

Aus dem Institut für Molekular- und Zellbiologie der Hochschule Mannheim

(Direktor: Prof. Dr. rer. nat. Mathias Hafner)

Isolation, characterization, and expansion of heterogeneous circulating
tumor cell (CTC) populations from cancer patients using microfluidic
technologies

Inauguraldissertation

zur Erlangung des Doktor scientiarum humanarum (Dr. sc. Hum.)

der

Medizinischen Fakultät Mannheim

der Ruprecht-Karls-Universität

zu

Heidelberg

vorgelegt von

Mina Zeinali

aus

Tehran, Iran

2019

Dekan: Prof. Dr. med.Sergij Goerd
Referent: Prof. Dr. Sunitha Nagrath
Prof. Dr. rer.nat Mathias Hafner

Dedication

To my baba jon and maman jon, each equally my pride and joy.

To my mentor and my role model, Dr. Sunitha Nagrath, who believed in me and gave me the opportunity to change and build my career path.

To my sister, Mahnaz, for being a turning point in my life, forever.

And to my other family members who support and love me unconditionally.

I love you all.

#HopeToCureCancer

Table of Contents

1	Introduction	10
1.1	Circulating Tumor Cells (CTCs)	10
1.1.1	Clinical implications	10
1.1.2	Biology of CTCs.....	11
1.2	BioMEMS in life science	13
1.2.1	Fabrication and structure	14
1.2.2	Bioapplications of Microfluidic Devices	14
1.3	CTC enrichment strategies.....	15
1.3.1	Technology challenges	15
1.3.2	Immunoaffinity-based enrichment methods	16
1.3.3	Biophysical properties enrichment methods	19
1.3.4	Direct imaging modalities.....	22
1.3.5	Functional Assays	23
1.3.6	Perspectives	23
1.4	CTC detection in pancreatic cancer	28
1.4.1	Pancreatic cancer	28
1.4.2	The biology of pancreatic cancer	29
1.4.3	Detection and diagnosis	30
1.4.4	Staging of pancreatic cancer	32
1.4.5	Treatment	32
1.4.6	CTCs in pancreatic cancer	33
1.5	CTC detection in lung cancer	38
1.5.1	Lung cancer	38
1.5.2	The biology of lung cancer.....	38
1.5.3	Detection and diagnosis	39
1.5.4	Staging of lung cancer	40
1.5.5	Treatments	40
1.5.6	CTCs in lung cancer	40
2	Materials and Methods	42
2.1	Microfabrication.....	42

2.1.1	Computational analysis of the microposts	42
2.1.2	Photolithography.....	43
2.1.3	Rapid prototyping	44
2.1.4	Bonding, surface chemical modification and functionalization	46
2.2	Cell culture	48
2.2.1	CellTracker dye protocol.....	49
2.2.2	Primary human pancreatic cancer and cancer-associated fibroblast (CAF) cell lines.....	49
2.2.3	Patient-derived CTC expansion.....	50
2.3	Western blot	51
2.4	Flow cytometry analysis (FACS)	51
2.5	Capture efficiency in single CTC Carpet Chip	52
2.6	Capture efficiency in dual CTC Carpet Chip.....	52
2.7	Characterization experiments for Labyrinth (Cell lines)	53
2.8	Pancreatic cancer patient CTC capture using CTC Carpet Chip and Immunofluorescence staining (IF).....	53
2.9	Pancreatic and NSCLC cancer patient CTC isolation using Labyrinth and Immunofluorescence staining (IF).....	54
2.10	RNA extraction and quantitative reverse transcription polymerase chain reaction (qRT-PCR) analysis	56
2.11	Immunohistochemistry (IHC).....	57
2.12	Fluorescence in situ hybridization (FISH) analysis.....	58
2.13	In Vivo tumorigenicity assays	58
2.14	RBC lysis buffer	59
2.15	Drug testing.....	59
2.16	Statistical analysis.....	60
3	Results.....	62
3.1	Different design configurations of immunoaffinity microfluidic devices.....	62
3.1.1	General optimization of the microfluidic CTC chip	64
3.2	CTC Carpet microfluidic Chip technology	67
3.2.1	CTC Carpet Chip optimization	68
3.3	Dual capture.....	71

3.3.1	Optimization and re-evaluation of the dual CTC Carpet Chip	72
3.4	Application of the CTC Carpet Chip to evaluate heterogeneity in pancreatic cancer patient samples	80
3.4.1	Epithelial CTCs (EpCs) and EMT-like CTCs (EMTCs) recovered from pancreatic cancer patients	81
3.4.2	Pancreatic CTCs enrichment using the CTC Carpet Chip compared to healthy control samples	82
3.4.3	Pancreatic CTCs enrichment using the CTC Carpet Chip to explore associations with clinical outcomes	84
3.5	Gene expression profiling of EpCs and EMTCs by quantitative reverse transcription polymerase chain reaction (qRT-PCR)	86
3.5.1	Gene expression profiling on the captured CTCs on EpCAM Chip vs. CD133 Chip	86
3.5.2	Hematoxylin & Eosin (H&E) staining and immunohistochemistry (IHC) analysis of primary tissues	88
3.5.3	Gene expression profiling on stage IIA pancreatic cancer patients (n=5) ..	89
3.5.4	Gene expression profiling on stage IIB&III pancreatic cancer patients (n=18)	91
3.5.5	Gene expression profiling on stage IV pancreatic cancer patients (n=12) ..	92
3.6	Molecular signature and prognosis	93
3.7	Monitoring patients based on the treatment regime	95
3.7.1	CTC burden monitoring	95
3.7.2	Gene expression profiling	95
3.8	Application of the CTC Carpet chip in PDAC xenograft model	98
3.9	Application of the Labyrinth technology in pancreatic cancer patients	104
3.9.1	Optimization of Labyrinth using pancreatic cancer cell line	104
3.9.2	CTC enumeration for treatment naïve cohort	107
3.9.3	CTC enumeration before and after the treatment regime	109
3.9.4	CTC counts to predict the prognosis in pancreatic cancer	112
3.10	High throughput label-free isolation of heterogeneous CTCs from non-small cell lung cancer (NSCLC) patients for targeted therapy using Labyrinth	114
3.10.1	Optimization of Labyrinth for lung cell line recovery	114
3.10.2	Isolation of CTCs from NSCLC Patients	119

3.10.3	Identification of heterogeneous CTC subpopulations isolated using Labyrinth.....	120
3.10.4	Presence of clusters in CTCs isolated using Labyrinth.....	123
3.10.5	Genomic analysis of NSCLC patient CTC samples using Fluorescence in situ hybridization (FISH) analysis.....	126
3.11	Patient-derived CTC expansion	127
3.11.1	Optimization of CTC expansion methods	127
3.11.2	Recovered CTCs were expanded from NSCLC patient samples (n=2) using 3D model	134
3.12	CTC enumeration of follow-up NSCLC patient samples	138
3.13	Drug testing.....	140
3.13.1	Optimization of drug testing methods using NSCLC cell lines	140
3.13.2	Drug testing on the patient-derived expanded CTCs.....	146
4	Discussion	149
5	Conclusion.....	162
6	Summary	170
7	ZUSAMMENFASSUNG.....	173
8	References	176
9	Appendix.....	193
9.1	Different design configurations of immunoaffinity microfluidic devices.....	193
9.1.1	Original vs. Split CTC chip.....	193
9.1.2	Original vs. Modified CTC Chip	194
9.1.3	Modified vs. Rotated CTC Chip	195
9.1.4	Rotated vs. Carpet CTC chip.....	196
9.2	List of Tables.....	197
9.3	Table of Figures	219
9.4	Table of Tables	223
10	Curriculum Vitae.....	224
11	Professional Work and Research Cited.....	225
12	Acknowledgments	228

Table of abbreviations

sec	second(s)
min	minute(s)
hr	hour(s)
μl	microliter
mL	millilitre
μm	micrometer
rpm	Revolutions per minute
°C	centigrade degree
UV light	ultraviolet light
Å	angstrom
v/v	volume per volume
RT	room temperature
μg mL ⁻¹	microgram per milliliter
w/v	weight per volume
mmol	millimoles
L	liter
mg kg ⁻¹	milligram per kilogram
nM	nano molar
mm	millimeter
u mL ⁻¹	Unit per milliliter
ng mL ⁻¹	nanogram per milliliter

1 Introduction

1.1 Circulating Tumor Cells (CTCs)

1.1.1 Clinical implications

Tumor-derived circulating tumor cells (CTCs) represent a heterogeneous population of malignant cells that disseminate from tumors into the bloodstream, as single cells or tumor cell clusters, enabling their transportation to distant sites and the seeding of metastatic tumors.¹⁻³

One avenue that holds promise in developing accurate predictive tools and pharmacodynamic biomarkers to guide patient care is the analysis of viable CTCs.^{1, 4-17} Monitoring CTCs in cancer patients has been described as a “liquid biopsy” or “live biopsy”,¹⁸ which could be a potential alternative to invasive biopsies for detection of metastasis and monitoring therapies¹⁹ if one can capture the entire heterogeneity of the disease. Detection, quantification, and molecular characterization of CTCs in peripheral blood have been recognized as a highly valuable emerging technique in the diagnosis of cancer and detection of metastasis.^{1, 7, 20, 21}

In early stage disease, CTCs might be used to predict the risk of metastasis, while over the course of therapy they may be useful for evaluating response to therapy and choosing the most suitable therapeutic regime. Furthermore, molecular analysis of CTCs may provide insight into the process of metastasis, revealing new biological therapeutic pathways.¹⁹ If CTCs are demonstrated to be useful as biomarkers, eventually they could represent a new way to diagnose cancer.¹

1.1.2 Biology of CTCs

Thomas Ashworth, an Australian physician, observed CTCs for the first time in the blood of a man with metastatic cancer in 1869. He postulated, “Cells identical with those of the cancer itself being seen in the blood may tend to throw some light upon the mode of origin of multiple tumors existing in the same person.”²² After comparing the morphology of the CTCs with tumor cells, he concluded that “one thing is certain, that is they (CTC) came from an existing cancer structure, they must have passed through the greater part of the circulatory system to have arrived at the internal saphena vein of the sound leg”.²² Researchers have been studying metastasis for about 149 years and research has indeed demonstrated the critical role of CTCs in these phenomena recently.

1.1.2.1 Seed and soil hypothesis

Stephen Paget in 1889 proposed the seminal “seed and soil” hypothesis based on the idea that metastasis depends on cross-talk between selected cancer cells (the seeds) and specific organ microenvironments (the soil), and that metastasis only happens when the soil and seed are compatible.²³

1.1.2.2 The relation between CTCs and EMT

CTCs are cells that extravasate from the primary tumor and enter the blood stream, enabling their transportation to distant sites and potential formation of metastatic tumors.¹⁻³ CTCs may enter the blood circulation in two ways: by passive shedding of tumor cells from the primary tumor, which may occur in large numbers and in early stages of tumor formation, or by an active mechanism involving the epithelial-to-

mesenchymal transition (EMT).² EMT is a complex molecular and cellular program by which cells of epithelial origin lose their apical-basal polarity and adhesiveness to neighboring cells and gain mesenchymal features, including aggressiveness, motility, invasiveness, and resistance to apoptosis.^{2, 5, 12, 20, 24-26} Thus, EMT can be molecularly defined by tumor cells losing intracellular adhesions, with down-regulation of epithelial markers (e.g. epithelial cell adhesion molecule (EpCAM) and cytokeratins) and up-regulation of mesenchymal markers (e.g. CD133, Vimentin).²⁷ Furthermore, EMT is known as “Cadherin switching”; down regulation of E-cadherin and up regulation of N-cadherin.²⁷⁻³³ EMTs are encountered in three general subgroups: type I EMT is correlated with implantation, embryogenesis, and organ development and can generate mesenchymal cells; type II EMT is associated with wound healing, tissue regeneration, and organ fibrosis; and type III EMT occurs in cancer progression and metastasis (Table 1-1).³⁴

Table 1-1: Classification of EMT according to the biological context ^{34, 35 36}

Characteristics	Types of EMT		
	Type 1	Type 2	Type 3
Moment of appearance during human life	Embryo formation: ✓ Organ development	Adult life: ✓ Trauma ✓ Inflammation	Adult life: ✓ Epithelial cancer
Physiological processes in which EMT is involved	Generates the first set of mesenchymal cells = primary mesenchyme	Wound healing Tissue regeneration Organ fibrosis	
Pathological processes in which EMT is involved	Without	Ongoing fibrosis with organ destruction	Systemic progression = metastases

It has been shown that Vimentin contributes to EMT via i) gene expression (regulates gene expression of proteins required for execution of EMT like Axl), ii) protein-protein interaction, and iii) phosphorylation.³² Vimentin is a type III intermediate filament protein which is the major cytoskeletal component of mesenchymal cells.^{27, 33}

This 57-kDa protein is responsible for maintaining cell shape, integrity of the cytoplasm, and stabilizing cytoskeletal interactions.³³ Evaluating the expression of this protein in normal and cancerous tissues can be of great value in tumor diagnosis as well as in the development and progression of cancers.²⁷ Therefore, because of dramatic compositional changes in intermediate filaments during EMT, Vimentin has been recognized as a selective expression marker of EMT.^{27, 31}

Recent studies have shown that a small number of cells have stem cell-like characteristics in various cancers and are called cancer stem cells (CSCs).^{37, 38} CSCs and cells undergoing EMT play important roles in tumorigenesis, metastasis, and chemo and radio-resistance.^{39, 40} Therefore, detecting and analyzing these cells among CTCs in circulation could lead to better understanding of EMT and tumor metastasis.

1.2 BioMEMS in life science

BioMEMS stand for biomedical microelectromechanical systems which have become an important subset of MEMS (microelectromechanical system) or MST (microsystem technology) devices that have biological and/or biomedical functions or applications for the improvement of human health.^{41, 42} BioMEMS brings together the skills of electrical, mechanical, optical and chemical engineers, material specialists, clinical laboratory scientists, and physicians.⁴³ BioMEMS are increasingly being used for miniaturization of implantable medical devices for diagnostic and therapeutic applications⁴⁴.

BioMEMS research and applications include diagnostics, therapeutic and organ development, bio-microelectrodes, tissue engineering, and bio-inspired materials for self-healing.^{41, 45-47} For diagnostic applications they are normally used to detect cells,

proteins, microorganisms, viruses, and molecules of interest.⁴¹ Microfluidics as powerful network of BioMEMS platforms is commonly used for rapid detection and cell characterization in diagnosis.⁴¹ The applications of the microfluidic technologies in the cancer disease are explained in details in section 1.3.2.1.2.

1.2.1 Fabrication and structure

BioMEMS refer to systems which use micro- and nanoscale (200 μm -100 nm) fabrication techniques for the analysis and delivery of biological and chemical particles.⁴¹ They may be platforms for nanotechnologies, or they may be key constituents of much larger devices such as a medical imaging machines.⁴³ They may also operate *in vivo* or *in vitro*. Generally, devices and integrated systems using bioMEMS are also known as lab-on-a-chip (LOC) and micro-total-analysis systems (μTAS).⁴¹ μTAS may be hybrids of multiple chips, integrated electronic and external supports, while LOC refers to a microfluidic chip.⁴⁸ Both techniques result in increased efficiency through smaller scales and therefore are capable of performing analyses that cannot be done conveniently by other methods.

Traditional microfabrication approaches require expensive equipment, access to cleanroom facilities, multistep processes, and are often limited to rigid and non-transparent substrates.⁴⁹ However, microfabricated on-chip microfluidics do have the advantage of achieving high sensitivity, quantitative detection, low costs, and shorter turnaround times compare to traditional microfabrication approaches.⁴⁹

1.2.2 Bioapplications of Microfluidic Devices

Microfluidics can be used to study fluid transport processes, in channels with dimension of tens to hundreds of microns.^{47, 50} The use of microfluidic channels has

scaled down fluidic processes, shortened reaction times, and lowered costs.^{47, 50} Many new techniques are being used for molding, replication, casting, and bonding which are essential for mass production, reproducibility, and functional reliability at low cost in the bioMEMS field.

Microfluidic technologies are widely used in different areas of research from bioengineering and biomedical science, to chemistry and nanotechnology.⁵¹ For instance in immunoassays, DNA sequencing, polymerase chain reaction (PCR), electrophoresis, DNA separation, enzymatic assays, cell counting, cell sorting and cell culture.⁵¹ The small volumes of reagents required, short reaction time, portability, low cost, low consumption of power, versatility in design and potential of parallel operation in microfluidic systems, make these technologies attractive and powerful platforms.⁵¹

Innovation in modern healthcare diagnosis techniques continues to improve patient outcomes. There is a huge interest in lab-on-a-chip devices for point-of-care detection as low-cost and portable solutions to health screening, diagnosis, and personalized medicine.⁴⁹

1.3 CTC enrichment strategies

1.3.1 Technology challenges

Detection and isolation of CTCs is challenging due to the low number of CTCs in the blood of cancer patients (on the order of 1 CTC per 10^6 – 10^9 normal blood cells) and the biological heterogeneity of CTCs.⁵² Therefore, both high efficiency and high purity isolation of CTCs from patient blood is urgently needed. Over the past decades, researchers have focused on the enrichment and identification of CTCs in blood. The

main approach for enrichment has been to capture cells of interest using specific epithelial markers on the cell surface to distinguish them from leukocytes.¹

Multiple approaches have been considered to overcome the limitation of low numbers of CTCs in peripheral blood. CTC enrichment technologies are based on the exploitation of either biological (label-dependent or immunoaffinity-based) or physical (label-independent or size-based) properties of cells.^{1, 53-60} CTC isolation technologies are summarized in Table 1-2.⁶¹

1.3.2 Immunoaffinity-based enrichment methods

These methods use specific cell surface biomarkers to capture cells either by positive or negative selection. During positive selection, tumor-associated cell surface antigens such as epithelial cell adhesion molecule (EpCAM) are targeted. Negative selection methods deplete hematopoietic cells by targeting the common white blood cell antigen CD45.⁶²

1.3.2.1 Positive enrichment

With positive enrichments methods, antibodies targeting tumor-associated antigens are tethered to either magnetic particles or device surfaces to capture CTCs.⁶¹ Positive enrichment techniques include immunomagnetic, microfluidic-based, and *in vivo* enrichment methods.

1.3.2.1.1 Immunomagnetic

Immunomagnetic methods capture CTCs by attaching micron sized magnetic beads to the CTCs via formation of an antigen-antibody complex, and then isolating CTCs by passing them through a magnetic field.¹ CellSearch is the

only FDA-cleared immunomagnetic semi-automated CTC enrichment device for prognostication of breast, prostate, and colorectal cancers.⁶³ Some drawbacks to this method are the fact that only EpCAM positive CTCs are detected, and the possibility of false positive and false negative.⁶³

Another approach is the magnetic activated cell sorting (MACS) method.⁶⁴ Some advantages of this method are flexibility and preserved cell integrity, and some difficulties of these methods are the possibility of false positives due to the expression of the same antigens on non-tumor cells and false negatives due to the loss of antigens on CTCs.^{65, 66}

The AdnaTest is another established method for CTCs enrichment, which is based on the use of specific antibodies against epithelial and tumor markers. Some advantages of this test are recognition of fixed markers, the ability of downstream analysis (e.g. RT-qPCR), and the possibility of characterization for stemness and EMT. The disadvantages of using this method are the possibility of both false positives and false negatives as with other immunomagnetic based methods.⁶³ The MagSweeper technology is another immunomagnetic CTC enrichment method isolates CTCs by sweeping through wells containing pre-mixed samples with antibody-coated magnetic bead.⁶⁰

1.3.2.1.2 Microfluidic-based

1.3.2.1.2.1 Micropost arrays and surface-based

Microfabrication methods create structures at the nano/mico scale, providing a unique advantage for CTC separation. The first implementation of a microfluidic device for this purpose, the CTC-Chip, consisted of an array of 78,000 microposts chemically

functionalized with anti-EpCAM antibody.⁴ 60% capture efficiency with 50% purity was obtained using a flow rate of 1 mL hr⁻¹.⁴ Since then, different microfluidic-based technologies have been investigated by various research groups focused on the development of CTC enrichment methods (e.g. GEDI,⁶⁷ OncoCEE,⁶⁸ and OncoBean⁶⁹).

Due to limitations with imaging of captured CTCs on microposts arrays, surface-based microfluidic devices have been developed by different groups (e.g. herringbone (HB) chip,⁷⁰ geometrically enhanced mixing (GEM) chip,⁷¹ graphene oxide (GO) chip,⁷² and Modular Sinusoidal Microsystem⁷³).

One of the drawbacks of using these types of enrichment is the inability of retrieving the captured CTCs which are immobilized on the post/surface of the device, therefore the downstream analysis is challenging.

1.3.2.1.2.2 Immunomagnetic

Immunomagnetic microfluidic techniques utilize antibody-conjugated magnetic beads to facilitate CTC separation (e.g. Ephesia,⁷⁴ Magnetic Sifter,⁷⁵ LiquidBiopsy,⁷⁶ Isoflux,⁷⁷ and CTC-iChip⁷⁸). The CTC-iChip technology uses either negative or positive selection of cells. Using positive selection ≥ 0.5 CTCs mL⁻¹ was detected in 90% of patient samples in one study and ≤ 30 CTC 7.5 mL⁻¹ from patient samples in another study.⁶¹ The technology has some drawbacks including, low purity yield and biased pre-processing of blood samples with magnetic beads. In positive selection cells are sorted based on their EpCAM expression. Negative selection depletes leukocytes immunomagnetically. Although, the negative selection module of CTC-iChip allows isolation of

heterogeneous populations of CTCs, the isolated CTCs are a mixed population of CTCs.

1.3.2.1.3 *In vivo* enrichment

The GILUPI Cell Collector captures CTCs using a structured medical Seldinger guidewire functionalized with anti-EpCAM.⁷⁹ The guidewire is inserted into a patient's peripheral vein to allow continuous sampling of a relatively large volume of blood compared to other CTC enrichment methods. One drawback is that the method can be considered invasive to the patient.

1.3.2.2 Negative enrichment

As mentioned above, negative enrichment methods deplete unwanted background cells by utilizing antibodies targeting leukocyte-associated antigens conjugated to magnetic particles or the device surface. EasySep Human CD45 Depletion Kit,⁸⁰ QMS,⁸¹ MACS,⁸² Negative selection disk,⁸³ and CTC-iChip⁷⁸ are some examples of the available negative selection methods. These methods provide unbiased CTC isolation, however at the cost of lower purity compared with positive enrichment.⁶¹

1.3.3 Biophysical properties enrichment methods

In order to overcome the limitation of biased cell selection using biological properties, researches have proposed CTC enrichment based on biophysical properties. These are mainly referred to as “label-free” technologies, relying on physical characteristics such as density, size, deformability, and electric charge.⁶¹ Size-based CTC enrichment technologies rely on the size of CTCs, which has a larger morphology

(12-25µm) than leukocytes (8-14 µm).^{84, 85} One of the drawbacks of the size-based technology is the loss of smaller CTCs during enrichment.⁶¹

1.3.3.1 Density Gradient Centrifugation

Centrifugation is one of the first methods recorded for CTC isolation.⁸⁶ Blood samples were centrifuged to separate different cells populations based on their relative densities. Density gradient methods separate CTCs and mononuclear cells using different methods including Ficoll-Paque,⁸⁷ OncoQuick,⁸⁸ RosetteSep CTC Enrichment Cocktail,⁸⁹ and Accucyte Enrichment and CyteSealer.⁹⁰ OncoQuick has the advantage of preventing cross contamination by using an additional barrier, however the specificity is still low.^{1, 88, 91} RosetteSep CTC Enrichment Cocktail is based on negative selection, though there is still the possibility of cross contamination with this method.^{92, 93}

1.3.3.2 Microfiltration

Microfiltration technology uses pore sizes around 7-8 µm or 3D geometries for CTC enrichment.⁶¹ Microfiltration methods include 2D microfiltration systems (isolation by size of epithelial tumor cells (ISET),⁹⁴ ScreenCell,⁹⁵ CellSieve,⁹⁶ and Flexible Micro Spring Array (FMSA)⁹⁷) and 3D microfiltration systems (FaCTChecker,⁹⁸ Resettable Cell Trap,⁹⁹ and Cluster Chip¹⁰⁰).

ISET technology uses a filter with 8 µm pores to separate smaller leukocytes from the larger epithelial cells. Advantages of this method are that it is simple to use and inexpensive, as well as capable of capturing both EpCAM positive and negative tumor cells. The fundamental disadvantages of ISET are its low specificity in capturing CTCs, the possibility of loss of smaller CTCs which can pass through the pores, and the

enrichment of large leukocytes.^{1, 94} Although microfiltration systems in general allow rapid processing of blood, they are prone to clogging, parallel processing with multiple filters, achieving very low purities (<10%), large variability in CTC recovery, and concentrated stresses that affect the viability of enriched CTCs.^{61, 101} These complications leave an opportunity for improvement of these types of technologies.¹⁰²

1.3.3.3 Inertial focusing

Inertial focusing passively separates CTCs from other blood cells based on cell size. The relative positioning of cells passing through microfluidic flow channels is affected based on the equilibrium between lift forces and dean flow.^{61, 103} In general, inertial focusing methods exert minimal stress on isolated cells and allow viable cell recovery.⁶¹ Some methods that apply inertial focusing include Vortex,⁸⁵ Dean Flow Fractionation,¹⁰⁴ and Labyrinth.¹¹³ Labyrinth technology is explained in detail in section 1.4.6.1.2

1.3.3.4 Dielectrophoresis (DEP)

Dielectrophoresis (DEP) separates cells based on their electrical signature using an applied electric field.^{61, 105} The electrical signature of different cells depends on the composition, morphology, and phenotype of the cells.^{105, 106} ApoStream,¹⁰⁷ DEPArray,¹⁰⁸ and MOFF and DEP chip¹⁰⁹ are some examples of technologies that apply DEP for the CTC enrichment. DEPArray is a commercially available technology that is likely to be limited to samples with high CTC numbers due to the ~40% CTC lost during sample loading.¹¹⁰

1.3.3.5 Acoustophoresis

Acoustophoresis Chip separates CTCs based on the acoustophoretic mobility, by exposing them to acoustic waves.¹¹¹ Separation depends on physical characteristics of the cells including, size, density, and compressibility.¹¹¹ 87% cell recovery and 99.3% purity at a flow rate of 4.2 mL hr⁻¹ using cell lines was reported.¹¹¹ However, due to the low sample volume (100 µL) using this technique, it is not feasible to generate data for samples with any clinically relevant low concentrations of CTCs.¹¹¹ Increasing sample volumes results in long processing times which may affect long-term stability.¹¹¹

1.3.4 Direct imaging modalities

All of the mentioned technologies require subsequent verification to identify the captured cells. Hence, researchers have developed technologies to improve efficiency of imaging following CTC enrichment. Some of these technologies listed as Microfluidic Cell Concentrator (MCC),¹¹² ImageStream,¹¹³ EPIC Science,¹¹⁴ FASTCell,¹¹⁵ CytoTrack,¹¹⁶ and Photoacoustic flow cytometry (PAFC).¹¹⁷

MCC technology uses passive pumping between small transport channels and a large collection ring to concentrate samples, therefore reducing imaging time.¹¹² ImageStream combines flow cytometry with fluorescence imaging.¹¹³ However, the capture efficiency is variable, and highest with elevated CTC numbers.¹¹⁸ The enrichment-free CTC detection technology, EPIC Science, uses HD-CTC imaging system to screen a monolayer of three million nucleated cells spread on custom glass slides.¹¹⁴ CTCs were detected in 68% of NSCLC patient sample using this technology.⁶¹ In another study ≥ 5 CTC mL⁻¹ was detected in 50% of patients with pancreatic cancer.¹¹⁹

FASTcell and CytoTrack technologies both rely on imaging only. The first technology uses an array of optical fibers to form a wide collection aperture that provides a much larger field of view than traditional optical systems.¹¹⁵ CTCs were detected in a rate of ≥ 2 CTC mL⁻¹ in 42% of patients with NSCLC.¹²⁰ The latter technology prescreens the samples at high rates and records potential CTC targets for additional image analysis and verifications.¹¹⁶ PAFC platform is a laser-based technology for real-time CTC detection within patient veins by interrogating the blood flow through the skin.¹¹⁷

1.3.5 Functional Assays

Functional assays exploit viable CTC enrichment based on bioactivity of cells, such as protein secretion (e.g., EPISPOT¹²¹) or cell adhesion (Vita-Assay¹²²). Various groups have utilized the Epithelial ImmunoSPOT Assay (EPISPOT) to capture CTCs based on specific secreted/released/ shed tumor-associated proteins.^{121, 123-125}

1.3.6 Perspectives

It is important to develop optimal CTC isolation techniques that enable us to achieve high recovery and high purity of CTCs by depleting off-target cells, while employing a high throughput system to ensure handling of large sample volumes. As mentioned earlier, each technology has advantages and disadvantages. Below is the summary of pros and cons of the immunoaffinity and size-base separation methods.

1.3.6.1 Advantages and disadvantages of Immunoaffinity CTC isolation

Immunoaffinity methods offer very high specificity for CTC capture. Using these technologies, CTC isolation needs to be tailor-made to answer relevant biological

questions. By utilizing the right antibodies, an assorted pool of CTCs can be recovered from cancer patients regardless of the cell morphology. This isolation method can capture CTCs in various size ranges ($>4\text{-}30\text{ }\mu\text{m}$).¹²⁶ Although there is no need to pre-process the samples, the purity of recovered CTCs is high, therefore more options for downstream analysis are feasible.⁶⁷ The immunoaffinity method also offers the ability to capture CTC clusters.^{70, 127} However, they suffer from a few limitations including, low throughput,⁷⁸ and difficulties releasing the cells from the chip for single cell analysis and CTC derived xenografts models.¹²⁸

1.3.6.2 Advantages and disadvantages of size-based separation CTC isolation

The main advantage of using biophysical properties for CTC enrichment is that cell selection is not biased according to expression of a particular biomarker. Hence, these methods can recover heterogeneous CTC populations that are viable and not immobilized on a surface. Therefore, off-chip standard cell culture techniques for expanding patient derived CTCs and further downstream analyses are feasible. Another advantage is the ability to process a large sample volume (high throughput), however, clogging difficulties may still remain.¹²⁹ The main disadvantage of size-based separation methods is the loss of smaller CTCs, which may result in losing valuable information from the patient.^{126, 130}

In light of the limitations of current CTC enrichment technologies, we applied two different microfluidic technologies (the immunoaffinity CTC Carpet Chip, and the size-based separation device, Labyrinth) to study CTCs in pancreatic and non-small cell lung cancers patient samples.

Table 1-2: CTC isolation technologies⁶¹

Principle	Technology	Selection criteria	Flow rate	Capture efficiency	Purity	Application	Ref
Immunofluorescence	Immunomagnetic	CellSearch				FDA-Approved	131
		AdnaTest				CTCs captured then multiple cancer markers measured by RT-PCR	132
		MACS				Pos/Neg enrichment, high surface area to volume	64
		MagSweeper	9 mL hr ⁻¹	62%	51%	17 metastatic breast cancer patients, whole blood	60
	Microfluidic Micropost Arrays	CTC-Chip	1 mL hr ⁻¹	60-65%	50%	Micropost array optimized for cell-antibody contacts, 116 patients with metastatic lung, prostate, pancreatic, breast and colon cancer	4
		GEDI	1mL hr ⁻¹	85%	68%	20 patients with prostate cancer	67
		CTC Carpet Chip	1mL hr ⁻¹	97.5%	76%	Heterogeneous CTCs separation from whole blood of 36 pancreatic cancer patients	133
		OncoCEE				Staining procedure labels capture antibodies	68
		OncoBean	10 mL hr ⁻¹	>80%		6 patients with lung, breast, and pancreatic cancer	69
	Microfluidic Surface Capture	Herringbone Chip	1.5-2.5 mL hr ⁻¹	90%		Microvortices mix sample, 15 patients with metastatic prostate cancer, clusters observed	70
		GEM	3.6 mL hr ⁻¹			Microvortices mix sample	71
		Graphene Oxide Chip	1 mL hr ⁻¹	82.30%		20 patients with breast, pancreatic, and lung cancer	72
		Modular Sinusoidal Microsystem	>7.5 mL hr ⁻¹		>86%	Three modules; selection, impedance, and imaging, clusters observed	73
	Microfluidic Immunomagnetic	Ephesia	>3 mL hr ⁻¹			Self-assembly of magnetic μ m-beads into columns	74
		Magnetic Sifter	10 mL hr ⁻¹			Vertical flow configuration	75
		LiquidBiopsy	5 mL hr ⁻¹			Automated, sheath flow minimizes non-specific binding, continuous flow	76
		Isoflux™				Automated, continuous flow	77
		CTC-iChip	8 mL hr ⁻¹			Pos/neg enrichment, size-based separation, whole blood, inertial focusing aids in magnetic deflection	78
	Immunomagnetic, <i>in vivo</i>	GILUPI CellCollector™				Can process large volumes of blood	79
Negative Enrichment	Immunomagnetic	EasySep				Simple, easy-to-use batch separation	80
		QMS				Continuous flow, high throughput	81
		MACS					82
		Negative selection disk		60%		Isolation of breast cancer cells from mononuclear cells mixture	83
	Microfluidic Immunomagnetic	CTC-iChip				CD45, CD66b, Size	78

Biophysical	Density Gradient Centrifugation		Ficoll-Paque	Density	84%	Inexpensive, easy-to-use	87		
			OncoQuick	Density, Size	70.60%	Porous membrane above separation media for additional separation by filtration	88		
			RosetteSep CTC Enrichment Cocktail	Density, Antibody Cocktail		Antibody-labeling alters cell density	89		
			Accucyte Enrichment and CyteSealer	Density		Sequential density fractionation enriches target cells. Additional CyteFinder™ and CytePicker™ modules for high throughput imaging and single-cell recovery	90		
	Microfiltration		ISET	Size, Deforma- bility	NA	Filters fixed samples through 8 μm pores, 10–12 wells can process 1 mL each, clusters observed	94		
			ScreenCell			Hydrophilic surface, fixed/live samples, 7.5-6.5 μm pores	95		
			CellSieve			Constructed from a transparent, flexible, non-fluorescent photoresist, 7 μm pores	96		
			Flexible Micro Spring Array (FMSA)			Constructed from parylene-C, can process whole blood, captures viable cells, clusters observed	97		
			FaCTChecker			Constructed from parylene-C, captures viable cells between membrane layers	98		
			Resettable Cell Trap			Pneumatically-controlled microvalves	99		
			Cluster Chip			Triangular pillars designed for CTC clusters	100		
	Inertial Focusing		Vortex	Size	7.5 mL 20 min ⁻¹	~18% with cell lines	57-94%	No RBC lysis required, captures viable cells, clusters observed, tested with 12 patient samples (breast and lung cancer)	85
			Dean Flow Fractionation		7.5 mL 8 min ⁻¹	>80% with cell lines	~4 log dep	Tested with 10 patient samples (breast and lung cancer)	104
			Labyrinth		2.5 mL min ⁻¹	>95%	600 WBCs mL ⁻¹	RBC removal required, capture viable cells, easy to manufacture, clusters observed	103
	Electrophoresis		ApoStream	Electrical Signature	>10 mL hr ⁻¹		DEP-FFF, continuous flow, captures viable cells	107	
			DEPArray				Requires pre-enrichment, allows recovery and manipulation of viable, single cells through DEP cages	108	
			MOFF and DEP chip		126 μl min ⁻¹	99%	Isolation of breast cancer cells from blood	109	
	Acoustophoresis		Acoustophoresis Chip	Size	Acoustic pre-alignment and separation			111	
Direct Imaging Modalities	Pre-Enrichment Required	Microfluidic Cell Concentrator (MCC)	None	Passive pumping concentrates samples ~5x			112		
		ImageStream	CK, CD45, DRAQ5	Hybrid of flow cytometry and fluorescence microscopy, 5000 cells/sec			113		
	Enrichment-Free	EPIC	CK, CD45,	Automated digital microscopy, clusters observed			114		

Functional Assays	<i>In vivo</i>	FASTCell	DAPI	Fiber-optic array allows larger field-of-view, 25 M cells min ⁻¹ , low resolution	115
		CytoTrack		Special glass disc scanned as it spins, clusters observed, 100 M cells/min	116
		Photoacoustic flow cytometry (PAFC)	Absorption spectra	Non-invasive label-free interrogation of large blood volumes	117
		EPISPOT	Protein secretion	Discriminates between viable and apoptotic CTCs using protein secretion	121
		Vita-Assay	Cell adhesion matrix	Enriches for viable CTCs based on preferential CAM adhesion, clusters observed.	122

1.4 CTC detection in pancreatic cancer

1.4.1 Pancreatic cancer

Pancreatic ductal adenocarcinoma (PDAC) is the fourth leading cause of cancer-related death in the United States.¹³⁴ The median survival time is less than 6 months, with a bleak 5-year survival rate of 8%, making it one of the most lethal malignancies in humans.¹³⁴ The inability to detect pancreatic cancer in early stages means that tumor invasion to other organs has often already occurred by the time of diagnosis. This may be due to the aggressive nature of pancreatic cancer. Hence, there is an urgent need for methods that enable early detection.

There are two main types of pancreatic cancers: exocrine tumors, which are called adenocarcinomas, and endocrine tumors (islet cell tumors or pancreatic neuroendocrine tumors (PNETs)), which are most often benign and affect the hormone-producing cells, making up about 1% of pancreatic cancers.¹³⁵

Approximately 95% of pancreatic tumors originate from the ducts of the pancreas and are known as PDAC.¹³⁵ They may evolve from premalignant lesions to fully invasive cancer.¹³⁶ This type of cancer can penetrate into neighboring tissues such as lymphatics, spleen, peritoneal cavity, and, in advanced stages of metastasis, the liver and lungs.¹³⁵ Three known human PDAC precursor lesions have been identified in clinical and histopathologic studies, including pancreatic intraepithelial neoplasm (PanIN), mucinous cystic neoplasm (MCN), and intraductal papillary mucinous neoplasm (IPMN).^{135, 137} PanIN is the most common of these lesions and is graded into different stages from I to III, representing the earliest through advanced stages, and

ultimately transforms into invasive PDAC¹³⁷ (Figure 1-1). Genetic alterations are the drivers of these defects, and will be explained in detail in section 1.4.2.

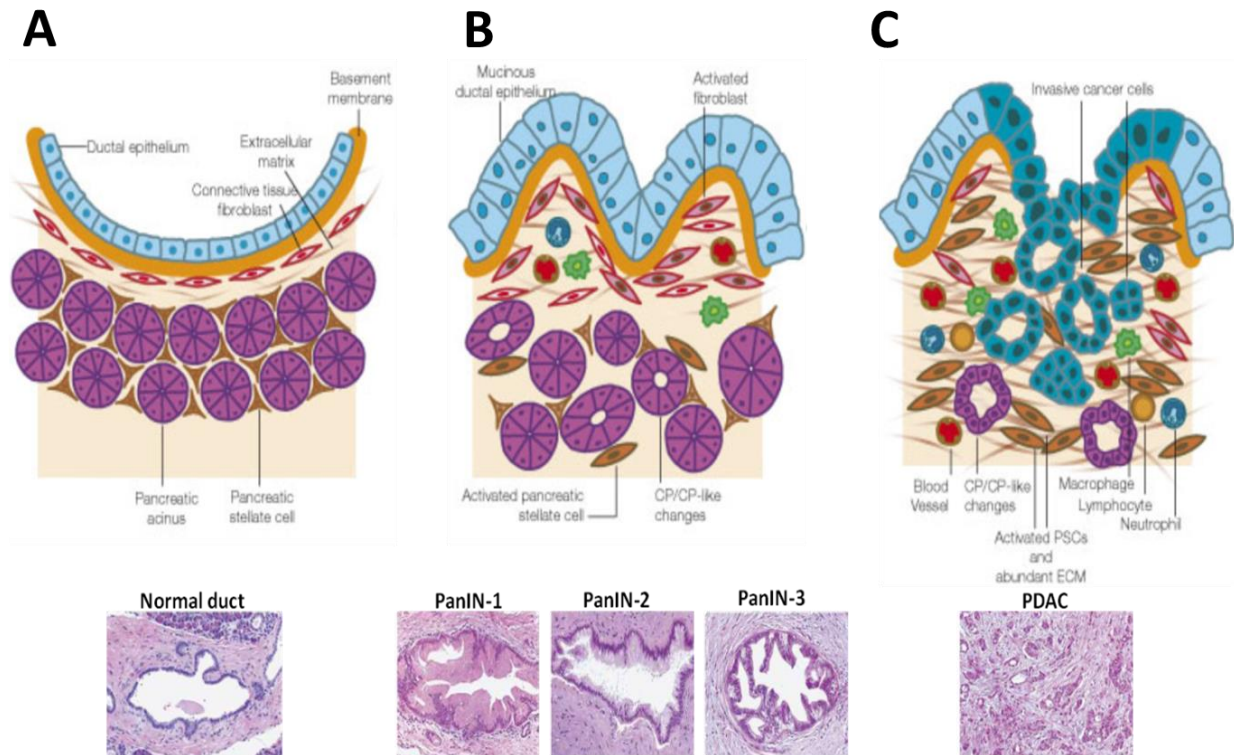


Figure 1-1: Pancreatic precursor lesions in pancreatic adenocarcinoma progression. A) Normal duct, B) pancreatic intraepithelial neoplasm (PanIN), and C) PDAC.^{135, 137}

1.4.2 The biology of pancreatic cancer

Almost all patients with pancreatic cancer carry one or more of four genetic defects: activation of KRAS2 oncogene (90% of tumors), inactivation of the tumor-suppressor gene CDKN2A (95%), inactivation of the tumor-suppressor genes TP53 (50%-75%), and deleted in pancreatic cancer4 (DPC4 or SMAD4) (50%).¹³⁶ These sequences of events are extremely complex and heterogeneous. Furthermore, these arrangements were also observed in mouse models.^{136, 138-141}

Pancreatic cancers are composed of several elements (Figure 1-2), including pancreatic cancer cells (carries an average of 63 genetic alterations per cancer, which can be grouped into 12 main signaling pathways),¹⁴² pancreatic cancer stem cells ($\leq 5\%$

of cells population), and the tumor stroma (mainly pancreatic stellate cells which are responsible for the poor vascularization).¹³⁶

The 12 cancer-relevant pathways that are involved in pancreatic cancer cells include: apoptosis, DNA damage repair, cell-cycle control, RAS, TGF- β , cell adhesion, Hedgehog, Integrin, JNK, wingless in drosophila (Wnt)- β -catenin, invasion, and small GTPases.¹³⁶ Pancreatic cancer stem cell populations are capable of asymmetric division; therefore, they are able to generate mature cells as well as cancer stem cells.

Pancreatic cancer stem cells, which can be identified with some specific markers such as CD24, CD44, CD133, and ALDH are resistant to chemotherapy and radiography but they have alterations in developmental pathways such as, Notch, Hedgehog, and Wnt- β -catenin which may result in a new therapeutic targets.¹³⁶

Tumor stroma is a dense formation of both cellular (e.g., fibroblasts, pancreatic stellate cells, endothelial cells, immune and inflammatory cells and adipocytes) and extracellular matrix components (e.g., collagen I and III, laminin, fibronectin, MMP, TIMP, SPARC, and CTGF).¹³⁶ The stroma is critically involved in tumor formation, progression, and metastasis.^{137, 143}

1.4.3 Detection and diagnosis

Lack of early symptoms and reliable screening tests for early detection are major reasons why over 85% of PDAC patients are inoperable at the time of diagnosis.¹⁴⁴ The inability to detect pancreatic cancer in early stages means that tumor invasion to other organs has often already occurred by the time of diagnosis. This may be due to the aggressive nature of pancreatic cancer.

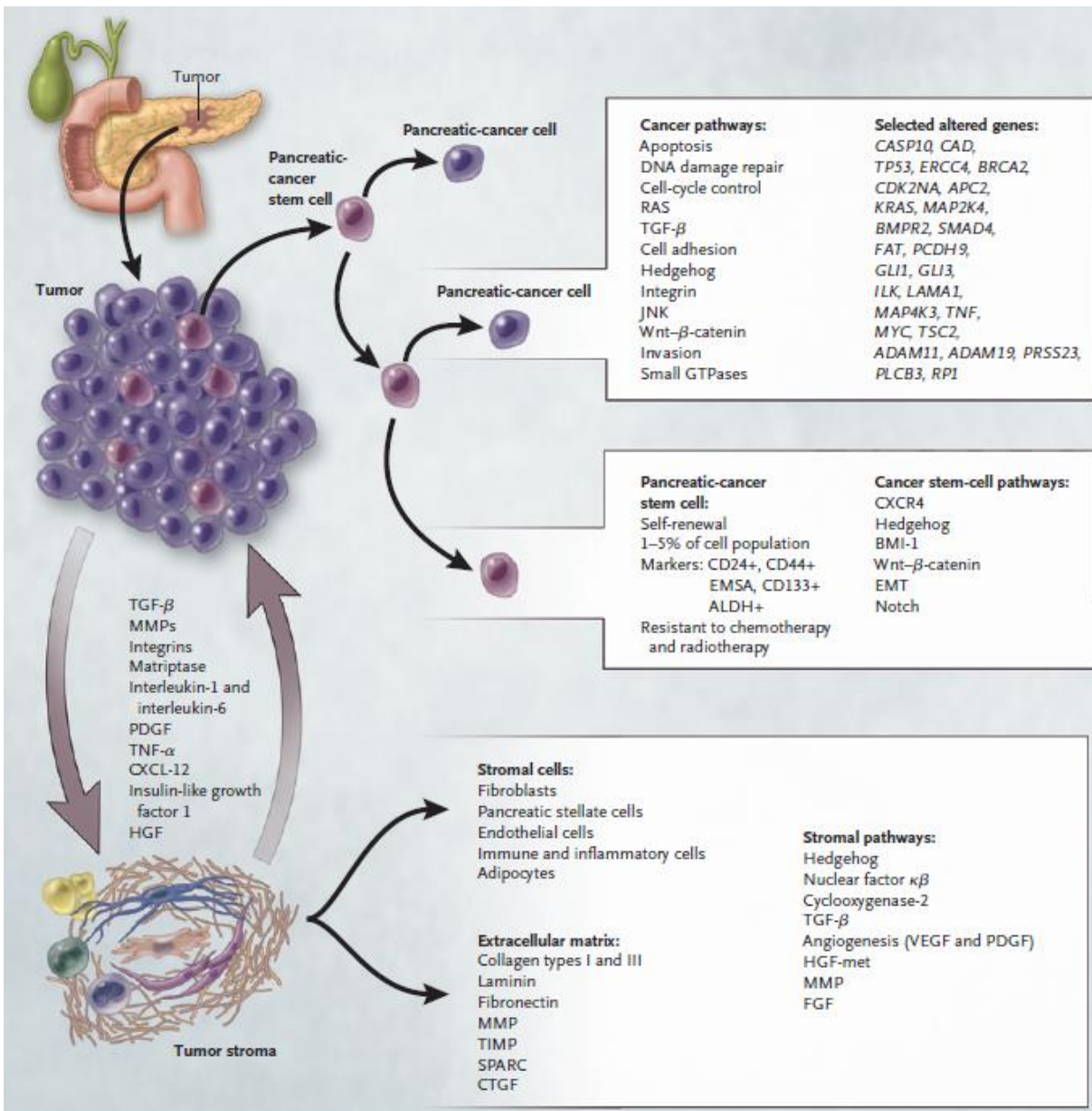


Figure 1-2: Cell components of pancreatic cancer. Pancreatic cancers are composed of several distinct elements, including pancreatic cancer cells, pancreatic cancer stem cells, and the tumor stroma.¹³⁶

For the initial evaluation for detection and staging in suspected pancreatic patients helical computed tomography (CT) is the most widely used technique.¹⁴⁵ Other than CT, contrast-enhanced Doppler ultrasound (US), enhanced magnetic resonance imaging (MRI), and endoscopic US (EUS) techniques are used in the diagnosis of pancreatic cancers of different stages and zones.¹⁴⁵

Presently, measuring the carbohydrate antigen 19-9 (CA19-9), and the carcinoembryonic antigen (CEA) are the only blood-based markers for diagnosis, monitoring of treatment, and prediction of survival in pancreatic cancer patients.¹⁰ CA19-9 is a sialylated Lewis antigen of the mucin 1 (MUC1) protein with an overall sensitivity of 80% and specificity of 82%.¹⁴ However, this biomarker is not applicable to all patients, since, not all patients are in a Lewis blood group. Patients with blood type of Lewis A- and B- genotype are incapable of synthesizing the CA- 19-9 epitope.¹⁰

1.4.4 Staging of pancreatic cancer

Pancreatic cancer is staged based on the American Joint Committee on Cancer (AJCC) tumor-node-metastasis (TNM) classification which is based on assessment of resectability by means of CT.¹³⁶ Each cancer is assigned a letter (T, N, and M stands for tumor, node, and metastases) and number. TX means the tumor cannot be measured, T0 shows there is no evidence of primary tumor, and Tis indicates that the cancer cells are only growing in the most superficial layer of tissue without growing into deeper tissues, which may be called in situ cancer or pre-cancer. Finally, T1, T2, T3, and T4 describe the tumor size and/or the spread into nearby tissues. The same explanations apply for N and M. Additional information about pancreatic cancer staging is provided in appendix section (Table 9-1).

1.4.5 Treatment

The inaccessibility of the pancreas limits the possibility of surgical removal, and the aggressive nature of the tumor leads to a rapid progression, which is strongly resistant to chemotherapy.¹⁵ In select patients with localized PDAC (only less than 20%

of patients),¹³⁶ surgical resection is the only treatment offering long time survival.¹⁴⁶ Adjuvant and neoadjuvant treatments for pancreatic cancer include chemo-radiotherapy and chemotherapy which have been evaluated in several trials with the goal of improving patient prognosis.¹⁴⁶ In advanced stages, chemo-radiotherapy and chemotherapy in locally advanced disease, fluoroprimitidines, cisplatin, and gemcitabine or more recently FOLFIRINOX is applied.¹⁴⁶ Although administering these treatments has been successful at reducing tumor burden and prolonging survival, effects of these treatments are limited and they cannot eliminate all PDAC cells.¹⁴⁷ Furthermore, molecularly targeted therapies have failed to show an additional advantage over chemotherapy.¹⁰ Obtaining tissue from pre- and post- treatment pancreatic cancer patients to monitor pharmacodynamic responses during clinical trials is challenging.¹⁰ A critical factor in the frequently poor outcome is the silent nature of pancreatic cancer until late in the disease process.¹⁴⁸

Therefore, early detection is an essential strategy to improve outcomes, such as screening of high-risk individuals.¹⁴⁹⁻¹⁵¹ Therefore, there is an urgent need to establish new sensitive prognostic methods capable of identifying patients. Meanwhile, better understanding of the biology of pancreatic cancer could open new avenues for treatment.

1.4.6 CTCs in pancreatic cancer

Since access to tumor biopsies in pancreatic cancer is quite challenging due to its anatomical position, biomarkers are required to provide better diagnosis and explore alternative therapies. Isolation of CTCs from pancreatic cancer is possible, however, due to poor sensitivity of many CTC assays for patients with PDAC^{2, 3} the investigation

of their clinical utility has proven less successful than in other cancer types. Some examples of CTC enrichment techniques using immunoaffinity, size-based separation, negative enrichment, and some other methods in pancreatic cancer field are summarized in details in appendix Table 9-2.

1.4.6.1 CTC detection methods in pancreatic cancer

Among various developed technologies for the CTC enrichment, some have been used to detect CTCs in pancreatic cancer (e.g., CellSearch,⁶³ ISET,¹⁰ CTC-Chip,⁴ CTC iChip,⁷⁸ GEM,⁷¹ and GEDI⁶⁷). CellSearch is the only FDA-cleared CTC isolation technology, which is able to detect only 2 ± 6 CTC per 7.5 mL of blood in pancreatic cancer patients.⁶³ Using the same technology, other groups reported 11-45% CTC detection among PDAC patients.^{6, 152, 153} Utilizing CTC-iChip 66.7% of PDAC patients had detectable CTCs.⁷⁸

Although Rhim et al. developed a sensitive method to tag and track pancreatic epithelial cells in a mouse model of pancreatic cancer,¹⁵⁴ there is no specific method available for human studies of pancreatic cancer in the clinic. Recently, another microfluidic technique, which is an optimized version of HB-chip, was applied to study pancreatic cancer.⁷¹ A geometrically enhanced mixing (GEM) chip was designed to be able to get higher performance of captured cells (90%) compared to HB-chip.⁷¹

1.4.6.1.1 CTC Carpet Chip

CTC Carpet Chip is designed to capture heterogeneous populations of rare pancreatic CTCs (epithelial CTCs (EpCs) and EMT-like CTCs (EMTCs)) using antibody-coated microposts (Figure 1-3).¹³³ Successful capture of heterogeneous CTC populations with high specificity and sensitivity was dependent on the flow velocities

and shear forces within the device. Flow velocity is optimized to allow maximal contact between cells and microposts, while shear forces are sufficient to prevent non-specific cell attachment to posts.

In order to increase the sensitivity of capture of phenotypically distinct CTCs, the previous CTC-Chip developed by Nagrath et al.⁴ was modified by implementing an 18° rotation of hexagonal arrays of 100 µm x 100 µm microposts with an average distance of 50 µm between them. We have incorporated novel rearrangements of the posts which greatly enhances the capture of different CTCs subpopulations on different chips. This employs a dual immunoaffinity and physical discrimination approach enabled by the lateral flow distribution and cell post interactions within the CTC Carpet Chip.

For a more thorough representation of biologically diverse CTCs in patients with pancreatic cancer sequential microfluidic devices were set up using antibodies against EpCAM, to capture EpCAM+ CTCs, and antibodies against CD133 to capture more stem cell like cells, or putative EpCAM- CTCs.¹⁵⁵

CD133 (Prominin-1 or alias PROML1 or AC133) expressed on the cell surface is now recognized as a prospective marker for the isolation and characterization of pancreatic stem and progenitor cells.¹⁵⁶⁻¹⁵⁸ CD133+ pancreatic CSCs showed more aggressive behavior such as increased cell proliferation, migration, and invasion compared with the CD133- cells because they underwent EMT more readily.¹⁵⁹⁻¹⁶¹

Therefore, this finding suggests that CD133 might be a meaningful cell surface marker for pancreatic cancer cells. In the progression of pancreatic cancer, CSCs are linked with the aggressiveness of pancreatic cancer with association of EMT,⁴⁰ by changing the expression of cell surface marker of stem-cell like phenotype and

increasing formation of tumor.¹⁶⁰ Other than CD133, CD44, CD24, CXCR4, ATP-binding cassette subfamily G member2 (ABCG2), and Nestin are also known as pancreatic CSCs specific membrane markers.¹⁴⁷

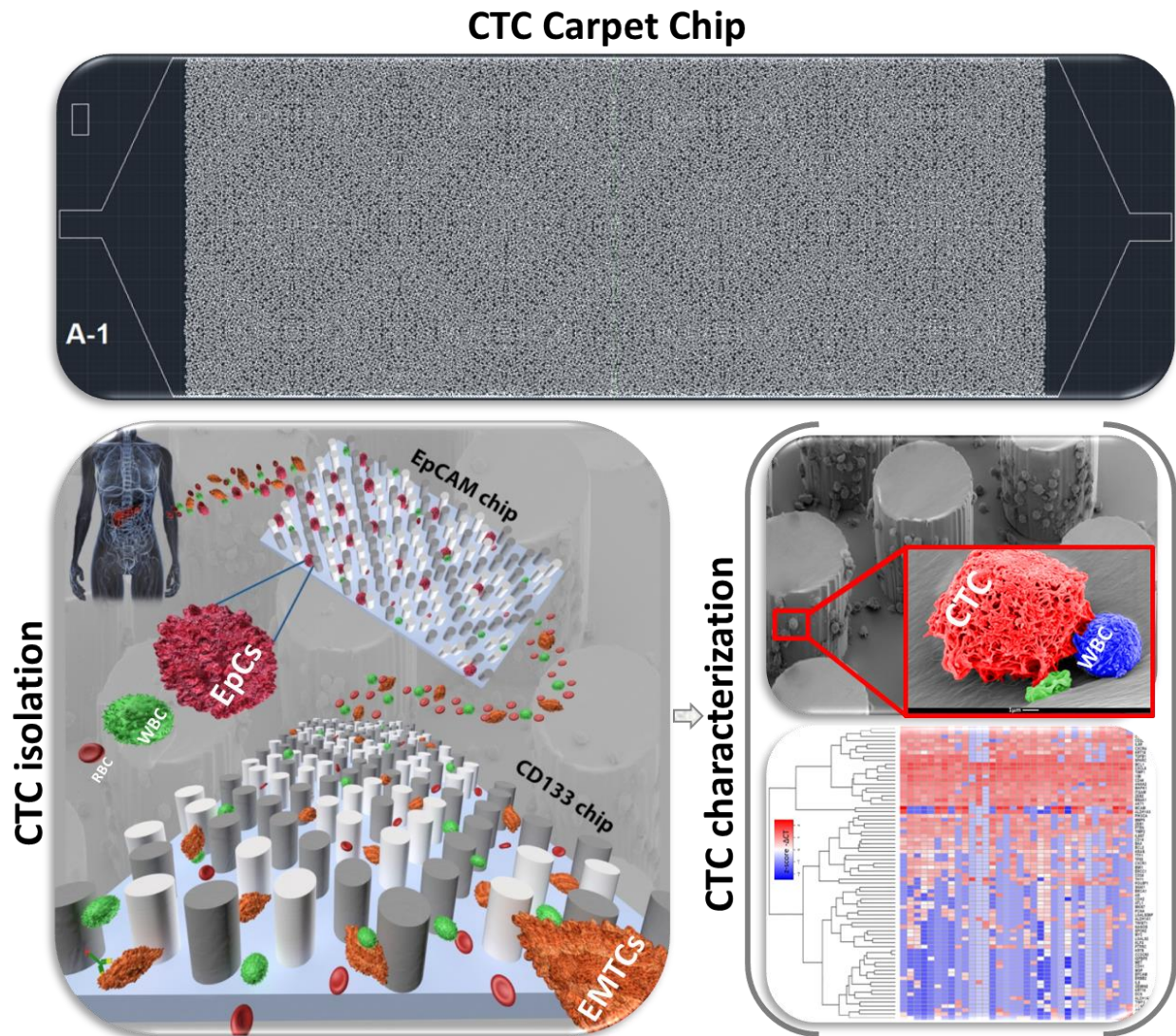


Figure 1-3: Schematic representative images of the immunoaffinity CTC Carpet Chip. The device uses sequential immunoaffinity-based microfluidics to study the biological relevance of heterogeneous circulating tumor cell (CTCs). Rare CTCs including both circulating epithelial cells (EpCs, dark pink) and EMT-like cells (EMTCs, orange) can be captured simultaneously from the peripheral blood of pancreatic cancer patients by using two markers of interest, anti-EpCAM and anti-CD133, in two different chips. The white/red blood cells are shown in green/red respectively. The posts are displayed in different colors only for visualization of the device pattern.

Obtaining pure CTC populations is crucial for robust downstream gene analysis. Therefore, applying the novel sequential microfluidic Carpet CTC Chip we can demonstrate enumeration, detection, and downstream molecular analysis of distinct CTC populations from pancreatic cancer patients.¹³³

1.4.6.1.2 Labyrinth device

The high throughput, label-independent, size-based inertial microfluidic separation device, Labyrinth, which was developed in the Nagrath lab, has been used to detect CTCs in breast, pancreatic, and lung cancer patients.¹⁰³

The design of the Labyrinth device is inspired by the Labyrinth in Greek mythology.¹⁰³ Both inertial focusing and dean flow were incorporated for sized-based separation, enabling continuous focusing of all cells while separating CTCs from smaller blood cells at the outlet.¹⁰³ The equilibrium between inertial lift forces and dean flow result in migration of particles during laminar flow through the microfluidic device within curved channels.¹⁰³ The Labyrinth device employs a combination of long curvature structure with loops and sharp corners to enhance differential focusing, allowing ease of separation of CTCs and white blood cells (WBCs) from patient blood samples.¹⁰³ The CTCs can be recovered from other blood components in curved microfluidic devices by focusing different sized cells into different stream lines and collecting them into individual outlet channels (Figure 1-4).¹⁰³ Particles are focused by inertial forces which can be considered as the driving forces, while particle migrates away from the center of the channel by drag forces from dean flow, leading to size-based separation.¹⁰³

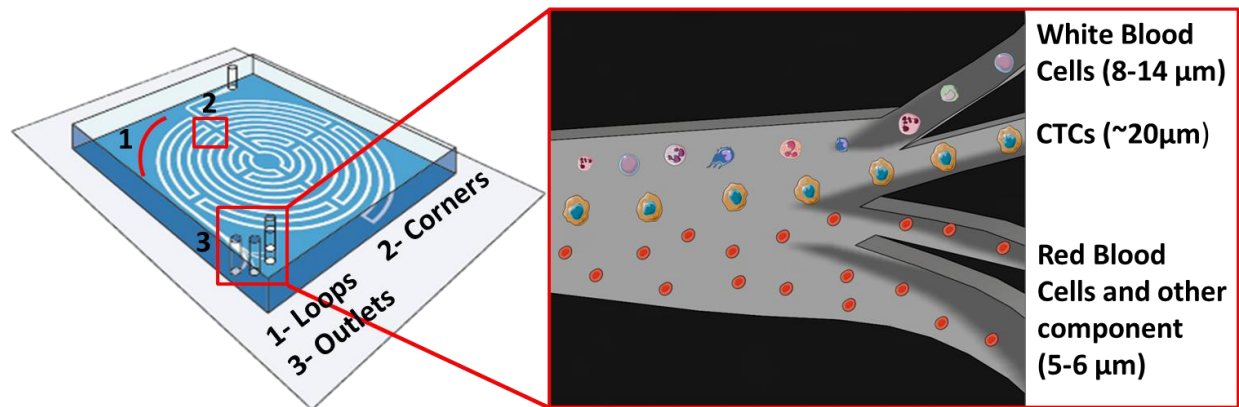


Figure 1-4: Size-based separation Labyrinth device. The device contains loops and corners to separate CTCs from other blood components individually into different streams (outlet channels).

1.5 CTC detection in lung cancer

1.5.1 Lung cancer

Lung cancer is among the most prevalent forms of cancer and has one of the highest mortality rates (>234,000 new cases and >154,000 death cases in the United State in 2018), with a 5-year survival rate of only 18%.^{134, 162, 163}

There are two major types of lung cancers based on the appearance of lung cancer cells under the microscope, small cell lung cancer (SCLC) and non-small cell lung cancer (NSCLC). About 10-15% of lung cancers are SCLC, while 80-85% of lung cancers are classified as NSCLC which mainly comprises adenocarcinoma (~40%), squamous cell (epidermoid) carcinoma (25-30%), and large cell (undifferentiated) carcinoma (10-15%).¹⁶⁴

1.5.2 The biology of lung cancer

A recent study revealed that less than two thirds of lung cancers have an underlying driver mutation responsible for tumor proliferation (e.g. *KRAS*, *EGFR*, *ALK*, *MET*, *HER2*, *FGFR1*, *ROS1*, *RET*, *BRAF*, *PI3KCA*, *MEK1*, *AKT1*, *MAP2K1*, and *NRAS*)

(Figure 1-5).¹⁶⁵ Of the known driver mutations, about 30% have FDA-cleared targeted therapies.¹⁶³

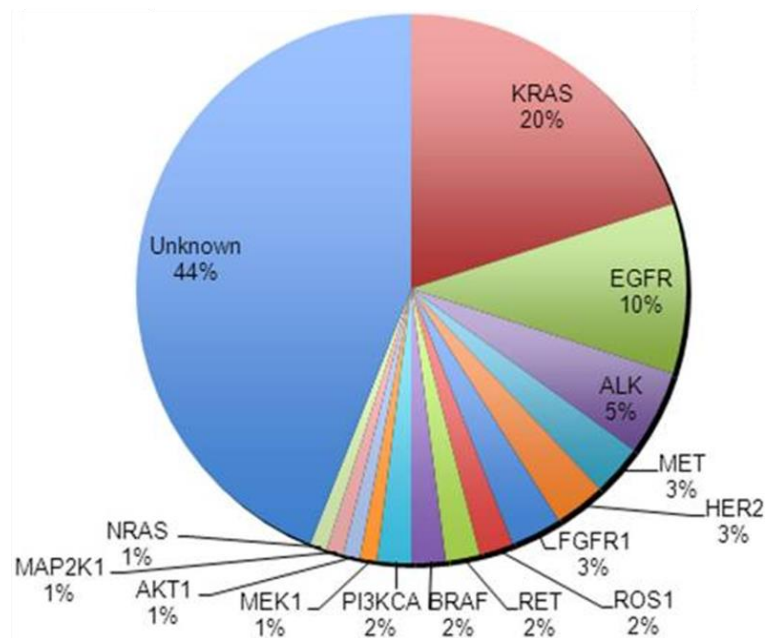


Figure 1-5: Pie chart of NSCLC mutations¹⁶⁵

1.5.3 Detection and diagnosis

Imaging tests including chest x-ray, CT scan, MRI scan, positron emission tomography (PET) scan, and bone scan are some examples of the commonly used screening tests for NSCLC.¹⁶⁶ Upon the non-small lung cancer detection, further diagnostics are performed, including, sputum cytology, thoracentesis, needle biopsy, and bronchoscopy.¹⁶⁶ The commonly used low-dose CT scan technique is not an ideal screening test for patients with lung cancer primarily due to poor specificity (high false positive rates).¹⁶⁷ In addition, CT scans are expensive and require tissue biopsies for confirmation of cancer. Alternative methods to detect cancers that can either supplant or complement the existing screening tests are an unmet need.¹⁶⁸

1.5.4 Staging of lung cancer

Lung cancer is staged based on the American Joint Committee on Cancer (AJCC) tumor-node-metastasis (TNM) system. Additional information about lung cancer staging is provided in appendix section (Table 9-3).

1.5.5 Treatments

The most effective treatment option for NSCLC patients is surgical intervention, however, patients are usually not diagnosed until advanced stages.¹⁶⁹ The practice of non-invasive liquid biopsy as a diagnostic, prognostic, and theranostic tool may be an attractive approach in NSCLC patients.¹⁷⁰ This approach may provide complementary data for prognostication and treatment responsiveness, and allow identification of newer genomic alterations that inform treatment resistance and alternative therapies.¹⁷⁰

1.5.6 CTCs in lung cancer

As mentioned above, CTCs have been detected in blood of patients with various solid tumors, including lung cancer, where their presence is associated with poor clinical outcomes.¹⁷¹⁻¹⁷⁸ Lung cancer CTCs have shown similar morphology and greater than 70% common histology with the primary tumor.¹⁷⁹ Therefore, CTCs may eventually serve as important blood-based biomarkers that could aid in early detection of lung cancer and the identification of early recurrence following therapy. However, there are currently no FDA-cleared CTC platforms for analyzing CTCs in lung cancer. The following section describes the merits and demerits of current CTC platforms for lung cancer.

1.5.6.1 CTC detection methods

Several studies have demonstrated the presence of CTCs using different detection technologies in patients with lung cancer.^{4, 174-178, 180, 181} It has been reported that in metastatic NSCLC patients only 21-39% of patients had detectable CTCs at baseline using CellSearch.^{174, 181-184} In contrast, the presence of CTCs (>5 CTC mL^{-1}) has been demonstrated in 100% of patients with metastatic lung cancer using the immunoaffinity microfluidic CTC-Chip.⁴ In another study using NanoVelcro technology, 4-17 CTCs mL^{-1} were detected in NSCLC patients.¹⁸⁵ One drawback of these label-dependent technologies is that they miss EpCAM- CTCs in NSCLCs that have undergone EMT. Among label-independent isolation approaches, ISET technology has detected 1-5 CTCs mL^{-1} in 36%-56.7% of NSCLC patients.^{186, 187} Recently, using Dean Flow Fractionation (DFF), CTCs were isolated (39.1 ± 24.8 CTCs mL^{-1}) at a flow rate of 3 mL hr^{-1} in metastatic NSCLC patients.¹⁸⁸ Additional information about CTC detection methods in lung cancer is provided in appendix section (Table 9-4).

There is a need for a simple, reliable, inexpensive, efficient, and high throughput system to enrich and characterize all relevant CTC subsets from lung cancer patient samples. Taking the advantage of the Labyrinth device, we can isolate heterogeneous populations of CTCs in NSCLC patients.

2 Materials and Methods

2.1 Microfabrication

Microfabrication is the method of fabrication of miniature structures of micro-nanometer scales. The microfabrication device pattern is first designed by employing AutoCAD software (version 2011), and then it was converted to a photomask (FineLine Imaging) for fabrication. The photomask was fabricated using traditional soft lithography,¹⁸⁹ bonded to a substrate, and then finally surface functionalized (Figure 2-1A). All microfabrication processes were done at the clean room facility available at Lurie Nanofabrication Facility at College of Engineering University of Michigan (Figure 2-1B).

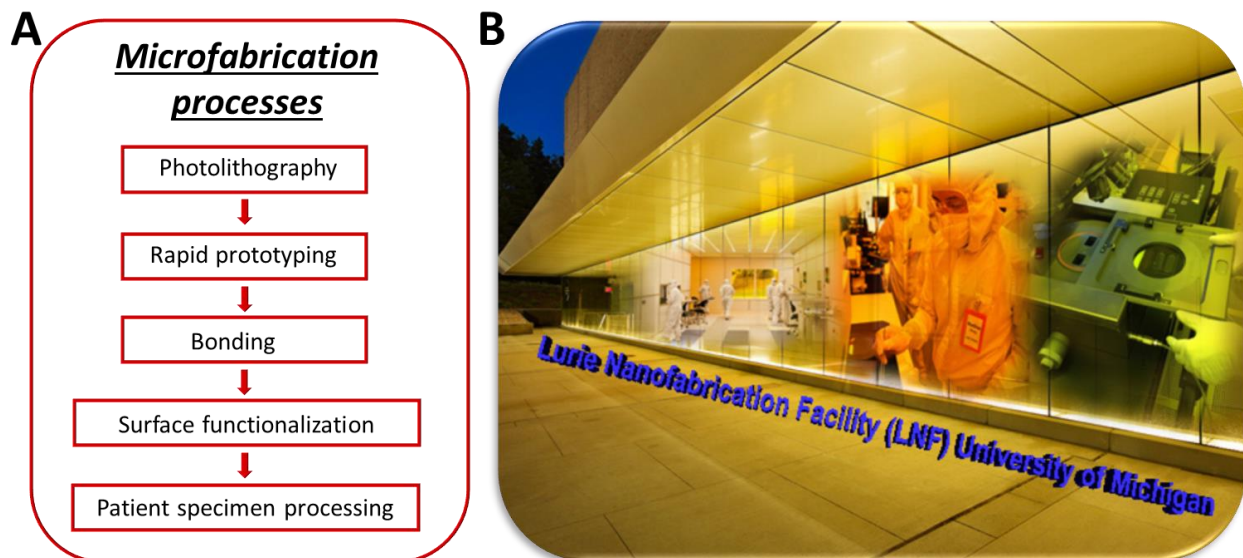


Figure 2-1: Microfabrication process. A) The flow chart of the microfabrication processes. B) The clean room facility available at Lurie Nanofabrication Facility at College of Engineering University of Michigan.

2.1.1 Computational analysis of the microposts

Finite element simulations were performed in COMSOL Multiphysics 4.2 (Comsol Inc.) with an inlet flow rate of 1 mL hr^{-1} on a portion of diamond shape of the CTC

Carpet Chip. A symmetry boundary condition was applied on the two similar boundaries flanking the posts. A wall (no slip) boundary condition was applied on the post outlines. The particle tracing plot was simulated with rigid particles 15 μm in size, with a condition of sticking to any encountered wall being applied.

2.1.2 Photolithography

Photolithography is a process by which an image is optically transferred from one surface to another, most commonly by the projection of light through a mask onto a photosensitive material such as photoresist. Photoresists are radiation sensitive materials that typically consist of a polymer resin, a radiation sensitizer, and a carrier solvent. Photoresist can be classified as either positive or negative based on their solubility following UV exposure. The solubility of exposed areas in positive resists increases, whereas in the negative photoresist the solubility is decreased.¹⁹⁰ Generally, a negative photoresist is strengthened by radiation exposure so the remaining pattern after being subject to a developer solution appears as the inverse of the opaque regions of the mask.

In our study, SU-8 100 (MicroChem Corp) was selected as a negative photoresist, and was used to prepare a mold with a final thickness of range 100 μm . The SU-8 was spin coated onto a silicon wafer at 500 rpm for 10 sec and then 2350 rpm for 60 sec. This was followed by two steps of soft baking, first at 65°C for 10 min and then 95°C for 1 hr, after which the coated wafer was exposed to UV light for 15 sec using a Karl Suss MA6 aligner. Post exposure baking was done first at 65°C for 3 min followed by 95°C for 10 min and the pattern was developed in SU-8 developer for 2 min, followed by rinsing with isopropyl alcohol for 2 min and hard baking at 150°C for 3 min.

The resulting thickness was confirmed to be within the range of 98-100 Å as determined using Dektak 6M Surface Profilometer. The steps involved in photolithography techniques for our study were shown in Figure 2-2.

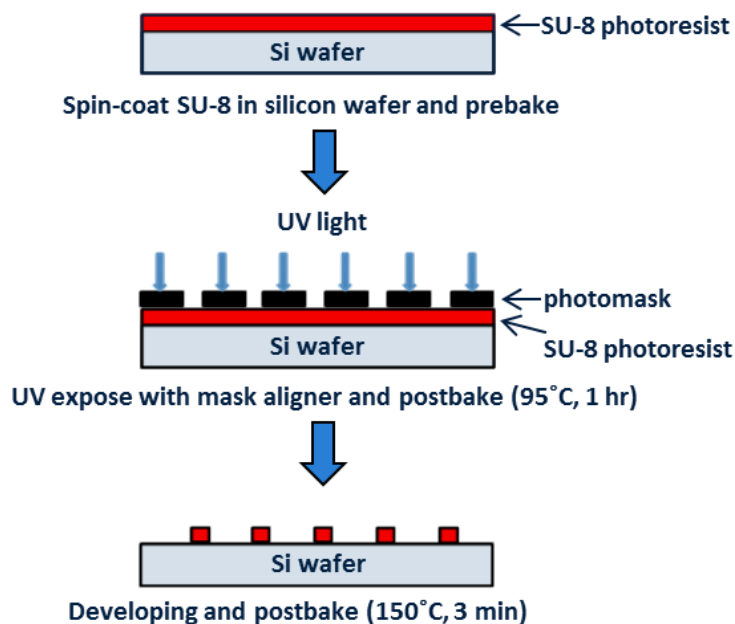


Figure 2-2: Photolithography process. A negative photoresist (SU-8) spin coated onto a silicon wafer followed by baking and exposure through a photomask, and developing to achieve the desired pattern.

2.1.3 Rapid prototyping

Rapid prototyping the microfabrication of the chambers can be done using transparent polymers such as, poly-dimethyl siloxane (PDMS) and poly-methyl methacrylate (PMMA).^{189, 191} PDMS is popular because it is not only optically transparent, but also allows for additional histochemical stains and markers to be applied post-enumeration, and is conducive to bright field imaging (currently a limitation in the silicon CTC Chip).^{189, 191} PDMS is a flexible elastomeric polymer that is an excellent material for microfluidic device fabrication. In order to produce an inexpensive, disposable, and high throughput point-of-care multiplex microfluidic chip, the current design is reproduced in PDMS elastomer, Sylgard® 184 (Dow Corning). Sylgard is a

two part resin system containing vinyl groups and hydrosiloxane groups. Mixing the two resin components together leads to a cross-linked network of dimethyl siloxane groups. Because this material is flexible, it can be unmolded (peeled) from the SU-8 master, leaving the master intact and ready to produce another device.

PDMS (mixed in a 10:1 ratio of PDMS base with curing agent, Sylgard® 184) was degassed in a desiccator for about 30 min, after which it was cast over the SU-8 mold, and degassed again for about 2 hr. Degassed PDMS was placed in an oven at 65°C overnight. The cured PDMS casting was released by peeling it away from the mold and fluidic ports were punched at the designated ends of the chamber to create inlet and outlet holes. These holes were later used for incorporating tubing inputs. The punched hole was slightly smaller than the outer diameter of the tubing being used, providing adequate sealing for typical fluidic pressures. The schematic of the rapid prototyping of PDMS devices and its bonding to glass slides is shown in Figure 2-3.

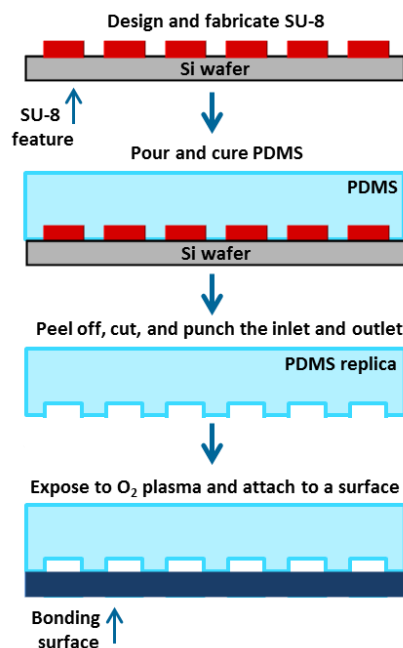


Figure 2-3: Rapid prototyping of PDMS devices. The silicon master mold is used to create PDMS molds, which are bonded to the substrate (glass) by plasma bonding.

2.1.4 Bonding, surface chemical modification and functionalization

One of the most useful properties of PDMS is that its surface can be chemically modified in order to obtain the interfacial properties of interest. The most reliable method to covalently functionalize PDMS is to expose it to oxygen plasma, whereby surface Si-CH₃ groups along the PDMS backbone are transformed into Si-OH groups by the reactive oxygen species in the plasma. These silane surfaces are easily transformed with alkoxy silanes to yield much different chemistry as shown in Figure 2-4.

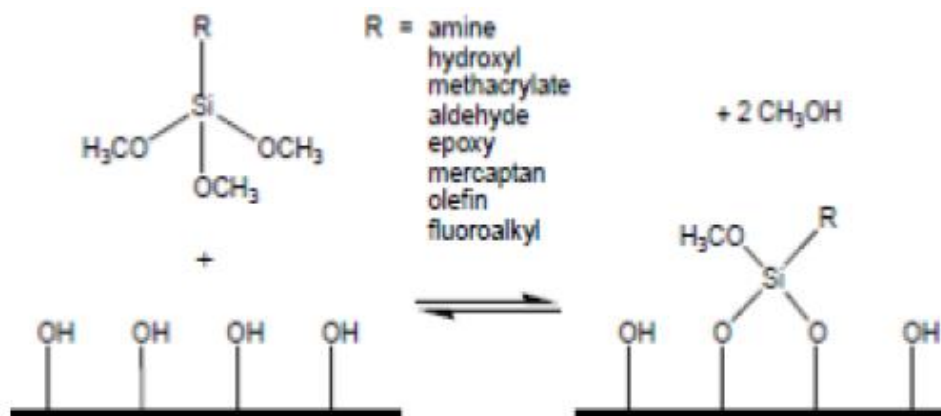


Figure 2-4: Silanization of plasma-exposed PDMS

PDMS replicas and glass slides were cleaned with oxygen plasma and then immediately placed in contact to bond the surfaces irreversibly. The PDMS slab was bonded with a glass substrate, post oxygen plasma treatment for oxidization the surfaces, and therefore for having a hydrophilic area, along with a 10 min baking at 80°C hot plate for having a stronger bonding (Figure 2-3).

The chemical modification and functionalization of the surface of the device was done immediately after the bonding as depicted. Initially, the surface of the device was modified with 4% (v/v) 3-mercaptopropyl trimethoxy silane (Gelest) in ethanol (1:25 ratio) for making the surfaces more hydrophilic, at room temperature (RT) for 1 hr. Then

it was treated with the coupling agent *N*-gamma-Maleimidobutyryloxy-Succinimide (GMBS) (Pierce) in ethanol (1:357 ratio) for 30 min, resulting in GMBS attachment to the microposts as a linker. Next, the device was treated with 100 $\mu\text{g mL}^{-1}$ Neutravidin (Invitrogen) in phosphate buffered saline (PBS) 1:10 ratio) at RT, leading to immobilization onto GMBS, and then flushed with PBS to remove excess of avadin. The functionalization process was checked with Biotin fluorescence labeled at a concentration of 10 $\mu\text{g mL}^{-1}$ in PBS with 1% (w/v) bovine serum albumin (BSA) with a positive control device, the negative one does not coated with Avadin, hence it doesn't show the fluorescence (Figure 2-5).

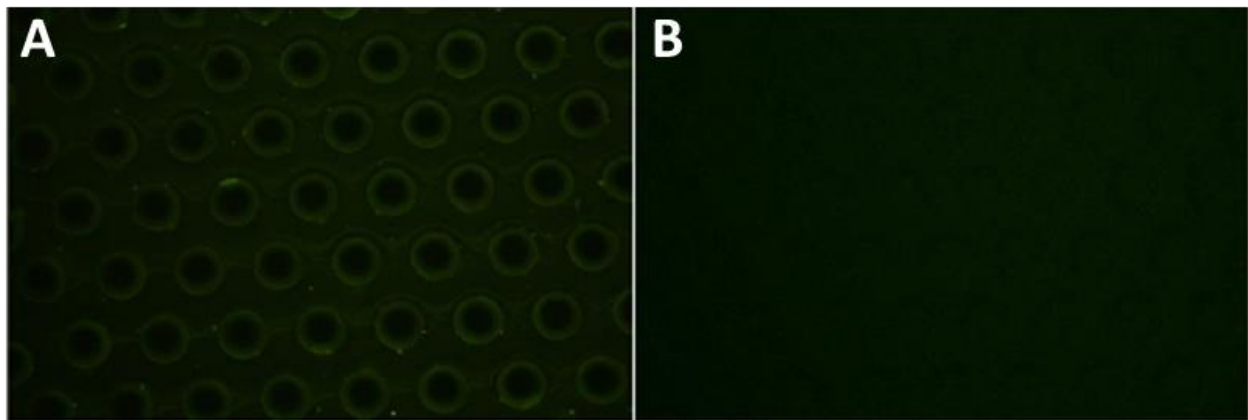


Figure 2-5: Biotinylated functionalized PDMS micropost chamber. Representative photomicrograph showing FITC conjugated biotinylated functionalized PDMS micropost chamber with (A) and without (B) inclusion of Avidin coating.

Finally, biotin-conjugated anti-Epithelial cell adhesion molecule (EpCAM) (RnD Systems) antibodies or anti-CD133 (Miltenyi Biotec) antibodies at a concentration of 20 $\mu\text{g mL}^{-1}$ in PBS with 1% (w/v) Bovine Serum Albumin (BSA) (Sigma) was allowed to react for 30 min for each inlet and outlet before washing with PBS. The device was immediately used for capturing CTCs or cancer cells (Figure 2-6).

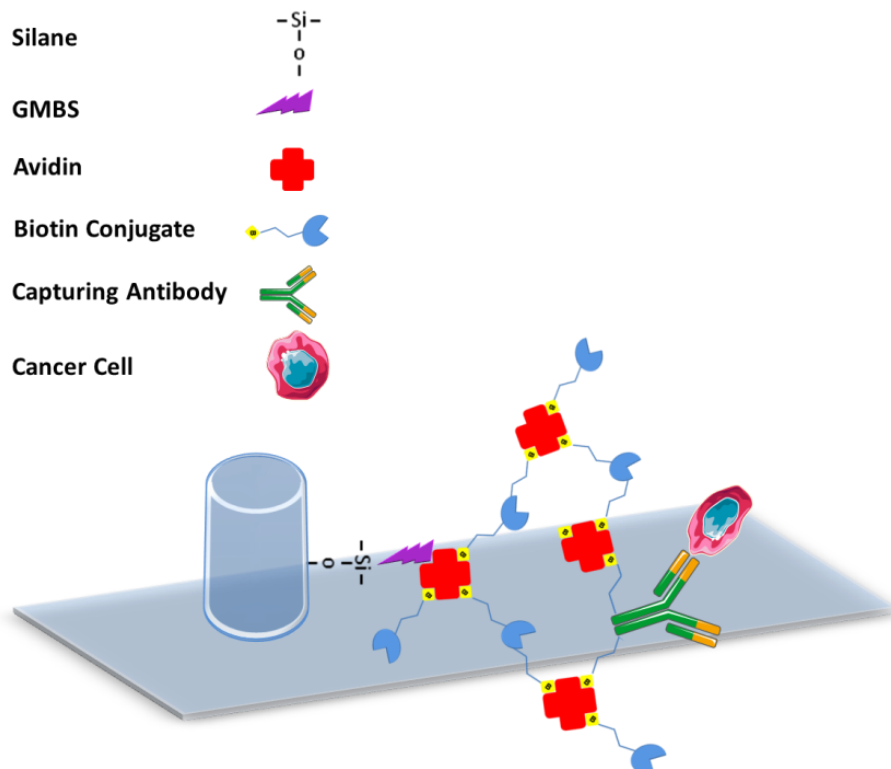


Figure 2-6: PDMS surface modification and functionalization. Antibodies can be immobilized on PDMS by silanization.

2.2 Cell culture

Six different human cancer cell lines, colon adenocarcinoma cell line (HT-29), pancreatic cell line (Panc-1), prostate cancer cell line (PC-3), and breast cancer cell lines (MCF-7, SUM-159, and Hs-578T) were obtained from ATCC. Capan-1 cancer cell line was obtained from Dr. Howard Crawford's lab at University of Michigan. Human non-small lung cancer cell lines H1650, PC-9, A549, HCC827, and H1975 were obtained from the Beer and Hassan laboratories at the University of Michigan.

The HT-29 cells were cultured in McCoy's 5A Medium (ATCC), PC-3, SUM-159, and Hs-578T cells in low-glucose Dulbecco's modified Eagle's-F12 medium (DMEM-F12) (Invitrogen), MCF-7 and Panc-1 cells in DMEM+++ medium (Invitrogen), Capan-1 cells in IMDM medium (HyClone), H1650, PC-9, HCC827, H1975, and A549 cells in

RPMI 1640 medium (Invitrogen). All supplemented with 10% Fetal Bovine Serum (FBS) (Invitrogen) and 1% penicillin-streptomycin (Pen-Strep) (Sigma) and maintained in an incubator at 37°C in 5% CO₂ and 95% relative humidity. The cells were cultured in sterile 25 or 75 cm² flasks (Corning) and media replaced every 48 hr. Upon reaching >75-80% confluence, the cells were harvested with 0.05% Trypsin-EDTA (Invitrogen). Prior to characterization experiments, cells were labeled with green CellTracker fluorescent dye (Invitrogen).

2.2.1 CellTracker dye protocol

Sub-confluent monolayers of cells were detached using 0.05% Trypsin-EDTA solution and washed in standard media, followed by centrifugation at 1000 rpm for 5 min. Cell pellet was washed two times with phosphate buffered saline (PBS) and resuspended with 5 mL of serum free media plus 5 µL dye (green CellTracker) followed by incubation for 30 min at 37°C. The cells were washed with PBS and incubated in complete media at 37°C for 30 min. After washing the pellet with PBS, 1000 cells mL⁻¹ were prepared by serial dilution. The density of cell suspensions were counted using a hemocytometer and spiked into PBS or healthy control (HC) blood for analysis of CTCs using CTC Carpet Chip or Labyrinth.

2.2.2 Primary human pancreatic cancer and cancer-associated fibroblast (CAF) cell lines

Primary human pancreatic cancer cell lines (UM18 and cancer associated fibroblast (CAF)) were generated from primary PDAC patient in Dr. Diane Simeone's laboratory at the University of Michigan hospital under Institutional Review Board (IRB) guidelines.¹⁹² Both cell lines were cultured in RPMI 1640 supplemented with 10% heat-

inactivated FBS, 2 mmol L⁻¹ L-glutamin, 100 units mL⁻¹ penicillin, 100 µg mL⁻¹ streptomycin (Invitrogen) in 95% air and 5% CO₂ at 37°C.

2.2.3 Patient-derived CTC expansion

Prior seeding the recovered CTCs from NSCLC patient samples using Labyrinth, the 48-well plates were coated with 100 µl of Matrigel (Corning), 51.6 µl of Collagen I (Invitrogen), and 48.4 µl of HEPES (Invitrogen) to make a 3D culture models. For making a 2D culture models, the well plates were coated with 5 µg of Fibrinectin (Corning) diluted in distilled water (Invitrogen). The well plates were incubated for 1 hr at RT and then washed with distilled water prior the culture.

After CTC enrichment, small portion of the samples were stained for CTC counts. The rest of the samples were seeded on a 3D coated 48-well plate using media #1 for 3-4 weeks under normoxic conditions (5% CO₂) and 95% relative humidity at 37°C. Media #1 contains 200 µl of conditioned media (from pancreatic cancer-associated-fibroblast 19 (CAF-19)) supplemented with 10% FBS, 1% Pen-Strep, 8 µl of human platelet lysates (hPL-MAX) (Mill Creek), and 0.06 µl of insulin (Sigma).

To be able to passage the cells from the 3D culture, 10 µl of collagenase type I (Invitrogen) diluted into 400 µl of HBSS (Invitrogen) and were added to the well plates to dissolve the Matrigel. The well plates were incubated 3-4 hr in the incubator, following centrifugation at 1000 rpm for 10 min. The cell pellet was resuspended with media #2 and then were seeded into a 2D culture condition for another 3-4 weeks. Media #2 contains 200 µl of conditioned media from CAF-19, 10% FBS, 1% Pen-Strep, and 8 µl of hPL-GOLD (Mill Creek)). Upon the cell confluency on 2D culture, the cells were passaged using 0.25% Trypsin-EDTA (Invitrogen). The cell pellet was resuspended with

media #2 and seeded into a 2D culture model. A small portion of this sample was used for the CTC counts.

2.3 Western blot

Whole cell lysates were prepared from PC-3 and HT-29 cell lines. For the Western blotting analysis, equal amount of proteins were separated using SDS-PAGE (RnD Systems) and transferred to a PVDF membrane (RnD Systems) and then incubated with anti-EpCAM and anti-CD133 antibodies. Proteins were visualized using horseradish peroxide-conjugated secondary antibodies followed by exposure of immunoreactive bands to photographic film. Glyceraldehyde 3-Phosphate Dehydrogenase (GAPDH) (Santa Cruz) was used as an internal loading control.

2.4 Flow cytometry analysis (FACS)

After harvesting the cell lines by trypsinization, cells were washed with PBS and the pellet resuspended with 4% paraformaldehyde (PFA) (Pierce), and 0.2% Triton X-100 (Sigma), followed by 30 min incubation time for each step. Next, the cells were washed with PBS and blocked with 3% BSA plus 2% goat serum (Invitrogen), followed by 30 min incubation time. Then cells were divided into unstained, isotype, and stained groups. The specific antibodies, anti-EpCAM and anti-CD133 were added followed by 1 hr incubation time. After PBS washing, the pellet was resuspended with secondary antibodies followed by 1 hr incubation in dark, and then PBS wash. All steps were followed by centrifuge at 2500 rpm for 4 min.

2.5 Capture efficiency in single CTC Carpet Chip

Four different cancer cell lines with different EpCAM expression levels, HT-29, Panc-1, PC-3, and Hs-578T, and a CD133 positive cell line, Capan-1, were fluorescently-labeled with green CellTracker (section 2.2.1). To determine the percentage of cells captured on a functionalized CTC Carpet Chip, coated with either anti-EpCAM (for EpCAM expression cell lines) or anti-CD133 (for CD133 expression cell line), 1000 cells from each of the fluorescently-labeled cancer cell lines were spiked into whole blood collected from HCs and flowed through the microfluidic device at a constant flow rate (1 mL hr^{-1}). Then cells were fixed and permeabilized on the chip by using Cytofix/Cytoperm (BD Bioscience) followed by staining with DAPI (4',6-diamidino-2-phenylindole) (Invitrogen) to identify DNA content. Capture efficiency was calculated as the percentage of captured cells on the device divided by the total number of cells flowed through the chip. Captured cancer cells were identified and enumerated by scanning the entire micropost chamber of the device using a Nikon Eclipse Ti fluorescence microscope.

2.6 Capture efficiency in dual CTC Carpet Chip

In order to facilitate separating circulating epithelial (EpCAM-expressing) and EMT-like (CD133-expressing) cells in different devices in sequential order from the same sample, two separate CTC Carpet Chips were connected to each other using a 2-inch piece of connective tubing (Fisherbrand™ Tygon S3™ E-3603 Flexible Tubings). The first chip was coated with anti-EpCAM and the second one with anti-CD133. Blood sample was then processed through each chip in succession. After this step, the chips

were disconnected from one another, and washed with PBS (10 mL hr^{-1}) for the immunofluorescence staining process.

2.7 Characterization experiments for Labyrinth (Cell lines)

The Labyrinth device was primed with 1% Pluronic acid solution (Sigma) at a flow rate of $100 \text{ } \mu\text{L min}^{-1}$ for 10 min followed by 10 min incubation time to prevent cell adhesion to channel walls. To demonstrate cell specificity in the Labyrinth, same number of pre-labeled cancer cells (from cell lines) and DAPI-labeled WBCs ($1000 \text{ cells mL}^{-1}$) were mixed and spiked into PBS and flowed through the device at different flow rates ranging from, $1500\text{-}3000 \text{ } \mu\text{L min}^{-1}$. Products from outlet #2 were collected after 1.5 min flow stabilization for cell counting to calculate the recovery and percent of depleted WBCs. Images were taken using a fluorescence microscope under FITC and DAPI filters to categorize and document cancer cells in isolation from other blood components.

2.8 Pancreatic cancer patient CTC capture using CTC Carpet Chip and Immunofluorescence staining (IF)

This study was approved by the institutional review board (IRB) of the University of Michigan. 1 mL of whole blood from each pancreatic cancer patient was processed through two CTC Carpet Chips connected in series at the designated flow rate (1 mL hr^{-1}), followed by fixation and permeabilization with 4% PFA and 0.2% Triton X-100 respectively, followed by blocking with 3% BSA plus 2% goat serum.

In order to identify and characterize sub-populations of pancreatic CTCs and distinguish them from other blood cells, we used the following criteria: cells that were captured on the anti-EpCAM coated chip and stained positive for pan-cytokeratin

(PanCK) (Biorad), negative for CD45 (Biorad), and positive for cell nucleus staining (DAPI) were characterized as epithelial CTCs (EpCs); and cells that were captured on the anti-CD133 coated chip and stained positive for Vimentin (BD Bioscience), negative for CD45, and positive for DAPI were characterized as EMT-like CTCs (EMTCs.)¹ Alexa Fluor 488-, 546-, 647-conjugated secondary antibodies (Invitrogen) were applied in order to detect CD45, PanCK, and Vimentin respectively.

2.9 Pancreatic and NSCLC cancer patient CTC isolation using Labyrinth and Immunofluorescence staining (IF)

The experimental protocol was approved by the Ethics (Institutional Review Board) and Scientific Review Committees of the University of Michigan and all patients and healthy blood donors gave their informed consent to participate in the study. Briefly, blood samples (~7-10 mL) from metastatic pancreatic cancer and (~20 mL) from NSCLC patients were collected in EDTA tubes and processed through the Labyrinth within 2 hr of collection. RBCs in the blood samples were removed using density separation with 6% dextran (Spectrum) prior to Labyrinth processing. The blood sample mixed with dextran solution was kept at RT for 1-1.5 hr to settle the RBCs driven by density difference. The supernatant, which included all whole blood components except RBCs, was carefully removed and diluted with PBS (1:3). The diluted dextran supernatant was then processed through the Labyrinth at a flow rate of 2000 $\mu\text{L min}^{-1}$ for pancreatic cancer patient samples and 2500 $\mu\text{L min}^{-1}$ for NSCLC patient samples. The product from outlet #2 was collected after stabilization.

The product from outlet #2 was processed using a Thermo Scientific™ Cytospin Cytocentrifuge. A poly-lysine coated slide was placed into the cytospin funnel and 250

μL of sample was added to each cytopsin funnel and cytrocentrifuged at a speed of 800 rpm for 10 min. Samples were fixed on the cytoslides using 4% PFA and cytrocentrifuged at the same conditions as described above. Slide samples were permeabilized by applying 0.2% Triton X-100 for 3 min. Slides were then washed with PBS (times 3) for 5 min and blocked using 10% donkey serum for 30 min at RT.

For the pancreatic cancer CTC enumeration, slides were incubated with the panel of primary antibodies including rabbit anti-human Zeb1 (Santa Cruz), mouse anti-human anti-PanCK (IgG1) (Biolegend), mouse anti-human anti-CK19 (IgG2a) (Santa Cruz), and rat anti-human CD45 (IgG2b) (Santa cruz) overnight at 4°C. The next day, slides were washed with PBS (times 3) for 5 min and then incubated with the secondary antibodies (Alexa Fluor 488, 549, and 647) in dark for 1.5 hr at RT.

For CTC enumeration of NSCLC patient samples, slides were incubated with the panel of primary antibodies including (mouse anti-human CD45 (IgG2a) (Biorad), mouse anti-human anti-PanCK (IgG1) (Biorad), anti-human anti-EpCAM, biotinlated (goat IgG) (R&D System), and rabbit anti-human anti-Vimentin (Abcam) overnight at 4°C, followed by PBS wash (times 3) for 5 min the following day. Slides were incubated in dark with secondary antibodies (Alexa Fluor 488, 549, 750, and 647) for 1.5 hr at RT. Finally, slides were washed with PBS (times 3) for 5 min and mounted using Prolong Gold Antifade Mountant with DAPI (Invitrogen). The immunofluorescently stained slides were imaged using a fluorescence microscope for the CTC enumeration.

2.10 RNA extraction and quantitative reverse transcription polymerase chain reaction (qRT-PCR) analysis

Isolated CTCs within the device were incubated at 42°C for 30 min with extraction buffer of Arcturus PicoPure kit (Invitrogen) to lyse the cells. Then RNase free water (Invitrogen) was passed through the chip to collect the cell lysate. Total RNA was then prepared from the CTC lysate using the Arcturus PicoPure kit and was subjected to a reverse transcription reaction followed by 18 cycles of pre-amplification of cDNAs of 96 cancer-related genes (**Error! Reference source not found.**) using the pooled TaqMan Gene Expression Assays and Cell-to-CT Ambion Kit (Invitrogen). Finally, the gene expression pattern of pre-amplified cDNAs was determined using TaqMan Gene Expression Assays for 96 genes and the BioMark HD qPCR platform (Fluidigm) (35 cycles) (Figure 2-7).

Table 2-1: Table of 96 genes analyzed by TaqMan Gene Expression Assays

96 genes analyzed by TaqMan Gene Expression Assays							
AKT1	BRAF	CDH2	ERCC1	KLF4	MCL1	PDX1	SPON2
ALDH1A1	BRCA1	cMYC	ESR1	K-Ras	MET	PGR	TGFB1
ALDH1a2	CCDC80	COL1a2	GAPDH	KRT18	MGP	PIK3CA	TIMP1
ALDH1a3	CCND1	COL3a1	GEMIN2	KRT19	MKI67	PON1	TIMP2
ALK	CD133	CTNNB1	GLi1	KRT20	MMP2	POU5F1	TIMP3
ANXA2	CD14	CXCR1	HPRT1	KRT5	MMP9	PTEN	TP53
AR	CD24	CXCR4	IGFBP5	KRT7	MS4A1	RAB7A	TTF-1
ATDC	CD3D	DCN	IL6	KRT8	NANOG	RB1	TWIST1
ATL1	CD44	EGFR	IL6R	LGALS3	NES	Shh	Vimentin
BAX	CD45	EMP2	IL6ST	LGALS3BP	NKX2-1	SNAI1	WNT2
BCL2	CD90	EPCAM	IL8	MAPK	p63	SNAI2	ZEB1
BMi1	CDH1	ERBB2	ITGAM	MCAM	PCNA	SPARC	ZEB2



Figure 2-7: BioMark HD Real-Time PCR system.

2.11 Immunohistochemistry (IHC)

A gastrointestinal pathologist reviewed each patient's hematoxylin & eosin (H&E) stained resection specimen and identified a representative section of formalin-fixed, paraffin-embedded tumor and normal tissue. The unstained 5 μ m-thick tissue section was reacted with anti-BMi1 (Cell Signaling), anti-MKi67 (Cell Marque), anti-PIK3CA (Abcam), anti-TP53 (Cell Marque), MCAM (Abcam), and CD133 (Miltenyi Biotec) antibodies using immunohistochemistry (IHC) technique to determine levels of tumoral protein expression of BMi1, MKi67, PIK3CA, TP53, MCAM, and CD133. The staining intensity and percentage of positive cells out of total tumor cells were graded by a pancreatic pathologist who was blinded to patients' outcomes. The intensity of IHC staining is graded on a scale of 0 to 3, where 0 is no staining, 1 is weak, 2 is moderate, and 3 is strong staining.

2.12 Fluorescence in situ hybridization (FISH) analysis

Interphase FISH was carried out as previously described by other groups.^{193, 194} Briefly, bacterial artificial chromosomes (BACs) were obtained from the BACPAC Resource Center (Oakland) for the preparation of probes.¹⁹⁵ For detection of gene rearrangements, deletion or amplification, the following probes were used: for *ROS1*, RP11-1110L9 (5' to *ROS1*) and RP11-605K7 (3' to *ROS1*), for *RET*, RP11-124O11 (5' to *RET*) and RP11-718J13 (3' to *RET*), for *EGFR*, RP11-23F4 (5' to *EGFR*) and RP11-56P1 (3' to *EGFR*), and for *ALK*, RP11-993C21 (5' to *ALK*) and RP11-984I21 (3' to *ALK*). The integrity and accurate localization of all probes were verified by hybridization to metaphase spreads prepared from normal peripheral lymphocytes. Slides were examined using a Zeiss Axioplan 2 microscope equipped with image processing software ISIS (Metasystems). FISH signals were scored manually under 100X oil immersion in morphologically intact and non-overlapping nuclei and greater than 100 cells from each slide were recorded.

2.13 In Vivo tumorigenicity assays

Six-week old NOD/SCID mice were housed under pathogen-free condition at the University of Michigan Animal Care center. Mice were anesthetized with intraperitoneal injection of xylazine (9 mg kg⁻¹) and ketamine (100 mg kg⁻¹). A median laparotomy was performed, and 10⁵ primary human pancreatic cells (UM18) infected with a lentivirus encoding GFP-luciferase (University of Michigan Vector Core) alone or with an equal number of DsRed-labeled CAF cells were injected into the pancreatic tail using a 30-gauge needle (n=5 per group). Six to 8 weeks following cell injections, mice were

ethanized with CO₂ inhalation. Blood was collected for enumeration analysis of circulating GFP-labeled tumor cells and DsRed-labeled CAF.

2.14 RBC lysis buffer

RBC lysis buffer (Qiagen) was utilized for RBCs removal from the products of either single or double Labyrinth. Recovered CTCs from outlet #2 of Labyrinth were incubated with this buffer (1:3) for 2 min on ice following the centrifugation step. A small portion of this solution was used for CTC enumeration, and the rest was used for the culture.

2.15 Drug testing

Different NSCLC cell lines were plated at a seeding density of 200, 400, and 2000 cells well⁻¹ on either 96-well or 384-well plates. Each drug concentration (0, 100, 500, 1000, 5000, and 10000 nM) had wells in triplicates. Cells were incubated with various drugs for 72 hr. After treatment, different cell viability assay kits including; CellTiter 96® Aqueous One Solution Cell Proliferation Assay (Promega), CellTiter-Glo luminescent cell viability assay (2D kit) (Promega), and CellTiter-Glo 3D cell viability assay (3D kit) (Promega) were used for 30 min, 1hr, 1.5 hr, and 2 hr to assess half maximal inhibitory concentration (IC₅₀) values of tyrosine kinase inhibitors (TKIs) along with relevant sensitive or resistant NSCLC cell lines. Luminescent signals were measured with a Biotek-Synergy Neo-Plate Reader (BioTek Instruments, Winooski, VT) and the optimal duration of incubation was determined. IC₅₀ values were calculated with nonlinear regression model using Prism Graphpad.

Various drugs including, Erlotinib and Crizotinib (Sigma), Ceritinib, Afatinib, and Osimertinib (Selleckchem) were reconstituted in DMSO, and Cetuximab (BioVision) was reconstituted in PBS ($1\text{ }\mu\text{g }\mu\text{L}^{-1}$) for *in vitro* drug testing.

2.16 Statistical analysis

For studying CTCs in pancreatic cancer using CTC Carpet Chip, all results present as mean \pm standard deviation. Unpaired t-tests (two-tailed) were used to compare the differences between total CTCs of patient samples (n=35) vs. healthy controls (n=9). Paired t-tests (two-tailed) were used to compare the differences between EpCs and EMTCs from patient samples (n=35). Unpaired t-tests (two-tailed) were used to evaluate the effect of stage, resection, tumor size, lymph node involvement, and metastasis on EpCs and EMTCs levels (n=35). Statistical significance was defined as a two-sided $p < 0.05$.

For the RNA expression analysis, non-detect values were replaced by a pseudo cycle number of 40 and in the analyzed samples typically out of 96 genes, around 50% of them showed positive data. Also a cut off $n > 2$ (greater than 2 patients displaying gene expression in each group for each gene) was applied when genes in different groups were compared to each other, and 75 of 96 genes met this criterion. GAPDH was used as an internal reference to normalize cycle threshold (Ct) values for the genes of interest by subtracting each gene expression value by GAPDH to generate a $-\Delta\text{Ct}$. Median fold changes were generated by dividing the median gene expression ($2^{-\Delta\text{Ct}}$) of group A by that of group B. Wilcoxon signed-rank test was used in RNA expression for paired samples (n=17). Mann-Whitney test was used to quantify differences in RNA expression for non-paired samples using the average $-\Delta\text{Ct}$ value across both sample

chips (n=17). Analyses were conducted using GraphPad Prism, Python, R software environment, and iPathwayGuide (Advaita). P-values were not adjusted for multiple testing due to the small number of patient samples. The median expressions of genes ($2^{-\Delta Ct}$) across all patients were used as cut-off points for Kaplan Meier graphs. Log-rank (Mantel-Cox) tests were used to analyze Kaplan-Meier overall survival (OS) and progression free survival (PFS) graphs in all patient CTCs samples (n=17). P-values threshold of 0.05 were used in the iPathwayGuide analysis.

For studying the CTCs in pancreatic cancer using Labyrinth, paired t-test was used to analyze the recovered CTCs from patient samples (n=141) in treatment naïve and treatment groups.

For studying CTCs in NSCLC cancer using Labyrinth, Mann-Whitney test (two-tailed) was used to compare the differences between total numbers of CTCs in patient samples (n=21) vs. healthy controls (n=3). Unpaired t-tests (two-tailed) were used to compare EpCAM+ and EpCAM- CTCs, Vimentin+ and Vimentin- CTCs, as well as single CTC versus CTC-clusters. The IC50 values were calculated with nonlinear regression model using Prism Graphpad. Results are shown as mean value with 95% confidence intervals calculated based on results triplicate wells. All drug testing experiments were repeated at least three times.

3 Results

3.1 Different design configurations of immunoaffinity microfluidic devices

As mentioned earlier, there are no unique technologies to enumerate CTCs from human pancreatic cancer in clinic. Therefore, to determine the highest CTC capture efficiency different micropost geometries and arrangements of the arrays and other parameters were explored in the process of optimization of the CTC Carpet Chip including, CTC Original, Split, Modified, Rotated, and Carpet Chip.

The Split and Modified Chips were different versions of the Original CTC Chip with some changes on the outliers to make them more specific and sensitive for capturing purpose. All had pattern of repetition of 10×10 arrays of $100 \mu\text{m}$ posts. The modifications were shown in red arrows (Figure 3-1).

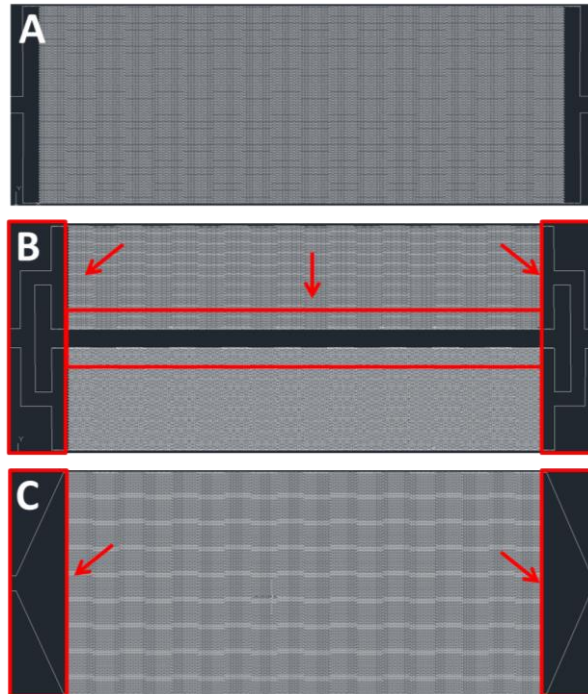


Figure 3-1: AutoCAD design of different version of the Original CTC Chip. A) Original, B) Split, C) Modified. The modification in the Split and the Modified CTC Chip were shown with red arrows.

In the Rotated device, the post arrays were rotated 10° relative to the previous array until reaching a total rotation of 180° and then decreasing rotation from 180° to 0° for the subsequent row (Figure 3-2B). CTC Carpet Chip is based on an 18° rotation of hexagonal arrays of $100\ \mu\text{m}$ posts (Figure 3-2C).

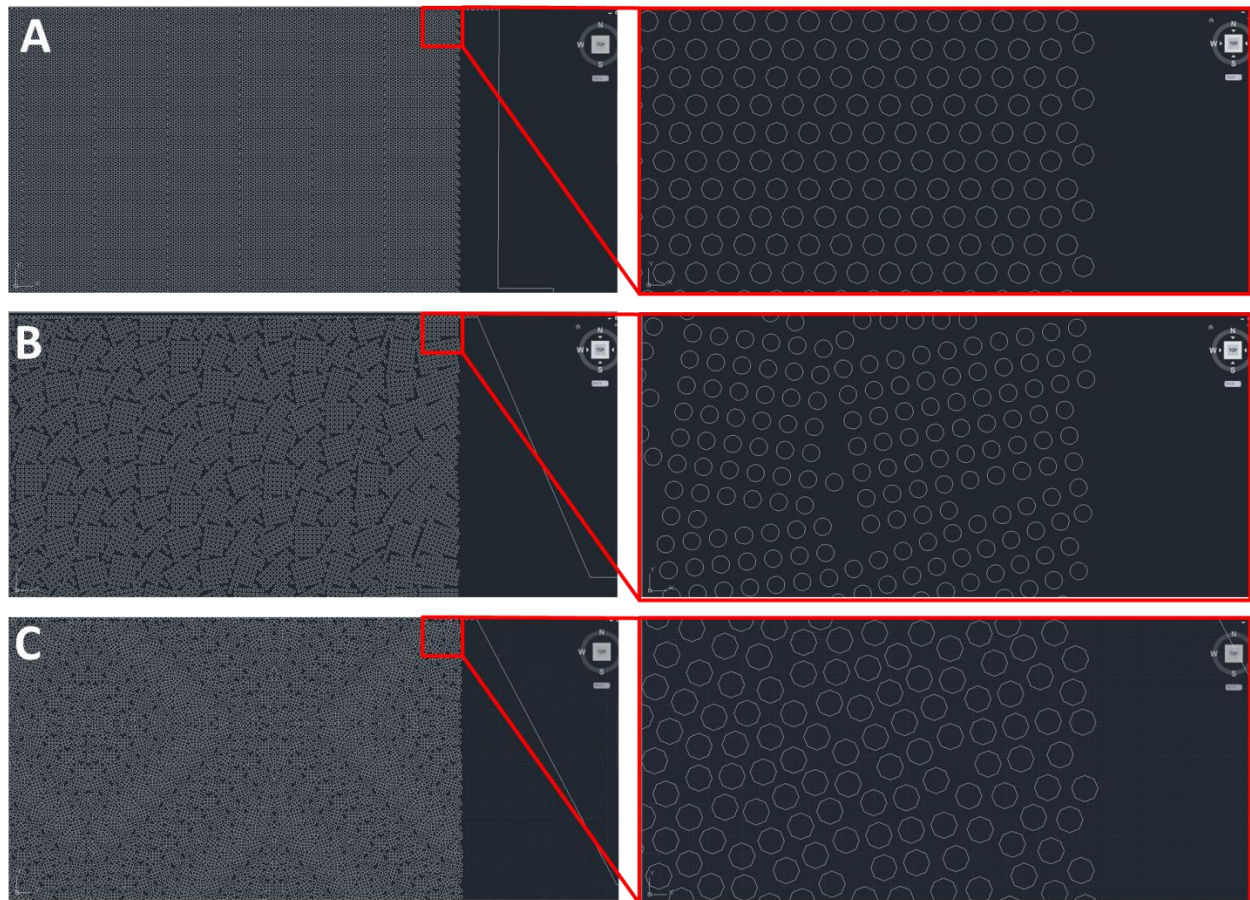


Figure 3-2: AutoCAD design of different configurations of the CTC Chip. A) Original, Split, Modified, B) Rotated, and C) Carpet.

Among all other CTC Chips, CTC Carpet Chip showed the highest % capture efficiency of spiked pre-labeled PC-3 cell line into buffer/blood at $1\ \text{mL hr}^{-1}$ as well as the purity among the other tested CTC Chips (Figure 3-3). The summary of the comparison between different devices is mentioned in Table 3-1. Different design configurations are explained in details in appendix section (9.1).

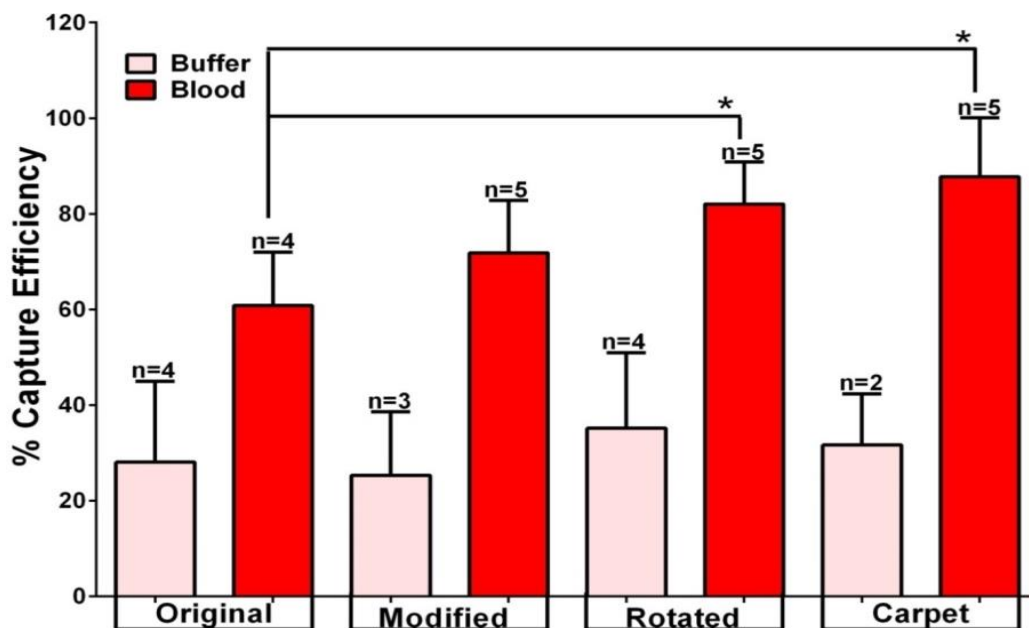


Figure 3-3: % Capture efficiencies among different configuration of the CTC Chip. % Capture efficiencies of EpCAM with pre-labeled cancer cells (PC-3) spiked into buffer and blood in 4 different CTC Chip, including Original, Modified, Rotated, and CTC Carpet Chip. Carpet CTC Chip showed the highest capture efficiency with PC-3 spiked into blood (87.73%) compared to the other CTC-Chips.

Table 3-1: Comparison between different microfluidic devices, including, Original, Modified, Rotated, and Carpet.

Microfluidic Devices	Array	Rotation	Capture efficiency in Buffer (%)	Capture efficiency in Blood (%)
Original	10 × 10	-	25.2	75.2
Modified	10 × 10	-	25.3	71.9
Rotated	10 × 10	10°	35.1	82
Carpet	8 × 8	18°	31.6	87.7

3.1.1 General optimization of the microfluidic CTC chip

3.1.1.1 Different confluency of cell lines

The effects of % cell confluency (40-50%, 70-80%, and 90-95%) on the EpCAM capture efficiencies were analyzed with HT-29 cell line with Original, Modified, and Rotated CTC Chips. The results showed the highest % capture efficiencies in the 70-80% cell's confluency group in buffer and blood samples among different devices (Figure 3-4).

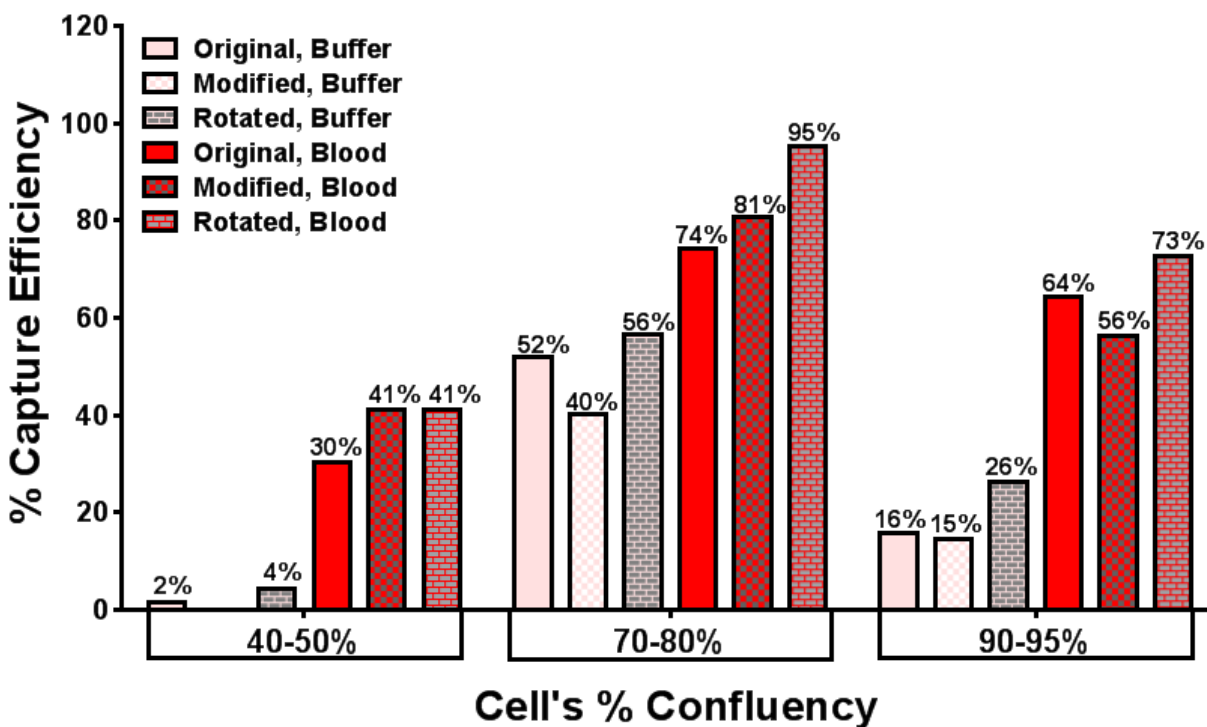


Figure 3-4: The effect of different cell %confluency of HT-29 cell line on the capture efficiencies of EpCAM. The 70-80% cell's confluency group showed the highest % capture efficiencies among the other groups.

3.1.1.2 Different blocking agent

In terms of increasing sensitivity as well as specificity using CTC Carpet Chip, different blocking reagents with different flow rates using MCF-7 cell lines were conducted. Different percentages of BSA alone or with the combination of different percentages of goat serum were used as a blocking reagent. The results in Figure 3-5 indicated that 3% BSA with 10 mL hr⁻¹ flow rates had the highest % purity (48.5%) among the other parameters with 71.7% of capture efficiency.

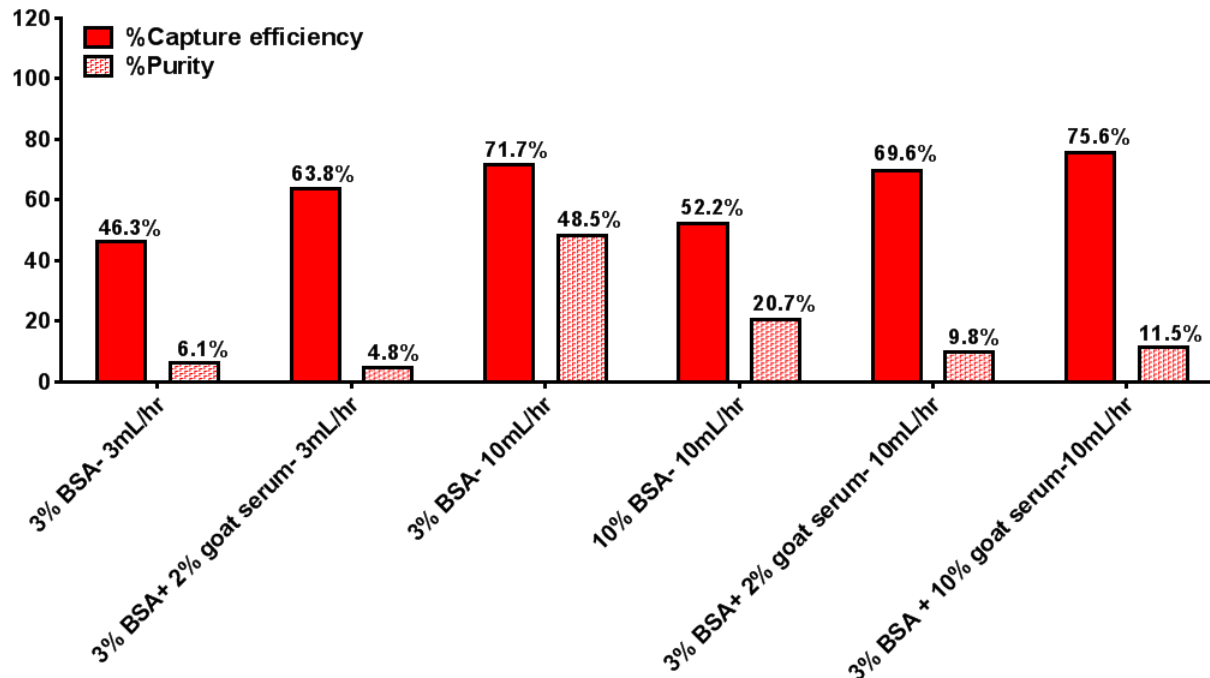


Figure 3-5: The effect of different blocking reagents on the capture efficiencies of EpCAM. BSA alone or with the combination of different percentages of goat serum with MCF7 cell line at different flow rates. 3% BSA at 10 mL hr⁻¹ flow rate had the highest sensitivity and specificity among the other parameters.

3.1.1.3 Forward vs. backward PBS washing

To be able to increase % purity, the effect of forward (from inlet to outlet) and backward (from outlet to inlet) PBS wash were checked within different CTC Chips (Original, Rotated, and Carpet) using HT-29 cell line. Backward wash had higher % purity in CTC Carpet Chip (76.4%) among the other parameters (Figure 3-6).

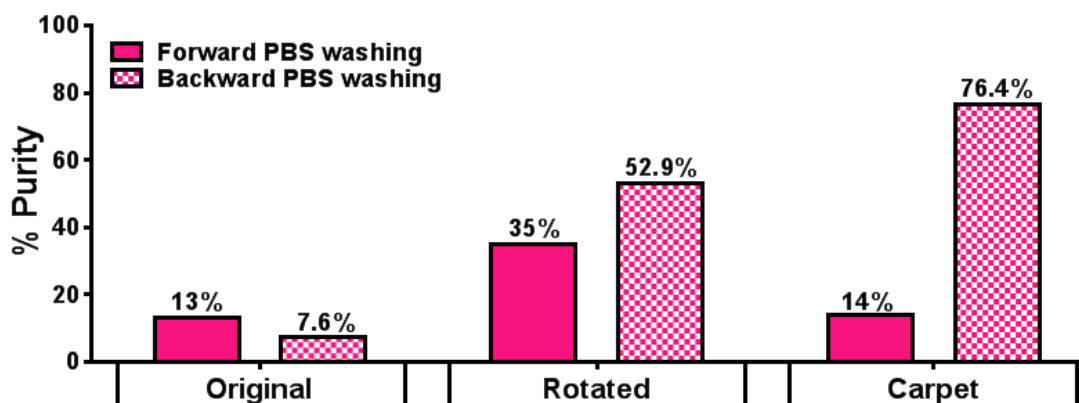


Figure 3-6: The effect of backward and forward PBS wash on the % purity.

3.2 CTC Carpet microfluidic Chip technology

CTC Carpet Chip has around 80,000 microposts and the overall size of the microfluidic device is 44.6 mm × 16.9 mm. The design of CTC Carpet Chip and representative SEM images of the microposts are shown (Figure 3-7A). The master mold of the Carpet Chip is shown in Figure 3-7B.

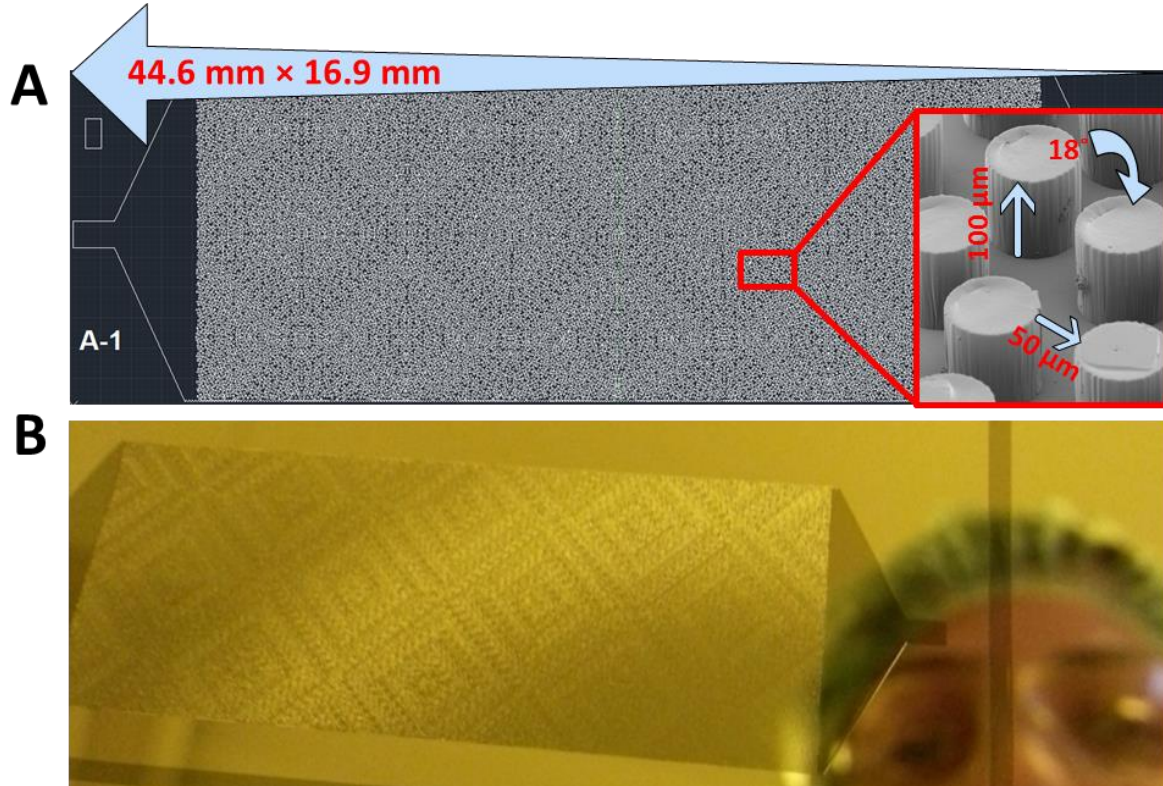


Figure 3-7: Schematic representation of CTC Carpet Chip. A) CTC Carpet Chip designed by AutoCAD software based on an 18° rotation of hexagonal arrays of 100 μm posts. It has around 80,000 post patterns with dimension of 100 μm × 100 μm, the distance between each post is 50 μm in which the posts are distributed in a way to have lateral flow. The overall size of the microfluidic device is 44.6 mm × 16.9 mm. The red box is showing the SEM image of some posts in the CTC Carpet Chip. B) The CTC Carpet Chip master mold.

Velocity magnitude profile and the particle tracing plot on a portion of the diamond shape of the CTC Carpet Chip are shown in Figure 3-8. Cell trajectories (blue lines) are based on particle tracing and the end position of the cells (15 μm rigid particles) is shown by red dots (Figure 3-8B). The simulations clearly had shown the

lateral distribution of fluid around the Carpet design as well as effective cell post interactions.

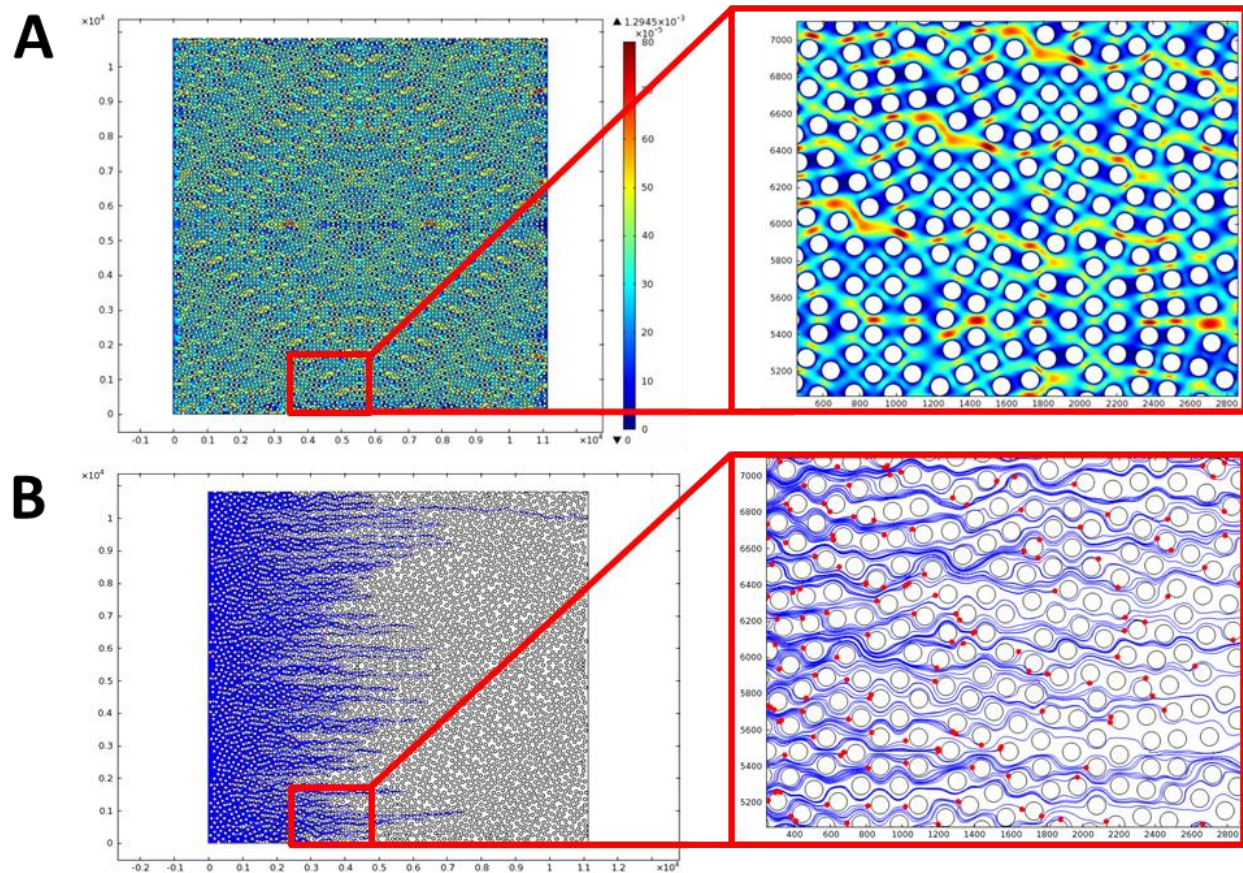


Figure 3-8: Finite element simulations of the CTC Carpet Chip. Simulation studies were done on $\frac{1}{4}$ of a diamond shape of the CTC Carpet Chip to ensure the sensitivity and specificity of the designed chip. A) Velocity magnitude of flow on a portion of diamond shape of the CTC Carpet Chip. B) Particle tracing plot around microposts near the inlet demonstrating typical streamlines (blue) and capture of 15 µm rigid particles (red) upon encountering a wall (post).

3.2.1 CTC Carpet Chip optimization

3.2.1.1 Different distance sizes and flow rates

The effects of different distance sizes (50 µm and 25 µm) between the CTC Carpet Chips and different flow rates (1, 3, 5, and 10 mL hr⁻¹) on the capture efficiencies were analyzed. The 50 µm distance showed higher % capture efficiency (94.9%) with Panc-1 cell line compared to the 25 µm (Figure 3-9A). By increasing flow rate from 1 mL

hr^{-1} to 10 mL hr^{-1} , capture efficiencies significantly decreased (Figure 3-9B). Therefore, 1 mL hr^{-1} flow rate was selected as a constant flow rate.

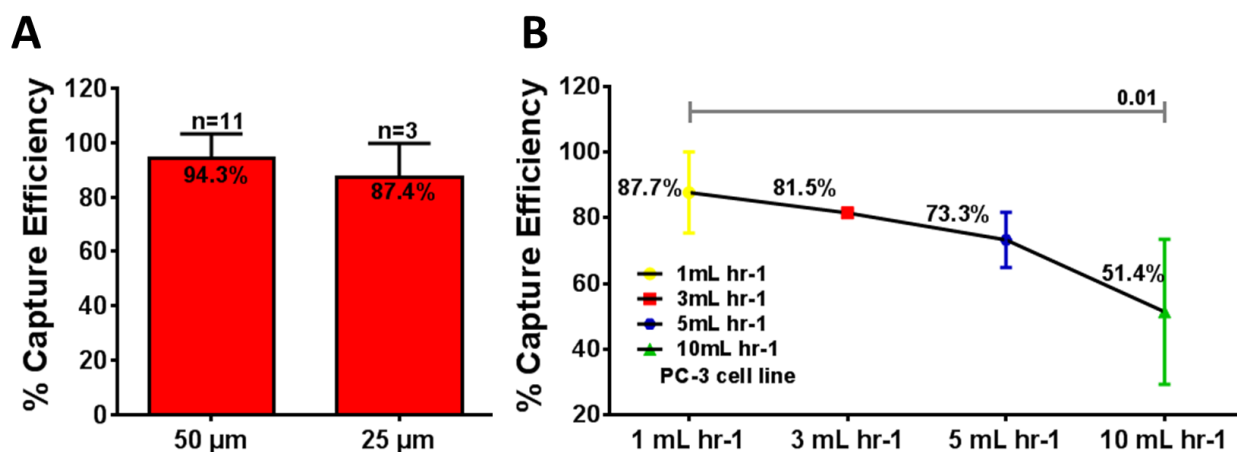


Figure 3-9: The effect of different distances between posts of CTC Carpet Chip and different flow rates on the capture efficiencies of EpCAM. A) Capture efficiencies were higher when there is a $50 \mu\text{m}$ distance between posts (94.9%). B) Capture efficiencies were higher when 1 mL hr^{-1} flow rate was used (87.7%) compared to the other flow rates (3, 5, and 10 mL hr^{-1}).

3.2.1.2 Different cell line

Four cancer cell lines with different levels of EpCAM expression and one cell line with high CD133 expression were used for testing and optimization of the CTC Carpet Chip; HT-29 and Panc-1 (high EpCAM expression), PC-3 (low EpCAM expression), Hs-578T (no EpCAM expression/negative control) and Capan-1 (high CD133 expression).¹⁹⁶ These cell lines were labeled with green CellTracker dye and spiked into blood at a concentration of $1000 \text{ cells mL}^{-1}$ to test the capture efficiencies of the single CTC Carpet Chip functionalized with either anti-EpCAM or anti-CD133 antibodies. The CTC Carpet Chip yielded the following efficiencies across the different cell lines; $97.5\% \pm 2.2$ (HT-29) and $94.9\% \pm 2.4$ (Panc-1), $87.7\% \pm 13.9$ (PC-3), 13.6% (Hs-578T), and $73\% \pm 16.6$ (Capan-1) (Figure 3-10).

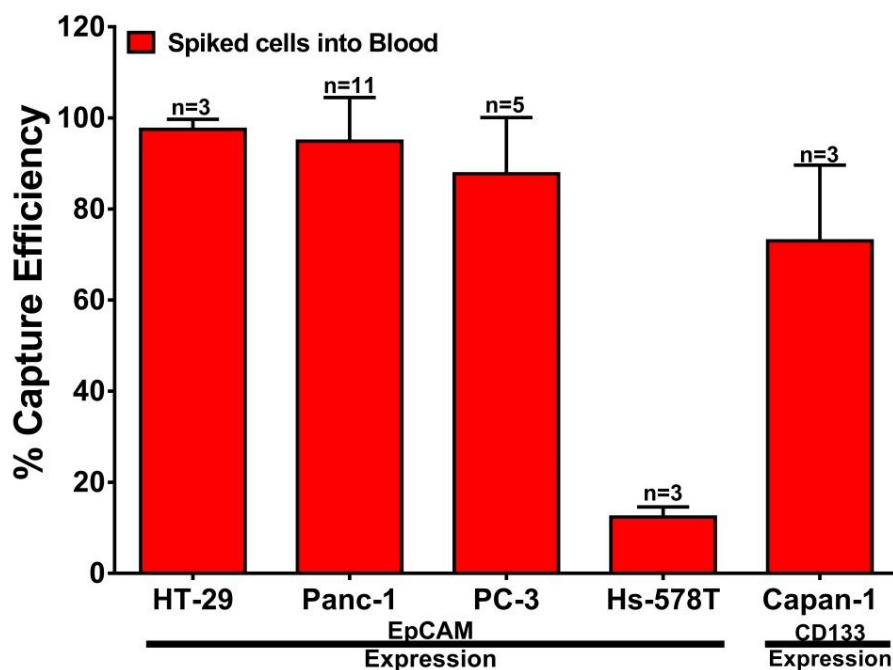


Figure 3-10: The effect of different cell line on the capture efficiencies of EpCAM. Different cell lines with various levels of EpCAM expression including; HT-29 and Panc-1 (high EpCAM expression), PC-3 (low EpCAM expression), and Hs-578T (none), and one cell line with high CD133 expression (Capan-1) were used. 1000 green CellTracker cells were spiked into blood and processed through single CTC Carpet Chip coated with anti-EpCAM or anti-CD133.

A representative image of entire chip with captured pre-labeled PC-3 cells is shown in Figure 3-11A. A pseudo-colored SEM image of captured cancer cells spiked into blood on the CTC Carpet Chip is shown in Figure 3-11B. In the Carpet design, the posts are arranged in a way to enhance lateral flow in addition to longitudinal flow. In order to further examine this phenomenon, the number of PC-3 cells captured along the length of the device was calculated. It was found that the density of the captured PC-3 cells in the Carpet device was high near the inlet (Figure 3-11C) similar density observations were made for the contaminating blood cells (Figure 3-11D).

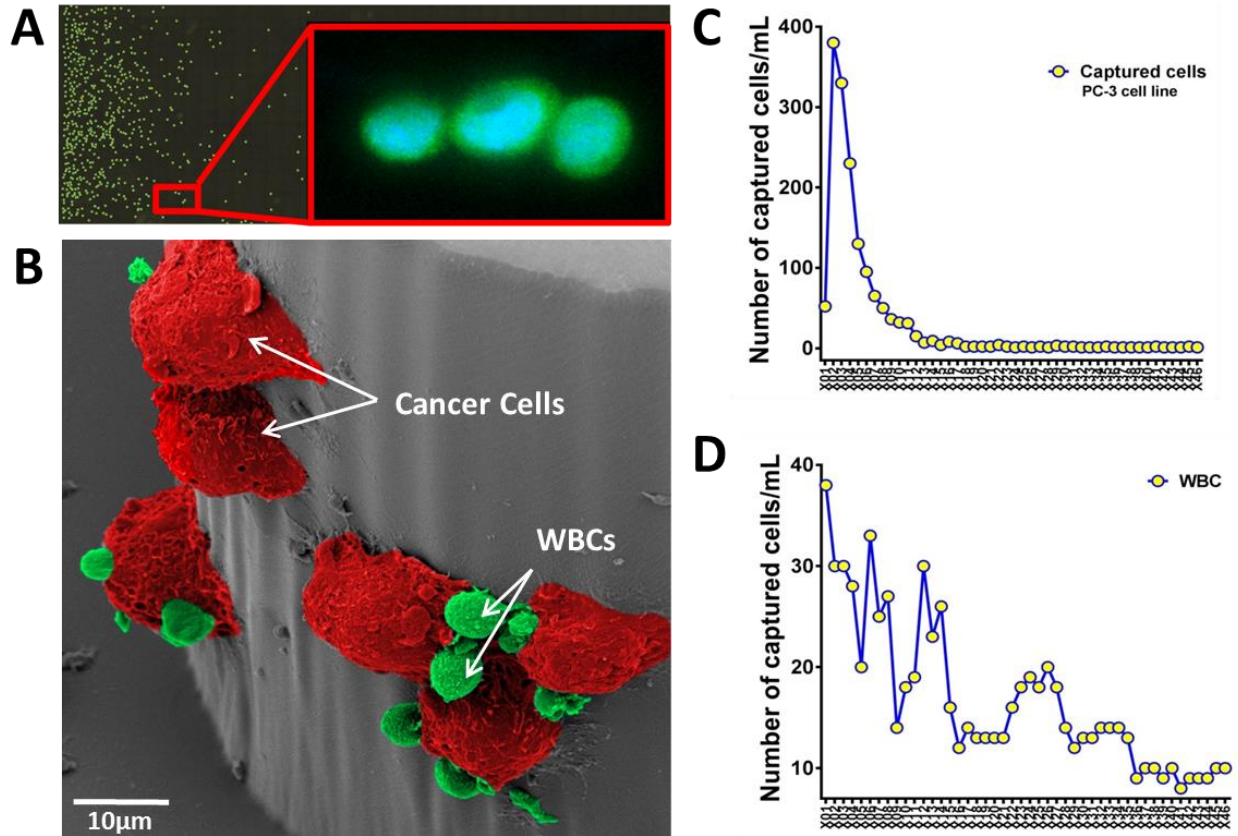


Figure 3-11: Profile capturing across the CTC Carpet Chip. A) Scanned image of the CTC Carpet Chip, shows increased cell capture near inlet area. B) Pseudo-colored SEM image of the captured cancer cells spiked into blood on the CTC Carpet Chip. Cancer cells and WBCs are shown in red and green respectively. C) Number of spiked PC-3 cells into blood captured along the X-axis of Carpet device indicates peak capture area near inlet, along with the number of WBCs captured along the X-axis of Carpet device (D).

3.3 Dual capture

In order to facilitate separating circulating epithelial EpCAM-expressing and EMT-like CD133-expressing cells in different devices in sequential order from the same sample, we connected two devices functionalized with different antibodies (anti-EpCAM in one device and anti-CD133 in the other device) in series as shown in Figure 3-12. Blood was passed through the connected chips at a flow rate of 1 mL hr^{-1} through the inlet of the first device.

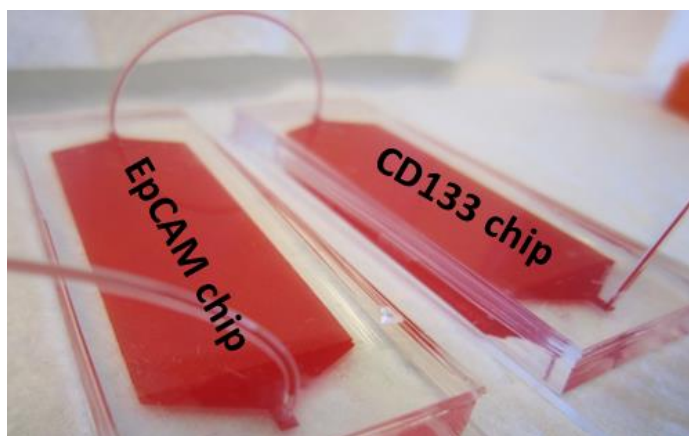


Figure 3-12: Representative image of a dual CTC Carpet Chip. 1 mL blood was sent through the anti-EpCAM coated CTC Carpet Chip which was connected to the anti-CD133 coated CTC Carpet Chip in sequence.

3.3.1 Optimization and re-evaluation of the dual CTC Carpet Chip

3.3.1.1 Western blot and FACS on the capture antibodies; EpCAM and CD133

In order to check the expression of EpCAM and CD133 on PC-3 and HT-29 cell lines, western blot analyses were conducted. The results indicated over/less-expression of EpCAM and high/none expression of CD133 on HT-29/PC-3 cell line respectively (Figure 3-13).

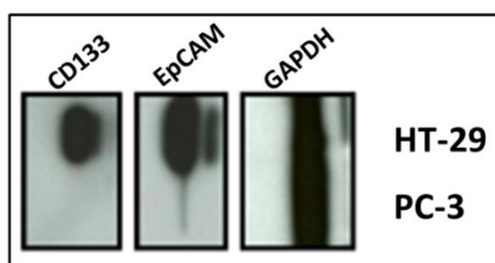


Figure 3-13: Western blot analysis of EpCAM and CD133 on HT-29 and PC-3 cell lines.

FACS analyses were conducted on HT-29 and Panc-1 cell line to check the expression of EpCAM and CD133. Results showing higher expression of EpCAM (99.7%) and CD133 (19.6%) in HT-29 cell line, compared to the Panc-1 cell line (70.9% and 0.7% of EpCAM and CD133 respectively) (Figure 3-14A-B).

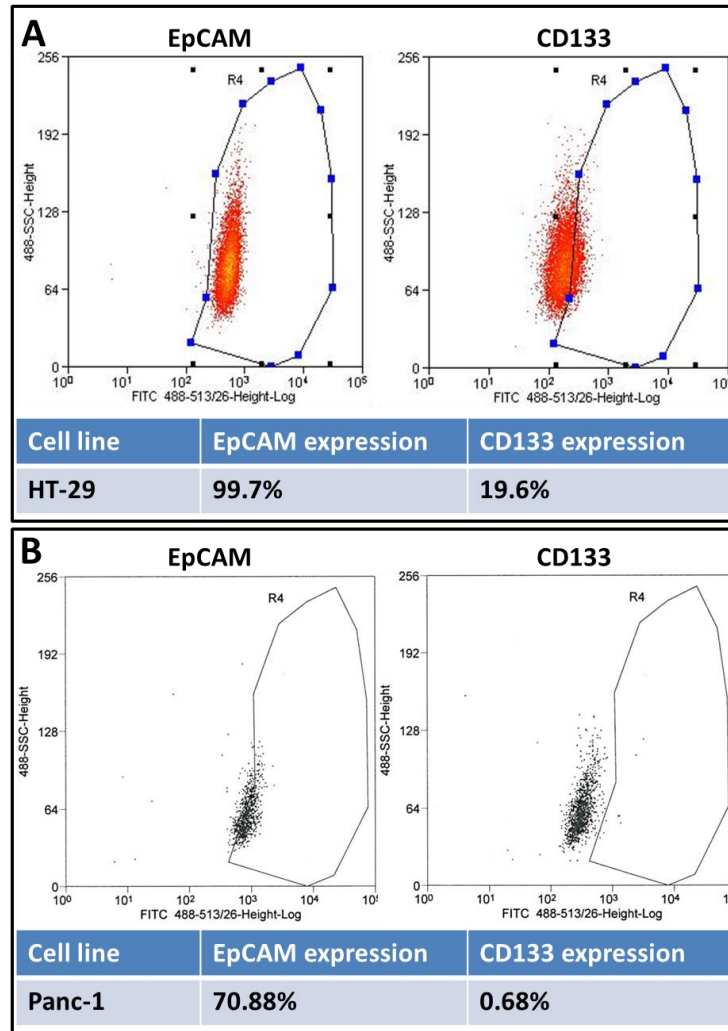


Figure 3-14: The FACS analysis to check the expression of capture antibodies (EpCAM and CD133) on different cell lines. The FACS results of HT-29 (A), Panc-1 (B) indicated over-expression of EpCAM (99.7% / 70.88%) and less expression of CD133 (19.6% / 0.68%) for HT-29 and Panc-1 respectively.

3.3.1.2 FACS analysis on the detection antibodies; Cytokeratin and Vimentin

The expression of the detection antibodies, CK and Vimentin, were checked with FACS analysis on three different cancer cell lines, PC-3, MCF-7, and SUM-159 (Figure 3-15 and Figure 3-16). The expression of CK7&8 and three different Vimentin antibodies from different resources (#1-Santa Cruz, #2-Cell Signaling, and #3-BD biosciences) and different hosts (rabbit and mouse) were checked.

The FACS analysis showed 99.3% of CK7&8 expression on PC-3 cell line (Figure 3-15A), 84.6% on MCF-7 (Figure 3-15B), and 31.6% on SUM-159

(Figure 3-15C). All three cell lines did not show any expression of Vimentin from source #1 and #2 (Figure 3-16A1, A2, B1, B2, C1, and C2). However, Vimentin #3 were expressed 33.5% on PC-3 (Figure 3-16A3), 53.9% on MCF-7 (Figure 3-16B3), and 88.8% on SUM-159 (Figure 3-16C3). Therefore, Vimentin #3 was selected for further analysis.

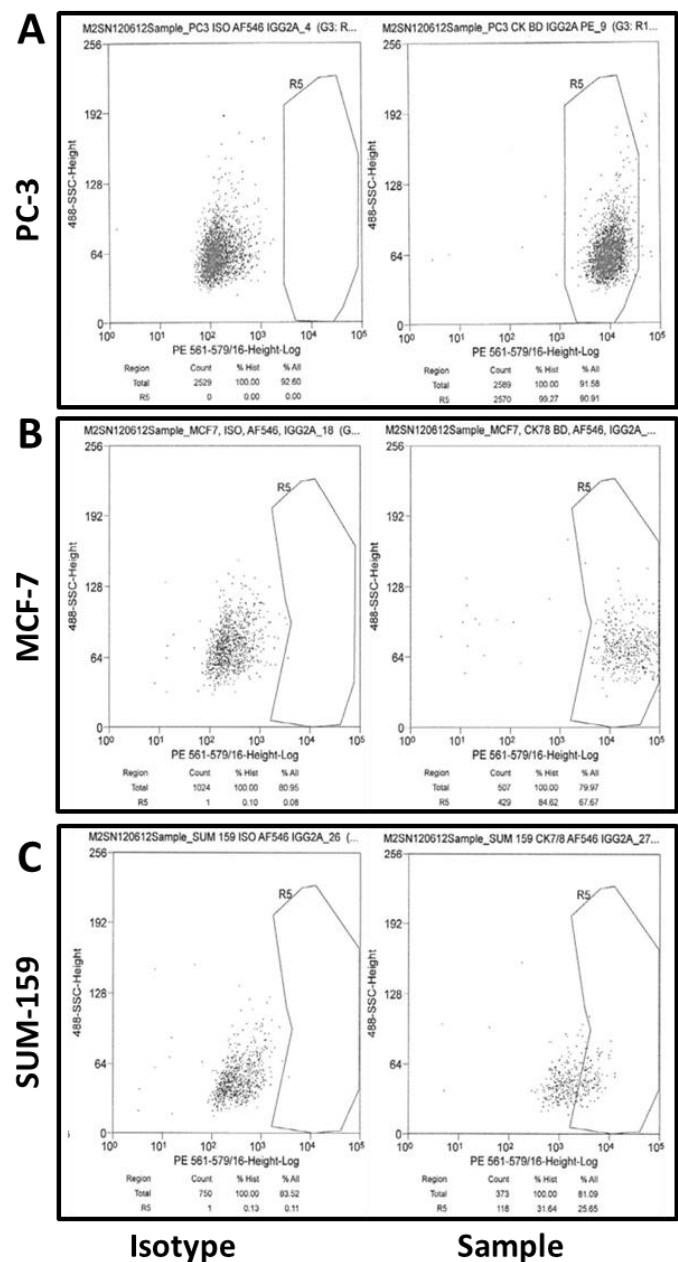


Figure 3-15: FACS analysis to check the expression of detection antibodies (CK) on different cell lines. (A) PC-3, (B) MCF-7, and (C) SUM-159 cell lines expressed 99.3%, 84.6% and 31.6% of CK7&8 respectively.

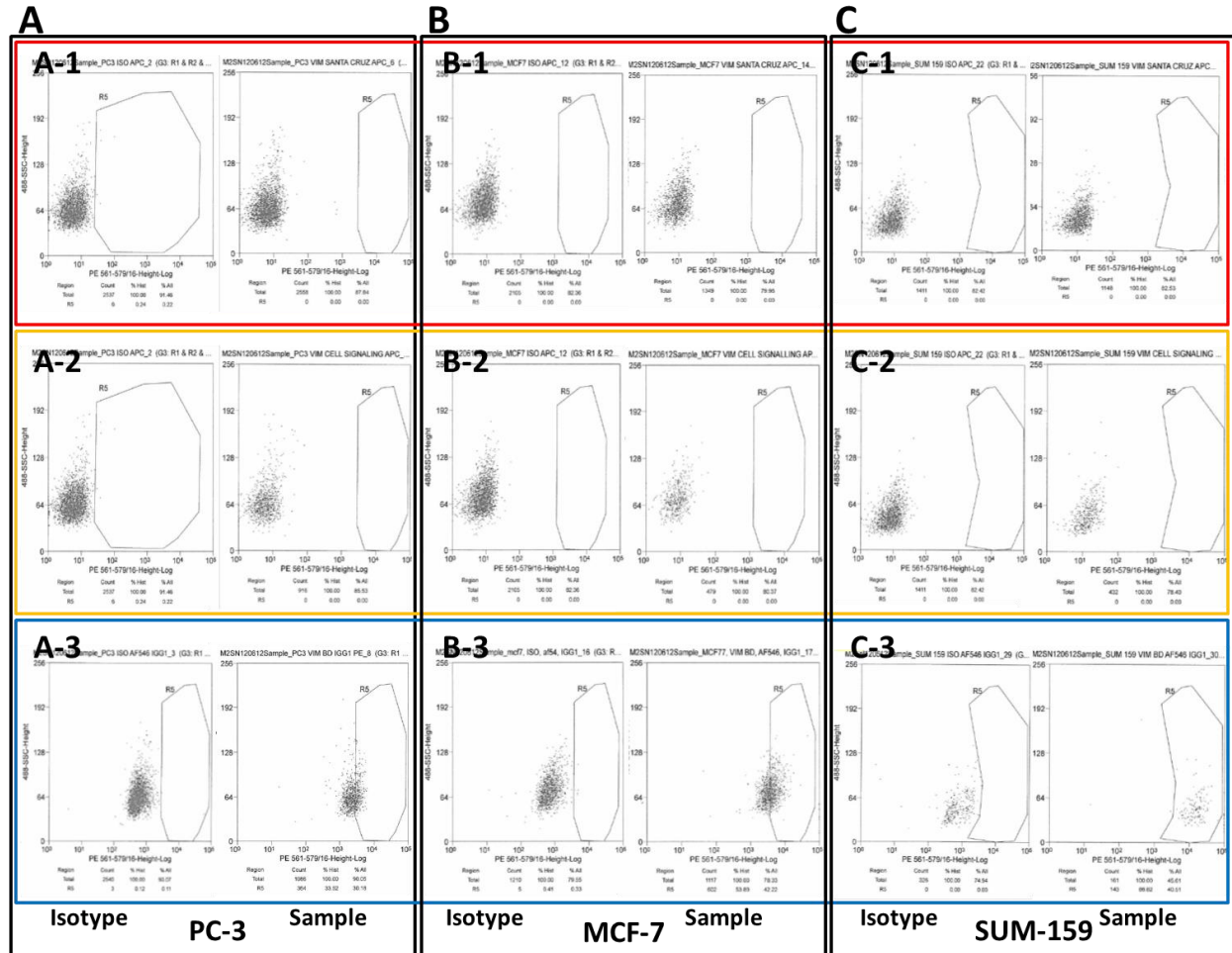


Figure 3-16: FACS analysis to check the expression of detection antibodies (Vimentin) on different cell lines. A) PC-3), B) MCF-7, and C) SUM-159 cell lines did not express Vimentin from source #1 (Santa Cruz) (A-1, B-1, and C-1) and #2 (Cell Signaling) (A-2, B-2, and C-2). However, Vimentin #3 (BD Bioscience) were expressed on PC-3 (33.5%), MCF-7 (53.9%), and SUM-159 (88.8%) cell lines (A-3, B-3, and C-3).

3.3.1.3 Sensitivity and specificity of the dual CTC Carpet Chip

Four different set-ups were tested in order to evaluate the sensitivity and specificity of the capture rates of the chips, each coated with and without the antibodies of interest (anti-EpCAM and anti-CD133), using Panc-1 spiked into blood. Chips coated with no antibodies (EpCAM- and CD133-) showed <3% capture efficiency (false positive). However, in the presence of antibodies (EpCAM+ and CD133+), efficiency rates increased to 89.8%±9.5 EpCAM+ cells and 6.6%±3.3 CD133+ cells. EpCAM+ and CD133- dual chips showed 90.2% and 0.7% EpCAM+ and CD133+ cells capture

efficiencies. EpCAM- and CD133+ dual chips captured 2.4% and 7.2% EpCAM+ and CD133+ cells capture efficiencies (Figure 3-17), demonstrating high specificity and consistent yields for both of the captured antibodies in the dual isolation. In summary, applying dual CTC Carpet Chip technology in terms of isolating different type of cancer cells was quite sensitive and specific.

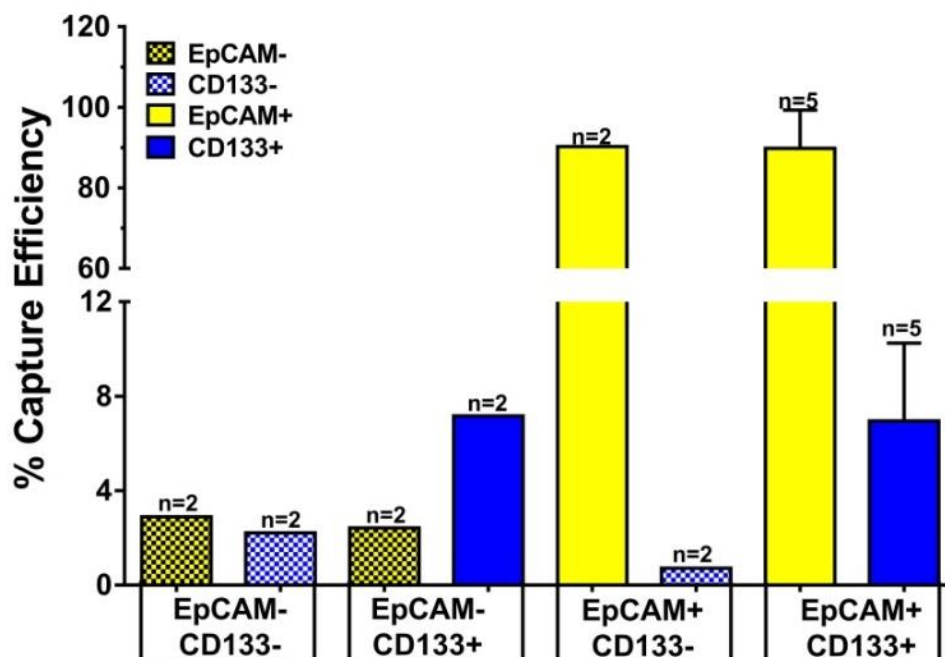


Figure 3-17: Sensitivity and specificity of the capture efficiencies of the dual CTC Carpet chip. % Capture efficiencies of Panc-1 cell lines spiked into blood with or without antibodies (EpCAM and CD133) in the dual chips. The solid/hatched yellow and blue bars show the presence/absence of EpCAM and CD133 antibodies.

3.3.1.4 Immunofluorescence staining

After cell capture, cancer cells were detected by immunofluorescence staining protocol described in section 2.8.

3.3.1.4.1 Optimization of the detection antibodies

In order to optimize the immunofluorescence staining protocol different antibodies, alone or in a combination form, including (Pan) cytokeratins, CD45, and Vimentin with different isotypes from different resources were tested in 16 pancreatic

cancer patient samples. Additional information about this optimization is provided in appendix section (Table 9-5).

Comparison between specificity of CK7&8 and PanCK antibodies on the number of EpCs per mL on EpCAM chip were checked on pancreatic cancer patient samples (n=3) (Table 9-5). Numbers of EpCs captured on the EpCAM chip were significantly higher when PanCK antibodies were used as detection antibodies compared to EpCs numbers when CK7&8 antibodies was used ($p=0.009$) (Figure 3-18).

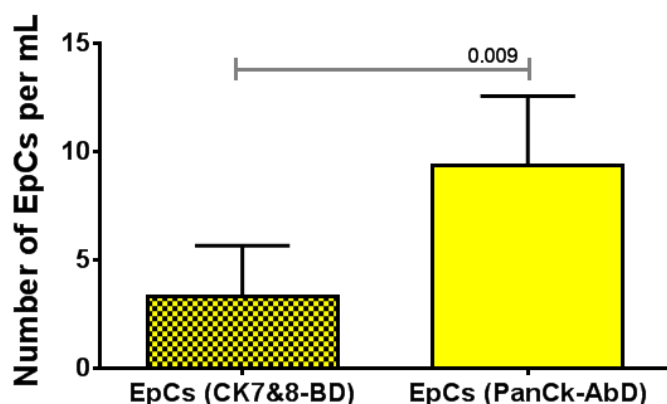


Figure 3-18: Comparison between CK7&8 and PanCK in detecting the EpCs in pancreatic cancer patient samples (n=3).

3.3.1.4.2 Triple staining of PanCK, Vimentin and CD45

To determine the presence of EpCs+ in the CD133 chip and EMTCs+ in the EpCAM chip, 16 patient samples were tested through triple staining of each chip (CK and Vimentin along with CD45) (Figure 3-19). Two out of 16 samples were Vimentin+ cells in the EpCAM Chip (1 and 4 cells), and two out of 16 were CK+ cells in the CD133 Chip (2 and 1 cells). As the results show in Figure 3-19, these markers were relatively specific for their origins, meaning there were few captured EMTCs (mean $0.3 \text{ cells mL}^{-1}$) in EpCAM Chips and few circulating EpCs in CD133 Chips (median 0.2 cell mL^{-1}). A

small number of double positive (PanCK⁺/CD45⁺) cells were found in some samples and were excluded from this study due to unknown origin and significance.

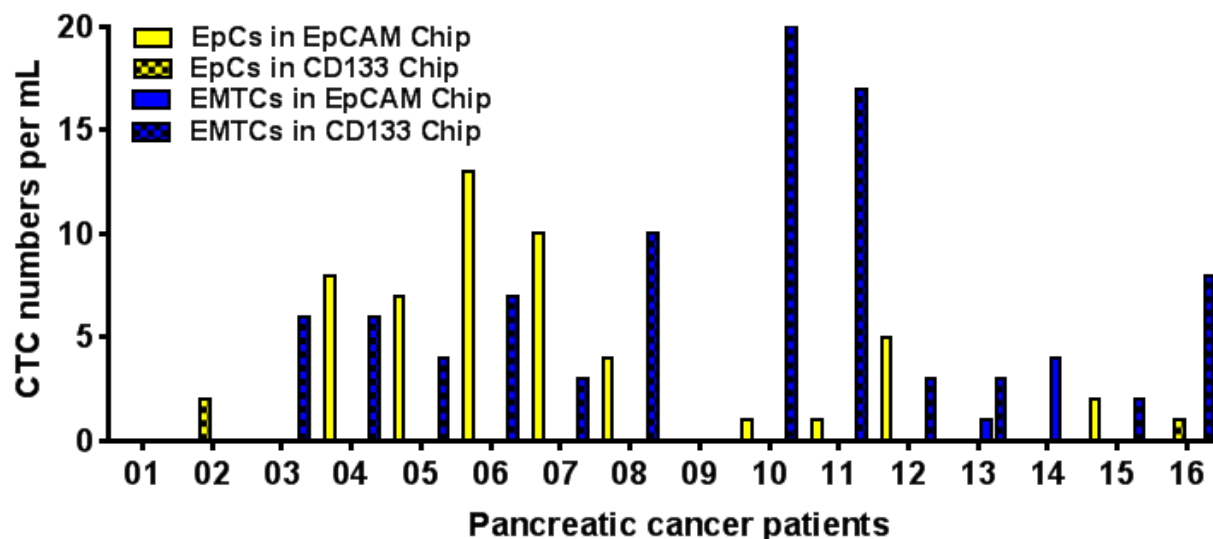


Figure 3-19: Analysis of pancreatic cancer patient samples (n=16) with triple staining (CK, Vimentin, and CD45) for each CTC Carpet Chip. Two out of 16 samples were Vimentin⁺ cells in the EpCAM Chip (1 and 4 cells). Two out of 16 samples were CK⁺ cells in the CD133 Chip (2 and 1 cells).

3.3.1.4.3 Finalized detection antibodies

Each chip was stained with either PanCK (for the EpCAM chip) or Vimentin (for the CD133 chip) antibodies. The leukocytes were identified by CD45 and neoplastic cells were identified as expressing EpCAM or CD133 and lacking expression of CD45. Figure 3-20A-B shows representative images of captured cancer cells stained for PanCK (red) and CD45 (green) to distinguish EpCs and WBCs. The captured EMTCs in the CD133 chip are shown in Figure 3-20C, with Vimentin (orange) and CD45 (green) used as detection antibodies for the EMTCs and WBCs respectively. In summary, PanCK⁺/CD45⁻/DAPI⁺, and Vimentin⁺/CD45⁻/DAPI⁺ phenotypes were determined and enumerated as EpCs and EMTCs respectively.

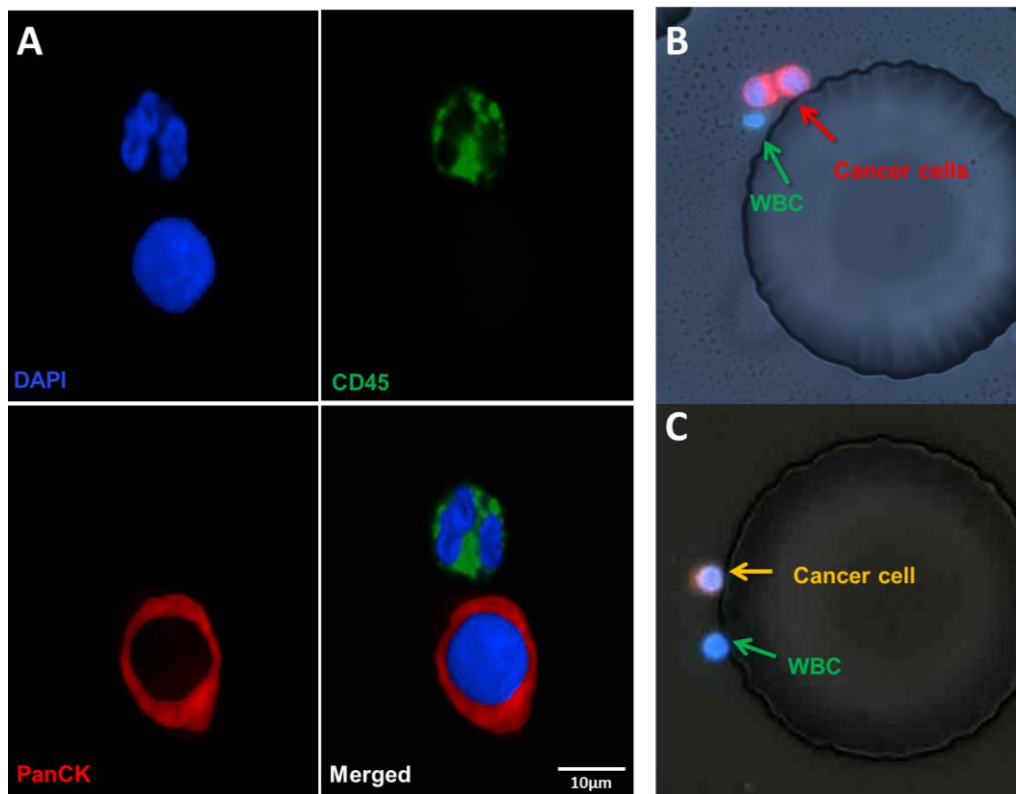


Figure 3-20: CTC Carpet Chip cell line immunofluorescence staining. Anti-human CD45, anti-human PanCK, and anti-human Vimentin antibodies were tested with cancer cell lines. A) Confocal image of a typical CK+ cancer cell. The PanCK+ CTCs were detected with PanCK (red) along with a CD45+ (green) WBC (B) Captured CK+ cells in the EpCAM chip using PC-3 cells spiked into blood (C) and Vimentin+ cells in the CD133 chip using SUM-159 cells spiked into blood.

3.3.1.5 CTC Carpet Chip sequence analysis

The effect of the device order (EpCAM Chip connected to the CD133 device (EpCAM → CD133: Ep1/CD2) and vice versa (CD133 → EpCAM: CD1/Ep2) on capture efficiencies of the spiked green CellTracker Panc-1 cell line into blood and pancreatic cancer patients samples (n=6) was tested (Figure 3-21). In the Panc-1 cell line, the % capture efficiency of the EpCAM Chip was 70.7% when the EpCAM Chip was run as the first Chip (Ep1) and 31.6% when the EpCAM Chip was conducted as the second Chip (Ep2), while, the % capture efficiency of the CD133 Chip was 15.7% and 7.1% when the

CD133 Chip being used as the first (CD1) compared to the second (CD2) Chip, respectively (Figure 3-21A).

The effects of the reverse study on the number of captured CTCs mL^{-1} from different pancreatic cancer patient samples ($n=6$) are shown in Figure 3-21B. The numbers of captured EpCs/EMTCs mL^{-1} were higher in the Ep1/CD2 (22.5/85.3 CTC mL^{-1}) group compare to the CD1/Ep2 (73.5/10 CTC mL^{-1}). In summary, the cell line results indicated when the EpCAM/CD133 Chip was arranged as a first device (Ep1 and CD1), the capture efficiencies were higher, while the numbers of captured $\text{EpCAM}^+/\text{CD133}^+$ were higher in the Ep1/CD2 group compare to the CD1/Ep2 from pancreatic cancer patients.

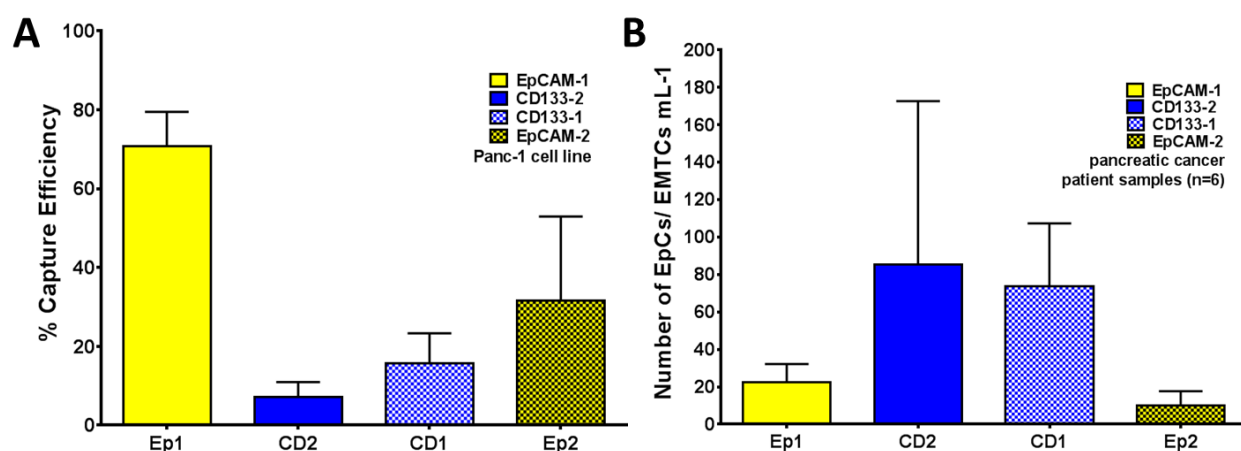


Figure 3-21: The effect of Chip's order on the numbers of captured cells on dual study. A) The effect of reverse study on the % capture efficiencies of Panc-1 cell line on different orders of EpCAM vs. CD133 CTC Chips (EpCAM \rightarrow CD133 (Ep1/CD2) and CD133 \rightarrow EpCAM (CD1/Ep2)). B) The effect of reverse study on the number of CTCs mL^{-1} in pancreatic cancer patient samples ($n=6$). Yellow/blue bars show EpCAM/CD133 Chips. Solid bars show EpCAM \rightarrow CD133 (Ep1/CD2), and hatched bars show CD133 \rightarrow EpCAM (CD1/Ep2).

3.4 Application of the CTC Carpet Chip to evaluate heterogeneity in pancreatic cancer patient samples

Thirty-five patients with histologically documented PDAC of varying stages were analyzed, with clinical data provided in details in appendix section (Table 9-6). Blood

samples from nine healthy controls were used for the CTC counts comparison (Table 9-6).

3.4.1 Epithelial CTCs (EpCs) and EMT-like CTCs (EMTCs) recovered from pancreatic cancer patients

The dual CTC Carpet Chips were connected in the sequential order of EpCAM first followed by CD133 in order to capture the EpCs and EMTCs (Figure 3-12) and then whole blood collected from the patients was flowed through the chips at 1 mL hr^{-1} . Figure 3-22A show representative images of EpCs cells on the EpCAM chip captured from pancreatic cancer patients. The EpCs and WBCs were stained with PanCK (red) and CD45 (green) respectively. EpCs demonstrating varied morphologies, ranging from round to oval in shape and in some cases occurring as cluster (Figure 3-22B).

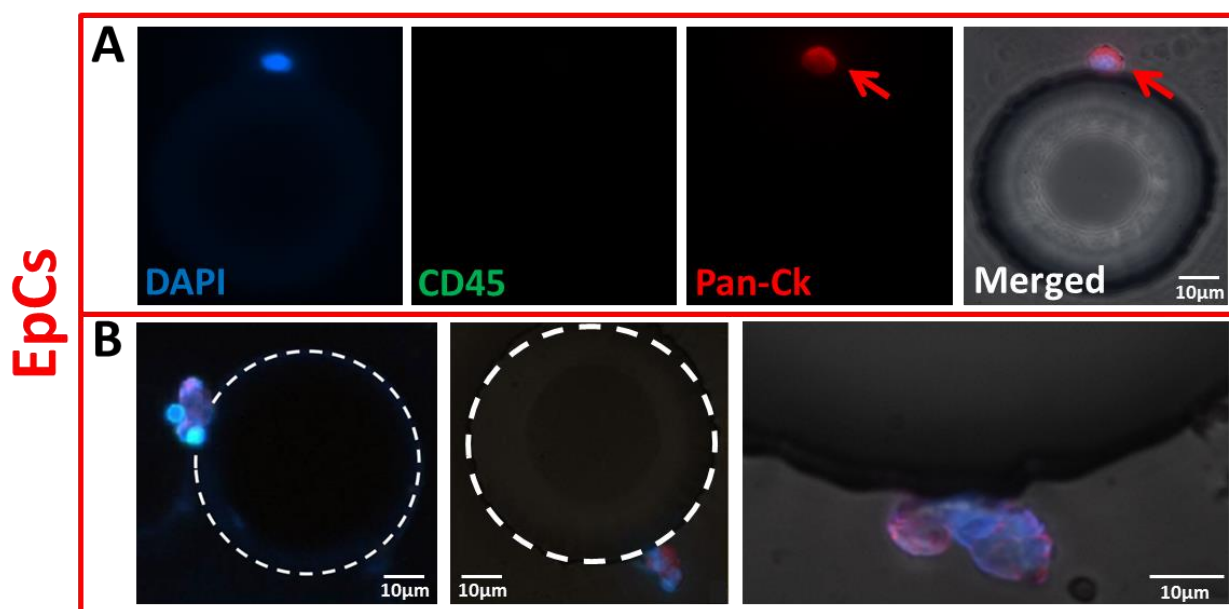


Figure 3-22: Characterization of circulating epithelial CTCs (EpCs) in the EpCAM Carpet Chip from pancreatic cancer patients. A) EpCs and WBCs were stained with PanCK and CD45 respectively, in addition to DAPI. Red arrow is showing a PanCK EpC. B) An EpC cluster captured around the posts. Post outlines are marked in white circle and bright field. The post outlines are marked with white circles.

Figure 3-23A shows images of an EMTC and a leukocyte. As shown in Figure 3-23B, EMTCs captured on the chip had a wide range of cell sizes. Red, orange,

and green arrows indicate PanCK, Vimentin, and CD45 staining respectively. Figure 3-23C shows a representative confocal image of a EMTC (pink) and a WBC (green) captured from a Pancreatic cancer patient on the CD133 chip.

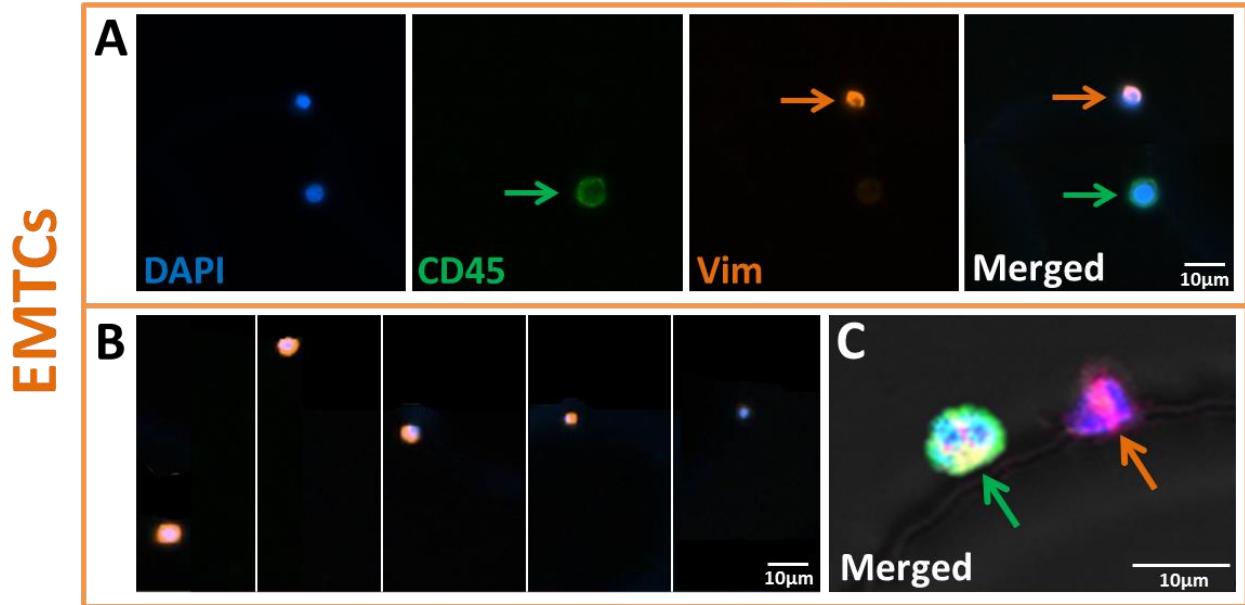


Figure 3-23: Characterization of circulating EMT-like CTCs (EMTCs) in the CD133 Carpet Chip from pancreatic cancer patients. A) Vimentin (orange) and CD45 (green) staining for detection of EMTCs and WBCs respectively. Orange and green arrows are showing Vimentin and CD45 positive cells respectively. B) Different sizes of EMTCs captured on the device. C) Confocal image of EMTC (pink) and WBC (green).

3.4.2 Pancreatic CTCs enrichment using the CTC Carpet Chip compared to healthy control samples

We quantified the captured EpCs and EMTCs on EpCAM and CD133 chips and found that 97.5% of the patients had EpCs+ (≥ 5 PanCK+ CTCs mL^{-1}) with a mean of $22.4 \pm 17.7 \text{ mL}^{-1}$, while all 35 patients had EMTCs (≥ 15 Vimentin+ CTCs mL^{-1}) with a mean of $85.7 \pm 59.5 \text{ mL}^{-1}$. In contrast, low numbers of EpCs ($0.9 \pm 0.9 \text{ mL}^{-1}$) and EMTCs ($1.9 \pm 2 \text{ mL}^{-1}$) were observed in the HCs samples (Figure 3-24). In summary, the results indicate significant differences between the overall number of CTCs in pancreatic cancer patients samples (108.1 ± 63.5) vs. HCs (2.8 ± 2.6) ($p < 0.0001$), as well as the number of EpCs (20.8% of overall CTCs) vs. EMTCs (79.2% of overall CTCs). We

found significantly higher numbers of EMT-like CTCs in circulation in pancreatic cancer patients compared to epithelial CTCs ($p<0.0001$).

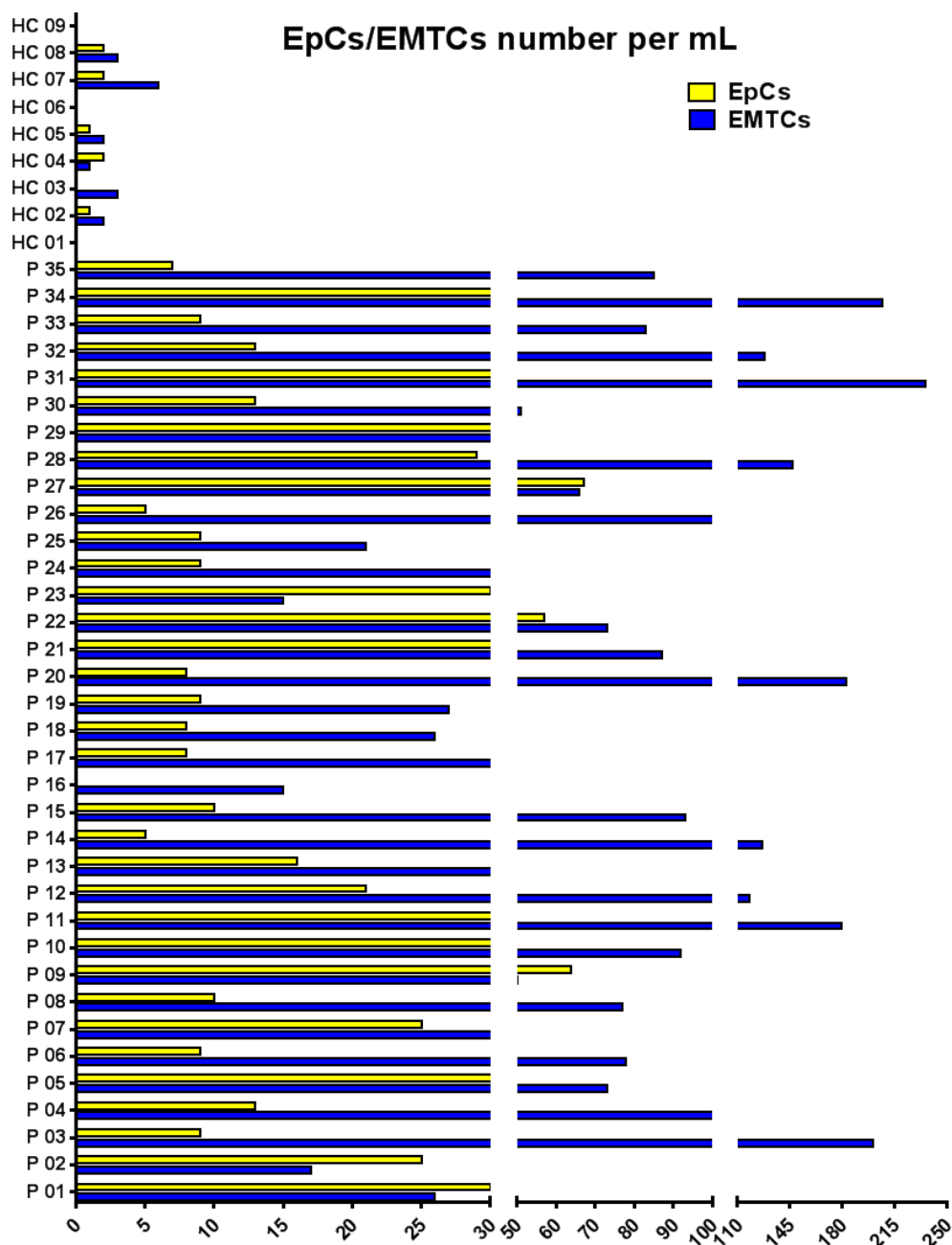


Figure 3-24: Analysis of EpCs and EMTCs from pancreatic cancer patient samples compared to the healthy controls. Enumeration of EpCs and EMTCs on the anti-EpCAM and anti-CD133 coated CTC Carpet Chips from pancreatic cancer patients ($n=35$) along with HCs ($n=9$). Significant difference between the overall number of CTCs in pancreatic cancer patients samples (108.1 ± 63.5) vs. HCs (2.8 ± 2.6) ($p<0.0001$) was observed using unpaired t-tests (two-tailed). Significantly higher numbers of EMTCs (85.7 ± 59.5) compared to EpCs (22.4 ± 17.7) were observed ($p<0.0001$) using paired t-tests (two-tailed) ($n=35$).

3.4.3 Pancreatic CTCs enrichment using the CTC Carpet Chip to explore associations with clinical outcomes

To further explore the relationship of EpCs and EMTCs and clinical outcomes in the pancreatic cancer patient cohort (n=35), the CTC counts from these two cell populations were analyzed based on clinical disease stages (Figure 3-25). All stages except stage IIA showed significantly higher numbers of EMTCs compared to the number of EpCs (Figure 3-25A). Patients with stage IV disease showed higher numbers of EMTCs than EpCs ($p=0.0008$).

Also, patients were categorized based on the tumor status as resectable (n=9), borderline resectable (n=2), locally advanced (n=13), and metastatic (n=11) groups. There were significantly higher numbers of EMTCs than EpCs between all these groups, except borderline resectable patients due to the small sample numbers (Figure 3-25B). The ratio of EpCs/EMTCs to total number of CTCs has a decreasing/increasing trend with later stages (Figure 3-25C). The percentage of EpCs decreased toward late stages, whereas the percentage of EMTCs increased.

Figure 3-25D-F summarize the frequencies of EpCs and EMTCs characterized in different patient subgroups, including tumor size <2cm vs. >2cm, no lymph node involvement (N0) vs. lymph node involvement (N1), and non-metastatic (M0) vs. metastatic (M1) groups. Significantly higher numbers of EMTCs ($p=0.04$) were observed when the patients were grouped based on lymph node involvement (N1) compared with no lymph node involvement (N0) patients.

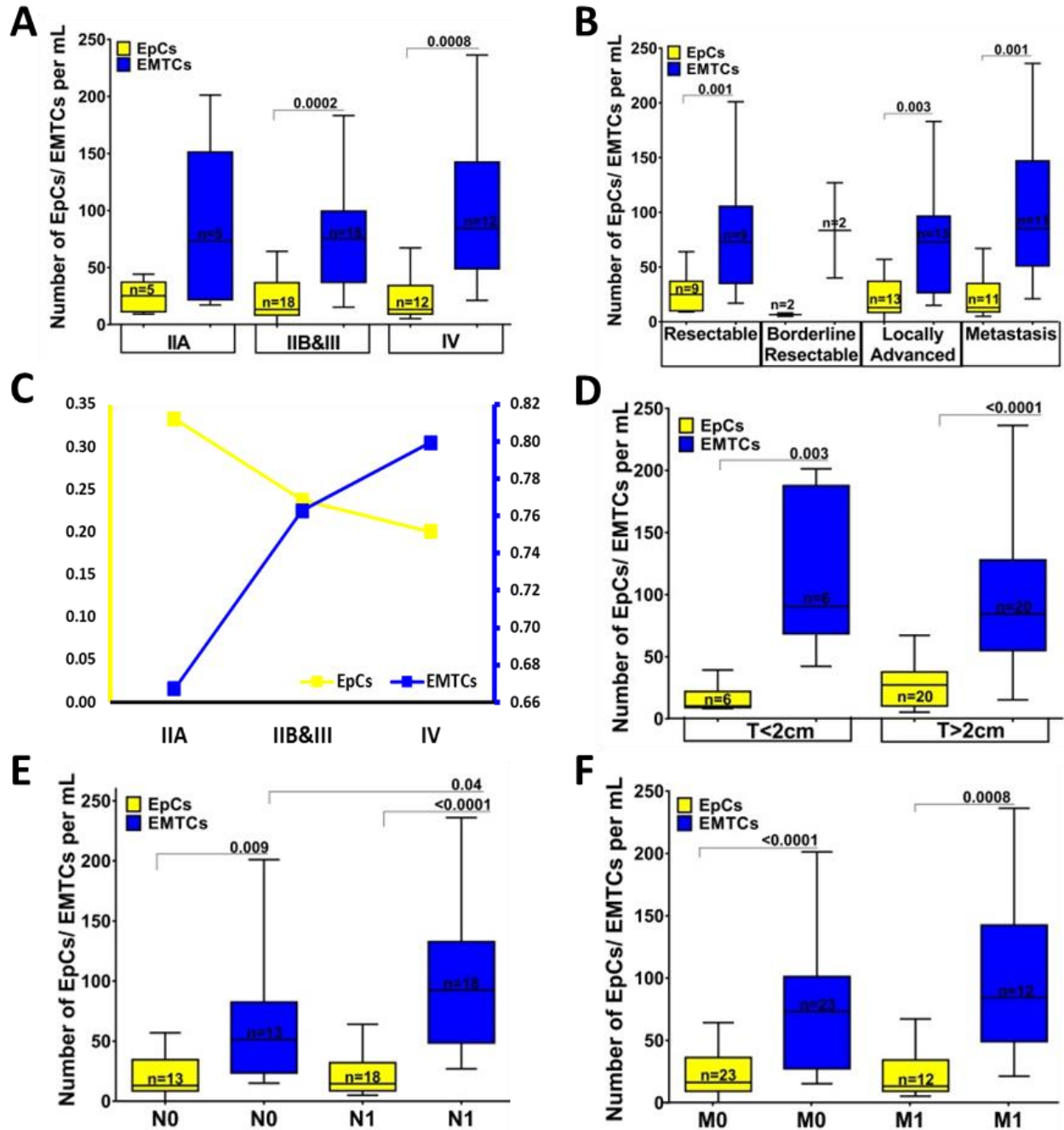


Figure 3-25: Analysis of EpCs and EMTCs from pancreatic cancer patient samples based on their clinical outcomes. A, B) Analysis of number of EpCs and EMTCs recovered in pancreatic cancer patient samples (n=35) based on their clinical disease stages from stage IIA (n=6), IIB&III (n=17), and IV (n=12), and based on tumor status (resectable (n=9), borderline resectable (n=2), locally advanced (n=13) and metastatic (n=11)). No significant differences were observed in the effect of stage and resection on the number of EpCs and EMTCs using unpaired t-tests. C) Ratio of EpCs to total number of CTCs and ratio of EMTCs to total number of CTCs from early to advanced stage disease. D-F) Enumerated EpCs and EMTCs grouped according to tumor size (> or <2cm (D), lymph node involvement (N0 or N1) (E), and metastasis (M0 or M1) (F). Unpaired t-tests were used to analyze the effect of tumor size, lymph node involvement, and metastasis. N1 group (n=18) showed significantly higher number of EMTCs compared to N0 group (n=13) (p=0.04). No significant correlation between tumor size and metastatic burden were observed.

3.5 Gene expression profiling of EpCs and EMTCs by quantitative reverse transcription polymerase chain reaction (qRT-PCR)

We profiled the mRNA expression of both of these populations using a panel of 96 cancer-related genes (Table 2-1). RNA was extracted from captured CTCs and utilized for gene expression profiling by RT-qPCR. Gene expression profiles of CTCs isolated from blood samples of pancreatic cancer patients (n=17) which were run through the dual CTC Carpet Chip are present as heat map (Figure 3-26).

3.5.1 Gene expression profiling on the captured CTCs on EpCAM Chip vs. CD133 Chip

Figure 3-27A presents the median log fold change (logFC) of select genes with $\log FC > 1.5$ in EpCAM Chip (yellow) and in CD133 Chip (blue). Figure 3-27B-C present box plots showing expression of significant differential expression of genes in patient CTCs isolated by EpCAM and CD133 chips. CXCR1 ($p=0.03$) in the EpCAM chip (Figure 3-27B), and POU5F1 (or Oct-4) ($p=0.008$) and MYC ($p=0.03$) in CD133 chip (Figure 3-27C) were significantly differentially expressed.

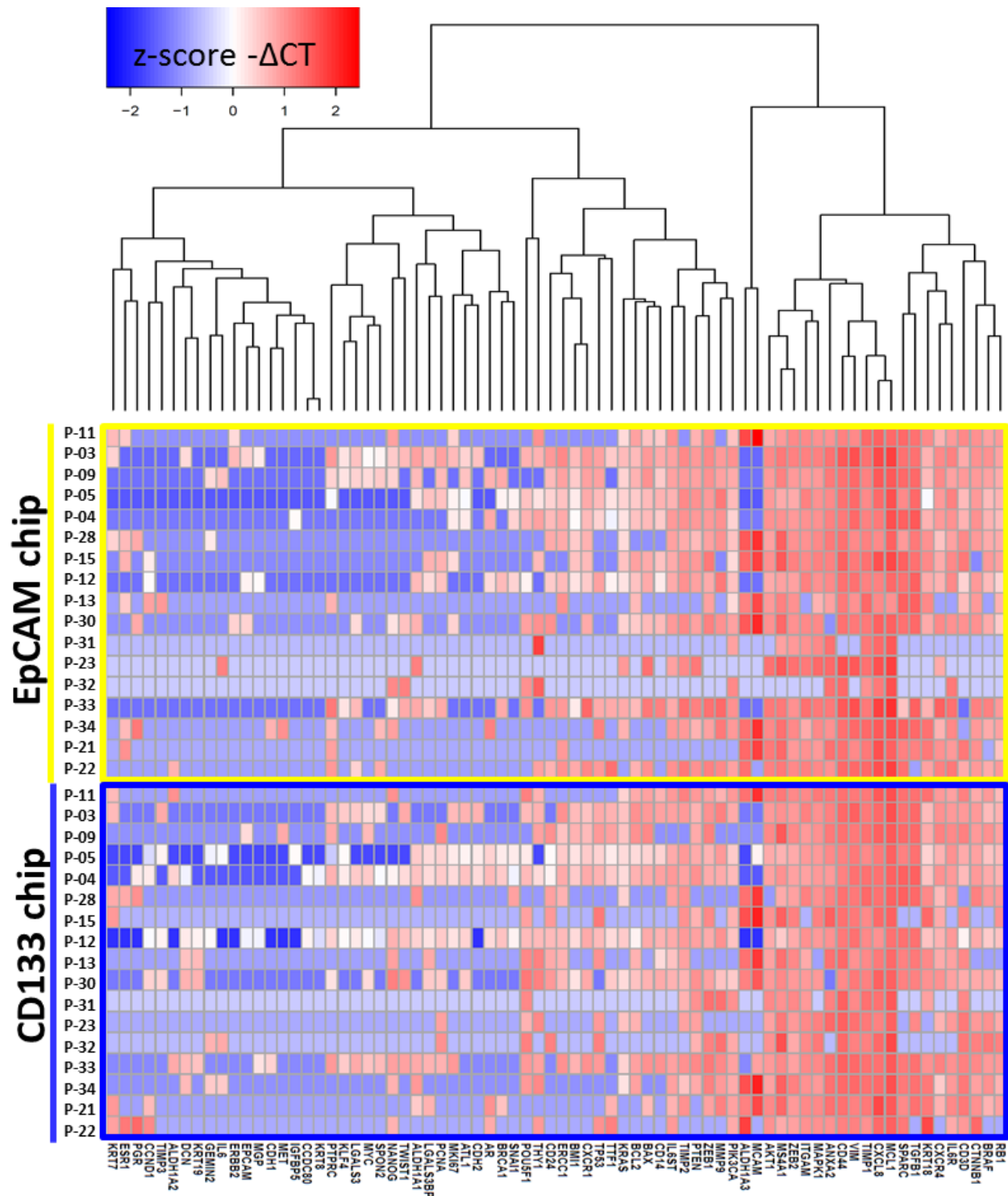


Figure 3-26: Clustering heat map of gene expression profiling of CTCs in pancreatic cancer patients samples (n=17). Clustering heat map analysis of gene expression data based on CTCs captured by EpCAM vs. CD133 CTC Carpet Chips was performed using $-\Delta Ct$. The top section shows the heat map of CTCs captured on EpCAM chip and the bottom section of the panel presents the CTCs captured on the CD133 chip. The color scale shown at the top illustrates the relative expression level of genes across the samples: red represents an expression level above the mean, blue represents expression lower than the mean.

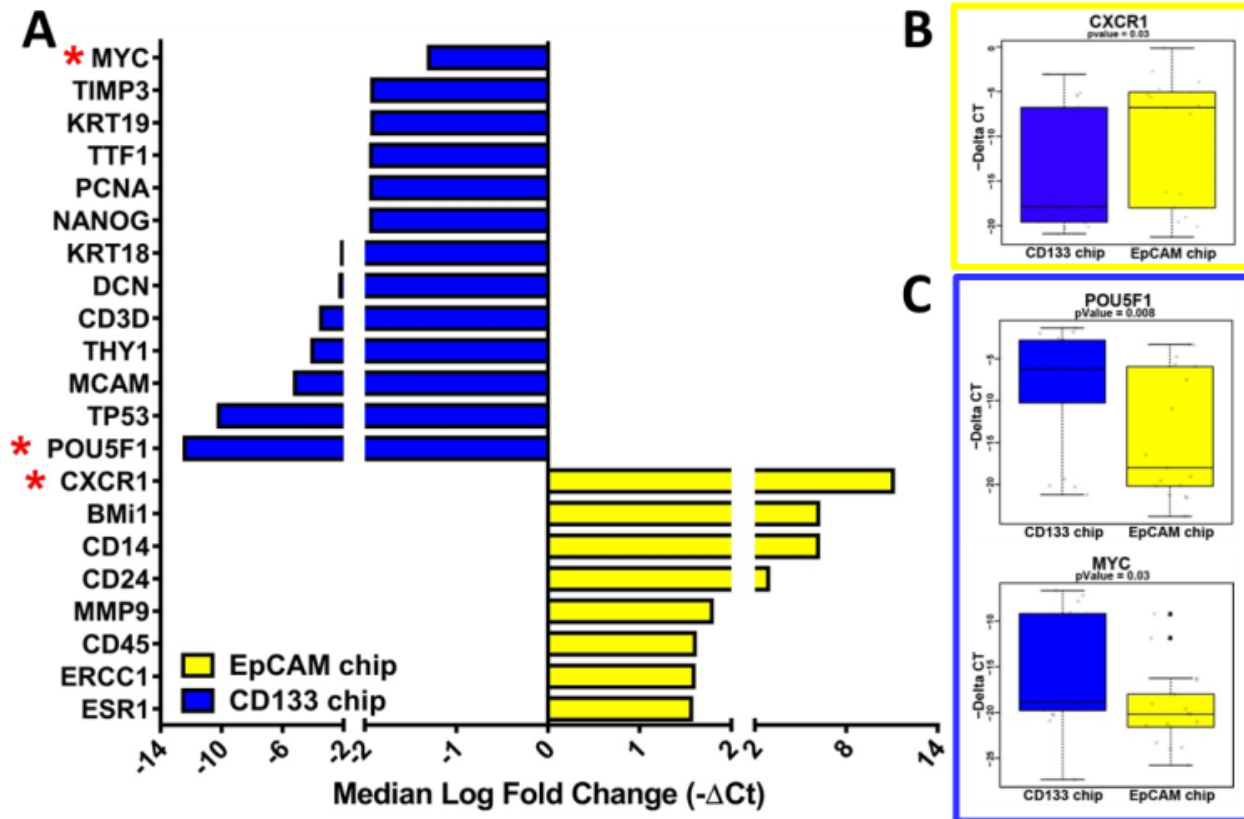


Figure 3-27: Gene expression profiling in pancreatic cancer patients CTC samples (n=17) based on the capture device. A) The median log fold change (logFC) of selected genes with logFC>1.5 is shown in yellow (for the EpCAM chip) and blue (for the CD133 chip). Each fold change is calculated from the $2^{-\Delta Ct}$. B-C) Box plot diagrams of significantly differently expressed individual genes in EpCAM chip (B), CXCR1 (p=0.03) and POU5F1 (or Oct-4) (p=0.008) and MYC (p=0.03) in CD133 chip (C). Yellow and blue bars represent the EpCAM and CD133 chips respectively. The Wilcoxon signed-rank test was used in RNA expression for paired samples (n=17).

3.5.2 Hematoxylin & Eosin (H&E) staining and immunohistochemistry (IHC) analysis of primary tissues

We obtained the PDAC tissues, and stained them for the markers of interest based on analysis of CTCs. We previously showed that genes including CXCR1 and BMI1 have ≥ 6 logFC in EpCAM Chip compared to CD133 Chip (Figure 3-27A). We found that, the primary tissues of early stage patients were highly positive (intensity of 3, 100% positivity) for BMI1 protein expression shown by immunohistochemistry (IHC) analysis (Figure 3-28A). The Hematoxylin & Eosin (H&E) staining of the corresponding primary tumor tissue is shown in Figure 3-28A.

We also reported that genes including POU5F1 (or OCT-4), TP53 and MCAM (or CD146) showing ≥ 5 logFC in CD133 Chip compared to EpCAM Chip (Figure 3-27A). IHC analysis of TP53 protein expression in the primary PDAC tissue showed high positivity (intensity of 2, 90% positivity) of this marker (Figure 3-28B). The H&E staining of the corresponding primary tumor tissue is shown in Figure 3-28B. IHC analysis of MCAM protein expression in the primary PDAC tissue was moderate positive (intensity of 2, 30% positivity) (Figure 3-28C). The H&E staining of the corresponding primary tumor tissue is shown in Figure 3-28C.

IHC analysis of CD133 protein expression in the primary PDAC tissue showed different range of positivity (intensity of 1 and 3, 5-60% positivity) of this marker (Figure 3-28D). The H&E staining of the corresponding primary tumor tissues are shown in this figure.

To further explore the gene signatures in different stages of disease, the patients were grouped based on their disease stages (Figure 3-29, Figure 3-30, and Figure 3-31). The summary of selected genes ($p < 0.05$) are shown in the box plots.

3.5.3 Gene expression profiling on stage IIA pancreatic cancer patients (n=5)

Stage IIA patients showed significant differential expression of genes including ATL1, BMi1, CD14, CDH2, ERCC1, MKi67, TTF1, and Vimentin compared to all other stages (Figure 3-29A). We also compared protein level expression of select differentially expressed markers by IHC of primary tissues. The H&E staining of the primary PDAC tissues of early stage patients is shown in Figure 3-29B. The corresponding primary tumor tissues were highly positive (intensity of 3, 100% positivity) for BMi1 protein

expression and moderate positive (intensity of 2, 10% positivity) for MKi67 protein expression shown by IHC analysis (Figure 3-29C).

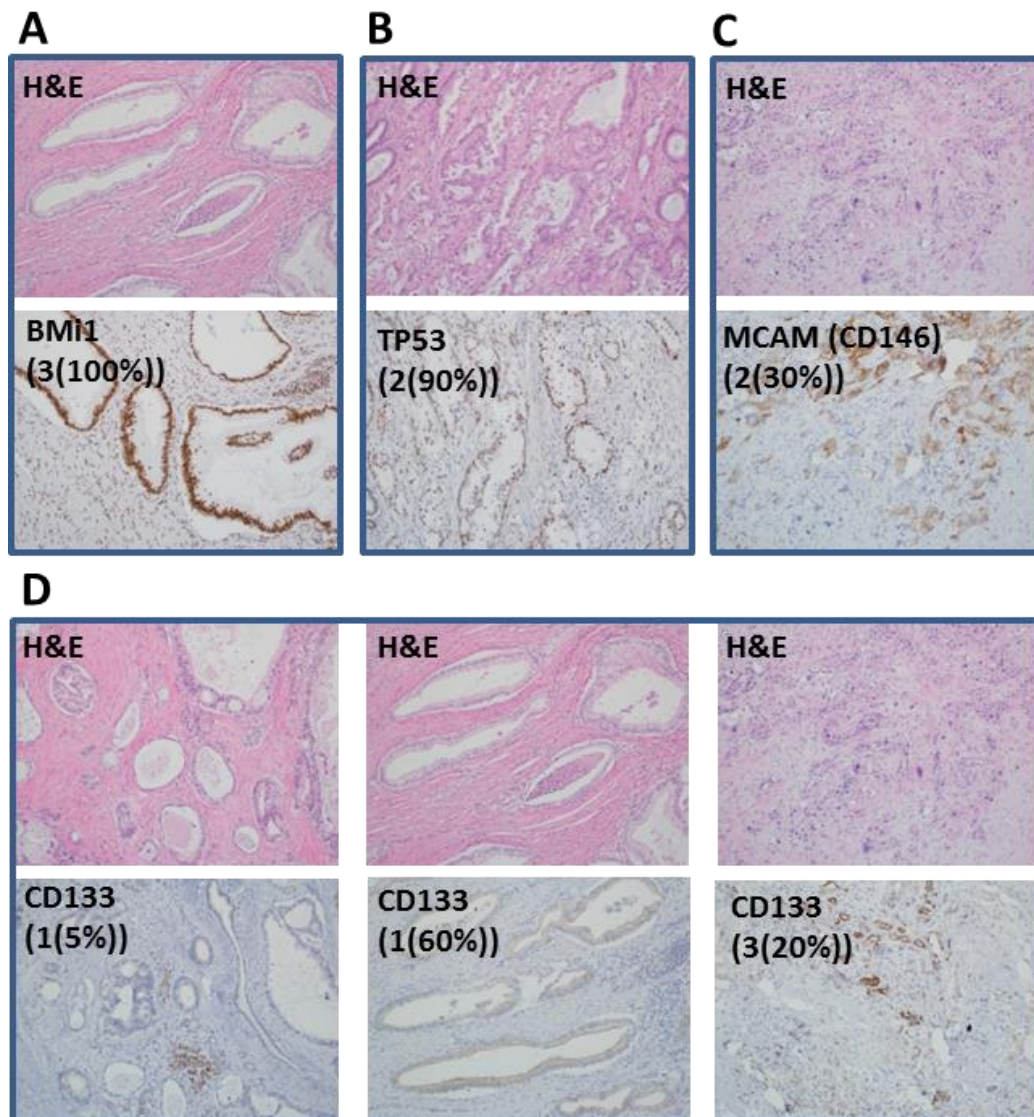


Figure 3-28: Immunohistochemistry of the primary tumor tissues of PDAC patients. A) BMI1 protein expressions (intensity of 3 in 100% tumor cells). B) TP53 marker (intensity of 3 in 90% tumor cells). C) MCAM marker (intensity of 2 in 30% tumor cells). D) CD133 marker from different tissue samples (intensity between 1 and 3 in 5-60% tumor cells). The H&E staining images of the corresponding primary tumor tissues of PDAC patients is shown. Original magnification: x100.

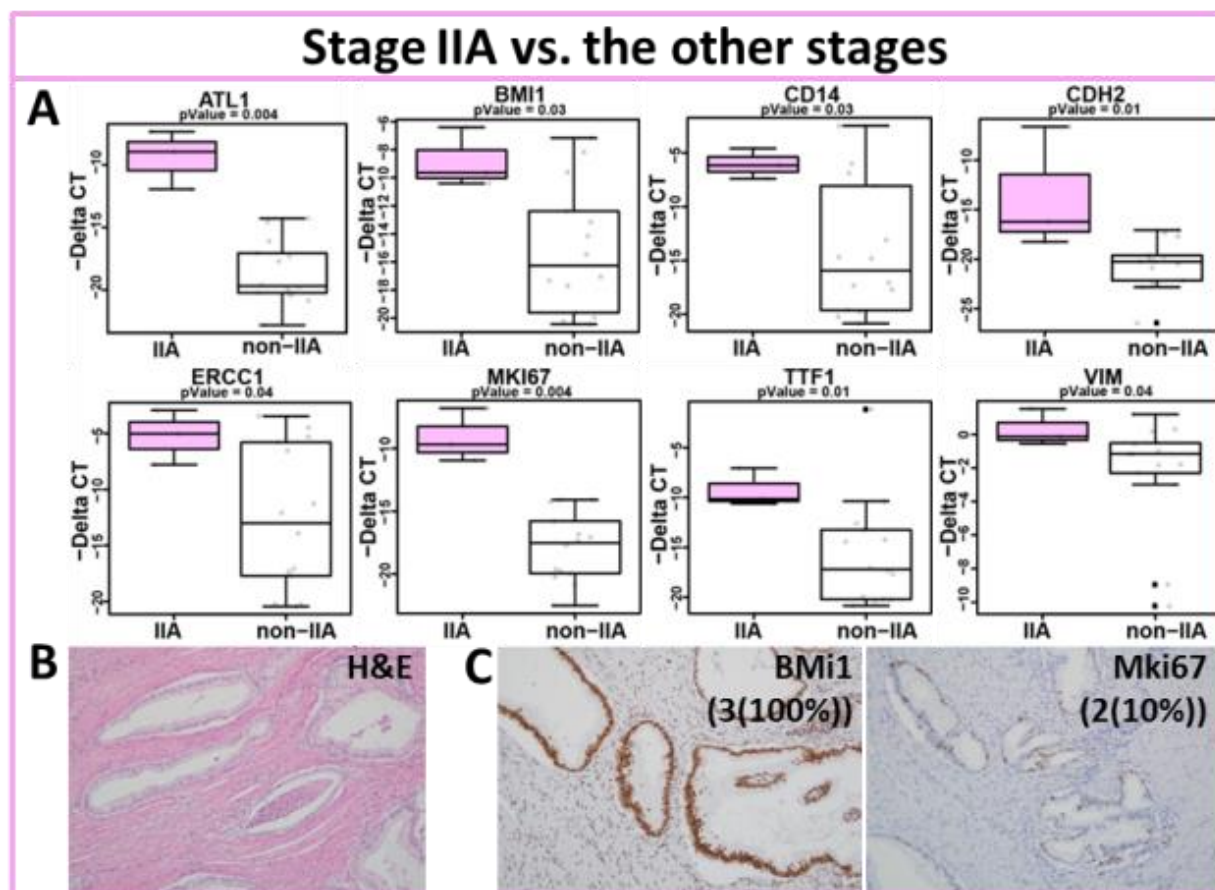


Figure 3-29: Gene expression profiling of CTCs based on stage IIA pancreatic cancer patients. Stage IIA samples (n=5) compared to the rest of stages (n=30) analysis. A) Box plot diagrams of significantly ($p < 0.05$) highly expressed individual genes in stage IIA CTC samples compared to the rest of stages including ATL1, BMI1, CD14, CDH2, ERCC1, MKI67, TTF1, and Vimentin genes. B) The H&E staining image of the primary tumor tissues of early stage patient. C) IHC analysis of the corresponding primary tumor tissues for BMI1 and MKI67 protein expressions revealed diffuse and strong positivity for BMI1 (intensity of 3 in 100% tumor cells), and patchy moderate positivity for MKI67 (intensity of 2 in 10% tumor cells) protein expression. The Mann-Whitney test was used to quantify differences in RNA expression for non-paired samples using the average $-\Delta\text{CT}$ value across both sample chips (n=17).

3.5.4 Gene expression profiling on stage IIB&III pancreatic cancer patients (n=18)

Pancreatic cancer patients in stages IIB&III showed significant differential expression of ALDH1A3, ESR1, KRT18 and KRT19 compared to stage IIA (Figure 3-30A). Comparing stages IIB&III with stage IV patients revealed significant differential expression of genes including AKT1 and CD3D (Figure 3-30B).

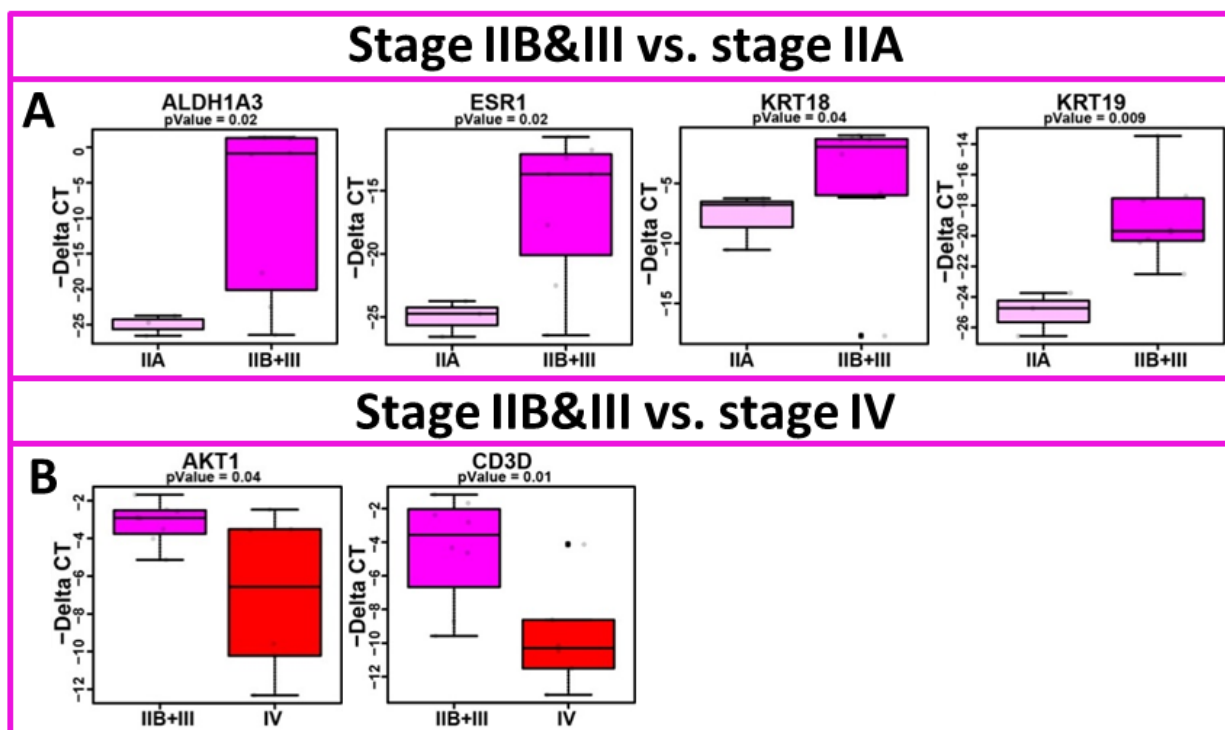


Figure 3-30: Gene expression profiling of CTCs based on stage IIB&III pancreatic cancer patients. A) Box plot diagrams of significantly highly expressed individual genes in stage IIB&III CTC samples (n=18) compared with the early stage (n=5) including ALDH1A3, ESR1, KRT18 and 19, and B) AKT1 and CD3D genes when stage IIB&III (n=18) compared with the late stage (n=12). The Mann-Whitney test was used to quantify differences in RNA expression for non-paired samples using the average $-\Delta Ct$ value across both sample chips (n=17).

3.5.5 Gene expression profiling on stage IV pancreatic cancer patients (n=12)

Stage IV patients showed significantly elevated expression of CDH1, DCN, KRT19, PGR, and PIK3CA genes compared to the rest of the stages (Figure 3-31A). The H&E staining of the primary PDAC tissue of late stage pancreatic cancer patients is shown in Figure 3-31B. The protein expression of PIK3CA in the corresponding primary tumor tissues was moderate (intensity of 2, 20% positivity) (Figure 3-31C).

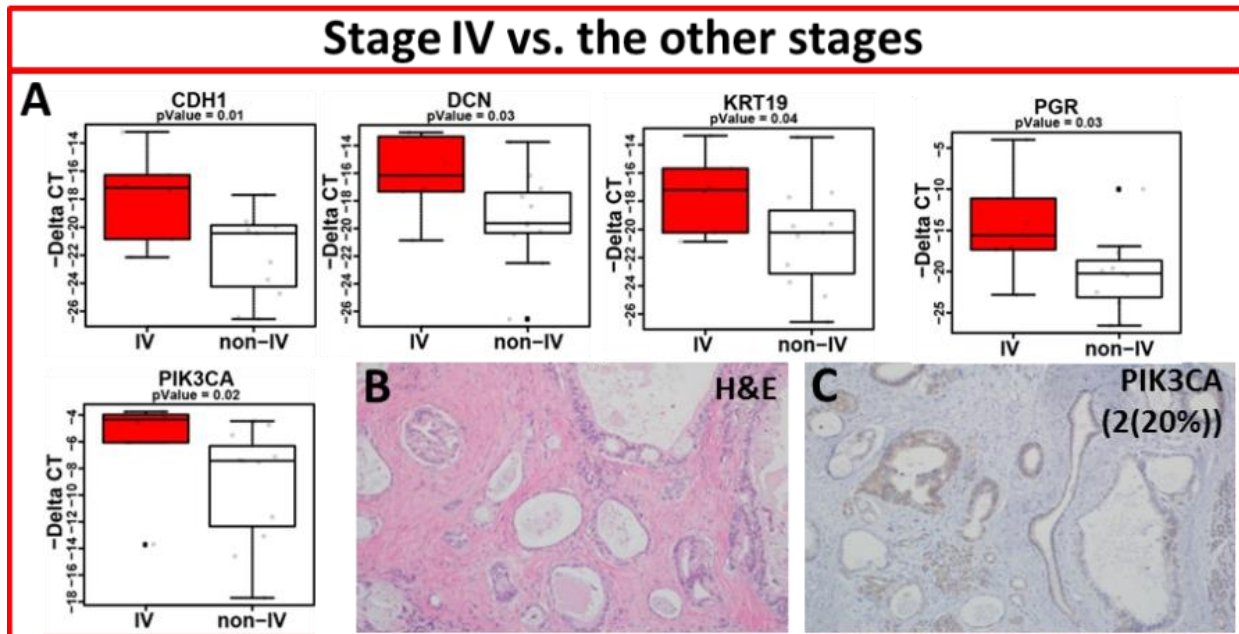


Figure 3-31: Gene expression profiling of CTCs based on stage IV pancreatic cancer patients. A) Stage IV samples (n=12) compared to the rest of the stages (n=23) showed significantly over expression of genes including, CDH1, DCN, KRT19, PGR, and PIK3CA. B) The H&E staining image the primary tumor tissues of late stage patient. C) PIK3CA protein expressions revealed patchy moderate positivity for this gene (intensity of 2 in 20% tumor cells) protein expression with IHC of primary tumor tissues. The Mann-Whitney test was used to quantify differences in RNA expression for non-paired samples using the average $-\Delta Ct$ value across both sample chips (n=17).

3.6 Molecular signature and prognosis

In the cohort considered in this study, the median overall survival (OS) of all patients was 15 ± 10.2 months (m) (2.5-33.7) and the median progression free survival (PFS) was 5.6 ± 10.5 m (1.7-33.5). The survival estimated by Kaplan Meier (KM) were significantly better for patients with high expression of AKT1 (21.1 vs. 6 m $p=0.08$ for OS, and 11.6 vs. 4.6 m $p=0.03$ for PFS), BMI1 (20.4 vs. 13.6 m $p=0.04$ for OS, and 9.2 vs. 4.6 m for PFS), CDH2 (30.2 vs. 14.8 m $p=0.04$ for OS, and 6.9 vs. 5.1 m for PFS), ERCC1 (22.3 vs. 10.6 m $p=0.04$ for OS, and 11.7 vs. 4.6 m $p=0.02$ for PFS), IL8 (21.1 vs. 6 m $p=0.08$ for OS, and 11.6 vs. 4.6 m $p=0.03$ for PFS), TTF1 (20.4 vs. 12.8 m $p=0.08$ for OS, and 9.3 vs. 2.5 m $p=0.04$ for PFS), and TP53 (18 vs. 11.4 m for OS, and 10 vs. 4.6 m $p=0.03$ for PFS) (Figure 3-32A-G). The H&E staining of the primary PDAC tissue of a pancreatic cancer patient is shown in Figure 3-32Hi. IHC analysis of TP53

protein expression in the corresponding primary tumor tissue showed high positivity (intensity of 2, 90% positivity) of this marker (Figure 3-32H-ii). Pancreatic cancer patients with higher expression of metastatic marker GEMIN2 (5 vs. 18 m $p=0.01^*$ for OS, and 4.6 vs. 7.7 m for PFS), and stem marker POU5F1 (13.4 vs. 20.4 m for OS, and 4.6 vs. 10.1 m $p=0.04^*$ for PFS) showed worse OS or PFS respectively (Figure 3-32I-J).

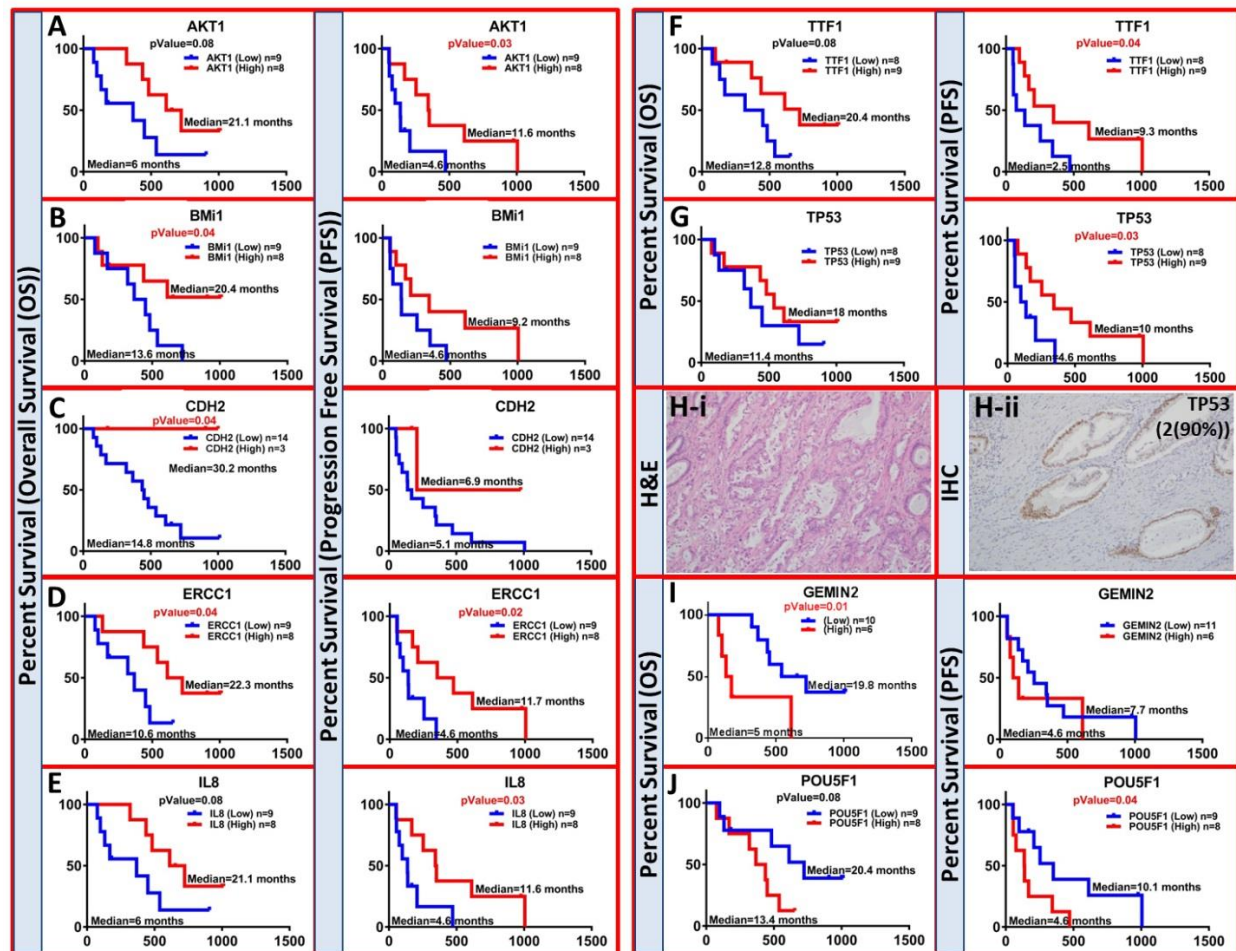


Figure 3-32: Relationship between CTCs gene expression and prognosis. Comparison of Kaplan-Meier overall survival (OS) and progression free survival (PFS) graphs in all patient CTCs samples (n=17) with low (blue) and high (red) expressions of selected genes are shown. The median expression of each gene ($2^{-\Delta Ct}$) across all patients was used as cutoff points. Log-rank (Mantel-Cox) tests were used to analyze the Kaplan-Meier OS and PFS. A-G) Higher expression of genes including BMI1, CDH2, and ERCC1 in pancreatic cancer patients showed significantly greater OS ($p=0.04$). Higher expression of genes including AKT1 ($p=0.03$), ERCC1 ($p=0.02$), IL8 ($p=0.03$), TTF1 ($p=0.04$), and TP53 ($p=0.03$) were significantly correlated with prolonged PFS. H) The H&E staining image of (i) the primary tumor tissue, (ii) and TP53 marker showed diffuse positivity (intensity of 2 in 90% of tumor cells) of this marker in the corresponding primary tumor tissues. I-J) Patients with high expression of genes including, GEMIN2 ($p=0.01$) and POU5F1 ($p=0.04$) had a worse OS and PFS respectively compared with those with low expression of these genes.

3.7 Monitoring patients based on the treatment regime

Analysis of heterogeneous population of pancreatic CTCs will provide greater insight into responses to therapeutic agents. In this study, we simultaneously isolated both EpCs and EMTCs at baseline (treatment naïve) and through treatment courses from limited number of pancreatic cancer patients.

3.7.1 CTC burden monitoring

In limited number of patients (n=8) we had multiple visits and subsequent molecular analysis (n=5) of these samples. Additional information is provided in appendix section (Table 9-7). All patients in visit 1 (treatment naïve) were naïve (n=8); however, 5 samples in visit 2 received chemo treatment in their second visit, and 3 samples were on chemo plus radiation treatment. Patients in visit 3 were received either chemo alone (n=2) or chemo plus radiation treatment (n=2). Patients in visit 4 either received chemo (n=2) or off chemo treatment (n=1). The CTC numbers of pancreatic cancer patient samples (n=8) in different visits are shown in Figure 3-33. EpCs (yellow) and EMTCs (blue) mL⁻¹ in different visits showed that the number of EMTCs were significantly higher in visit 1 and 2 compared to EpCs, also the number of EpCs significantly increased from visit 2 to visit 3 (Figure 3-33).

3.7.2 Gene expression profiling

Gene expression analysis were studied for some of these follow up patient samples (n=5) in their first (treatment naïve) and second (under chemo treatment) visits. The results showed that PIK3CA was significantly upregulated in visit 1 patients. Genes including, ERCC1, CD45, BAX, NANOG, and BCL2 in visit 1 patients, and ESR1,

MCAM, and KRas in visit 2 group showed >8.5 log FC compared to the other cohort (Figure 3-34A).

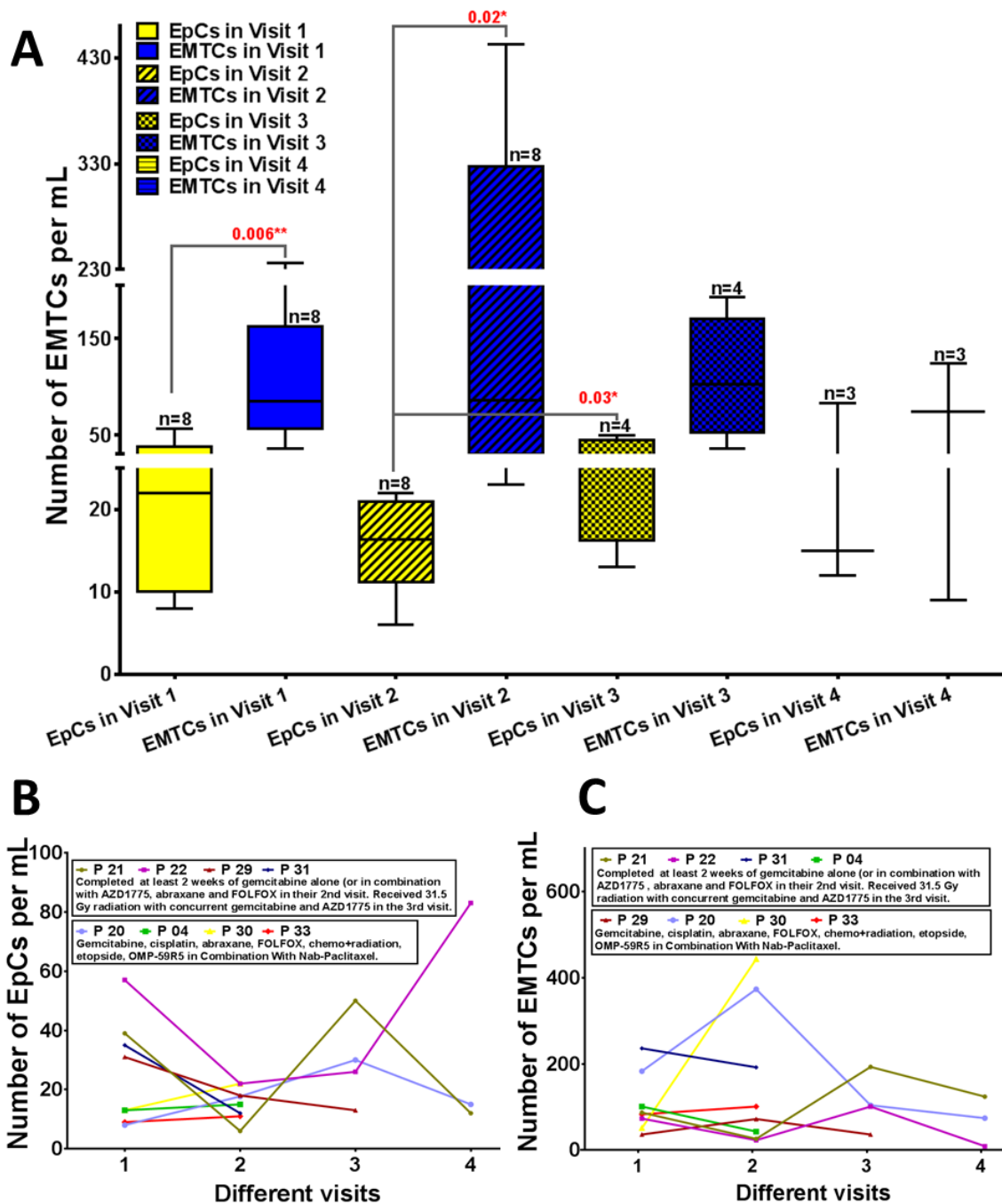


Figure 3-33: CTC numbers of pancreatic cancer patient samples (n=8) over the treatment. A) Numbers of EpCs (yellow) and EMTCs (blue) mL⁻¹ in different visits showed that the number of EMTCs in visit 1 and 2 are significantly higher compared to the EpCs. Numbers of EpCs significantly increased from visit 2 to visit 3. B-C) Numbers of EpC and EMTCs in individual patient samples. Patients were grouped based on increasing (P 20, 04, 30, and 33) and decreasing (P 21, 22, 29, and 31) group in EpCs numbers (B). Patients were grouped based on increasing (P 29, 20, 30, and 33) and decreasing (P 21, 22, 31, and 04) group in EMTCs numbers (C).

The KM estimates were analyzed for these follow up patients (n=5). Patients with high expression of AKT1, CTNNB1, and ERCC1 showed better PFS (24.1 vs. 13.6 m for OS, and 11.7 vs. 3.2 m p=0.03* for PFS) (Figure 3-34B). The OS were significantly worse for patients with high expression of genes including MYC, PGR and, TP53 (13.4 vs. 24.1 m p=0.03* for OS, and 5.1 vs. 11.7 m for PFS) (Figure 3-34C), and POU5F1 (14.6 vs. 28.9 m p=0.06 for OS, and 4.6 vs. 22.6 m p=0.06 for PFS) (Figure 3-34D).

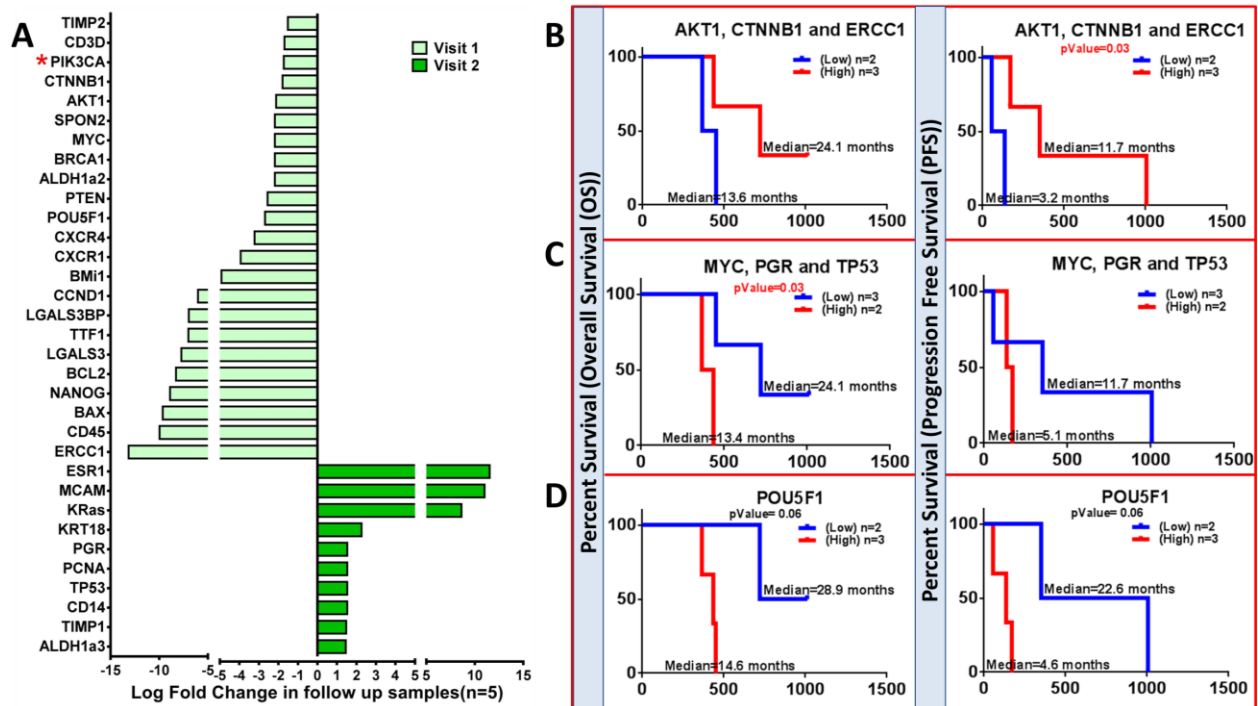


Figure 3-34: Gene expression analysis of pancreatic cancer patient samples (n=5) over the treatment. The median log fold change (log FC) of selected genes with log FC>1.5 is shown for the visit 1 (treatment naïve) patients samples (light green) and for the Visit 2 patient (under chemotherapy) samples (dark green). Each fold change is calculated from the $2^{\Delta\Delta Ct}$. PIK3CA gene showed significantly higher in patients with naïve patients. B-D) The KM for OS and PFS of the selected genes which had log FC >1.5 in different visits of patients (n=5). B) Higher expression of genes including AKT1, CTNNB1, and ERCC1 led to longer OS and PFS (*). C-D) Higher expression of genes including MYC, PGR, TP53, and POU5F1 (or OCT-4) led to worse OS and PFS.

3.8 Application of the CTC Carpet chip in PDAC xenograft model

PDAC is characterized by a dense stroma, which is heterogeneous and composed of both cellular and acellular components.¹⁹⁷ The cellular component mostly consists of mesenchymal-appearing spindle-shaped cells (cancer associated fibroblast or CAFs), immune and vascular cells.¹⁹⁷ It has been hypothesized that the stroma contributes to the aggressive nature of PDAC; however the precise role of the stroma in pancreatic tumorigenesis remains controversial. Earlier studies using in vitro assays, xenografts, and genetically engineered mouse models have suggested that activated cells promote tumor growth and metastasis.¹⁹⁷

The aim of this study was to isolate both CTCs and CFCs (circulating fibroblast cells) from a patient-derived PDAC xenograft model.¹⁹⁷ The model system was established by injecting 10^5 GFP (green fluorescent protein)-luciferase-labeled tumor cells mixed with the same number of DSRred (red fluorescent protein)-labeled cancer associated fibroblast (CAF) and cancer associated mesenchymal stem cells (CA-MSC) subcutaneously into NOD-SCID mice (n=26). GFP-luciferase-labeled tumor cells (CAF and CA-MSC) injected alone served as the experimental controls. Upon tumor formation in mice, blood samples were collected for the CTC and CFC counts. Tumors were harvested from mice, digested into single cells and then cultured for secondary reimplantation in a new cohort of NOD-SCID mice after FACS flow sorting. After the formation of the secondary tumors, blood samples were again collected for the CTC and CFC counts. An overview of the experimental plan is shown in Figure 3-35.

Injection of tumor cells alone resulted in the development of small tumors comparable in size to those generated by injection of tumor cells plus CAF cells over

the 1.4 week period of study, while larger tumors developed in the tumor cells plus CA-
MSC group¹⁹⁷ (Figure 3-36).

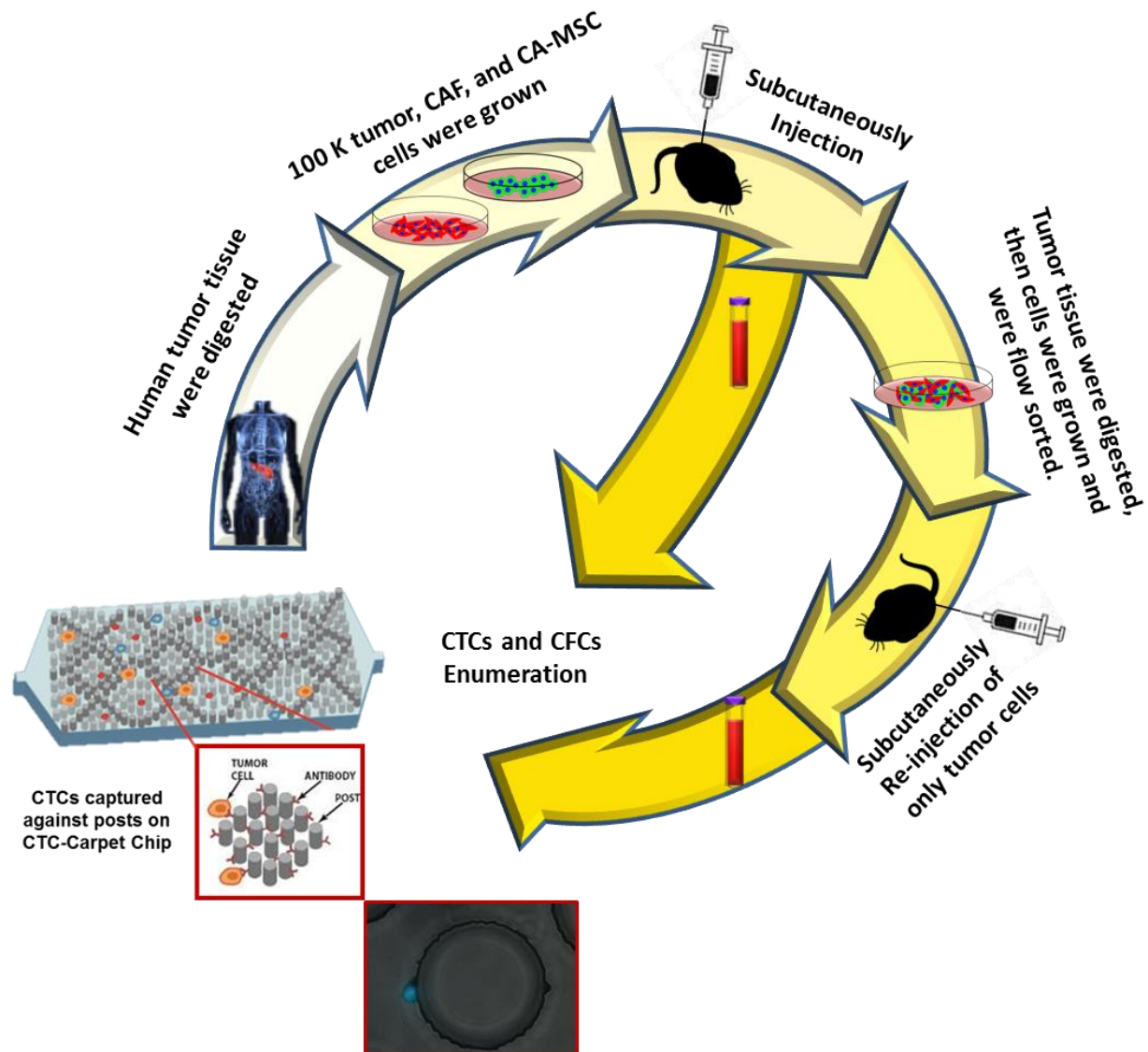


Figure 3-35: Strategies of the application of CTC Carpet Chip to isolate both CTCs and CFCs from pancreatic cancer mouse model.

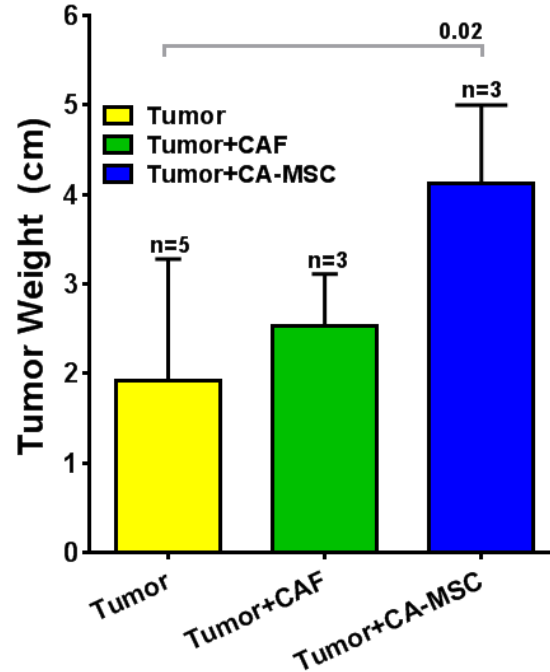


Figure 3-36: Pancreatic cancer cells transduced with a luciferase-expressing lentivirus were subcutaneously injected alone or with CAF or CA-MSC into NOD/SCID mice. Bioluminescent-based tumor growth (measured by signal intensity p/s/cm²) of luciferase tumors alone or in combination with CAFs or CA-MSCs (MSCs). Larger tumor sizes were found the tumor plus CA-MSC group.

For metastatic progression to occur, carcinoma cells must traverse through the basement membrane and disseminate into the bloodstream. Hence we examined the presence and extent of circulating GFP-labeled tumor cells and DSRed-labeled CAFs and CA-MSCs from the mouse blood samples using the CTC Carpet Chip. Figure 3-37 presents some examples of the captured GFP-labeled tumor cells (CTCs) in the form of single CTCs (Figure 3-37A) and clusters (Figure 3-37B) in the CTC Carpet Chip. H&E staining of some captured cells are also shown in Figure 3-37C.

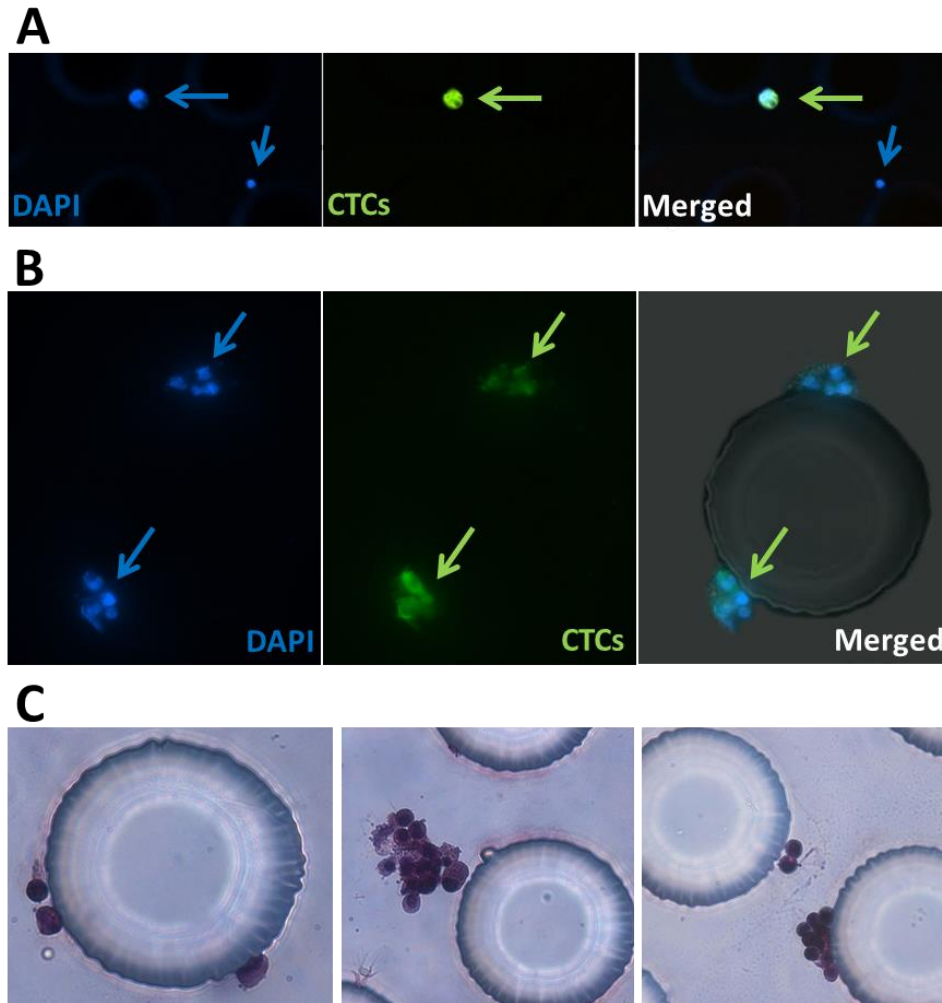


Figure 3-37: Representative images of captured circulating GFP⁺ tumor cells (CTCs) using CTC Carpet Chip from mice blood samples. A) A single captured CTC along with a WBC. B) Cluster form of CTCs. C) H&E staining of the capture CTCs around the posts.

Circulating GFP⁺ tumor cells were detected in all three groups; tumor alone, tumor plus CAF and CA-MSC, however there was a significant increase in the number of circulating GFP⁺ tumor cells in the tumor cells plus CA-MSC group compared to the tumor cells alone and tumor cells plus CAF groups (Figure 3-38 and Table 3-2). Further DSRred positive circulating cells were detected in only the tumor cells plus CA-MSC mice group.

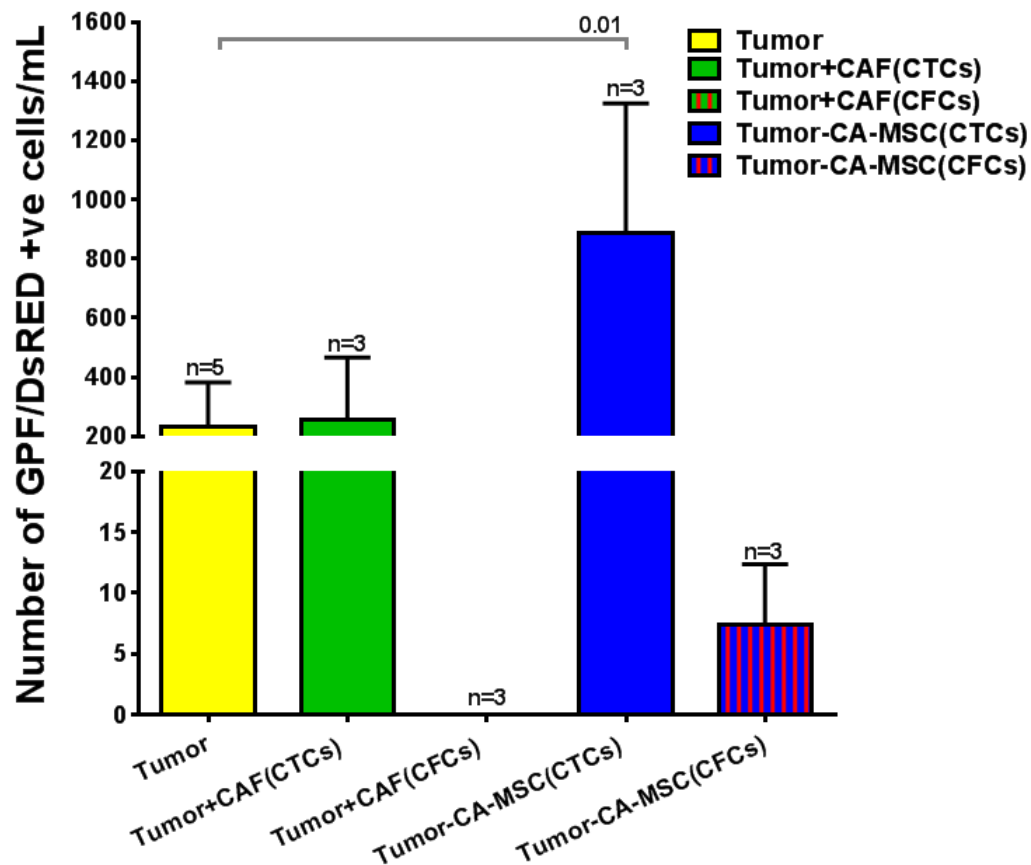


Figure 3-38: Quantification of circulating GFP+ tumor cells (CTCs) in tumor alone, tumor plus CAF, and CA-MSC groups and DsRed+ fibroblasts cells (CFCs) in tumor+CAF and CA-MSC groups. The presence of CA-MSC increased the number of CTCs compare to the tumor alone group significantly.

Table 3-2: Numbers of GFP+ tumor cells (CTCs) in tumor alone, tumor plus CAF, and CA-MSC groups and DsRed+ fibroblasts cells (CFCs) in tumor+CAF and CA-MSC groups.

Tumor	Tumor+CAF (CTCs)	Tumor+CAF (CFCs)	Tumor-CA-MSC (CTCs)	Tumor-CA-MSC (CFCs)
316	160	0	382	2
352	32	0	1180	12
82	104	0	1096	8
352	496	0	280	0
52	-	-	136	2

Furthermore, the primary tumors from the mice were harvested, digested, and both tumor and CAF/CA-MSC cells were grown in culture. This mixed population was then FACS sorted, and only tumor cells were re-injected subcutaneously into NOD-SCID mice (n=13). After the tumor formation, we examined the presence of circulating GFP-labeled tumor cells by using the CTC Carpet Chip. The number of the GFP positive cells (CTCs) in all tumor alone and tumor plus CAF/CA-MSC groups in the

second injection was significantly higher compared to the first injection group (Figure 3-39 and Table 3-3).

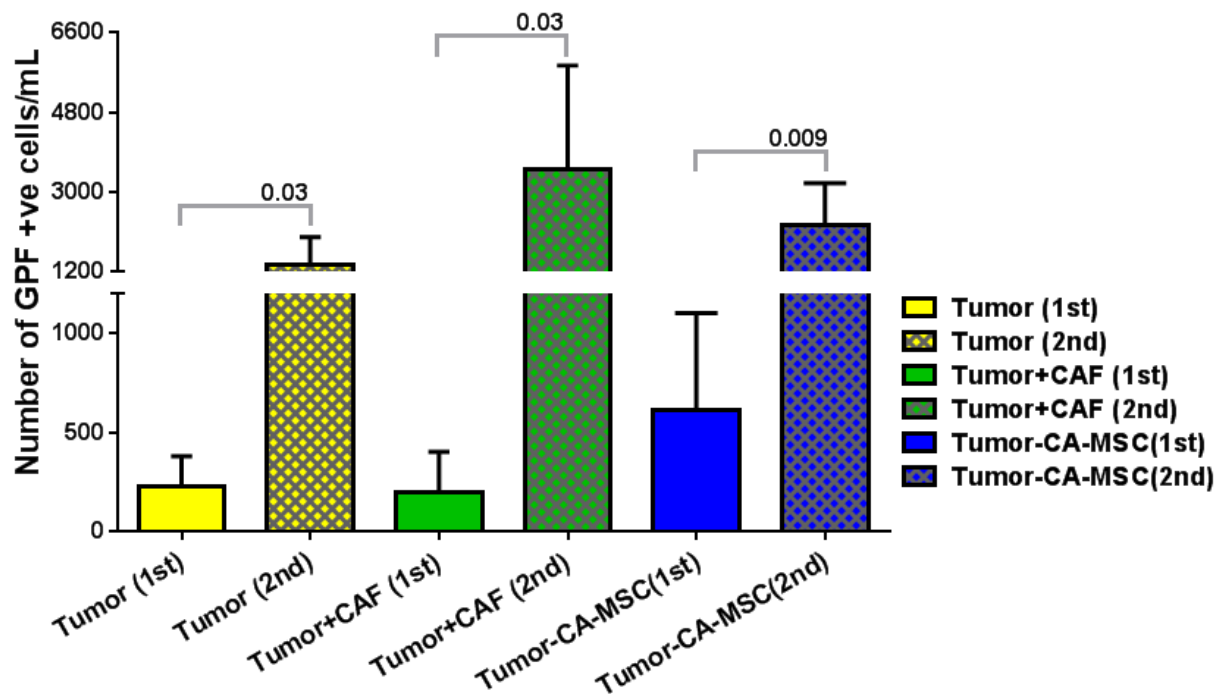


Figure 3-39: The effect of the reinjection on the number of GFP positive cells on the tumor, tumor plus CAF CA-MSC groups. The CTC numbers in all groups were significantly higher in the 2nd injection.

Table 3-3: Numbers of GFP positive tumor cells (CTCs) in tumor, tumor plus CAF and CA-MSC groups in the first and second injection.

Tumor (1st)	Tumor (2nd)	Tumor+CAF (1st)	Tumor+CAF (2nd)	Tumor-CA-MSC (1st)	Tumor-CA-MSC (2nd)
316	524	160	2750	382	2740
352	1245	32	6840	1180	1445
82	1530	104	1330	1096	1013
352	2055	496	3130	280	2945
52	-	-	-	136	3085

3.9 Application of the Labyrinth technology in pancreatic cancer patients

The overall strategy of this clinical study was to validate the utility of CTCs as a tool for assessing tumor response to the only three therapy options available for pancreatic cancer: surgery, chemotherapy, and radiotherapy (Figure 3-40).

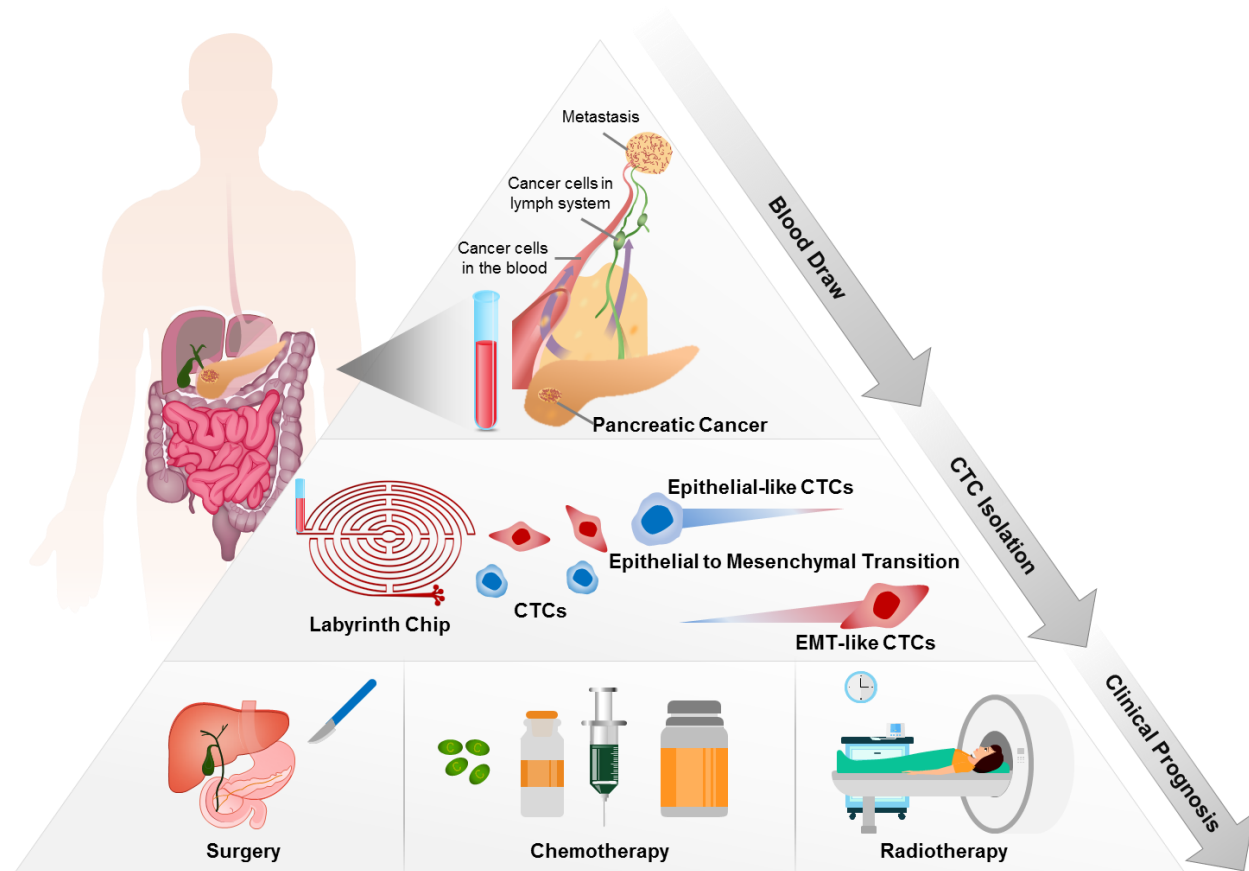


Figure 3-40: Experimental outline for isolation of CTCs in pancreatic cancer patients using Labyrinth technology.

3.9.1 Optimization of Labyrinth using pancreatic cancer cell line

As demonstrated previously, the long loops and sharp corners in the Labyrinth device enhance the separation of CTCs from other blood components.¹⁰³ The device consists of 11 loops and 56 corners. The loops have a small curvature ratio to provide enough channel length to achieve total focusing of CTCs from other blood cells. In contrast, the sharp corners have a high curvature ratio to enhance the focusing of blood

cells. Labyrinth has one inlet and 4 outlet channels (Figure 3-41A). The device has 637 mm channel length in total, with 500 μm in width and 100 μm in height (Figure 3-41B). The outlets were designed such that outlet #1 collects WBCs, outlet #2 collects CTCs, and outlets #3 and #4 collect red blood cells (RBCs) and other blood components. The device was loaded with red food dye to show the structure of Labyrinth (Figure 3-41C).

The Labyrinth was first tested and optimized for CTC isolation using Panc-1 cell line. Different cell concentrations (10, 100, and 10^5) were spiked into whole blood and processed through the Labyrinth (section 2.9). In all cases the cell recovery was above 88%, suggesting that the Labyrinth is a promising tool to isolate CTCs from pancreatic cancer patients (Figure 3-41D).¹⁹⁸

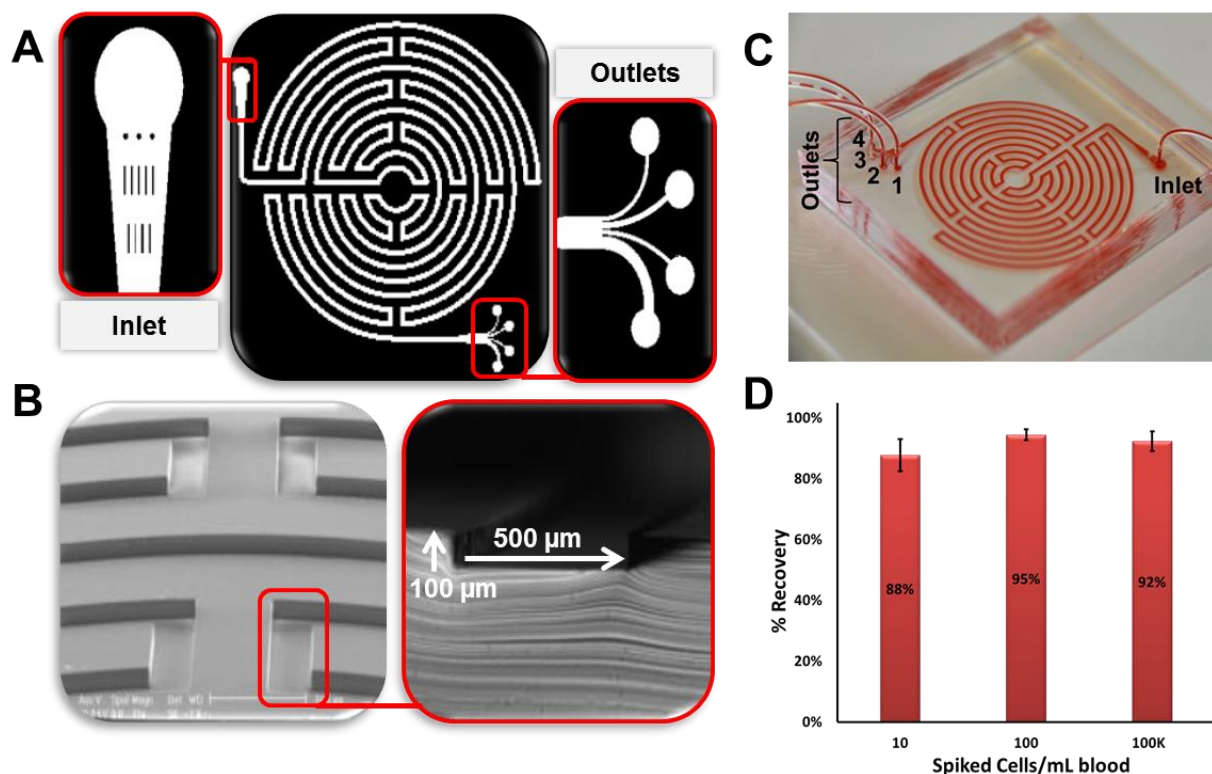


Figure 3-41: The illustration of Labyrinth device. A) Labyrinth device consisting of with one inlet and 4 outlets. B) SEM images of the channel in labyrinth and cross-sectional view of labyrinth taken with microscope. C) The Labyrinth was loaded with red dye to show the device's structure as well as the inlet and outlets. D) Optimization of Labyrinth with Panc-1 cell line.

One hundred and forty one treatment naïve pancreatic cancer patients were enrolled in this study. Additional information is provided in appendix section (Table 9-8). Similar to the Carpet CTC Chip study in pancreatic cancer (section 3.4.1), the isolated CTCs were classified as epithelial CTCs and EMT-like CTCs. The epithelial CTCs were enumerated as PanCK+/CD45-/DAPI+ (Figure 3-42A), while the EMT-like CTCs were identified as PanCK+/Zeb1+/CD45-/DAPI+ (Figure 3-42B). Total CTC number was equal to the sum of these two populations.

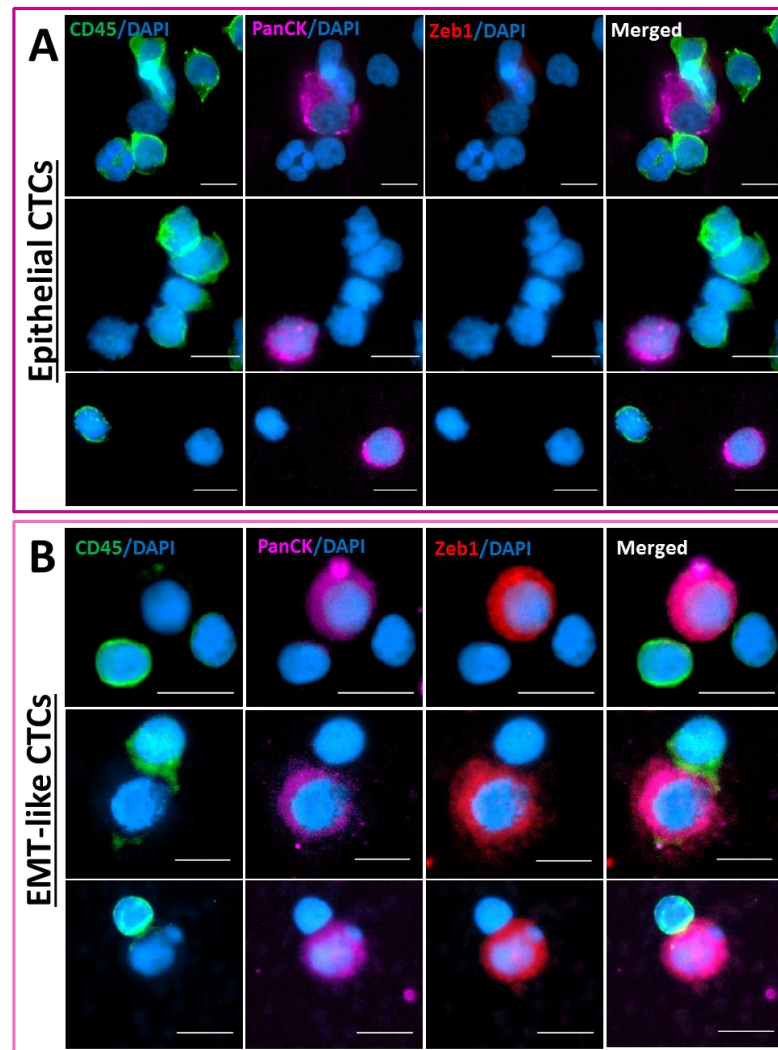


Figure 3-42: Characterization of heterogeneous CTC populations in pancreatic cancer using Labyrinth. A) Circulating epithelial CTCs (PanCK+/CD45-/DAPI+), B) EMT-like CTCs (PanCK+/Zeb1+/CD45-/DAPI+). Scale bar is 10µm.

3.9.2 CTC enumeration for treatment naïve cohort

Utilizing Labyrinth device, CTCs were isolated from treatment naïve pancreatic cancer patient blood samples (n=141). These patients were classified according to their tumor staging: resectable (n=35), borderline resectable (n=32), locally advanced (n=25), and metastatic (n=49). Figure 3-43A shows the epithelial and EMT-like CTCs counts for treatment naïve pancreatic cancer patients. Overall, 18.7 ± 21 total CTCs, 9.7 ± 15.7 epithelial CTCs, and 9 ± 9.8 EMT-like CTCs were observed across all samples (n=141).

The resectable group had 14.6 ± 16.6 total CTCs, 6.3 ± 10.1 epithelial CTCs, and 8.3 ± 8.8 EMT-like CTCs (n=35). The borderline resectable group had 29.5 ± 28.9 total CTCs, 16.3 ± 21.1 epithelial CTCs, and 13.2 ± 12.8 EMT-like CTCs (n=32). The locally advanced cohort had 15.6 ± 14.4 total CTCs, 8.3 ± 11.8 epithelial CTCs, and 7.3 ± 6.6 EMT-like CTCs (n=25). The metastatic group had 16.3 ± 18.5 total CTCs, 8.6 ± 15.7 epithelial CTCs, and 7.7 ± 9.1 EMT-like CTCs (n=49) (Figure 3-43B). Statistical significance was observed when the borderline resectable cohort was compared to the resectable group (p=0.01), locally advanced group (p=0.03), and metastatic cohort (p=0.01) using the unpaired t-test.

Figure 3-44 shows the overall survival probability for the treatment naïve cohort (Figure 3-44A). Classification based on the stages confirms the increased mortality rate in advanced stages (Figure 3-44B).

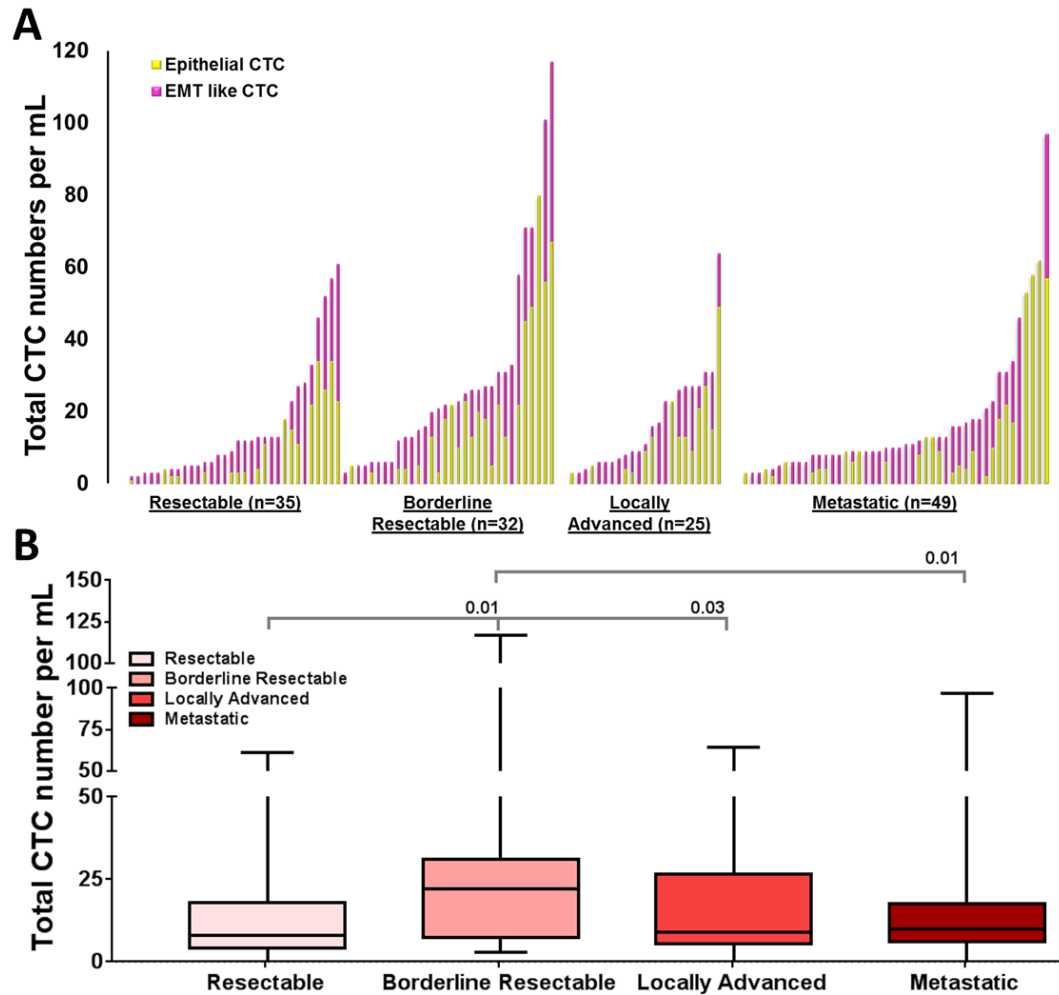


Figure 3-43: CTC enumeration of treatment naïve pancreatic cancer patients using Labyrinth. A) Enumeration of both epithelial CTCs and EMT-like CTCs across all the treatment naïve patient samples (n=141). B) Box plot graph of total CTCs counts stratified by cancer stage, resectable, borderline resectable, locally advanced, and metastasis. The CTC numbers were significantly higher in borderline resectable cohort compared to the other groups using unpaired t-test.

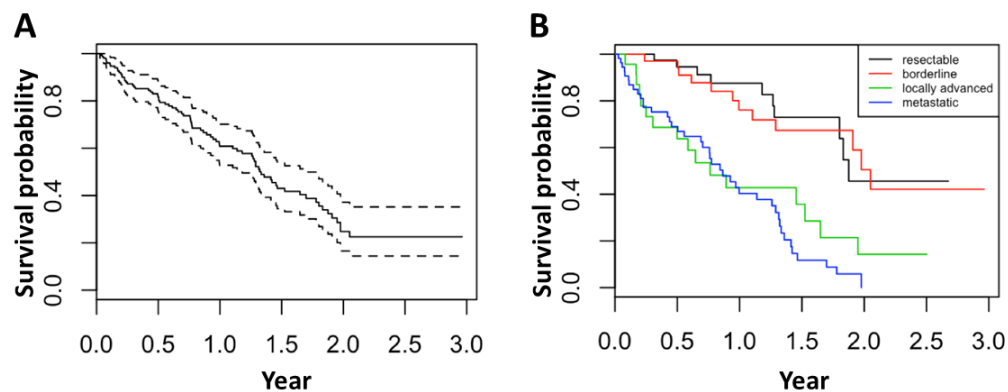


Figure 3-44: KM curve for overall survival probability in treatment naïve (A), and in treatment naïve samples grouped by cancer stage (B). Advanced stages patient samples showed lower OS compared to the early stages samples.

3.9.3 CTC enumeration before and after the treatment regime

Changes in CTC counts were evaluated for pancreatic cancer patients who were undergoing surgery, chemotherapy, and radiation. Additional information is provided in appendix section (Table 9-9) for the surgery cohort (n=29). The blood samples were collected 22 days (median) prior to surgery and 33 days (median) post-surgery. The total CTC numbers were decreased in the post-surgery cohort but not significantly (Figure 3-45A). However, when patients were categorized based on the stages, the CTC numbers were significantly decreased in the pre- and post-surgery samples ($p=0.02$) (Figure 3-45B).

The effect of chemotherapy on CTC numbers was evaluated prior, during, and after the course of treatment. The blood samples (n=35) were collected 20 days (median) prior to the chemotherapy (pre-chemo), and 85 days (median) post treatment (on-chemo). Additional information is provided in appendix section (Table 9-10). The numbers of CTCs (total CTCs ($p=0.04$), epithelia CTCs ($p=0.01$), and EMT-like CTCs ($p=0.03$)) were significantly decreased from the pre-chemo group to on-chemo cohort (n=35) (Figure 3-46).

For the pre- and post-chemotherapy group, the blood samples (n=22) were collected 13 days (median) prior to the chemotherapy (pre-chemo), and 51 days (median) post treatment (post-chemo). Additional information is provided in appendix section (Table 9-11). The numbers of total and epithelial CTCs were significantly decreased from the pre-chemo group to on-chemo cohort ($p=0.002$ and 0.005 respectively) (Figure 3-47).

We also evaluated the effect of radiotherapy on CTC counts for 12 patient samples. Sample collection was performed 135 days (median) prior to the treatment

and 72 days (median) post treatment. Additional information is provided in appendix section (Table 9-12). A statistically significant decrease was observed in total CTC counts after the treatment ($p=0.04$) (Figure 3-48).

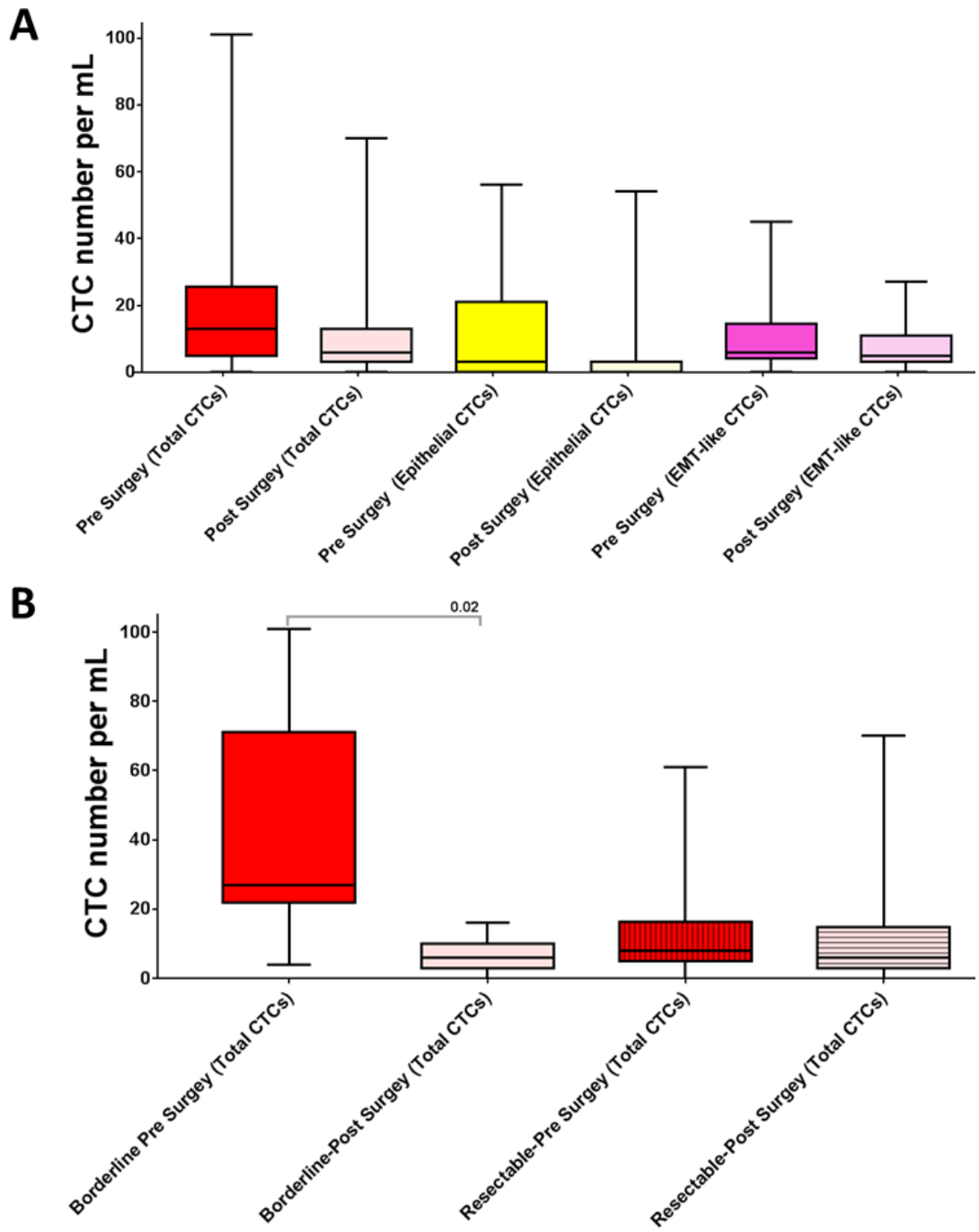


Figure 3-45: CTC enumeration for pre- and post-surgery cohort (n=29). A) No significant differences were observed across different CTC subpopulations (total CTCs, epithelial CTCs and EMT-like CTCs). B) Significantly lower numbers of CTCs were observed in the borderline group after surgery. Paired t-test was used to analyze the effect of surgery on the CTC numbers.

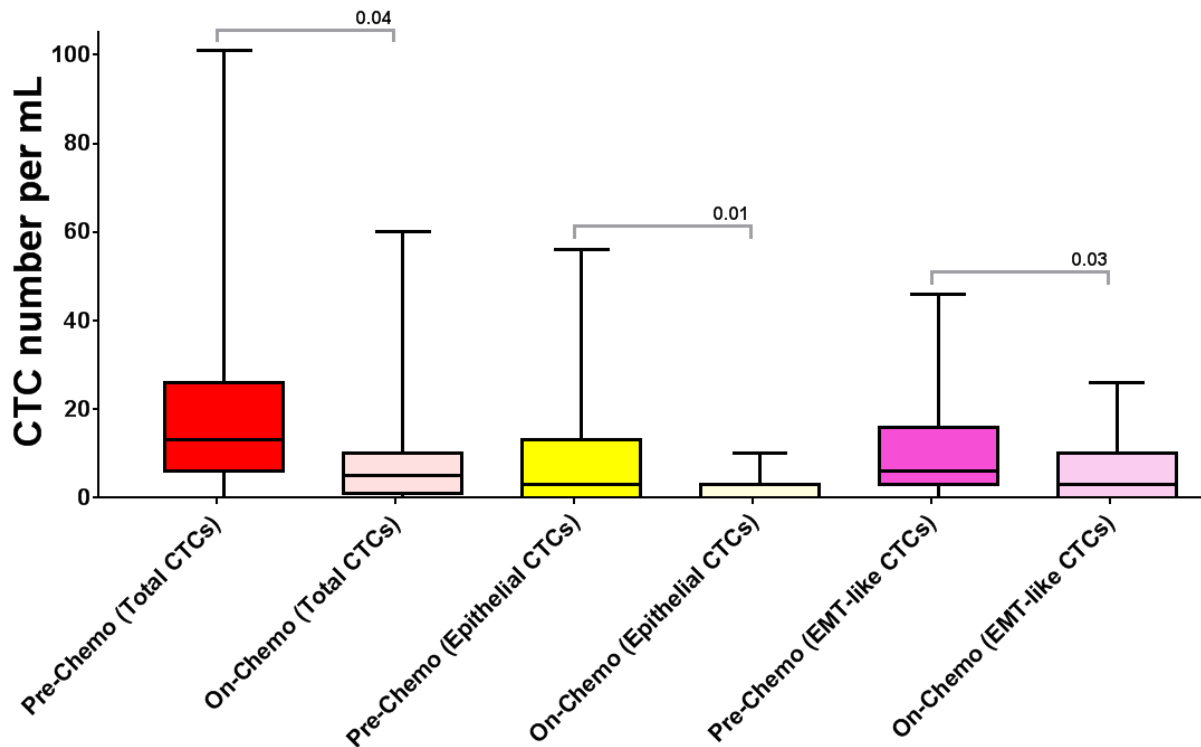


Figure 3-46: CTC enumeration for pre- and on-chemotherapy cohort (n=35). Significantly lower number of CTCs were observed across different CTC subpopulations (total CTCs $p=0.04$, epithelial CTCs $p=0.01$, and EMT-like CTCs $p=0.03$). Paired t-test was used to analyze the effect of chemotherapy on the CTC numbers.

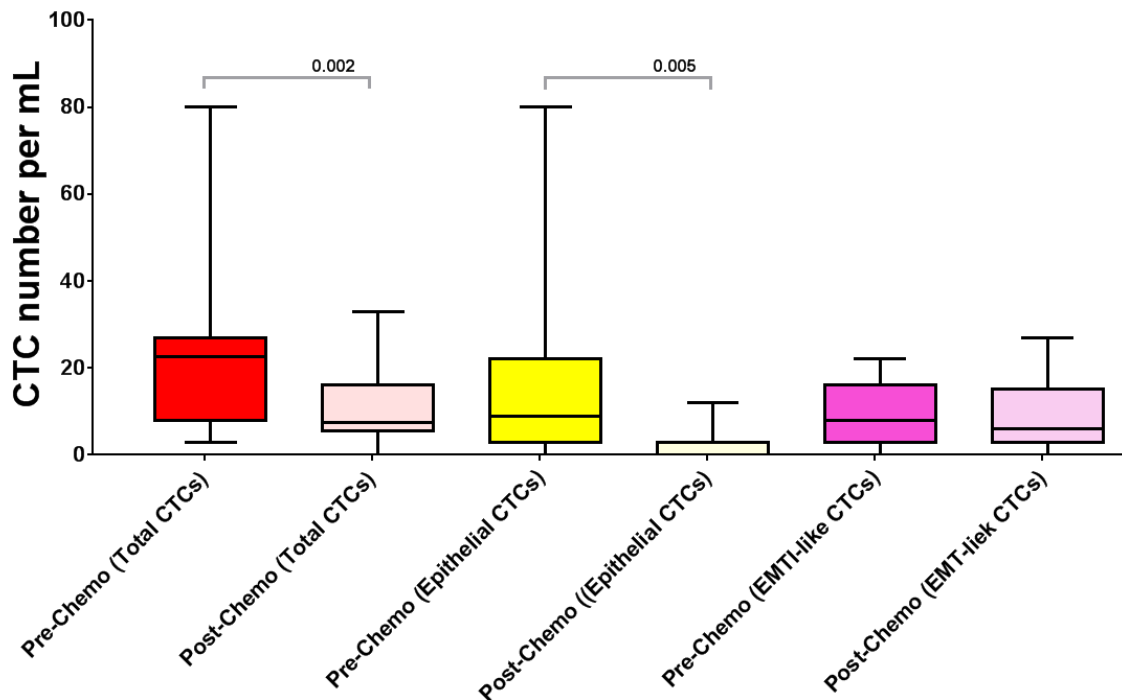


Figure 3-47: CTC enumeration for pre and post chemotherapy cohort (n=22). Significantly lower number of CTCs were observed across different CTC subpopulations (total CTCs $p=0.02$ and epithelial CTCs $p=0.005$). Paired t-test was used to analyze the effect of chemotherapy on the CTC numbers.

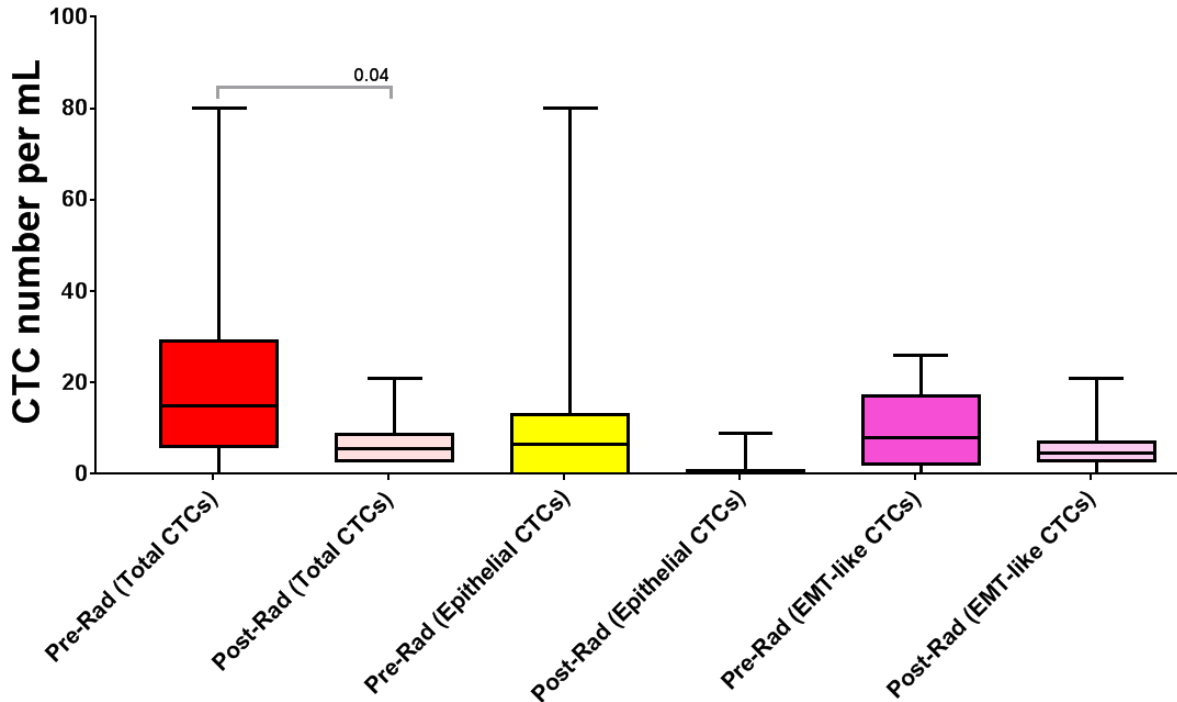


Figure 3-48: CTC enumeration for pre- and post-radiation cohort (n=12). Significantly lower number of CTCs were observed in total CTCs $p=0.04$. Paired t-test was used to analyze the effect of chemotherapy on the CTC numbers.

3.9.4 CTC counts to predict the prognosis in pancreatic cancer

The correlation of overall survival with the decrease of CTC counts after treatment was evaluated for all of the mentioned treatments options. The KM curve for pre- and post-surgery (Figure 3-49A), pre- and on-chemotherapy (Figure 3-49B), pre- and post-chemotherapy (Figure 3-49C), and pre- and post-radiation (Figure 3-49D) cohort was graphed. In the surgery group, 17/29 patient samples had a decrease in CTC numbers. For chemotherapy treated patients sample groups, 24/35 and 18/22 samples had significantly lower CTC numbers in pre-/on-chemotherapy and pre-/post-chemotherapy groups respectively. The CTC numbers dropped in 9/12 radiotherapy-treated patient samples. Therefore, a decrease in CTC counts was correlated with a higher probability of survival across all treatment options.

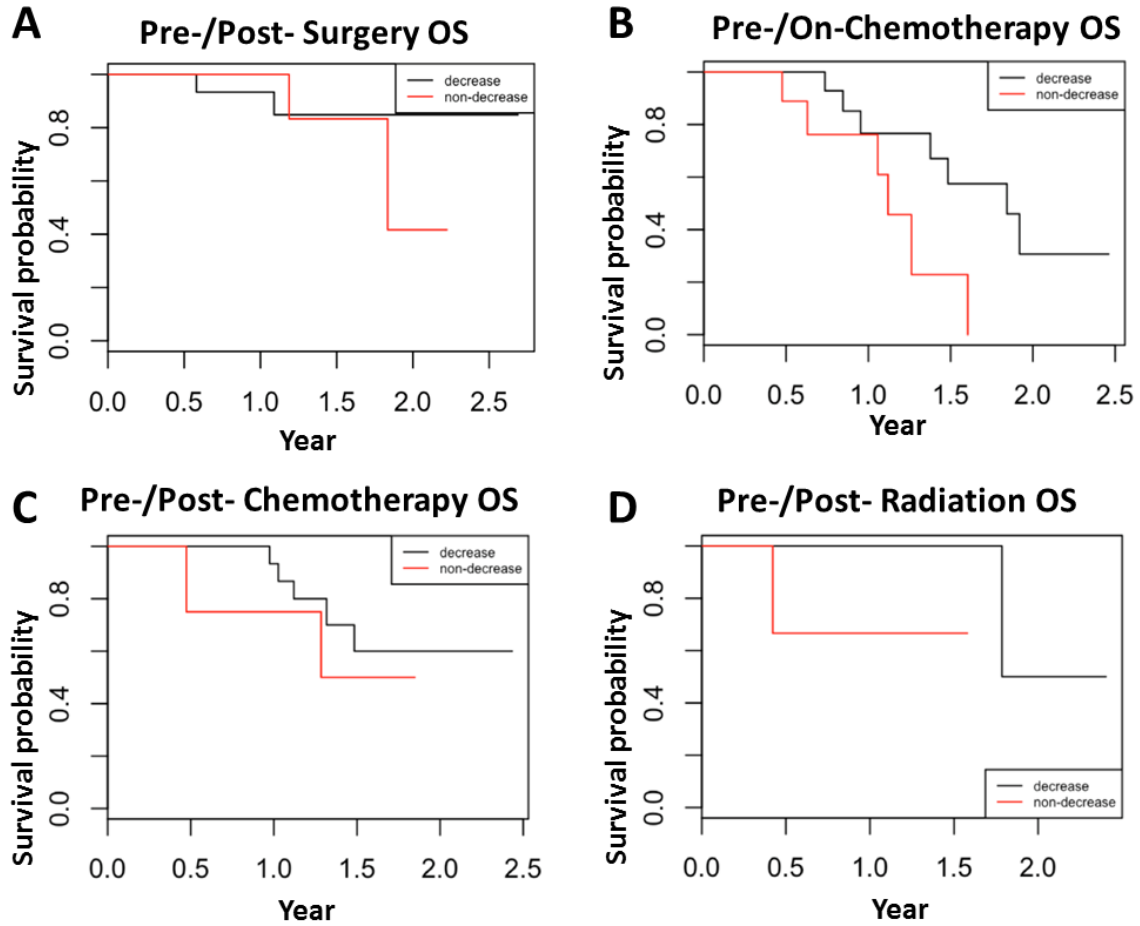


Figure 3-49: CTC counts to predict the prognosis in pancreatic cancer. KM curve for overall survival in A) surgery, B-C) chemotherapy, and D) radiotherapy patient cohorts. In all groups decrease in CTC numbers in post treatment patient samples prolong their OS.

3.10 High throughput label-free isolation of heterogeneous CTCs from non-small cell lung cancer (NSCLC) patients for targeted therapy using Labyrinth

The overall strategy of this clinical study was to utilizing the Labyrinth device to isolate CTCs from non-small cell lung cancer patients (NSCLC) (Figure 3-50).

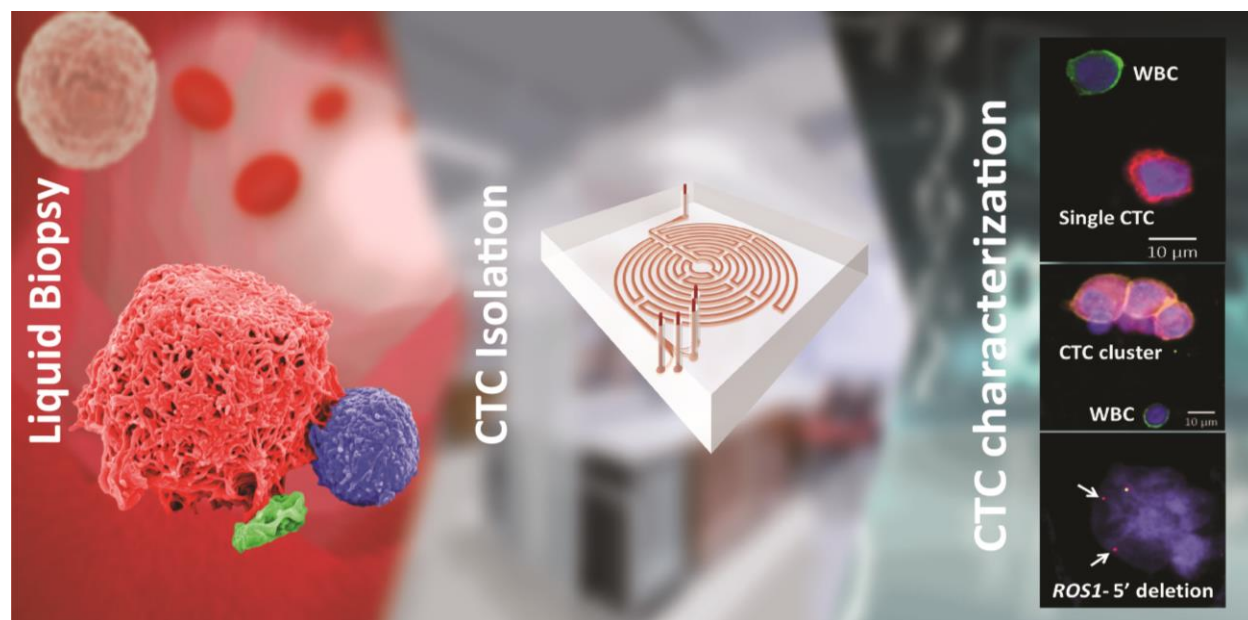


Figure 3-50: High throughput and label-free Labyrinth device demonstrated the advantages of marker-independent separation methods in identifying heterogonous CTC sub-population in non-small cell lung cancer patients.

3.10.1 Optimization of Labyrinth for lung cell line recovery

Labyrinth was optimized and tested for inertial separation of cancer cells using different human lung cancer cell lines. To demonstrate cell focusing in the device, the same concentration of pre-labeled cancer cells with green CellTracker and pre-labeled WBCs with DAPI (1000 cells mL⁻¹) were spiked into PBS and separated using the Labyrinth. First, various flow rates ranging from 1500-3000 µl min⁻¹ were tested to check the focusing and separation of labeled WBCs with DAPI (blue stream) and the pre-labeled lung cancer cell lines (green stream) into individual outlets (Figure 3-51A, Figure 3-52A, Figure 3-53A, and Figure 3-54A).

Products were collected after flow stabilization (1.5 min) for calculating the percentage of CTC recoveries and WBC depletion. Meanwhile, the intensity of separation of WBCs and cancer cells were measured (Figure 3-51B, Figure 3-52B, and Figure 3-53B). Afterward, the % cell recovery (Figure 3-51C, Figure 3-52C, Figure 3-53C, and Figure 3-54B) and % WBCs depletion were analyzed (Figure 3-51D, Figure 3-52D, Figure 3-53D, and Figure 3-54C).

Using PC-9 cell line, 95% of cells were recovered from outlet #2 at a flow rate of $2400 \mu\text{L min}^{-1}$ (Figure 3-51C), with 93% WBCs depletion from outlet #1 (Figure 3-51D).

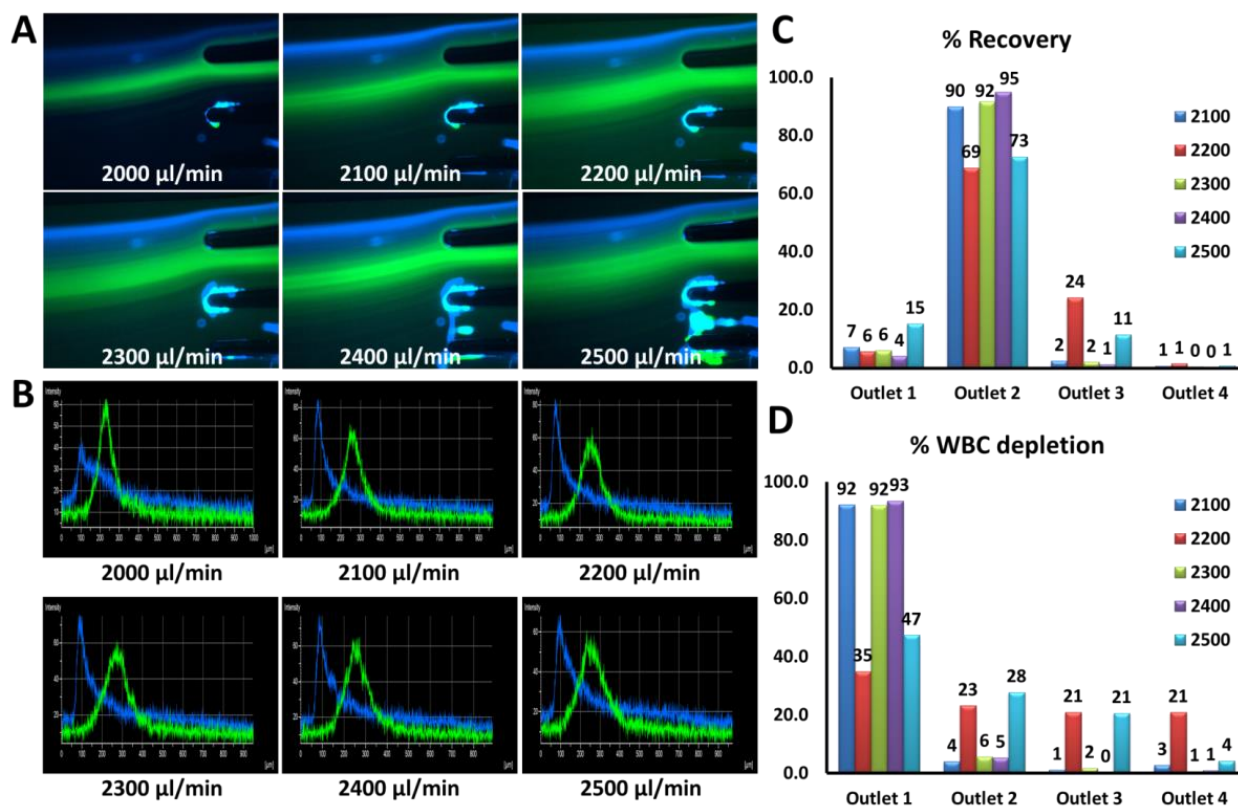


Figure 3-51: Labyrinth optimization using PC-9 cell line for cell recovery. A) The separation of labeled WBCs (blue) and PC-9 cell line (green) into individual outlets. B) The intensity of these separations was measured. C) % Recovery of PC-9 from all five tested flow rates ($2100\text{-}2500 \mu\text{L min}^{-1}$). D) % WBCs depletion from the all five flow rates ($2100\text{-}2500 \mu\text{L min}^{-1}$). 95% of the PC-9 cells were recovered from outlet #2 using $2400 \mu\text{L min}^{-1}$ with 93% WBCs depletion from outlet #1.

Using H1975 cell line, 46% of cells were recovered from outlet #2 at a flow rate of 2300 $\mu\text{L min}^{-1}$ (Figure 3-52C), with 78% WBCs depletion from outlet #1 (Figure 3-52D).

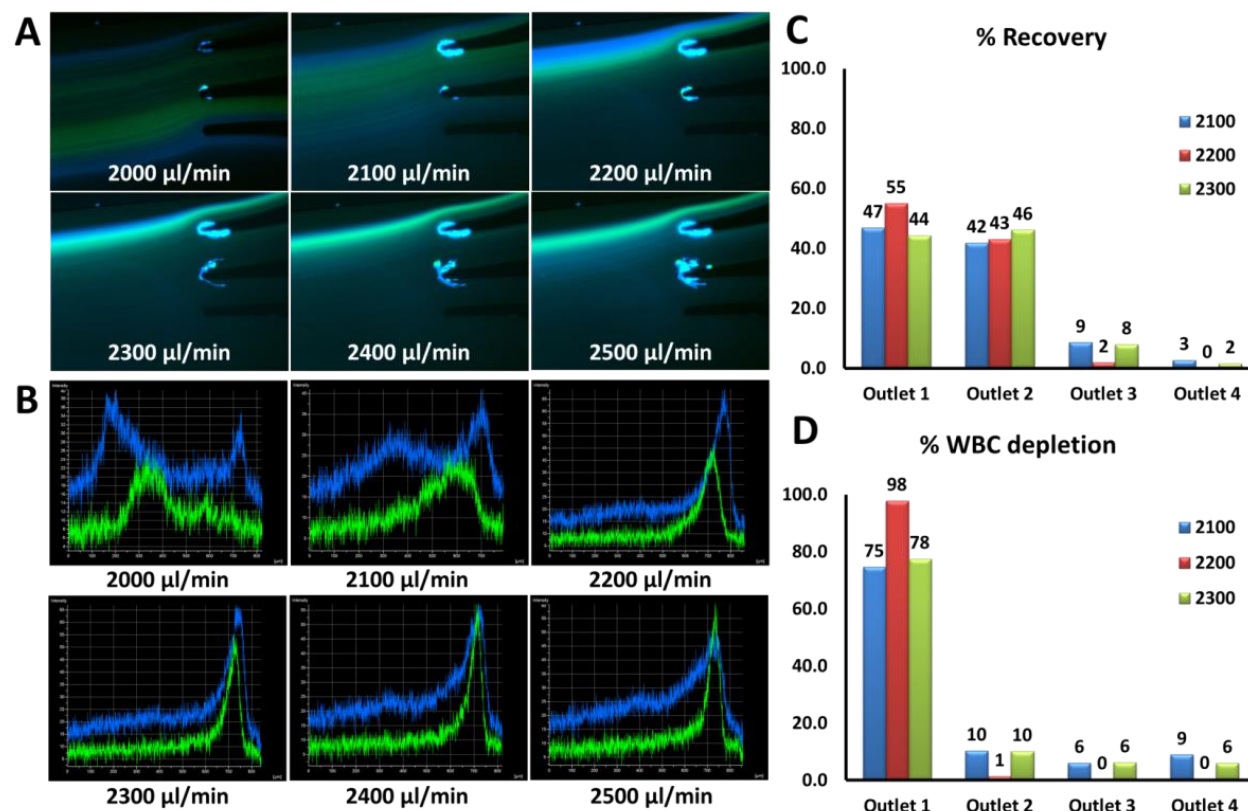


Figure 3-52: Labyrinth optimization using H1975 cell line for cell recovery. A) The separation of labeled WBCs (blue) and H1975 cell line (green) into individual outlets. B) The intensity of these separations was measured. C) % Recovery of H1975 from all three tested flow rates (2100-2300 $\mu\text{L min}^{-1}$). D) % WBCs depletion from the all five flow rates (2100-2300 $\mu\text{L min}^{-1}$). 46% of the H1975 cells were recovered from outlet #2 using 2300 $\mu\text{L min}^{-1}$ with 78% WBCs depletion from outlet #1.

Using HCC827 cell line, 63% of cells were recovered from outlet #2 at a flow rate of 2400 $\mu\text{L min}^{-1}$ (Figure 3-53C), with 67% WBCs depletion from outlet #1 (Figure 3-53D). Finally using the H1650 cell line, 82% of cancer cells were recovered at a flow rate of 2500 $\mu\text{L min}^{-1}$ (Figure 3-54B), while 78% of WBCs were removed (Figure 3-54C). This flow rate was used to process the patient samples.

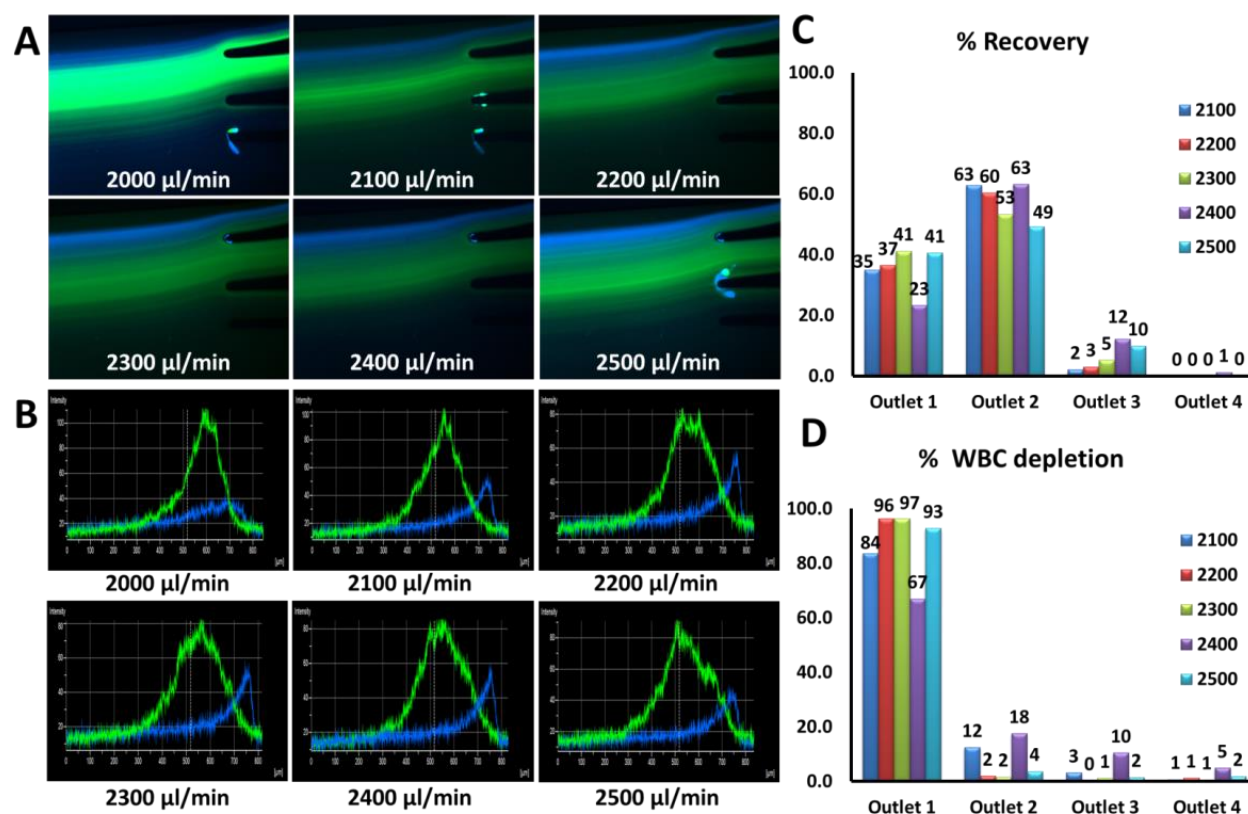


Figure 3-53: Labyrinth optimization using HCC827 cell line for cell recovery. A) The separation of labeled WBCs (blue) and HCC827 cell line (green) into individual outlets. B) The intensity of these separations was measured. C) % Recovery of HCC827 from all three tested flow rates (2100-2500 $\mu\text{l min}^{-1}$). D) % WBCs depletion from the all five flow rates (2100-2500 $\mu\text{l min}^{-1}$). 63% of the HCC827 cells were recovered from outlet #2 using 2400 $\mu\text{l min}^{-1}$ with 67% WBCs depletion from outlet #1.

To identify CTCs in patient samples, immunofluorescence staining was optimized with a panel of antibodies (anti-CD45, anti-PanCK, anti-EpCAM, and anti-Vimentin) using NSCLC cell lines including H1975 and A549 (section 2.9) (Figure 3-55). Using the optimized immunofluorescence staining protocol, both H1975 and A549 were positive for PanCK and negative for CD45. Furthermore, these cells expressed EpCAM and Vimentin as expected.

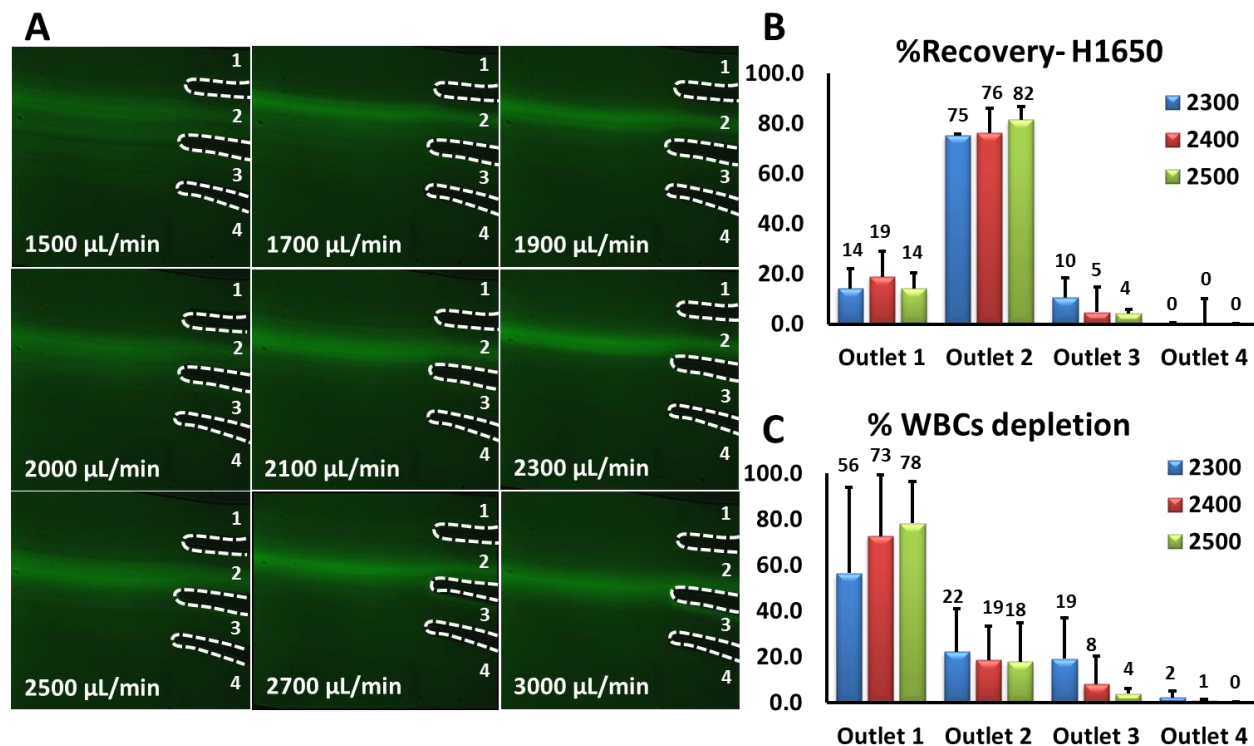


Figure 3-54: Labyrinth optimization using H1650 cell line. A) Device's optimization with H1650 cell line. 10^5 cells of pre-labeled H1650 cell line were spiked into PBS and processed through the Labyrinth with different flow rates ranging from 1500-3000 $\mu\text{L min}^{-1}$. B-C) Pre-labeled H1650 cell line and DAPI-labeled WBCs (1000 cells) were spiked into PBS and processed through the Labyrinth. Using flow rate at 2500 $\mu\text{L min}^{-1}$, 82% \pm 5% of H1650 cells were recovered from outlet #2 and 78% \pm 18% of WBCs were removed through outlet #1.

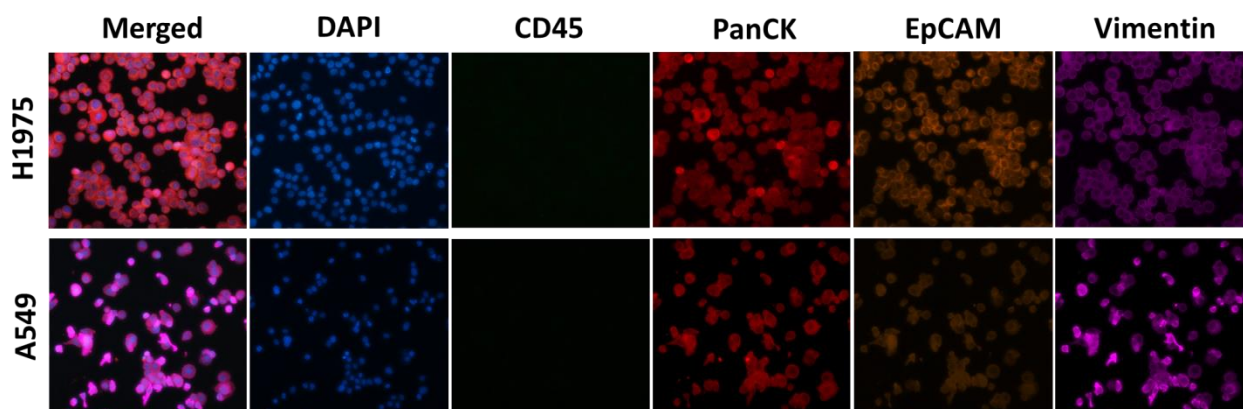


Figure 3-55: Immunofluorescence staining optimization using NSCLC cell lines. Anti-human CD45, anti-human PanCK, anti-human EpCAM, and anti-human Vimentin antibodies were tested with lung cancer cell lines, H1975 and A549.

3.10.2 Isolation of CTCs from NSCLC Patients

CTCs were isolated from peripheral blood samples collected from 21 patients with metastatic, stage IV NSCLC. Additional information is provided in appendix section (Table 9-13). These patient samples were processed through the Labyrinth (section 2.9). After isolation, the product from the outlet #2 was analyzed for CTCs. CTCs were detected by immunofluorescence staining (section 2.9). Cells with the PanCK+/CD45-/DAPI+ phenotype were identified and enumerated as CTCs. Figure 3-56A shows immunofluorescence staining of an isolated single CTC stained for PanCK (red) and CD45 (green) to distinguish CTCs from WBCs. Figure 3-56B and Figure 3-56C illustrate confocal images of isolated CTCs in clusters of 2 cells (Figure 3-56B) and 3 cells (Figure 3-56C).

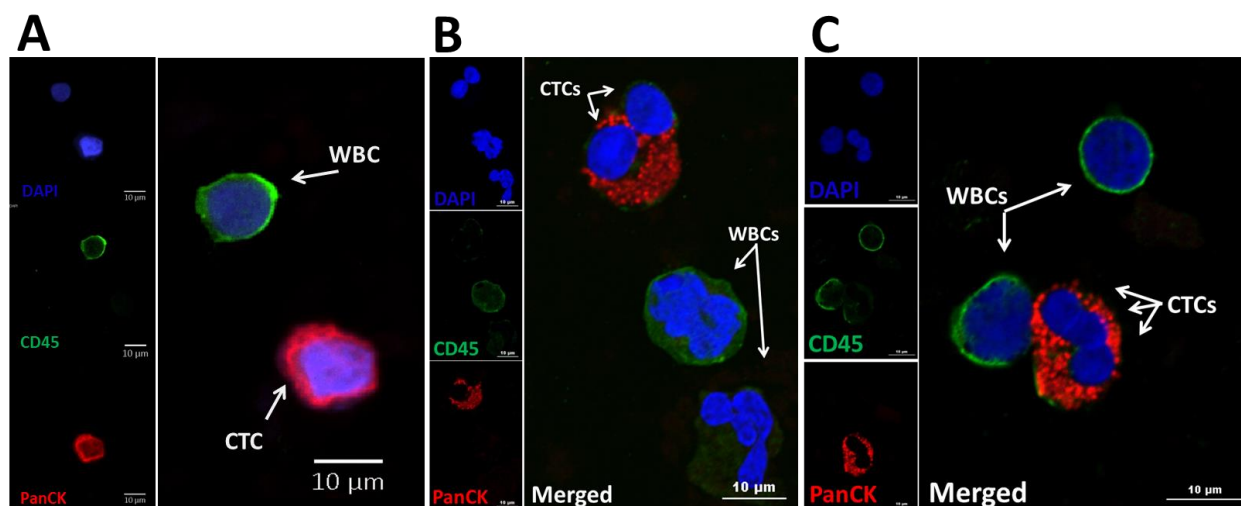


Figure 3-56: Immunofluorescence staining images of the representative images of some CTCs recovered from NSCLC patients samples. A) Fluorescent microscope image of a single CTC. Cells are stained with DAPI (blue), PanCK (red) and CD45 (green). B-C) Confocal microscopy images of some CTC clusters.

We determined that all 21 patients (100%) had detectable CTCs with an average of 180 CTC mL⁻¹ (10.2-631.4). In contrast, low numbers of CTC mL⁻¹ (0-

3) were observed in the HCs (Figure 3-57). Additional information is provided in appendix section (Table 9-14).

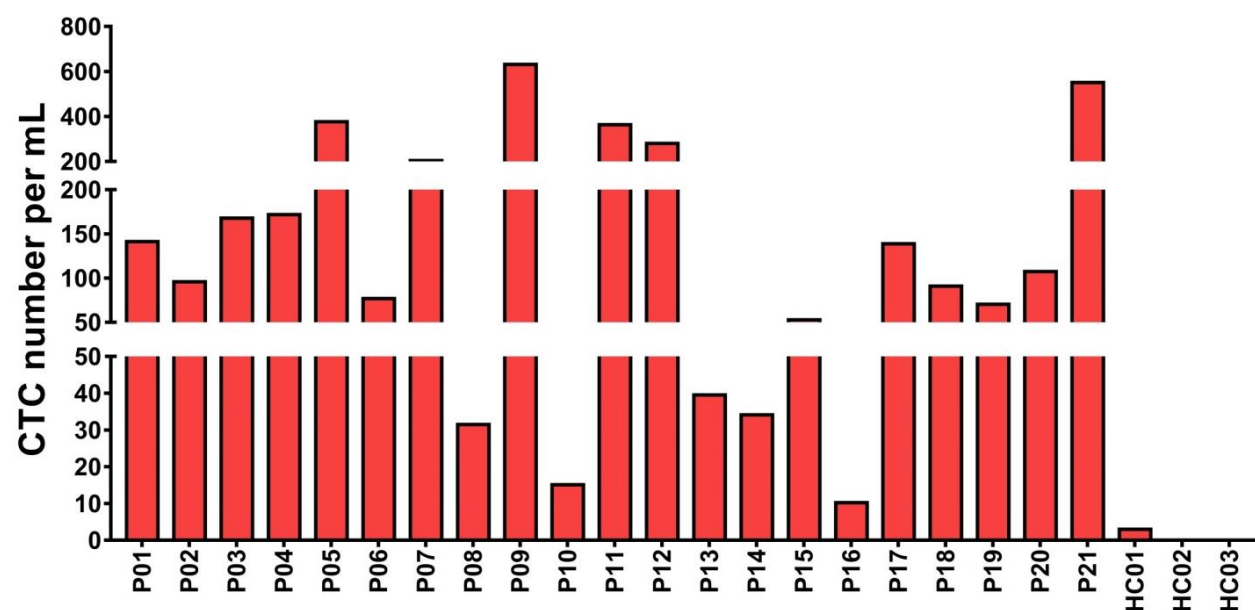


Figure 3-57: Isolation of CTCs from NSCLC patients (n=21). An individual bar plots of number of CTCs recovered from NSCLC patient samples, using Labyrinth, at baseline. Significant differences between the overall numbers of CTCs in NSCLC patients samples ($180 \pm 167.9 \text{ mL}^{-1}$) vs. HCs ($1 \pm 1.7 \text{ mL}^{-1}$) was observed ($p=0.001$). Mann-Whitney unpaired t-test analysis was used for comparing patient cohort vs. healthy controls.

3.10.3 Identification of heterogeneous CTC subpopulations isolated using Labyrinth

Isolated CTCs from a subset of NSCLC patients (n=19) were further examined to determine the percentage of cells that displayed epithelial and mesenchymal markers. We used EpCAM (for epithelial phenotype) and Vimentin (for mesenchymal phenotype), in addition to PanCK (tumor marker), CD45 (leukocyte marker), and DAPI (nuclear marker). CTCs were defined as cells positive for PanCK, and DAPI, but negative for CD45. We further categorized CTCs into subpopulations based on expression of EpCAM, Vimentin, or double expression of EpCAM and Vimentin (Figure 3-58).

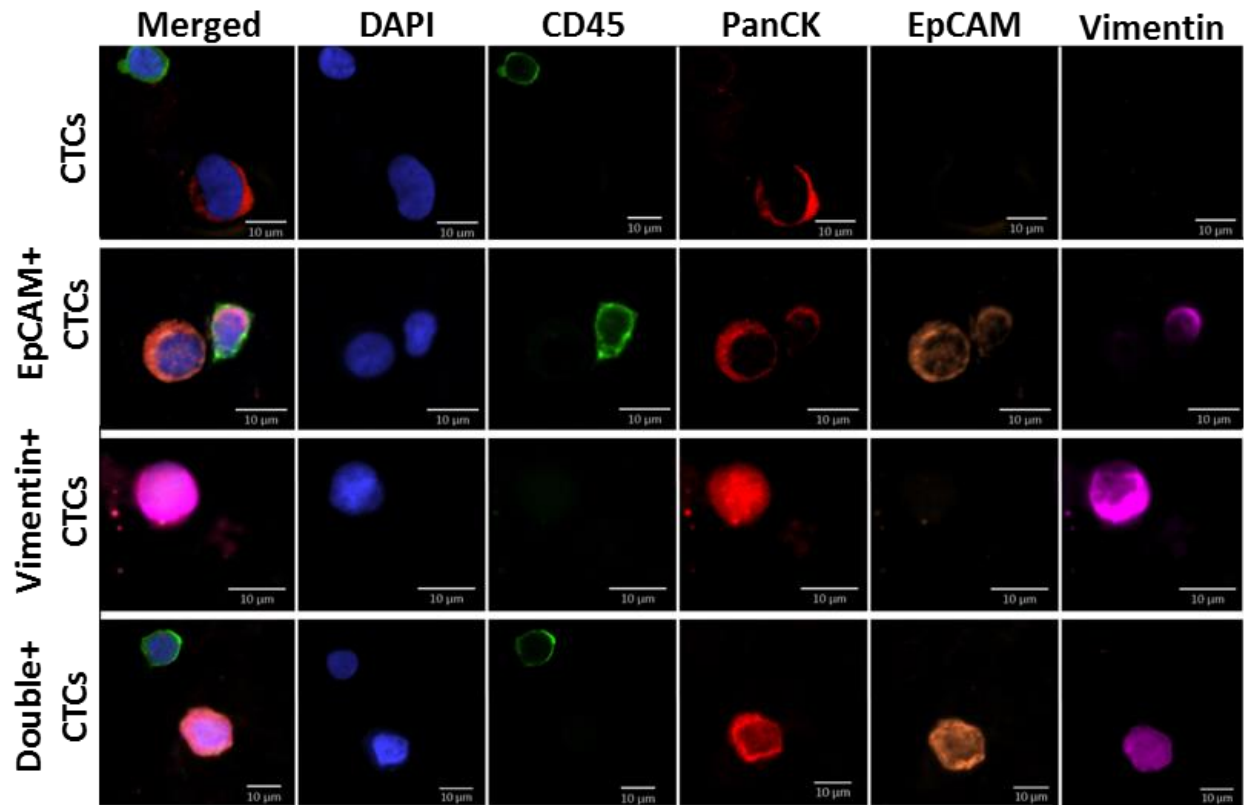


Figure 3-58: Immunofluorescence staining images of the representative images of heterogeneous CTC subpopulations recovered from NSCLC patients samples. Fluorescent microscope images of different subpopulations of CTCs (CTCs, EpCAM+ CTCs, Vimentin+ CTCs, and Double+ CTCs). Cells are stained with DAPI (blue), CD45 (green), PanCK (red), EpCAM (orange), and Vimentin (pink).

Figure 3-59A-B demonstrates the percentage of CTCs expressing EpCAM (EpCAM+/- in dark/light orange, respectively) and CTCs expressing Vimentin (Vimentin+/- in dark/light pink, respectively) of each patient. Of 19 patient samples, 15 samples had more EpCAM- CTCs than EpCAM+ CTCs, whereas only 4/19 patients (P 02, P 07, P 10, and P 19) had a higher number of EpCAM+ CTCs than EpCAM- CTCs.

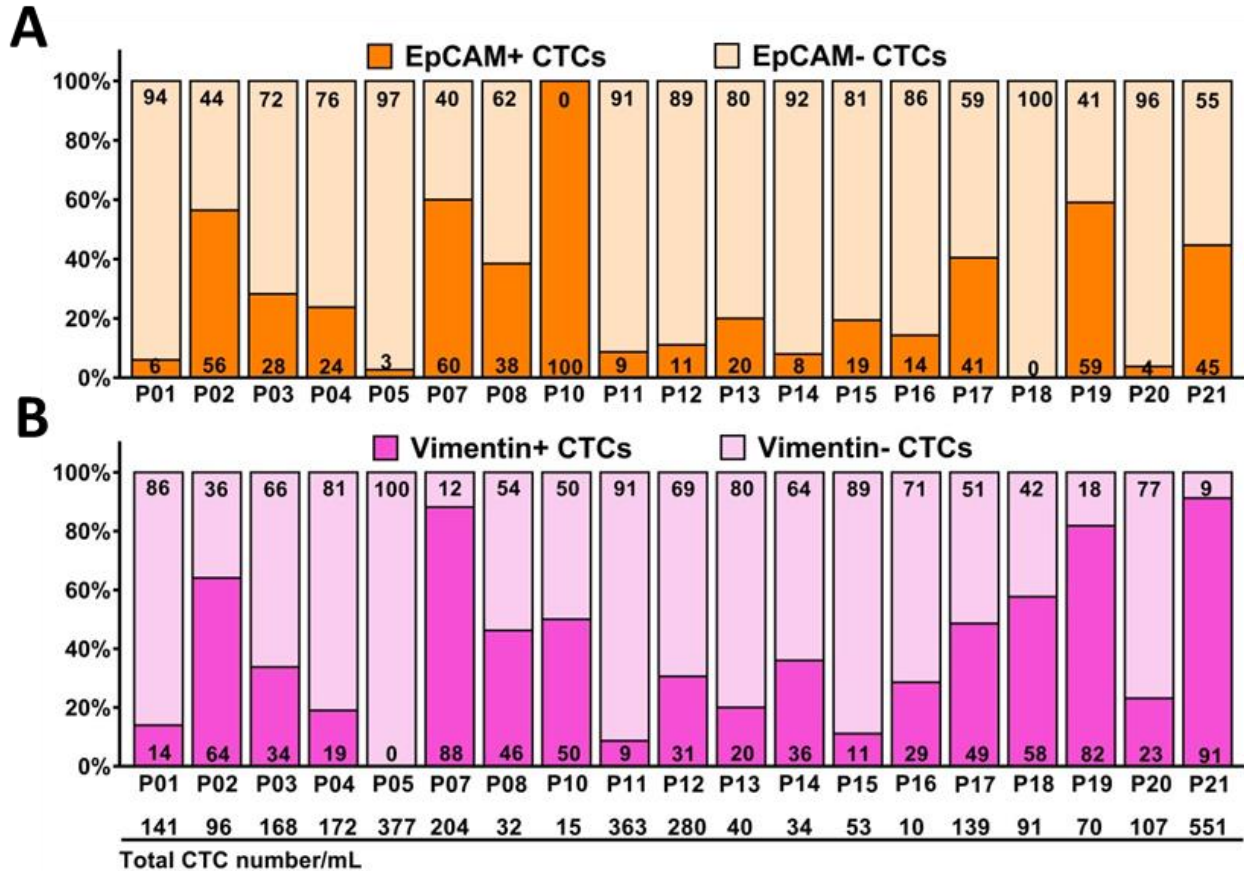


Figure 3-59: Identification of heterogeneous CTC subpopulations isolated from NSCLC patient samples (n=19). A-B) The percentage of CTCs expressing both EpCAM (A) and Vimentin (B) recovered from each NSCLC patient sample (n=19). The EpCAM+/- CTCs is shown in dark/light orange respectively and the Vimentin+/- CTCs is shown in dark/light pink respectively. An average of 28.7% of the captured CTCs was EpCAM+ and 71.3% were EpCAM- CTCs. An average of 39.6% of the captured CTCs were Vimentin+ and 60.4% were Vimentin- CTCs. Total number of CTCs/mL across all patient samples is shown on the bottom of the graph.

An average of 71.3% (115.7 CTCs mL⁻¹) of the captured CTCs were EpCAM- and 28.7% (39.1 CTCs mL⁻¹) were EpCAM+ (p=0.01) (Figure 3-60). Checking the mesenchymal phenotype on the recovered CTCs demonstrated that 39.6% were Vimentin+ CTCs (64.4 CTCs mL⁻¹), and 60.4% were Vimentin- CTCs (90.4 CTCs mL⁻¹) (p=0.5) (Figure 3-60).

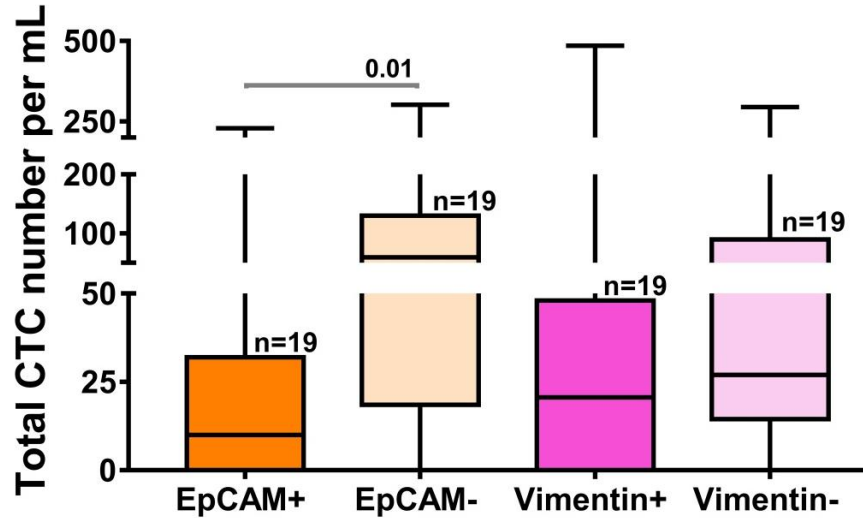


Figure 3-60: Analysis of total numbers of CTCs mL^{-1} in different subpopulation of CTCs. Significantly higher number of EpCAM- CTCs were observed ($115.7 \text{ CTCs mL}^{-1}$) compared to EpCAM+ CTCs ($39.1 \text{ CTCs mL}^{-1}$) ($p=0.01$). While 39.6% of the recovered CTCs were Vimentin+ CTCs ($64.4 \text{ CTCs mL}^{-1}$), and 60.4% were Vimentin- CTCs ($90.4 \text{ CTCs mL}^{-1}$). Unpaired t-test (two-tailed) analysis was used for comparing between these groups.

3.10.4 Presence of clusters in CTCs isolated using Labyrinth

In addition to single CTCs recovered from NSCLC patient samples, a large number of CTCs were observed in cluster forms (2 to 7 CTCs/cluster) (Figure 3-61). On an average, $28.9 \pm 27 \text{ CTCs mL}^{-1}$ were in the form of single CTCs, whereas $125.9 \pm 138.9 \text{ CTCs mL}^{-1}$ were in cluster forms ($p=0.005$). (Figure 3-62A-B). Among the analyzed NSCLC patients, 1/19 had only single CTCs and 18/19 (95%) had CTCs in cluster forms. Of the 19 samples, 17 had ≥ 2 clusters. The majority ($n=16$) presented with at least 3 CTC clusters. There were others with 4 clusters ($n=7$), 5 clusters ($n=4$), 6 clusters ($n=1$) and 7 clusters ($n=2$) (Figure 3-62C). Significantly higher numbers of recovered clusters from Labyrinth were EpCAM- CTC-clusters ($p=0.009$) (Figure 3-63) and 36% of the recovered CTC in cluster form displayed mesenchymal markers (Figure 3-62D).

Analyzing recovered clusters from Labyrinth, we found that significantly higher numbers of clusters did not express EpCAM (EpCAM-) ($p=0.009$) and 35% of clusters expressed the EMT marker, Vimentin ($p=0.3$) (Figure 3-63).

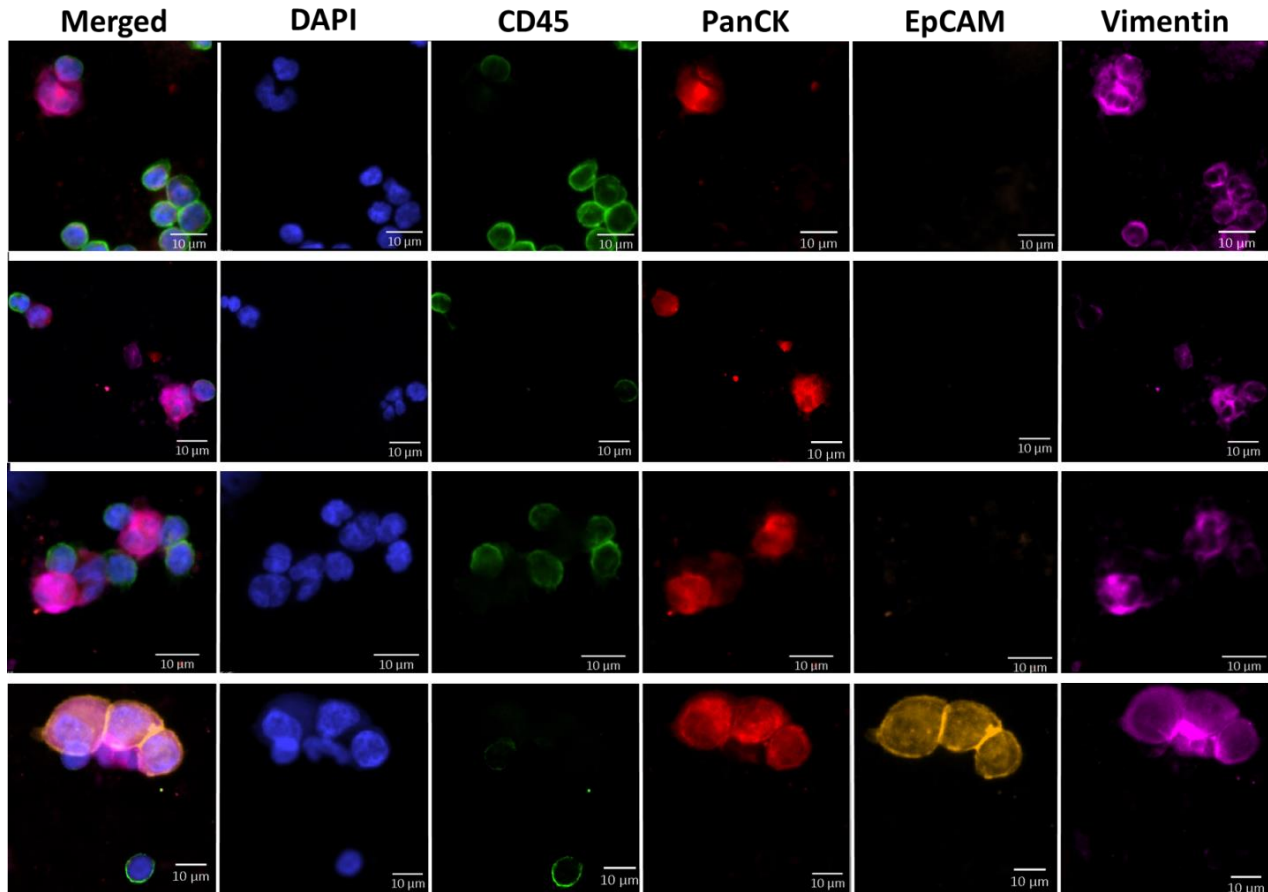


Figure 3-61: Immunofluorescence staining images of the representative recovered CTC clusters in NCSLC patients. CTCs are stained with DAPI (blue), CD45 (green), PanCK (red), EpCAM (orange), and Vimentin (pink).

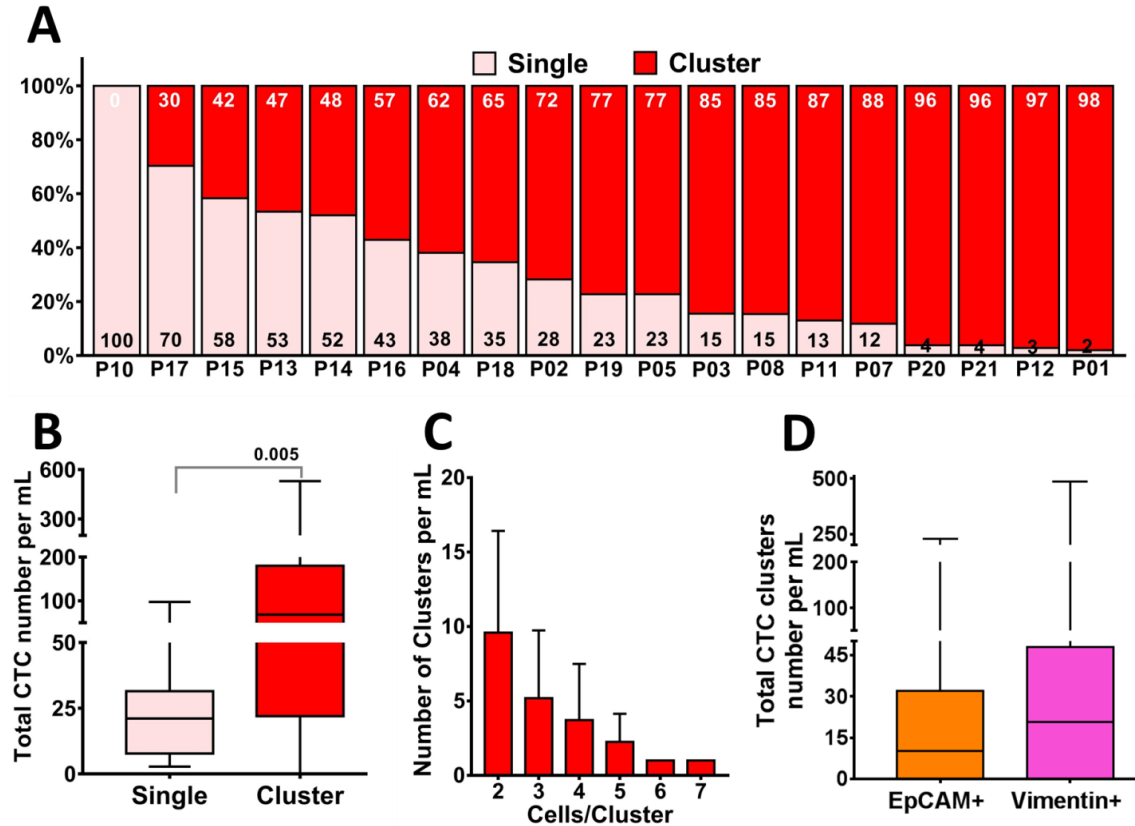


Figure 3-62: Identification of CTC clusters recovered from NSCLC patient samples (n=19). A) The percentage of CTCs in single (light pink) vs. cluster (red) forms. Across all patients, only one patient did not have CTCs in cluster forms. B) The comparison between the total CTC numbers in single vs. cluster forms. Significantly higher numbers of clusters compared to the single CTCs were observed in the captured CTCs from NSCLC patients (n=19). C) Cell clusters of 2-7 CTCs were observed in 95% of patients. D) 36% of the recovered CTC clusters displayed a mesenchymal or EMT phenotype (53.4 CTCs mL⁻¹). Unpaired t-test (two-tailed) analysis was used for comparing single vs. clusters CTCs.

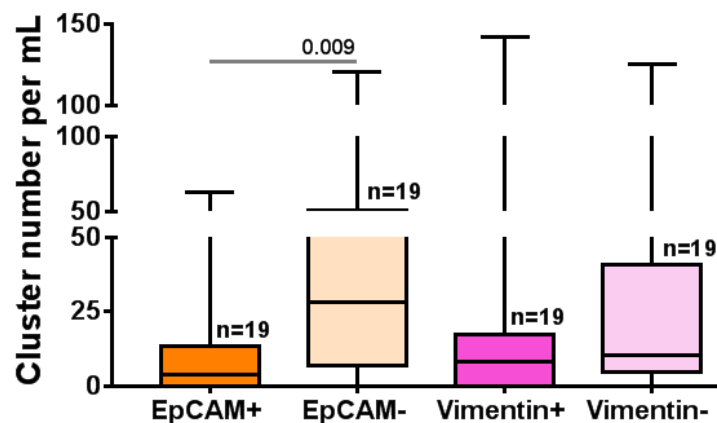


Figure 3-63: Analysis of CTCs clusters mL⁻¹ in different subpopulation of CTCs. Analyzing recovered clusters from Labyrinth, we found that significantly higher numbers of clusters were not expressing EpCAM (EpCAM-) (p=0.009), and 35% of clusters expressing the EMT marker, Vimentin. Unpaired t-test (two-tailed) analysis was used for comparing between these groups.

3.10.5 Genomic analysis of NSCLC patient CTC samples using Fluorescence in situ hybridization (FISH) analysis

To investigate whether CTCs isolated by Labyrinth carry the genomic signature of the primary tumor, we analyzed CTCs for genomic alterations in *ROS1*, *ALK*, and *RET*. A 5' deletion of *ROS1* was detected by FISH in recovered CTCs from a patient with a known *ROS1* rearrangement in the primary tumor (P 03) (Figure 3-64A). Similarly, an *ALK* rearrangement was noted in the CTCs, matching the patient's primary tumor (P 17) (Figure 3-64B) and a 3'deletion of *RET* was found in recovered CTCs from a patient with a *RET* rearranged tumor (P 21) (Figure 3-64C).

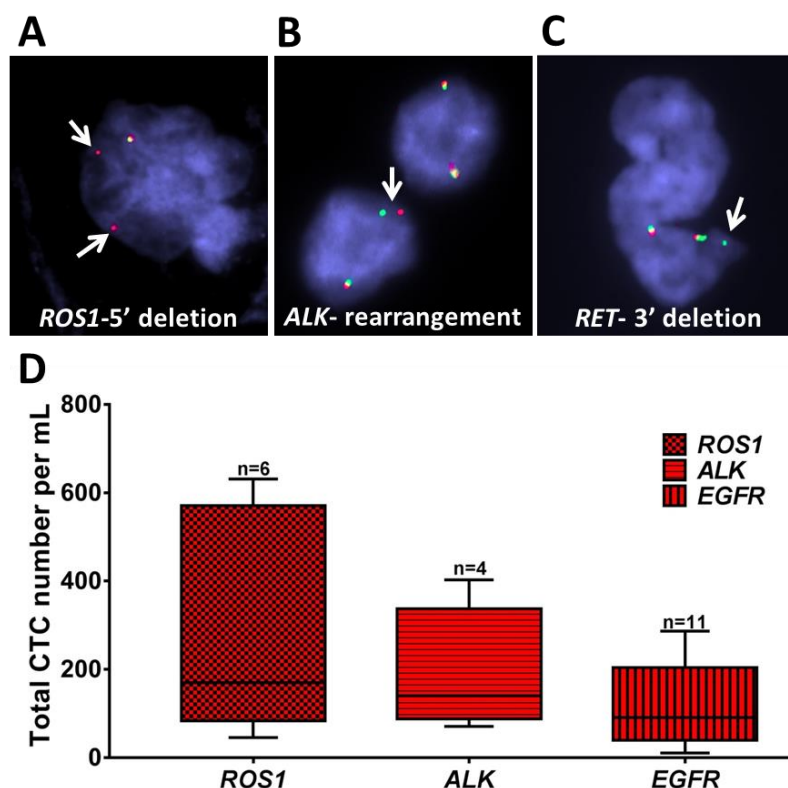


Figure 3-64: Genomic analysis of NSCLC patient samples using Fluorescence in situ hybridization (FISH) analysis. A-C) Recovered CTCs from selected patient samples with different mutation (*ROS1*, *ALK*, and *RET*) were evaluated A) A patient with *ROS1* rearrangement showed 5' deletion in some of the cells. B) A patient with aberration in *ALK* showed *ALK* rearrangement C) A patient with aberration in *RET* showed 3' deletion. Arrows indicate specific aberration in each gene. D) Box plot of the total number of CTCs recovered from patients with different mutation (*EGFR* (n=11), *ROS1* (n=6), *ALK* (n=4) and *RET* (n=1)).

The total numbers of CTCs mL^{-1} in all patients with respect to their *EGFR/ALK/ROS1* status are shown in Figure 3-64D. NSCLC patients with *ROS1* rearrangements (n=6) had an average of 277.2 total CTCs mL^{-1} (45.2-631.4). Patients with *ALK* rearrangements (n=4) had an average of 188.3 total CTC mL^{-1} (70.4-402.6), and patients with *EGFR* mutations (n=11) had an average 124 total CTCs mL^{-1} (10.2-286.3). However, the differences in the number of CTCs according to genotype were not statistically significant.

3.11 Patient-derived CTC expansion

3.11.1 Optimization of CTC expansion methods

To be able to expand the recovered CTCs from NSCLC patients for *ex vivo* drug testing, different CTC culture methods were tested. Sixteen samples were seeded in three conditions including, a plain 48-well plate (plastic), a “Fibronectin coated” 48-well plate (2D), and a “Matrigel-Collagen” coated 48-well plate (3D). After 3-4 weeks the expanded CTCs were passaged and then seeded onto 2D 48-well plates. The “possible CTCs” were counted and the results showed that the growth rate was significantly higher in the 3D model (Figure 3-65).

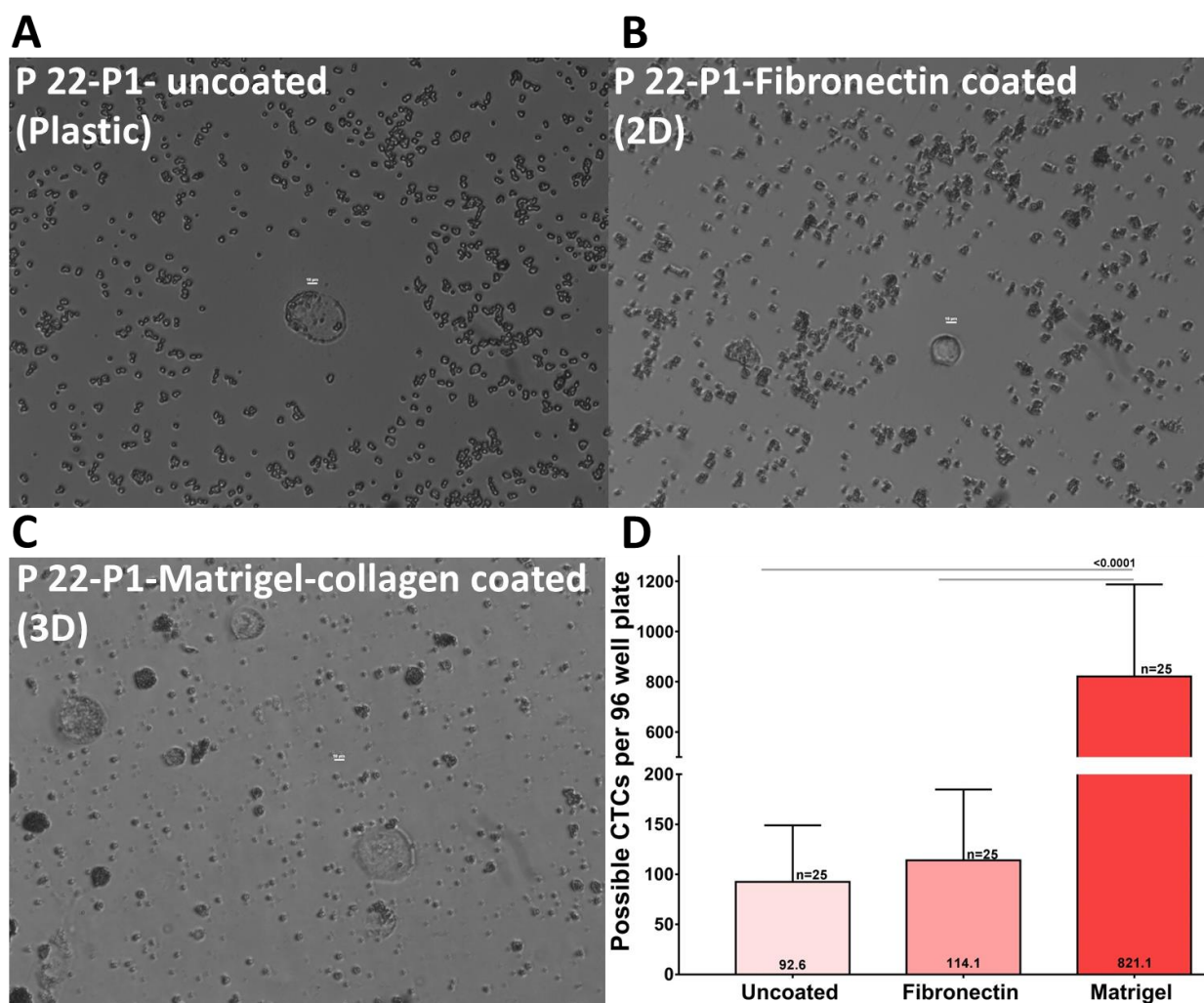


Figure 3-65: Patient-derived CTC expansion utilizing different culture conditions. Enriched CTCs separated from Labyrinth were cultured on A) uncoated 48-well plate B) Fibronectin coated 48-well plate), and C) Matrigel-collagen coated 48-well plate. D) The box plot of these 3 conditions shows significantly higher growth rate in the Matrigel condition.

Small portion of expanded CTCs were seeded in 96-well plate to check the cell viability. Cells were labeled with IncuCyte NucLight Rapid Red (IncuCyte) reagent for 30 min prior visualization with fluorescence microscopy (Figure 3-66). The NucLight Rapid Red reagent labels the nucleus of cells and their growth rate can be tracked for 72 hr. Alive cells show dim, and dead cells show bright fluorescent. Some bright field and fluorescently labeled images of expanded CTCs were shown in Figure 3-66A-B.

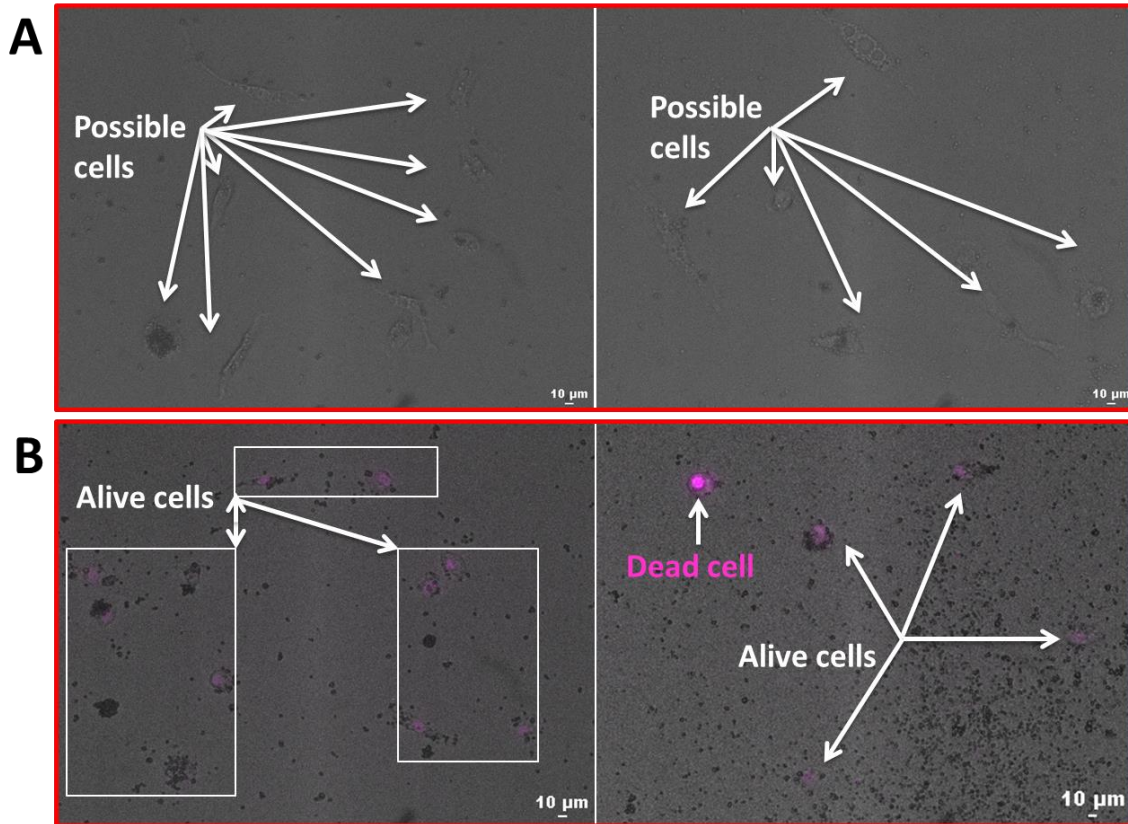


Figure 3-66: Cell viability check on the patient-derived expanded CTC using 3D models. A) Bright field images of possible expanded patient-derived CTCs. B) Possible expanded CTCs from different patient samples were labeled with IncuCyte NucLight Rapid Red. Alive cells show dim, and dead cells show bright fluorescent.

3.11.1.1 Red blood cells (RBCs) removal techniques

To be able to expand patient-derived CTCs *in vitro*, it is necessary to reduce the off-target cells (mostly RBCs) after CTCs enrichment. Even though by utility of Dextran, the majority of the RBCs are depleted at the first place, the high numbers of remain RBCs may still disturb the CTC expansion *in vitro*. Hence, we attempted to optimize the RBCs depletion methods while maintaining the numbers of the recovered CTCs from NSCLC patient.

3.11.1.1.1 Double Labyrinth

In the first attempt, we processed the second outlet's products of the Labyrinth (single) through another Labyrinth (double). The CTCs recovered from single vs. double

Labyrinth of 4 different patient samples were collected and stained with PanCK and CD45. The CTC lost was observed across all the samples (n=4) using the double Labyrinth (Figure 3-67A). For further investigation of the CTC lost in double Labyrinth using one NSCLC patient sample, the recovered CTCs from single Labyrinth compared to the ones recovered from different outlets (1, 2, and 3) of double Labyrinth. The results showed that the majority of the CTCs separated in the first outlet (Figure 3-67B).

3.11.1.1.2 RBC lysis buffer

Since the use of double Labyrinth was not a success, in the second attempt the RBC lysis buffer was used for further RBC depletion. The effects of both single vs. double, with or without RBC lysis buffer on the CTC counts were analyzed. The CTC numbers showed CTCs lost using both double Labyrinth and RBC lysis buffer (Figure 3-67C-D). In another attempt, the recovered CTCs from two patients divided into 2 groups; in one set the effect of RBC lysis buffer was checked on the CTC lost, and in the other set, the recovered CTCs (suspended into the media) sat overnight inside the refrigerator to allow the larger cells (CTCs) form a pellet. The following day, the media was removed and the pellet was resuspended. A small portion of the sample was checked for the CTC counts. The results showed that the number of CTCs decreased using the RBC lysis buffer/fridge compared to the CTC counts from Labyrinth without any post processing (After single) (Figure 3-67E).

3.11.1.1.3 Microbubbles

We further tested the RBC Depletion Kit (Akadeum) which is a microbubble-based cell isolation product designed to clean up samples with red blood cell

contamination. We tested 2 different concentrations of the bubbles and compared with the CTC count without any post processing. However, due to the steps of centrifugation we lost many CTCs (Figure 3-67F).

3.11.1.1.4 Cell strainer

Due to the CTC lost using the stated techniques which contains centrifugation steps, we decided to investigate the cell strainer technology for the RBC removal. The cell strainer (pluriselect) is a size-based sterile sieving device to separate cells of interest from the other cells. Any cell smaller than the pores, will go through the filter while the larger cells will remain on top of the filter. In theory, this method should allow RBCs/WBCs (smaller cells) pass through the filter and CTCs (larger cells) remain on top of the filter. The filter can then be inverted to recover the CTCs on top to obtain a more purified sample.

The experiment we conducted involved using two different types of cell strainers (Uber and Pluri (Figure 3-68C-D)), three different pore sizes (1, 5, and 10 μm), and two sample retrieval methods (washing from the top or from the bottom of the filter). Pluri uses a vacuum to send the sample through the filter and Uber uses pressure to send the sample through the filter.

1000 green CellTracker cell lines (A549) spiked into 1 mL treated blood with dextran were prepared to test RBCs depletion. Samples sent through different cell strainers and both waste and recovered samples were collected for further analysis. The results showed that the 1 μm Pluri cell strainer has the highest recovery compared to the Uber (>61% vs. 25%) and other filter sizes (>61% vs. 1% and 26%) (Figure 3-68A).

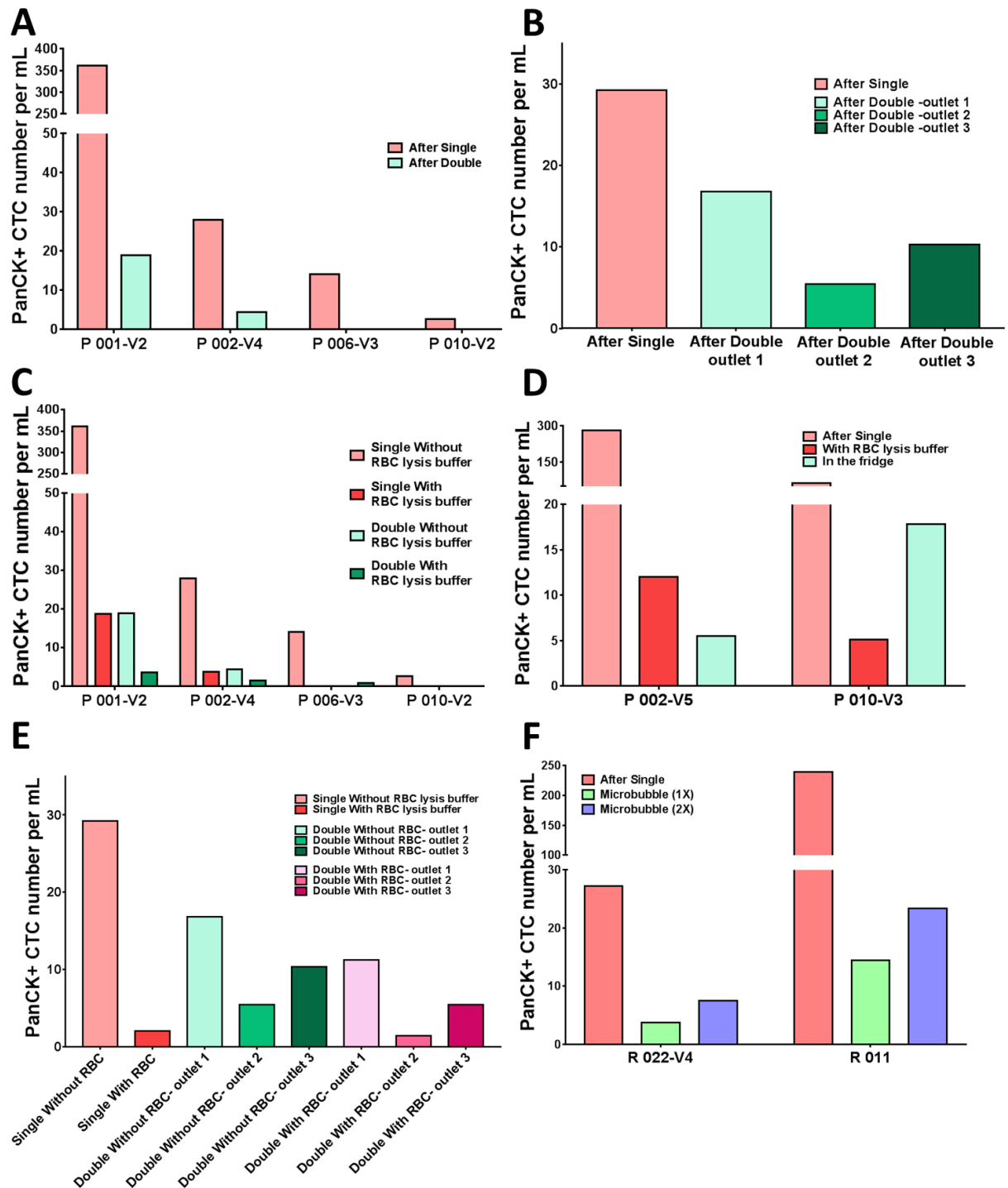


Figure 3-67: RBC removal techniques optimization. A) CTC numbers from single vs. double in different patient samples (n=4). CTC lost was observed using double Labyrinth. B) CTC numbers of different outlets from double Labyrinth vs single Labyrinth. C-D) The effect of using double Labyrinth, with or without RBC lysis buffer on the CTC counts. E) The effect of RBC lysis buffer and no post-processing (in the fridge) of the product from 2nd outlet of Labyrinth on the CTC counts. F) The effect of using microbubbles on the CTC counts. All the mentioned methods result in losing CTCs.

The 1 μm Pluri cell strainer was utilized with one patient sample to confirm their effectiveness and compatibility but no CTCs were collected after using the filter. Using 1 μm Pluri, the diameter of the cell lines in both waste and the recovered samples showed that the size of cells passing through or remaining on top of the filter are almost similar (16 μm vs 14 μm) (Figure 3-68B). This could be a reason for CTC loss using this technology.

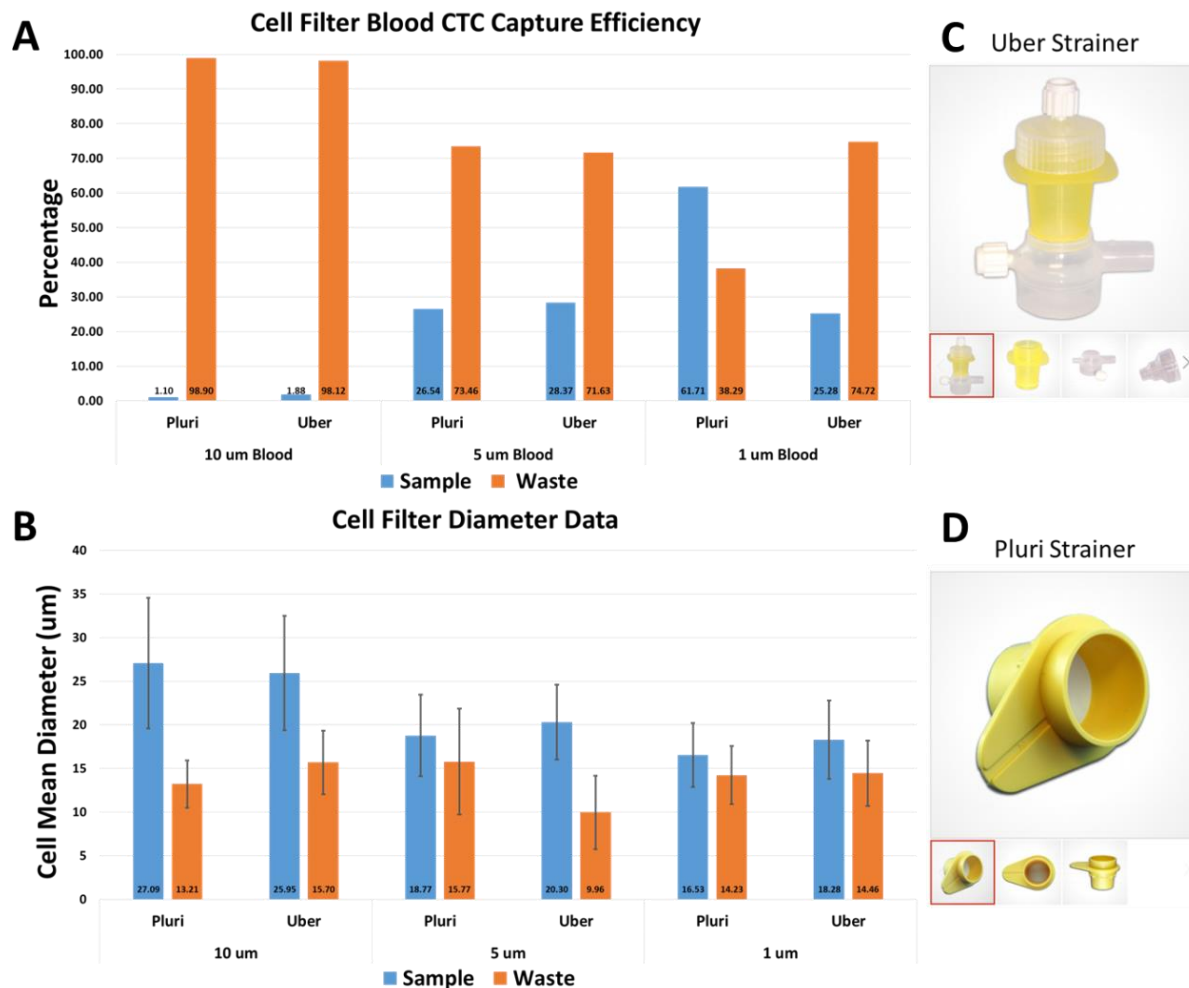


Figure 3-68: RBC removal techniques optimization using cell strainer. A) % of recovered cells from the sample and waste for each cell strainer. B) Cell diameter in both waste and the recovered samples. C-D) A representative image of Uber (C) and Pluri (D) strainer.

3.11.1.1.5 Ficoll-Paque™ PLUS Media

In another attempt, we applied Ficoll-Paque™ PLUS Media (GE Healthcare) for the RBC removal purpose before the CTC enrichment. Different NSCLC patient samples were treated with both Dextran and Ficoll before the enrichment (n=10). A small portion of the processed samples was stained for enumeration purposes, and the rest were seeded for the CTC expansion. The CTC numbers were higher in 6/10 of patient samples using Ficoll and the number of RBC was reduced significantly using Ficoll (Figure 3-69). Hence, this technique was carried on for the CTC expansion application for the rest of processed NSCLS patient samples.

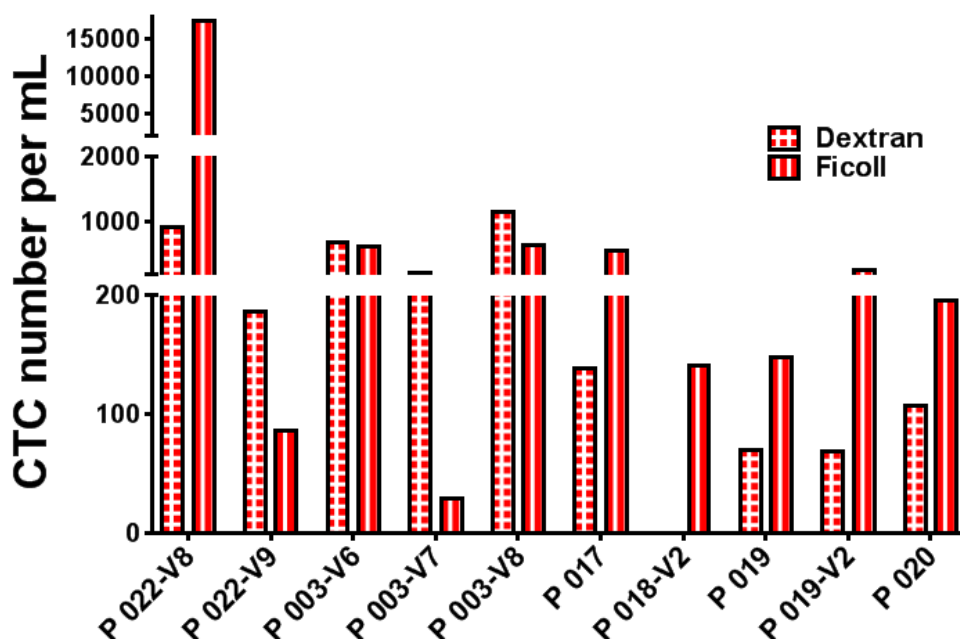


Figure 3-69: RBC removal techniques optimization using Ficoll. CTC numbers from Dextran vs. Ficoll from 10 different patient samples indicated higher CTC numbers in 6/10 of patients using Ficoll.

3.11.2 Recovered CTCs were expanded from NSCLC patient samples (n=2) using 3D model

We were able to successfully expand isolated CTCs from 2 patient samples (P 003 at visit 6 and P 022 at visit 8). A small portion of the expanded “potential CTCs” were

stained for the CTC panel of antibodies (PanCK, EpCAM, Vimentin, and CD45). Since the majority of the RBCs and WBCs are gone at this time, the cells expansions are faster. Eventually, we were able to expand CTCs from a 48-well plate to T175 flasks. Figure 3-70 and Figure 3-72 are representative images of the bright field and fluorescent images of the expanded CTCs from P 03 (Figure 3-70) and P 22 (Figure 3-72).

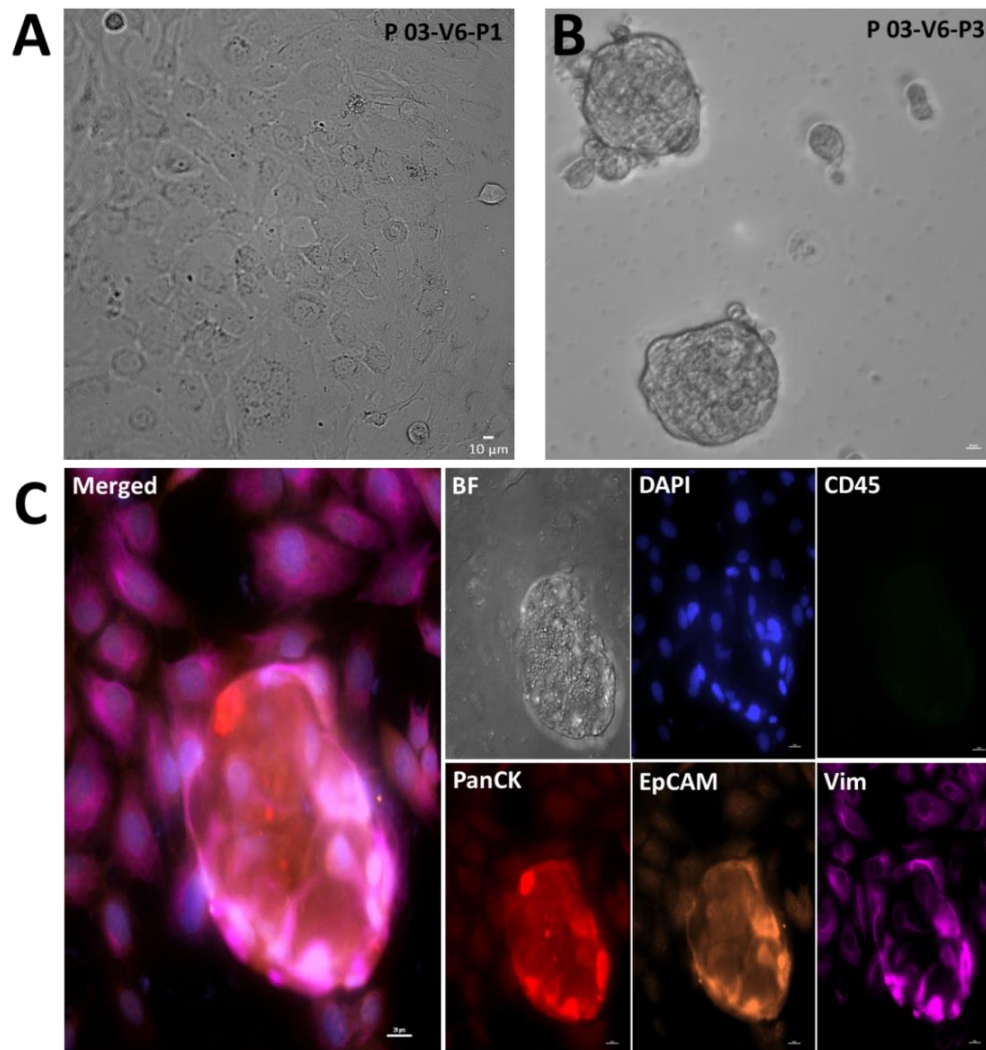


Figure 3-70: Representative images of the NSCLC patient-derived expanded CTCs (P 03). A-B) Bright filed images of expanded CTCs in single cell forms on a well plate culture (A) and in cluster forms in a low attachment well plate (B). C) Expanded CTCs are stained with DAPI (blue), CD45 (green), PanCK (red), EpCAM (orange), and Vimentin (pink).

To be able to verify the genomic signature (*ROS-1* rearrangement) from the CTCs at day 0 vs. the expanded CTCs, the cells were analyzed using FISH (Figure 3-71A). Similar to the results of FISH analysis on the tumor from the clinic, the FISH analysis on the CTCs expanded demonstrated the loss of 5' probe in some cells confirming *ROS-1* rearrangement (Figure 3-71B).

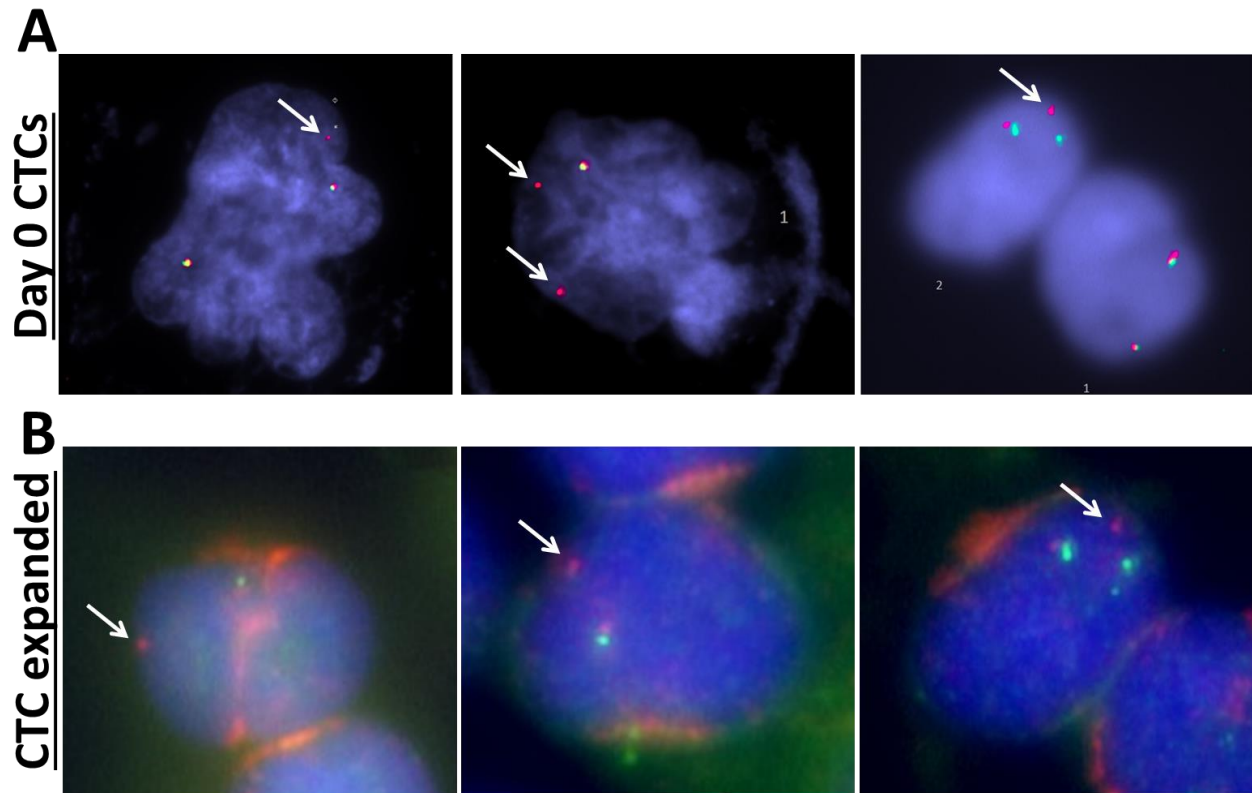


Figure 3-71: Genomic analysis of NSCLC patient sample (P 03) using FISH analysis. A) Recovered day 0 CTCs from patient P 03 with *ROS-1* rearrangement were evaluated. Patient P 03 showed 5' deletion in some of the cells. B) Expanded CTCs from same patient showed the loss of 5' probe in some cells.

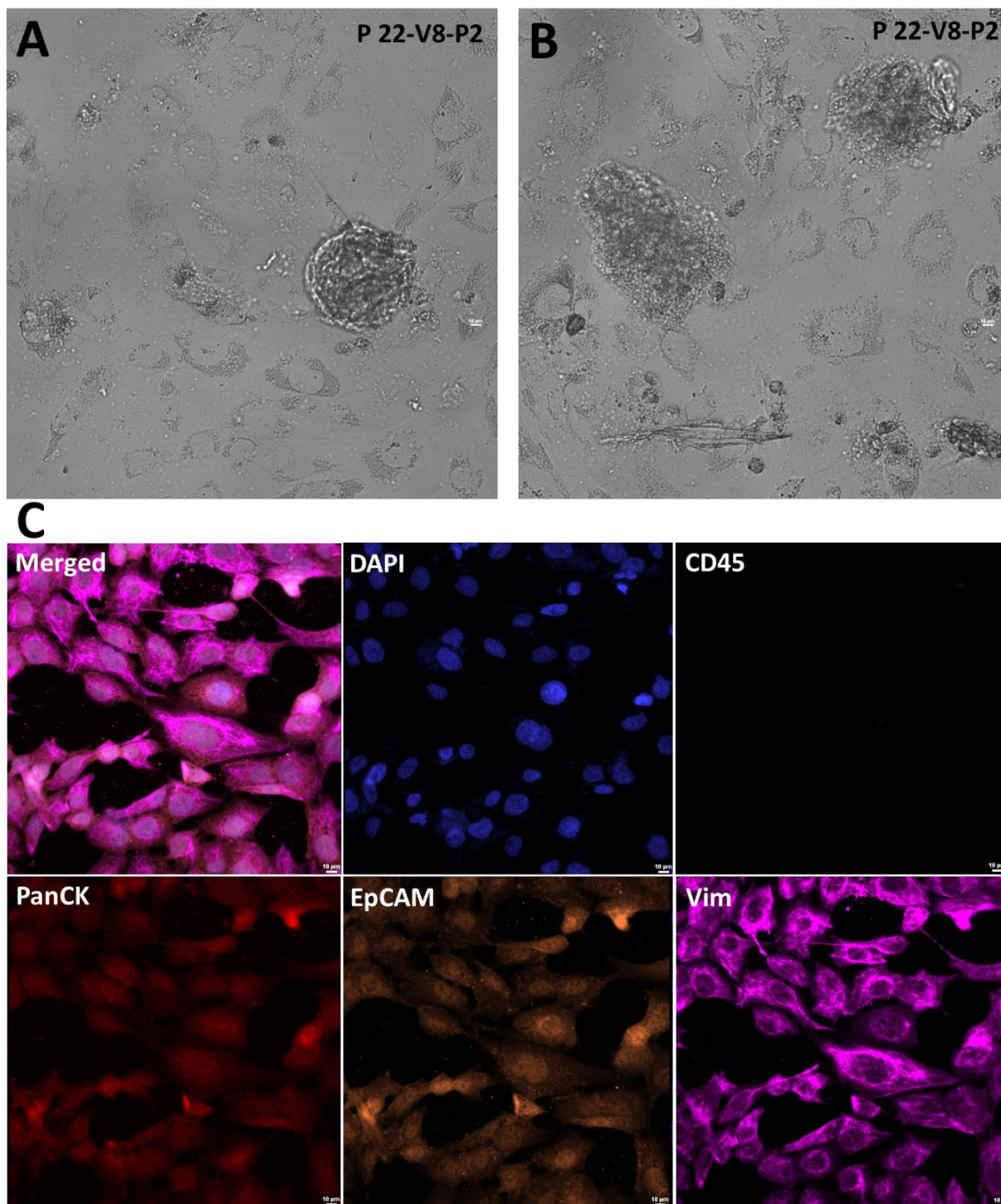


Figure 3-72: Representative images of the NSCLC patient-derived expanded CTCs (P 22). A-B) Bright filed images of the expanded CTCs in single cell forms on a well plate culture and in cluster forms. C) Expanded CTCs are stained with DAPI (blue), CD45 (green), PanCK (red), EpCAM (orange), and Vimentin (pink).

3.12 CTC enumeration of follow-up NSCLC patient samples

Blood samples were collected during subsequent clinic visits in addition to the baseline. The relevant clinical information for patients P 03 and P 22 over the course of treatment is shown in detail in appendix section (Table 9-15).

Ten consecutive samples from patient P 03 were collected during different treatment regimes. The numbers of CTCs were analyzed during the follow-up visits (Figure 3-73A). This patient enrolled at this study on 12/6/2016 while she was on Crizotinib treatment. The progression in the brain was observed after 350 days. Higher numbers of CTCs were observed in her 3rd visit compared to first and second visits.

After 412 days (visit 5), a slight increase in fullness of L frontal brain tumor was observed. Then, the treatment regime was switched to Entrectinib. Cancer progression at several spots in the brain was detected after 468 days and Entrectinib continued as treatment. The CTC numbers increased 3 folds at this visit (V6) compared to the previous visit (V5). We were able to establish the CTC cell line from the recovered CTCs at this visit (Figure 3-70). In summary, according to the available clinical information, the CTC numbers tracked the patient's outcome over the course of treatment.

Nine follow-up samples were collected during different treatments from patient P 22 and the CTC numbers were analyzed (Figure 3-73B). This patient enrolled at this study on 10/21/2016 and after one-week treatment with Docetaxel along with Ramucirumab was started. After 525 days at her 8th visit, the CTC numbers increased from the previous visits and we were able to expand CTCs from this visit (V8) (Figure 3-72). Due to fatigue and taste changes Docetaxel was discontinued after 539

days. After 602 days due to the progression on MR brain with two new lesions, her treatment regime was switched from Ramucirumab to Osimertinib.

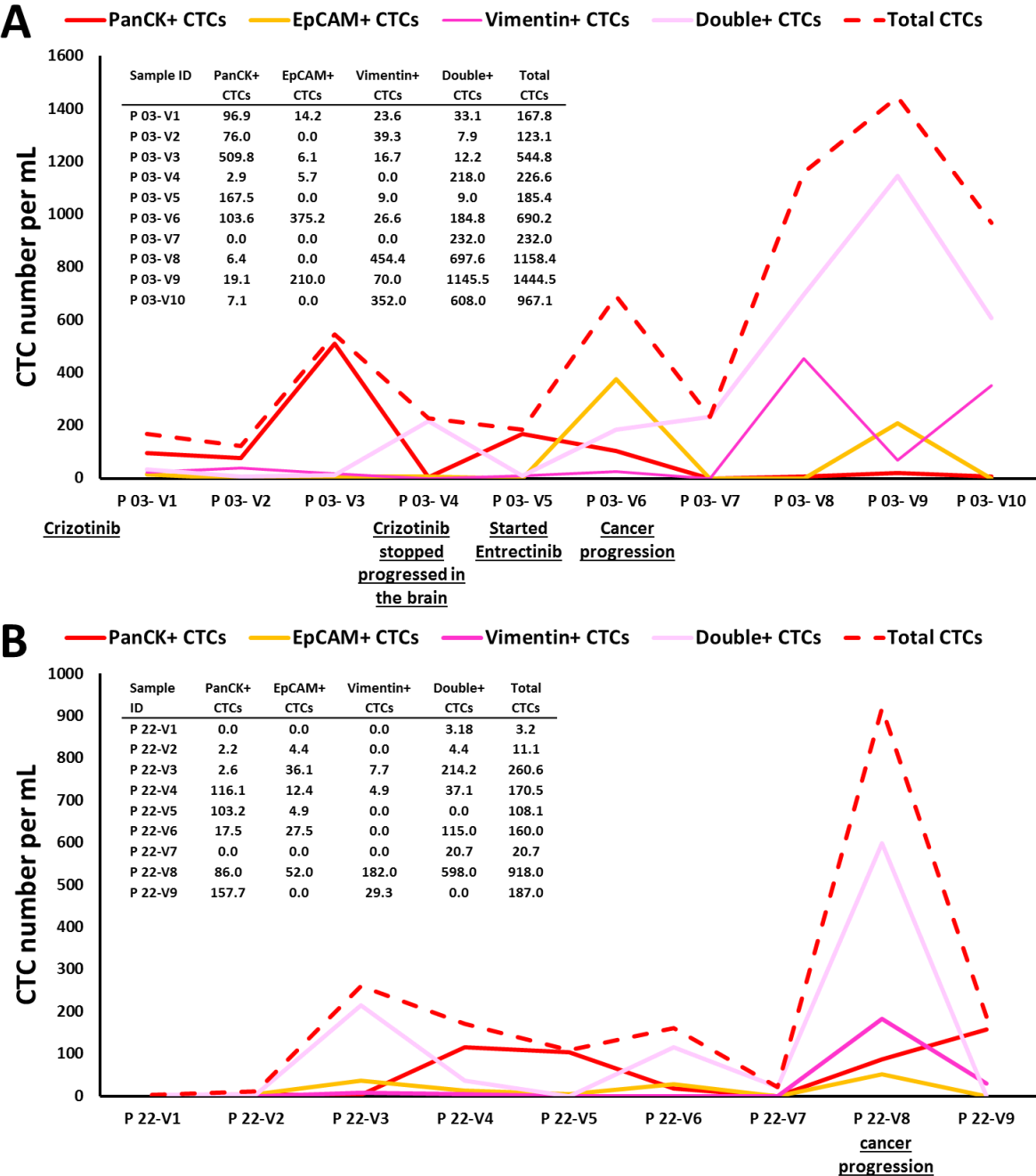


Figure 3-73: CTC enumeration of two NSCLC patients over the treatment regime. A) 10 different follow-up samples from patient P 03 (A) and P 22 (B) were collected and the CTC numbers were evaluated over different treatments.

3.13 Drug testing

3.13.1 Optimization of drug testing methods using NSCLC cell lines

To analyze the effect of each drug on different NSCLC cell lines including, both sensitive and resistant cell lines to drugs, the half maximal inhibitory concentration (IC₅₀) analysis using different methods was conducted.

3.13.1.1 CellTiter 96® Aqueous One Solution Cell Proliferation Assay

The tetrazolium-based MTS assay, CellTiter 96® aqueous one solution cell proliferation assay, was used to analyze IC₅₀ of each different drugs against potential sensitive or resistant NSCLC cell lines. 2000 cells were seeded in each well of a 96-well plate in triplicates.

Using a sensitive cell line (H3122) to Crizotinib and Ceritinib the IC₅₀ values were 151.8 nM and 14.3 nM respectively. The resistant cell line (A549) showed IC₅₀ of 6642 nM and 3761 nM for these two drugs respectively (Figure 3-74A-B). IC₅₀ of Erlotinib for the sensitive cell line (PC-9) was 112.2 nM, while the resistant cell line A549 showed IC₅₀ of 3761 nM (Figure 3-74C). HCC827 cell line was 2.6 fold more sensitive to Afatinib (IC₅₀= 332.1 nM) than the resistant cell line, A549 (IC₅₀=854.4 nM) (Figure 3-74D). The IC₅₀ of the sensitive cell line to Osimertinib (EGFR L858R/T790M double mutation cell line, H1975) was 139.8 nM compared to the resistant cell line (A549) which was 1790 nM (Figure 3-74E). The efficacy of Cetuximab, at inhibiting growth of EGFR mutant cell line, HCC827 (IC₅₀=8957 ng/mL) is more effective than the resistant cell line, A549 (IC₅₀=111287 ng/mL) (Figure 3-74F).

The IC₅₀ results of drug-testing studies conducted with Crizotinib, Ceritinib, Erlotinib, Afatinib, Osimertinib, and Cetuximab are summarized in

Table 3-4.

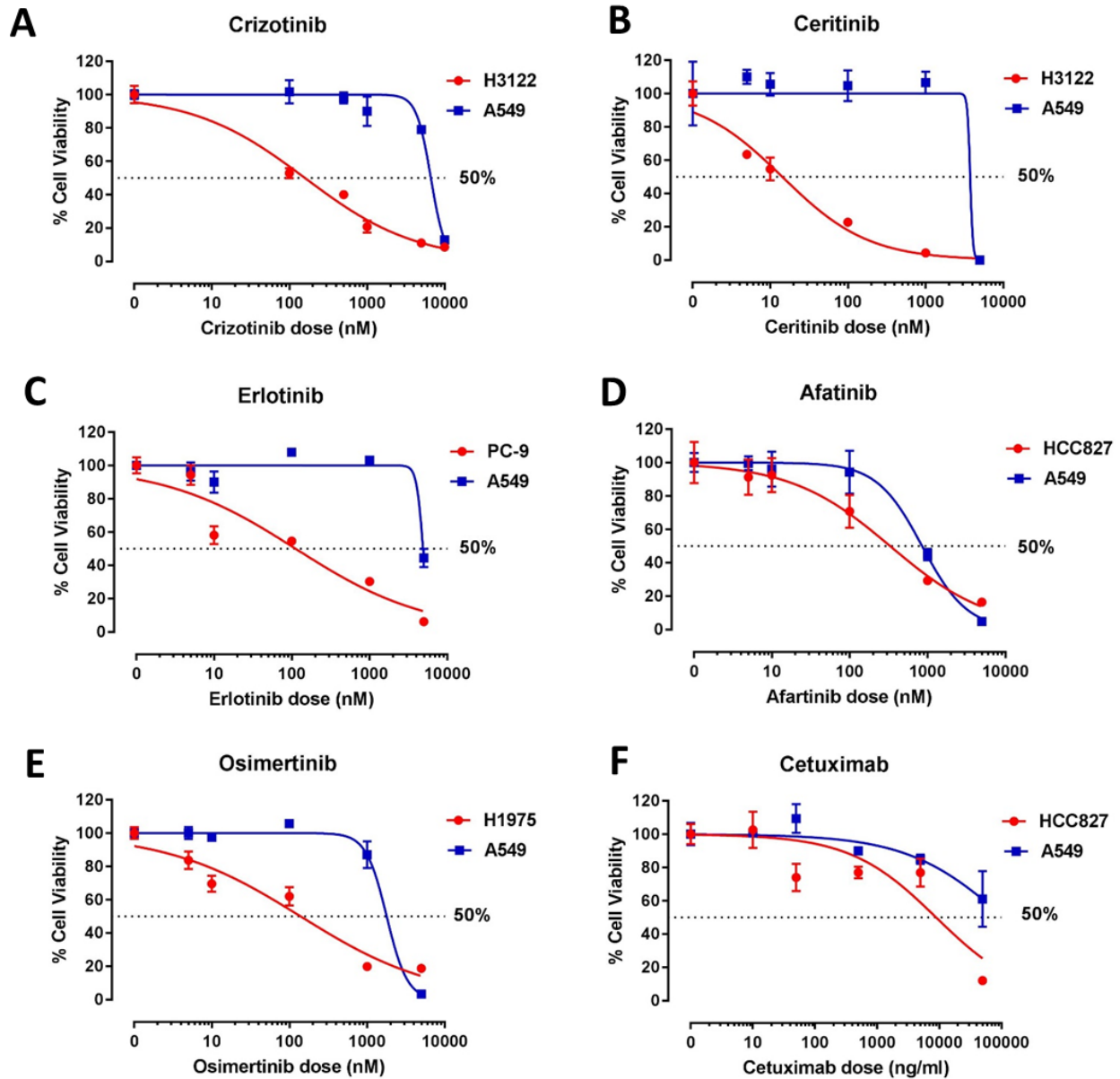


Figure 3-74: IC₅₀ values of different drugs on NSCLC cell lines using CellTiter 96® Aqueous One Solution Cell Proliferation Assay. A) H3122, A549 cell lines treated by Crizotinib; B) H3122, A549 cell lines treated by Ceritinib; C) PC-9, A549 cell lines treated by Erlotinib; D) HCC827, A549 cell lines treated by Afatinib; E) H1975, A549 cell lines treated by Osimertinib; F) HCC827, A549 cell lines treated by Cetuximab.

Table 3-4: The effects of different drugs on of NSCLC cell lines.

Compound	Range of concentration of compound	Sensitive cell line	IC50 of sensitive cell line	Resistant cell line	IC50 of resistant cell line
Crizotinib	100~10000 nM	H3122	151.8 nM	A549	6642 nM
Ceritinib	5~5000 nM	H3122	14.3 nM	A549	3761 nM
Erlotinib	5~5000 nM	PC-9	112.2 nM	A549	4894 nM
Afatinib	5~5000 nM	HCC827	332.1 nM	A549	854.4 nM
Osimertinib	5~5000 nM	H1975	139.8 nM	A549	1790 nM
Cetuximab	10~50000 ng/mL	HCC827	8957 ng/mL	A549	111287 ng/mL

3.13.1.2 CellTiter-Glo® luminescent cell viability assay (2D kit)

To assess IC50 values with a lower seeding density, we utilized the CellTiter-Glo® luminescent cell viability assay. All cell lines were seeded at a density of 400 cells well⁻¹ on 384-well plates. After treatment, each well was incubated with CellTiter-Glo® luminescent cell viability assay for 10 min. Absorbance was measured with LUM mode of Biotek-Synergy Neo-plate Reader.

Similar to the IC50 results we observed using CellTiter 96® aqueous one solution cell proliferation assay with 2000 cell well⁻¹ density in 96 well plate, we obtained comparable IC50 values using CellTiter-Glo® luminescent cell viability assay using 400 cells well⁻¹ in 384-well plate (Figure 3-75, Table 3-5).

Table 3-5: Comparison of IC50 values with two different cell viability assays.

Drugs	Cell lines	Concentrations nM	IC50 (nM) using CellTiter-Glo® Luminescent Cell Viability Assay	IC50 (nM) using CellTiter 96® Aqueous One Solution Cell Proliferation Assay	
Crizotinib	Sensitive cell line	H3122	100~10000	243	151.8
Ceritinib		H3122	5~5000	44	14.3
Erlotinib		HCC827	5~5000	97	112.2
Afatinib		HCC827	5~5000	95	332.1
Osimertinib		H1975	5~10000	37	139.8
Crizotinib	Resistant cell line	A549	100~10000	1502	6642
Ceritinib		A549	5~5000	1357	3761
Erlotinib		A549	5~5000	1064	4894
Afatinib		A549	5~5000	505	854.4
Osimertinib		A549	5~10000	1899	1790

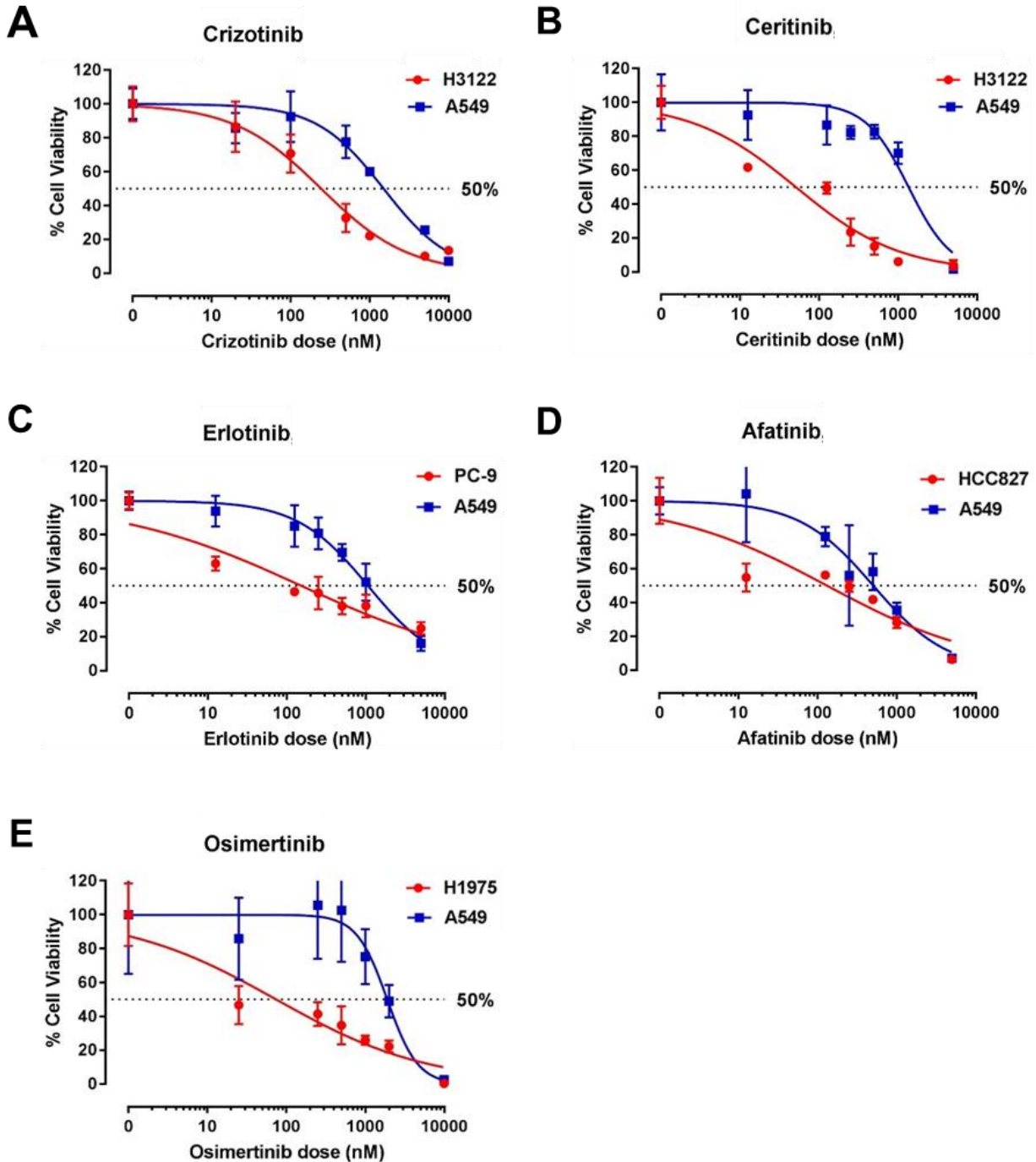


Figure 3-75: IC₅₀ values of different drugs on NSCLC cell lines using CellTiter-Glo® Luminescent Cell Viability Assay. A) H3122 and A549 cell lines treated with Crizotinib; B) H3122 and A549 cell lines treated with Ceritinib; C) PC-9 and A549 cell lines treated with Erlotinib; D) HCC827 and A549 cell lines treated with Afatinib; E) H1975 and A549 cell lines treated with Osimertinib.

3.13.1.3 CellTiter-Glo luminescent cell viability assay (2D kit) vs. CellTiter-Glo 3D Cell Viability Assay (3D kit)

To be able to expedite testing the effect of each drug on the recovered-seeded CTCs on the 3D culture model, the utilizing of the CellTiter-Glo 3D cell viability assay (3D) which is formulated with more robust lytic capacity to spheroids was investigated. We studied the IC₅₀ values of 2D and 3D cell viability kits with 2D and 3D cell culture conditions using sensitive (H3122) and resistant (A549) cell lines.

Utilizing Crizotinib on the 2D culture model using the 2D cell viability kit, the IC₅₀ of H3122 was 297 nM, and A549 was 2173 nM (Figure 3-76A). Expectedly, 3D culture with 2D cell viability kit showed IC₅₀ of 1565 nM for H3122 cell line. However, utilizing the 3D cell viability kit on 3D cells culture model drops the IC₅₀ to 291 nM (Figure 3-76B). The IC₅₀ values of this experiment are summarized in Table 3-6.

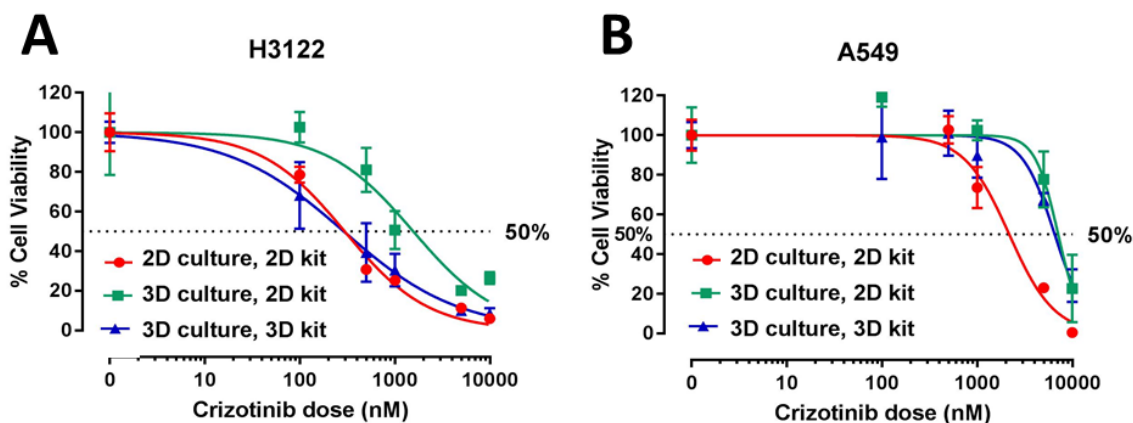


Figure 3-76: IC₅₀ values of crizotinib on NSCLC cell lines using CellTiter-Glo luminescent cell viability assay (2D kit) vs. CellTiter-Glo 3D Cell Viability Assay (3D kit). A) H3122 cells B) and A549 were cultured in 2D or 3D conditions and IC₅₀ values were analyzed by the 2D vs. 3D kit.

Table 3-6: Comparison of IC₅₀ values with two different cell viability assays 2D vs. 3D

Cell Culture and Cell Viability Kits	Cell lines	IC ₅₀ for crizotinib (nM)
2D culture, 2D kit	H3122	297
	A549	2173
3D culture, 2D kit	H3122	1565
	A549	7097
3D culture, 3D kit	H3122	291
	A549	6524

3.13.1.4 LIVE/DEAD viability/cytotoxicity kit optimization

Given that enrichment of a large number of CTCs *in vitro* is still a challenge, we investigated the LIVE/DEAD cell viability assays to assess drug efficacy tests by seeding less cell numbers (50-200 cells well⁻¹). The LIVE/DEAD viability/cytotoxicity kit (Thermo Fisher Scientific) was used to analyze IC₅₀ of tyrosine kinase inhibitors (TKIs) with directly counting live cells using Calcein AM (green) and dead cells using ethidium homodimer (EthD-1) (red) under fluorescence microscope from lower number of cells. The optimal dye concentrations for NSCLC cell lines H3122 and A549 were 10 μ M calcein AM /3 μ M EthD-1 (Figure 3-77A), and 20 μ M calcein AM /3 μ M EthD-1 (Figure 3-77B) respectively.

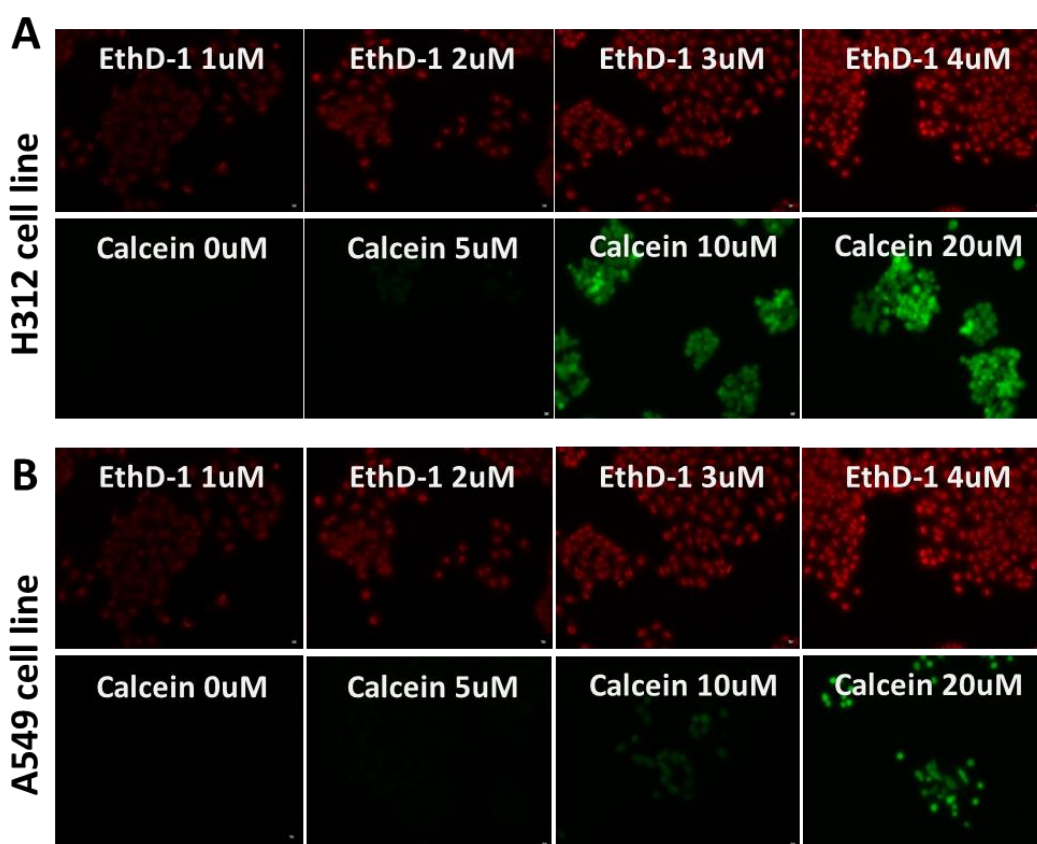


Figure 3-77: LIVE/DEAD viability/cytotoxicity kit optimization using different NSCLC cell lines. A) H3122 and B) A549 were cultured in 2D condition in 384-well plate. Treat and stain cells following manufacture's protocol and take picture under fluorescent microscope with amplification 20x.

3.13.2 Drug testing on the patient-derived expanded CTCs

As mentioned above, we have successfully expanded the isolated CTCs from 2 patient samples (P 03 at follow up visits of 6 and P 22 at follow up visits of 8). The drug screening was done subsequently with 2D kit using various TKIs directed against the genomic drivers. Appropriate positive and negative controls were used and experiments were confirmed in triplicates.

The first patient (P 03) had a *ROS1* rearranged NSCLC on Entrectinib therapy. The IC₅₀ value of this drug on the expanded CTCs is 2357 nM (Figure 3-78). Patient P 03 showed CNS progression on scans on Entrectinib, hence Lorlatinib was selected to test on her expanded CTCs (IC₅₀=15979 nM) (Figure 3-78). The third tested drug on her CTCs was TPX-0005 which has been shown overcoming a broad spectrum of mutations in *ALK* and *TRKA* (tropomyosin receptor kinase A) kinases (IC₅₀=278 nM) (Figure 3-78). The IC₅₀ values of different drug tested on this patient's expanded CTCs are summarized in Table 3-7.

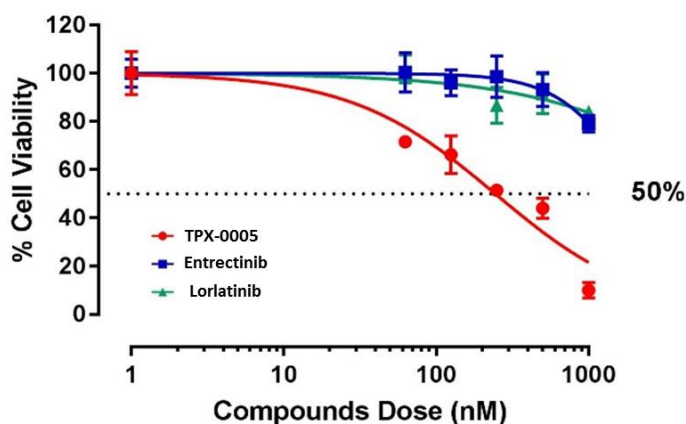


Figure 3-78: IC₅₀ values of different drugs on the expanded CTCs from patient P 03-V6. The expanded CTCs were treated with Entrectinib, Lorlatinib, and TPX-0005. The cells were resistant to both Entrectinib and Lorlatinib, but sensitive to TPX-0005.

Table 3-7: IC₅₀ values of different drugs on the expanded CTCs from patient P 03-V6. Data are means \pm standard deviation of three independent experiments.

CTC or Cell Line	TKI		
	IC ₅₀ (nM)		
	TPX-0005	Entrectinib	Lorlatinib
Expanded CTCs from P 03-V6	278 \pm 140	2357 \pm 802	12175 \pm 8324

The second patient (P 22) had an *EGFR* mutant NSCLC, on Osimertinib therapy. Following successful expansion during visit 8, we tested this patient's CTCs against Osimertinib, and a sensitive NSCLC cell line to this drug (PC-9) (deletion in exon 19 of the *EGFR* gene). Karachaliou N et al. has been reported that TPX-0005 was synergistic with Osimertinib in *EGFR*-mutated NSCLC cells.¹⁹⁹ Therefore, TPX-0005 was selected to test on the expanded CTCs from P 22, as well as evaluating whether a co-activation trait was shown between TPX-0005 and *EGFR* TKIs in treatment of *EGFR*-mutation-positive NSCLC patients.

Our results showed that PC-9 was more sensitive to Osimertinib (IC₅₀=135nM) than TPX-0005 (IC₅₀=830nM) (Figure 3-79B, Table 3-8). Meanwhile, the IC₅₀ of combining both TKIs displayed similar value (71 nM) as the one of Osimertinib treatment alone (135 nM). On the contrary, the expanded CTCs of P 22-V8 were resistant to Osimertinib (IC₅₀=34617 nM), but exhibited a modest sensitivity to TPX-0005 (IC₅₀=339 nM), as well as TPX-0005 + Osimertinib (IC₅₀=392 nM) (Figure 3-79A, Table 3-8).

Table 3-8: IC₅₀ values of TKIs tested in patients' CTCs or NSCLC cell line. Data are means \pm standard deviation of three independent experiments.

CTC or Cell Line	TKI		
	IC ₅₀ (nM)		
	TPX-0005	Osimertinib	TPX-0005+Osimertinib
Expanded CTCs from P 22-V8	339 \pm 113	34617 \pm 7938	392 \pm 223
PC-9	830 \pm 30	135 \pm 19	71 \pm 43

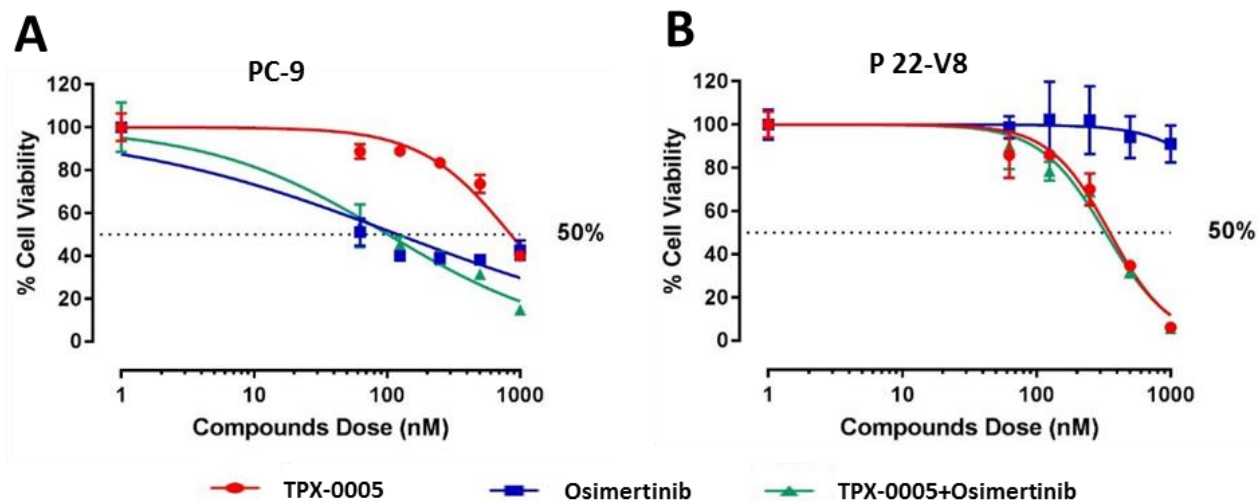


Figure 3-79: IC50 values of different drugs on the expanded CTCs from patient P 22-V8. A) The expanded CTCs and B) PC-9 cell line were treated with Osimertinib alone or the combination and TPX-0005. The expanded CTCs were resistant to Osimertinib but sensitive to TPX-0005.

4 Discussion

In the past decade, circulating tumor cells (CTCs) have been the subject of intense research as blood based biomarkers of diagnosis and prognosis in various cancers. In fact, CTCs have now been proposed as surrogate biomarkers in over 270 clinical trials.²⁰⁰

Many techniques have been developed to detect CTCs in the circulatory system, making them promising biomarkers for detection of different types of cancer. However, to date, CTCs have not been incorporated into clinical practice for management of patients with cancer. The main challenges to this field include sensitivity and specificity of various proposed approaches in detecting these cells which often number between 1-10 cells per 10 mL of blood.

Microfluidic isolation techniques have become attractive since the development of the first microfluidic CTC Chip due to their high sensitivity, high throughput, low cost, and enhanced spatio-temporal control abilities.^{4, 9} Immunoaffinity-based microfluidic technologies are capable of isolating CTCs from peripheral blood without pre-processing and with high specificity of the recovered assorted pool of CTCs.¹⁰² The main approach for enrichment thus far has been to capture cells of interest by using specific epithelial markers such as EpCAM on the cell surface to distinguish CTCs from leukocytes.¹ These technologies provide high purity, allowing for improved downstream analysis. However, they suffer from low throughput and bias in capturing specific subpopulations of CTCs.^{61, 102} Another drawback of immunoaffinity technologies is their inability to easily release cells from the device,³⁰ which can limit downstream applications such as single-cell analysis and CTC-derived xenografts assays.¹⁰²

During cancer progression, cancer cells undergo an epithelial-to-mesenchymal transition (EMT) process, whereby epithelial markers on the cell surface are down-regulated and mesenchymal markers are upregulated.^{154, 201} As such, CTC detection based only on EpCAM (EpCAM+) might miss a substantial number of other CTCs have lost expression of epithelial markers and have undergone the process of EMT (EpCAM-).^{21, 154, 202}

In this presented work, immunoaffinity-based and label-free microfluidic technologies have been developed to investigate heterogeneous CTC populations from pancreatic cancer and non-small cell lung cancer (NSCLC) patients.

The most prevalent form of pancreatic cancer, PDAC, displays a particularly aggressive biology with resistance to both conventional and targeted therapeutics. By the time a patient receives diagnosis, the disease has already advanced to an incurable state in the vast majority of patients.¹³⁵ These facts highlight the unmet challenge of identifying the lethal cells that survive and thrive even after treatment and predispose patients to recur, even after seemingly curative surgery.

Although isolation of CTCs from pancreatic cancer patients is feasible, investigating their clinical utility has proven less successful than other cancers due to limitations of epithelial cellular adhesion molecule (EpCAM)-only based CTC assays. CTC detection based only on EpCAM may miss a substantial number of other CTCs, which might have an aggressive phenotype such as EMT-like CTCs.^{21, 154} The only FDA-cleared CTC isolation technology, CellSearch,⁶³ suffers from drawbacks including low efficiency, low purity, and extremely low abundance of CTCs (0-1 CTC per 7.5 mL of blood) in pancreatic cancer patients.²⁰³ To our knowledge, there is no technique

available for detecting different cell populations of interest simultaneously from peripheral blood of pancreatic cancer patients. Herein, we present two different technologies to study heterogeneous CTCs in pancreatic cancer.

We developed an integrated technology and biology based translational approach, the immunoaffinity-based microfluidic, “CTC Carpet Chip” to study the biological relevance of rare circulating cells from pancreatic cancer patients (n=35). We have focused on a novel strategy based on obtaining separate populations of phenotypically distinct CTCs. Both circulating epithelial CTCs (EpCs) and EMT-like CTCs (EMTCs) were simultaneously isolated from the peripheral blood of pancreatic cancer patients by using multiple markers of interest. Sequential microfluidic devices were set up using antibodies against EpCAM, to capture EpCAM⁺ CTCs (detected by anti-cytokeratin), and antibodies against CD133 to capture more stem-like cells, potentially EpCAM⁻ CTCs (detected by Vimentin) in pancreatic cancer patients.^{1, 27, 31, 32, 155, 204, 205} Among the genes involved in EMT, Vimentin has been studied most in our work. It has been shown that pancreatic cancer has greater than threefold higher expression of Vimentin compared to other cancers.^{27, 204}

The EpCAM CTC Carpet Chip could capture ≥ 5 EpCs mL⁻¹ in 97.5% of pancreatic cancer patients assayed (mean 22.4 \pm 17.7 CTCs mL⁻¹). Moreover, 100% of those individuals showed ≥ 15 EMTCs/mL (mean 85.7 \pm 59.5 CTCs mL⁻¹) in the CD133 chip. We found the numbers of EMTCs were significantly higher compared to the number of EpCs within the stages from early stages to metastatic, and more interestingly, the ratio of EMTCs to total CTCs has an increasing trend toward late stages. The stage IV group patients showed higher number of EMTCs than EpCs

($p=0.0008$), suggesting the strong role of EMT process in the progression of pancreatic cancer.^{2, 5, 20, 25, 36, 206} Moreover, we observed that pancreatic cancer patients with lymph node involvement had significantly higher numbers of EMTCs compared to the patients without. This supports the observations from other studies, where the associations of EMT with lymph node metastasis have been reported.²⁰⁷⁻²⁰⁹ However, we were not able to observe any significant correlation between CTC abundance, disease stage, tumor size, metastatic burden, operability, and survival rate in this group, which could be due to the limited sample size.

The comparison between the EpCAM and CD133 chips in terms of gene expression profiling showed that CXCR1 was significantly upregulated in CTCs isolated by the EpCAM chip while POU5F1 (or OCT-4) and MYC were significantly elevated in the CTCs captured on the CD133 chip. Given the phenotypic differences we have observed between EpCs and EMTCs, it is not surprising that the stem cell related gene POU5F1 is highly expressed in EMTCs. Based on our results, over expression of this gene was significantly correlated with worse PFS.

It has been reported that the expression of the chemokine gene, CXCR1 is correlated with lymph node metastasis in pancreatic cancer.²¹⁰ The presence of POU5F1 has been reported in adult human pancreatic stem cells during differentiation and in pancreatic cancer cells and plays a crucial role in proliferation, cell cycle, stemness, and metastasis.²¹¹ Based on our results, over expression of this gene was significantly correlated with worse PFS ($p=0.04$). There are several studies showing that expression of the oncogene MYC is elevated in pancreatic cancer, the activation of which may be essential during carcinogenesis.^{212, 213} Signaling pathways based on

analysis of captured CTCs on EpCAM vs. CD133 chip with iPathwayGuide using a p value threshold of 0.05, suggested that these two genes were involved in signaling pathways regulating pluripotency of stem cells ($p=0.056$).

We found that the expression of ATL1, BMi1, CD14, CDH2, ERCC1, MKi67, TTF1, and Vimentin were significantly higher in our early stage pancreatic cancer patient cohort compared to the rest of the stages. Among these genes, BMi1, CDH2, ERCC1, and TTF1 genes were significantly associated with the prolonged OS and/or PFS. BMi1 has been implicated in progression of PDAC by the regulation of pancreatic cancer CSCs,^{37, 214} conversely, our results showed over expression of these genes lead to significantly prolonged OS and PFS. It has been shown that over expression of CDH2 (N-Cadherin) is associated with invasiveness in cancer and poor outcomes in pancreatic cancer patients,^{215, 216} however our results showed higher expression of this gene in early stage patients with longer OS.

ERCC1 has a key role in the removal of adducts from genomic DNA through the NER pathway and over expression of this gene enables DNA repair in tumor cells that promotes their viability and growth.²¹⁷ Similar to our findings, over expression of this gene has been reported in PDAC with better OS and outcomes.²¹⁸ TTF1 has been reported in PDAC with a prolonged disease control (≥ 10 months).²¹⁹

We observed genes including, ALDH1A3, ESR1, KRT18, KRT19, AKT1, and CD3D were significantly higher in stage IIB&III pancreatic cancer patients. Among these genes, AKT1 was significantly associated with PFS. AKT1 is increased in many types of cancer including pancreatic cancer, which is related to apoptosis resistance and cell proliferation, growth and energy metabolism.^{220, 221}

We also observed the expression of CDH1, DCN, KRT19, PGR, and PIK3CA genes significantly elevated in the stage IV pancreatic cancer patients cohort. Collagen-associated proteoglycan decorin (DCN) is an important component of extracellular matrix (ECM) and over expression of this gene has been reported in PDAC.²²² Somatic mutation in PIK3CA gene has been reported in several types of cancer including colorectal, gastric, thyroid, and breast.²²³ It has not been reported in conventional PDAC to date; however the presence of this gene has been reported in IPMN and MCN.^{223, 224}

Further, gene expression profiling revealed that IL8 and TP53 were significantly over expressed in patients with higher OS and/or PFS. IL8 (CXCL8) is a chemokine which is associated with cell proliferation, migration, invasion and cancer stem cells population in many types of cancers including pancreatic cancer.²²⁵ The TP53 tumor suppressor gene is a well-considered deregulated gene in pancreatic cancer.²²⁶ However, pancreatic cancer patients with higher expression of metastatic marker, GEMIN2 and stem marker, POU5F1 showed worse OS or PFS respectively.

Although the immunoaffinity CTC Carpet Chip enables us to isolate different CTC populations from pancreatic cancer patients, it's still a low throughput and biased CTC isolation system. Therefore, refinements including increasing throughput and using biomaterials and reversible conjugation of antibodies for CTC release of off the chip may be the important steps toward improving immunoaffinity technologies.¹⁰²

The other current challenge is to increase the yield and detection of CTCs that have undergone phenotypic changes such as EMT.²²⁷ To enable identification and enrichment of heterogeneous populations of CTCs, biomarker-independent technologies have been developed. Label-free technologies present high throughput

approaches with the ability to release and expand CTCs using off-chip standard cell culture techniques. However, they share some disadvantages including, limited recovery, throughput, purity, and the ability to couple with conventional biological assays or platforms for other downstream analyses.^{94, 163, 170, 176, 188, 228} Therefore, a high throughput microfluidic-based biomarker-independent CTC isolation technology with high sensitivity, specificity, and efficiency is needed to enable the study of heterogeneous CTC populations.

The size-based, label-free inertial microfluidic device, Labyrinth, uses the delicate balance of inertial and dean forces to differentially focus cells within microfluidic channels.¹⁹⁸ Particles are focused by inertial forces which can be considered as the driving forces, while particle migrates away from the center of the channel by drag forces from dean flow, leading to size-based separation.¹⁰³ It also induces fluidic path directional shifts by incorporating 56 high curvature turns.¹⁹⁸ The multi-course path traversing across inner loops to outer loops yields an increased hydrodynamic path length to enhance the focusing of both CTCs and WBCs, resulting in greater purity.¹⁹⁸ Herein, using this novel technology, we have isolated heterogeneous populations of CTCs expressing epithelial and mesenchymal markers in both pancreatic cancer patients and advanced non-small cell lung cancer patients (NSCLC).

As mentioned above, the treatment options for pancreatic cancer are limited to surgery, chemotherapy and radiotherapy. Only 15% of patients are qualified for surgery, which may result in increasing patient's survival only 10-20%. The efficiencies of chemotherapy and radiotherapy are also limited. Hence, the need of a biomarker for detecting and monitoring this disease is an urgent need.

Therefore, in order to study the efficacy of CTCs as tumor biomarkers,¹⁴¹ treatment naïve pancreatic cancer patients samples were studied for heterogeneous CTC populations including epithelial CTCs and EMT-like CTCs. Using Labyrinth, CTCs were detected in 94.3% of treatment naïve pancreatic cancer patients ranging from 0-117 total CTCs mL⁻¹. This cohort was further stratified based on their cancer stage: resectable, borderline resectable, locally advanced, and metastasis. Patients with borderline resectable disease had significantly higher numbers of total CTCs compared to the other categories. Our results showed the potential of cancer dissemination even in the earlier stage, as has been previously reported by other groups.¹⁵⁴

The CTC counts were analyzed for the patients who were under surgery and it compared with the CTC numbers before surgery. The total CTC numbers showed a slight decrease in post-surgery patients. However, when this cohort grouped based on their stages, significantly higher decrease change on the CTC counts was observed in the more advanced stage group of patients (borderline resectable). The correlation of overall survival of patients with a decrease compared to an increase or constant CTC counts shows a better OS in the patients who lost CTCs due to the treatment.

The effect of chemotherapy on CTC numbers was evaluated on pre-/on-chemotherapy cohort, and pre-/post-chemotherapy group. The numbers of epithelial, EMT-like, and total CTCs were significantly decreases in on-chemotherapy cohort. Patients who had a decrease in their CTC numbers show an improved on their OS. Furthermore, post-chemotherapy group of patients showed significantly lower number of total and epithelial CTCs, suggesting the effect of chemotherapy treatment on decreasing the CTC numbers in the circulatory system and result in a longer probability

survival. Furthermore, the effects of radiotherapy were studied on patients where the total CTCs counts significantly declined in response to treatment which is associated with prolonged OS.

Lung cancer causes approximately one fifth of all cancer-related deaths in the world. Most lung cancer patients are diagnosed when their disease is too advanced for surgical intervention. A small minority of patients with lung adenocarcinoma present to the clinic with oncogenic driver mutations in the *EGFR* (epidermal growth factor receptor) gene, or rearrangements in the *ALK* (anaplastic lymphoma kinase) or *ROS1* gene.^{164, 229} Additional genomic aberrations include fusions in the *RET* protooncogene.²³⁰

Over the last decade, a number of new therapies targeting signaling pathways that control cell growth and survival have been developed. The discovery and development of small molecule tyrosine kinase inhibitors (TKIs) has revolutionized therapy for specific molecular subsets of NSCLC patients. TKIs competitively bind in the ATP-binding pocket of kinases, thus interfering with tumor growth.²³¹ Examples include Erlotinib, Osimertinib, Gefitinib, and Afatinib for *EGFR*-mutant lung cancers and more recently, Alectinib, Certinib, and Crizotinib for lung cancers harboring chromosomal rearrangements of *ALK*.

Erlotinib is one of reversible *EGFR*-TKIs and recommended as first line treatments for NSCLCs harboring an activating *EGFR* mutation such as an exon 19 deletion or an L858R mutation. Afatinib belongs to a class of irreversible inhibitors of the human epidermal receptor family. However, *EGFR* T790M mutation leads to resistance to most *EGFR* TKIs such as Erlotinib or Afatinib. Osimertinib is the third-generation *EGFR* TKI

and it has shown effects against the T790M mutation. Cetuximab is a monoclonal antibody (mAb) against *EGFR* extracellular domain. Crizotinib is a non-specific small molecule *ALK* inhibitor and Ceritinib is the second-generation *ALK* inhibitor.

These therapies often induce marked responses and clinical remissions. However, the majority of patients will develop resistance to TKIs within a few years.²³²
²³³ The resistance is often mediated by a secondary mutation in the target gene or alternative pathways that supervene and bypass the original signaling pathway.²³⁴

Presently, the only way to ascertain mechanism of resistance is to perform a re-biopsy.^{235, 236} Once the resistance mechanism is identified, there are newer therapies available to target the resistance mechanism. However, there is no definitive method to identify which one of the various drugs that target the “resistance causing mutation” might be the most effective for that individual patient.²³⁴ There is therefore an unmet need, not only to identify resistance early and without a tissue biopsy, but also for drug sensitivity assays that predict response *ex vivo*.

CTC isolation as a non-invasive method could help to identify primary and secondary resistance mutations and allow for *ex vivo* drug testing to direct therapy specific to the patient. Current methods for isolation of lung CTCs mostly rely on biomarker dependent antibody-based capture, missing populations that may be stem-like in nature. Therefore, our technology needs to be highly sensitive and highly specific in order to test isolated cells for driver mutations and resistance mutations, as well as culture cells for *ex vivo* drug testing. Therefore, we utilized the Labyrinth technology to identify and study the CTCs recovering from non-small cell lung cancer patients.

We were able to detect CTCs in all analyzed NSCLC patients whose lung cancers exhibited specific driver mutations/rearrangements. CTCs were detected at numbers of ≥ 10 CTCs mL⁻¹ in 100%, ≥ 50 in 81%, ≥ 100 in 57%, ≥ 200 in 29%, ≥ 400 in 14%, and ≥ 600 in 5% of NSCLC patient samples. We have also found that the number of recovered EpCAM- CTCs (115.7 CTCs mL⁻¹) was significantly higher than the EpCAM+ CTCs (39.1 CTCs mL⁻¹) ($p=0.01$). As such, CTC detection based only on EpCAM (EpCAM+) might miss a substantial number of tumor cells.^{21, 154}

CTC clusters have been observed rarely in various cancers, including lung cancer.^{70, 127} We have previously demonstrated the presence of CTCs in clusters from patients with early-stage lung cancer.¹⁷² To investigate the ability of Labyrinth to isolate CTCs in cluster form, we analyzed the CTCs isolated from advanced NSCLC patients for the presence of clusters. In addition to the single CTCs (28.9 ± 27 CTCs mL⁻¹) recovered from these patients, we were able to isolate CTCs in clusters (125.9 ± 138.9 CTCs mL⁻¹) from 95% of patients ($p=0.005$). Of 19 patient samples, 17 had ≥ 2 clusters, 16 had ≥ 3 clusters, 7 had 4 clusters, 4 had 5 clusters, 1 had 6 clusters, and 2 had 7 clusters. It has been reported that the CTC clusters have a high propensity for survival in circulation and development of metastases.¹²⁷ We found that significantly higher numbers of recovered clusters were EpCAM- ($p=0.009$) and 36% of them displayed mesenchymal markers, suggestive of a preponderance of an EMT phenotype in CTC clusters.^{237, 238}

It has been shown previously that matched *EGFR* mutations were detected in CTCs in 84% of patients carrying *EGFR* mutations in their primary tumors.²³⁹ In another study, all NSCLC patients with *ALK* rearranged tumors had detectable

CTCs in their baseline blood samples.²⁴⁰ We utilized FISH analysis to explore whether the recovered CTCs from driver mutant lung adenocarcinoma patients with aberration in *ROS1*, *ALK*, and *RET* carry the genomic signature of the primary tumor. Our results revealed that a 5' deletion of *ROS1* in the recovered CTCs from a patient with a known *ROS1* rearrangement in the primary tumor, an *ALK* rearrangement in the CTCs, matching the patient's primary tumor, and a 3'deletion of *RET* in recovered CTCs from a patient with a *RET* rearranged tumor.

To be able to expand patient-derived CTCs for *ex vivo* drug testing, it is necessary to reduce the off-target cells (mostly RBCs and WBCs) after CTCs enrichment. We utilized many techniques for the RBCs removals including, RBC lysis buffer, cell strainer, and microbubbles. However, applying these techniques resulted in excessive loss of CTCs. Although, utilizing Ficoll-Paque showed a great promise on higher CTC enrichment and lower RBC numbers after Labyrinth, the need of a faster, reliable, and more robust system still is a challenge.

Patient-derived CTCs could be a useful method for therapeutic testing, but to date it has been difficult to expand this population of cells. To date, only few groups have been able to expand CTCs in *ex vivo*.^{125, 241-244} The challenge of culturing CTCs comes from not only the rarity of the captured population, but also from the physical distance between the cells. Therefore, the environment imposes stresses that may prevent cells from growing and instead, induce them to undergo apoptosis. To overcome these challenges, a Matrigel-Collagen culture model supplemented with conditional media

from human pancreatic cancer associated fibroblast cells, and human platelet lysates were utilized for the NSCLC patient-derived CTC expansion *ex vivo*.

The half maximal inhibitory concentration (IC₅₀) analysis is the most commonly used technique for drug testing analysis. The IC₅₀ numbers may be influenced by several conditions such as, number of cells, cell culture conditions, and the viability assay kits (for example the metabolism-based or DNA synthesis-based). Various NSCLC cell lines were used simultaneously as positive/negative controls along with the expanded CTCs for drug testing. The drug testing was performed on these expanded CTC using various TKIs directed against the genomic drivers.

The first patient (P 03) had a *ROS1* rearranged NSCLC on Entrectinib therapy. Following successful expansion during visit 6, we tested this patient's CTCs against Entrectinib, Lorlatinib, and TPX-0005. The IC₅₀ data could echo the clinical inefficiency of Entrectinib on this patient. Her expanded CTCs were not sensitive to Lorlatinib either. However, TPX-0005 could direct her to a clinical trial. Concurrently, it was noted that the patient was noted to have CNS progression on scans on Entrectinib. Given the relative sensitivity to TPX-0005, this patient could be directed to a clinical trial using this compound.

The second patient (P 22) had an *EGFR* mutant NSCLC, on Osimertinib therapy. Following successful expansion during visit 8, we tested this patient's CTCs against various *EGFR* TKIs as well as TPX-0005. We found that the expanded CTCs were resistant to Osimertinib, but sensitive to TPX-0005 as well as to the combination of Osimertinib and TPX-0005. Given the relative sensitivity to TPX-0005, this patient could be directed to a clinical trial using this compound.

5 Conclusion

Primary tumors are constituted of heterogeneous populations of cells from which circulating tumor cells (CTCs) are derived.²⁴⁵ Hence, CTCs may allow for dynamic, continual assessment of the tumor's biological activity and provide a relatively facile means of monitoring the important yet poorly understood epithelial-to-mesenchymal transition (EMT) of disseminated cells. Therefore, CTCs have emerged as important blood-based surrogate markers of primary tumors. By detecting and analyzing primary tumor-derived CTCs, we would obtain useful information about disease status noninvasively. The field of study involving CTCs has evolved at a rapid pace that may eventually provide a valuable point of care assessment of cancer prognosis and prediction of the effectiveness of therapy.

To develop the clinical applications of CTCs for personalized therapy in many types of cancers, there is a compelling need for sensitive and accurate approaches to distinguish CTCs from other blood cells. Microfluidic-based technologies have changed the existing paradigm for the recovery of CTCs from cancer patients. Two main approaches for the isolation of CTCs utilizing microfluidic devices are immunoaffinity capture and label-free size-based methods. We have developed and utilized both of these approaches in various cancer types including pancreatic, breast, prostate and lung cancer.^{69, 72, 103, 133, 168, 246}

Pancreatic cancer has one of the lowest survival rates among all cancers. Tumor invasion to other organs has often already occurred by the time of diagnosis. Hence, there is an urgent need for methods that enable early detection.

We presented an integrated technology and biology-based approach using a microfluidic “Carpet Chip” with different spacing between posts and arrays to study the biological relevance of heterogeneous CTC populations in pancreatic cancer.¹³³ Both epithelial CTCs (EpCs) and EMT-like CTCs (EMTCs) are isolated simultaneously from whole blood of pancreatic cancer patients (n=35) by separately targeting two surface markers: EpCAM to capture EpCAM+ CTCs, and CD133 to capture more stem cell like cells, or putative EpCAM- CTCs.^{133, 155}

Different spacing between posts and arrays, enabled us to increase the capture efficiencies (>97%) and purity (>76%), which is crucial for downstream gene analysis. Thirty-four patients had ≥ 5 EpCs mL^{-1} and 35 patients had ≥ 15 EMTCs mL^{-1} . Overall, significantly higher numbers of EMTCs than EpCs are recovered, reflecting the aggressive nature of pancreatic cancer. Furthermore, higher numbers of EMTCs are observed in patients with lymph node involvement compared to patients without. Our results indicate that enumeration, detection, and molecular characterization of these CTC populations show a great promise as a diagnostic and therapeutic tool for detection of cancer and metastasis.

Gene expression profiling of CTCs from 17 patients reveals that CXCR1 is significantly upregulated in EpCs, while known stem cell markers POU5F1 and MYC are upregulated in EMTCs. Our findings on gene expression profiling of CTCs from early stage pancreatic cancer patients may improve prediction of survival and outcomes. Based on our observations on EMTCs and lymph node involvement, targeting the genes involved in the EMT process and individualized therapy could reduce metastasis, thereby increasing the survival rate of pancreatic cancer patients.³⁶

Among the analyzed genes, BMI1, CDH2, ERCC1, and TTF1 showed higher expression in early stage patients (stage IIA) compared to the rest of stages which were also significantly associated with prolonged OS and/or PFS. However, pancreatic cancer patients with higher expression of stem marker POU5F1 showed worse PFS. In this study, successful isolation and genomic profiling of heterogeneous CTC populations are demonstrated, revealing genetic signatures relevant to patient outcomes. Overall, isolating different CTC populations separately may help us predict the patient's outcome.

Among the existing CTC isolation technologies, high throughput, label-free, microfluidic devices have advantages compared with other available techniques. By removing the bias of using molecular markers for CTC isolation, heterogeneous CTC subpopulations can be recovered using label-free isolation. Each different population may carry distinct, important information that could predict patient outcomes. Herein, we utilized a high throughput, continuous, biomarker-independent, and size-based microfluidic separation technology, Labyrinth, to isolate CTCs from whole blood of pancreatic and non-small cell lung cancer patients.¹⁹⁸

Using Labyrinth, we were able to isolate epithelial CTCs (9.7 ± 15.7 CTCs mL⁻¹) and EMT-like CTCs (9 ± 9.8 CTCs mL⁻¹) from treatment naïve pancreatic cancer patients (n=141). This cohort was stratified based on their tumor staging: resectable, borderline resectable, locally advanced, and metastatic. The CTC numbers were significantly higher in the borderline resectable group. This cohort was further stratified by each patient's treatment options, surgery, chemotherapy, and radiotherapy. For all the

treatment options, we observed a statistically significant decrease in CTC counts after treatment completion, which was associated with prolonged OS.

Lung cancer is the leading cause of cancer-related death in the world. CTCs have shown tremendous promise in lung cancer for therapeutic monitoring, especially in predicting drug resistance. We evaluated the detection of heterogeneous CTC populations isolated from NSCLC patient blood samples (n=19) using the Labyrinth device. The Labyrinth device was optimized and tested for inertial separation of cancer cells using the human lung cancer cell line H1650. The recovery and purity were >82% and >78%, respectively, operating at a flow rate of 2.5 mL min⁻¹.

Heterogeneous CTC populations were detected, including CTCs (PanCK+ and CD45-), CTCs expressing EpCAM or Vimentin, and CTCs expressing both markers representing an EMT-like population of CTCs. Using Labyrinth, we were able to isolate CTCs from 100% of patients with an average yield of 180±168 CTCs mL⁻¹, while the healthy control group showed 1±1.7 total CTCs mL⁻¹ (p=0.001). Among the captured CTCs, EpCAM- CTCs were significantly more common than EpCAM+ CTCs (115.7 vs. 39.1 CTCs mL⁻¹ respectively). Of recovered CTCs, on average, only 28.7% of CTCs expressed some level of EpCAM, emphasizing the need for label-free approaches for studying lung CTCs. In addition, an average 39.6% of CTCs expressed Vimentin. Among 21 analyzed patient samples, 20 samples had Vimentin+ CTCs, indicating the presence of Vimentin+ EMT-like cells in circulation in NSCLC.

In addition to single CTCs, we have observed CTC clusters (≥2 CTCs) in 95% of NSCLC patients. Among the total number of clusters (905.2 clusters mL⁻¹) recovered from all 19 patient samples, 79% of cell-clusters were negative for EpCAM expression,

whereas 35% of clusters expressed the EMT marker Vimentin, suggestive of an EMT phenotype in CTC clusters. These findings indicate the advantage of the label-free approach for isolating CTC subpopulations in both single and cluster forms.

We have been able to detect tumor related-mutations in the recovered CTCs from patients with driver mutant lung adenocarcinoma. Recovered CTCs from patients with *RET*, *ROS1*, and *ALK* rearranged tumors showed aberrations matching with the primary tumor for each gene using FISH analysis. The label-free Labyrinth device demonstrated the advantages of marker-independent separation methods in identifying heterogenous CTC sub-population in lung cancer.

The isolated CTCs were successfully expanded *ex vivo* from two patients and were screened for therapeutic efficacy. A Matrigel-Collagen (3D) model was utilized for *ex vivo* expansion and the drug testing was performed using various TKIs directed against known genomic drivers of lung cancer. We found that the expanded CTCs from a NSCLC patient with *ROS1* rearrangement were resistant to Entrectinib (IC₅₀=2357 nM) and lorlatinib (IC₅₀=15979 nM). The second successful expanded CTCs from NSCLS patient with *EGFR* mutation were resistant to Osimertinib (IC₅₀=34167 nM). The IC₅₀ results on the expanded CTCs were consistent with patients clinical outcomes. We have successfully found a new potential TKI, TPX-0005 (IC₅₀=278 nM for the patient with *ROS1* rearrangement, and IC₅₀=392 nM for the patient with *EGFR* mutation) which might be effective in these patients and would direct them to a clinical trial using this compound.

There is an unmet need to diagnose any kind of cancers by non-invasive methods as well as to develop methods to predict drug sensitivity, *ex vivo*. Although *in*

vivo applications of label-free technologies are still very limited, the capability of collecting recovered CTCs from the device using a continuous processing technique while in a suspension state opens the opportunities not only for CTC expansion off-chip but also for *ex vivo* drug testing to direct patient-specific therapies. The specificity of genomic aberration, as well as defined therapies for lung cancers, make them ideally suited to test our CTC platform for diagnosis, CTC expansion, and drug testing. However, in order to perform the drug testing for each patient samples, we still need to optimize the CTC expansion methods.

Moreover, single-cell diagnostics including those based on CTCs, are predicted to be instrumental for the realization of personalized medicine and for the development of completely novel therapeutic concepts. The single cell workflow process allows rapid and reliable isolation, processing, and profiling of individual cells for multiple genomics applications.

In order for CTCs to become a routine clinical test for personalized therapy in lung and other cancers that are associated with specific genomic alterations, there is a compelling need for sensitive, accurate, and validated approaches. There is currently no way to predict which of the many early phase compounds that target resistance mechanisms will actually lead to further response in the patient. Having the ability to culture CTCs *ex vivo* reproducibly and without loss of genetic fidelity may allow us to perform *ex vivo* drug testing as a parallel “co-clinical” trial.

Our recent and encouraging breakthroughs in optimizing conditions for CTC expansion and *ex vivo* drug testing in NSCLC patients (n=2) needs to be validated in additional patients in a prospective manner. We still need to understand molecular

mechanisms underlying therapeutic resistance in lung cancer as observed by CTCs' response to therapy. It is also beneficial to understand aberrations in intracellular RNA silencing pathways at a single cell level in the CTCs during the course of therapy in these specific driver mutant lung cancers. The expanded CTCs yet need to be validated via genomic characterization, as well as, test the patient derived CTCs for drug resistance. Furthermore, in order to validate the utility of the expanded CTCs, CTC-derived xenograft mice (Nod/Scid) model need to be utilized, which could serve as a method to examine expanded CTCs *in vitro* properties including tumorigenicity and drug susceptibility (Figure 5-1).

Due to the CTC enrichment and expansion challenges new approaches for CTC drug screening need to be established such as 3D single-cell analysis based on 3D culture platform. High throughput screening approaches for single CTCs will give further advance individually drug administration. However, breaking through the bottlenecks for single cell in 3D long-term culture still is a critical factor to overcome.

Last but not the least, we need to validate more CTCs from a variety of patients by variant TKIs in a prospective manner which might give benefit to optimize the systemic therapy and enable early decision-making to tailor effective antitumor strategies.

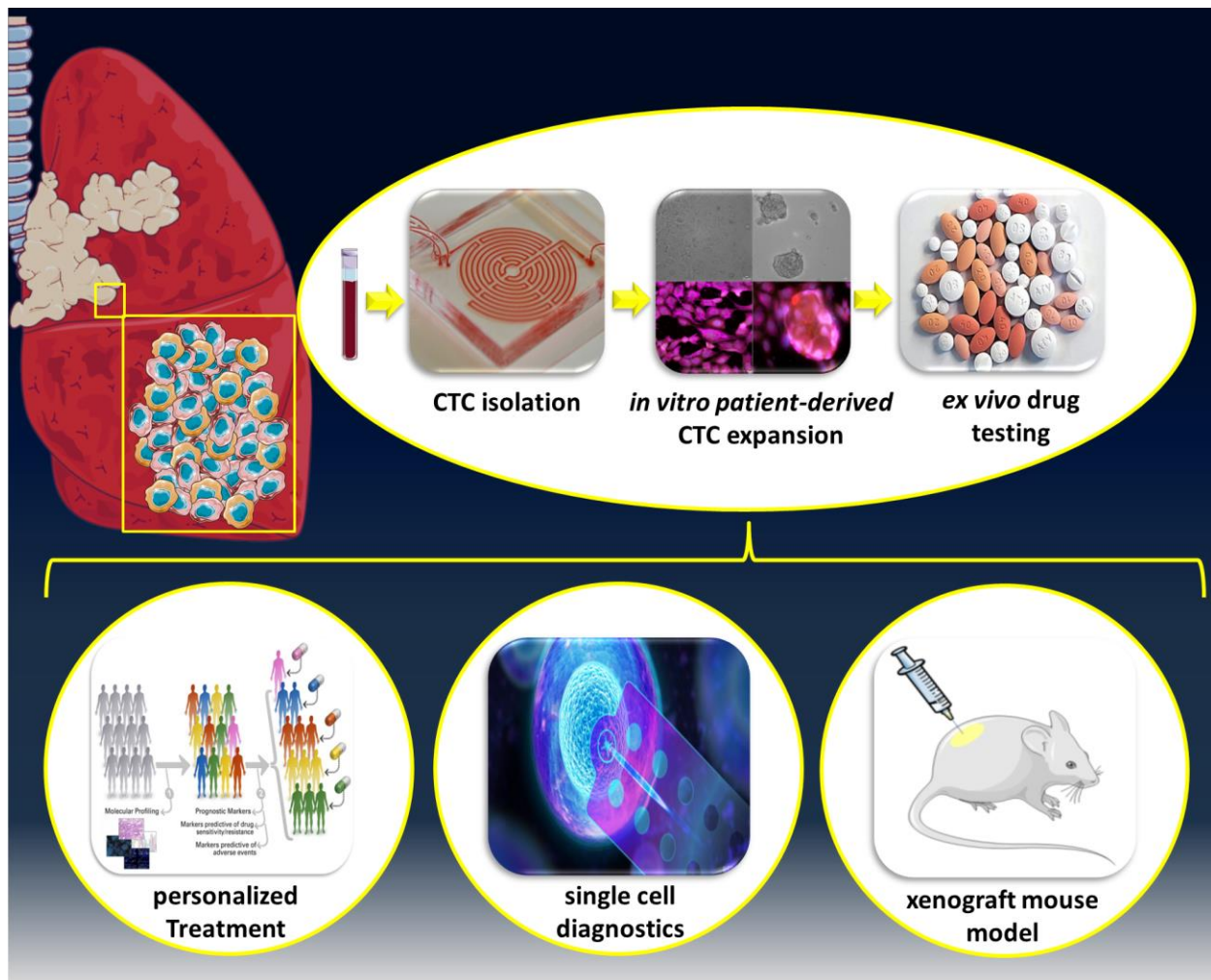


Figure 5-1: Biomarker independent microfluidics strategy and the future direction for CTC based tumor models in lung cancer.²⁴⁷⁻²⁴⁹

6 Summary

Circulating tumor cells (CTCs) are cancerous cells that shed from a primary tumor, intravasate into blood, travel through the blood circulation, and then extravasate to distant organs and form secondary tumors. Hence, CTCs are critical to understand the biological process of metastasis and could serve as potential blood-based surrogate markers to noninvasively evaluate tumor progression and response to treatment.

Although isolation of CTCs from pancreatic adenocarcinoma (PDAC) patients is feasible, investigating their clinical utility has proven less successful than in other cancers due to limitations of epithelial cellular adhesion molecule (EpCAM)-only based CTC assays. We developed a "Carpet Chip" using sequential immunoaffinity-based microfluidics to study the biological relevance of heterogeneous CTCs. Both epithelial (EpCs) and epithelial-to-mesenchymal transition (EMT)-like CTCs (EMTCs) were detected from the blood of PDAC patients (n=35). Thirty-four patients had ≥ 5 EpCs mL^{-1} and 35 patients had ≥ 15 EMTCs mL^{-1} . Overall, significantly higher numbers of EMTCs than EpCs were recovered, reflecting the aggressive nature of PDAC. Furthermore, higher numbers of EMTCs were observed in patients with lymph node involvement compared to patients without. Gene expression profiling of CTCs from 17 patients revealed that CXCR1 is significantly upregulated in EpCs, while known stem cell markers POU5F1, or Oct-4 and MYC were upregulated in EMTCs. Thus, successful isolation and genomic profiling of heterogeneous CTC populations were demonstrated, revealing genetic signatures relevant to patient outcomes. Individualizing therapies targeting genes involved in EMT could reduce metastasis and improve patient survival.

In further studies on PDAC patients, the utility of CTCs as a tool was validated for assessing tumor response to the only three therapy options currently available: surgery, chemotherapy, and radiotherapy. For all treatment options, we observed a statistically significant decrease in CTC counts after treatment completion, which was associated with prolonged OS.

Orthogonally, in an effort to develop label-free technologies for CTC isolation, a microfluidic Labyrinth device for high throughput, label-free, size-based isolation of CTCs was applied to study CTCs from metastatic non-small cell lung cancer patients (NSCLC). Current methods for isolation of lung CTCs mostly rely on biomarker dependent antibody-based capture, missing populations that may be stem-like in nature. Using Labyrinth operating at a flow rate of 2.5 mL/min, heterogeneous CTC populations were isolated from NSCLC patients (n=21). Detected populations included CTCs (PanCK+ and CD45-), CTCs expressing EpCAM or Vimentin, and CTCs expressing both markers representing an EMT-like population of CTCs. We were able to isolate CTCs from 100% of patients with an average yield of 180 ± 168 CTCs mL⁻¹. Among captured CTCs, EpCAM- CTCs were significantly more common than EpCAM+ CTCs (115.7 vs. 39.1 CTCs mL⁻¹ respectively). Cell clusters of 2 or more CTCs were also observed in 95% of patients; 79% of these clusters were negative for EpCAM expression, whereas 35% expressed Vimentin, suggestive of an EMT phenotype. Recovered CTCs from patients with *RET*, *ROS1* and *ALK* rearrangements in tumors showed aberrations matching the primary tumor for each gene using FISH analysis. We successfully expanded CTCs *in vitro* and the cultured cells carried matched mutations. The Labyrinth device demonstrated the advantages of marker-independent separation

methods for isolation of heterogonous CTC sub-populations in lung cancer for CTC expansion, allowing drug testing for therapies targeting specific driver mutations.

The capability of collecting recovered CTCs from the device using a continuous processing technique opens up opportunities for not only CTC expansion off-chip, but also ex-vivo drug testing to direct patient-specific therapies.

7 ZUSAMMENFASSUNG

Zirkulierende Tumorzellen (CTCs) sind Krebszellen, die aus einem Primärtumor ausgeschieden werden, sich in Blut intravasieren, durch den Blutkreislauf wandern und dann in entfernte Organe extravasieren und sekundäre Tumore bilden. Daher sind CTCs für das Verständnis des biologischen Prozesses der Metastasierung von entscheidender Bedeutung und könnten als mögliche Ersatzmarker auf Blutbasis dienen, um die Tumorprogression und das Ansprechen auf die Behandlung nicht-invasiv zu bewerten. Obwohl die Isolierung von CTCs aus Patienten mit Pankreasadenokarzinom (PDAC) durchführbar ist, hat sich die Untersuchung ihres klinischen Nutzens aufgrund von Einschränkungen der nur auf EpCAM-basierenden CTC-Tests auf Epithelzellen (EpCAM) basierenden Tests als weniger erfolgreich erwiesen.

Wir entwickelten einen "Carpet-Chip" mit sequenziellen Mikrofluidik auf Immunoaffinitätsbasis, um die biologische Relevanz heterogener CTCs zu untersuchen. Sowohl epitheliale (EpCs) als auch epithelial-mesenchymale Übergangs (EMT) - ähnliche CTCs (EMTCs) wurden aus dem Blut von PDAC Patienten (n = 35) detektiert. Vierunddreißig Patienten hatten ≥ 5 EpCs mL⁻¹ und 35 Patienten hatten ≥ 15 EMTCs mL⁻¹. Insgesamt wurden deutlich mehr EMTCs als EpCs gewonnen, was die Aggressivität von PDAC widerspiegelt. Darüber hinaus wurden bei Patienten mit Lymphknotenbefall im Vergleich zu Patienten ohne EMTC eine höhere Anzahl von EMTCs beobachtet. Genexpressionsprofile von CTCs von 17 Patienten zeigten, dass CXCR1 in EpCs signifikant hochreguliert ist, während bekannte Stammzellmarker POU5F1 oder Oct-4 und MYC in EMTCs hochreguliert wurden. So wurde die

erfolgreiche Isolierung und das genomische Profiling heterogener CTC-Populationen demonstriert, was genetische Signaturen aufzeigt, die für die Patientenergebnisse relevant sind. Durch die Individualisierung von Therapien, die auf Gene abzielen, die an der EMT beteiligt sind, könnte die Metastasierung verringert und das Überleben der Patienten verbessert werden.

In weiteren Studien an PDAC-Patienten wurde der Nutzen von CTCs als Instrument für die Bewertung der Tumorreaktion auf die drei derzeit verfügbaren Therapiemöglichkeiten validiert: Operation, Chemotherapie und Strahlentherapie. Bei allen Behandlungsoptionen beobachteten wir eine statistisch signifikante Abnahme der CTC-Werte nach Abschluss der Behandlung, die mit einem verlängerten OS verbunden war.

In dem Bestreben, kennzeichnungsfreie Technologien für die CTC-Isolierung zu entwickeln, wurde orthogonal ein mikrofluidisches Labyrinth-Gerät für die markierungsfreie, größenbasierte Isolierung von CTCs mit hohem Durchsatz angewendet, um CTCs von Patienten mit metastasiertem nicht kleinzelligem Lungenkrebs (NSCLC) zu untersuchen. Derzeitige Methoden zur Isolierung von Lungen-CTCs basieren meistens auf Biomarker-abhängiger Erfassung von Antikörpern, wobei Populationen fehlen, die möglicherweise stammähnlich sind. Unter Verwendung von Labyrinthbetrieb, das mit einer Flussrate von 2,5 ml / min betrieben wurde, wurden heterogene CTC-Populationen aus NSCLC-Patienten (n = 21) isoliert. Zu den entdeckten Populationen gehörten CTCs (PanCK + und CD45-), CTCs, die EpCAM oder Vimentin exprimieren, und CTCs, die beide Marker exprimieren, die eine EMT-ähnliche Population von CTCs darstellen. Wir konnten CTCs von 100% der Patienten

mit einer durchschnittlichen Ausbeute von 180 ± 168 CTCs/mL-1 isolieren. Unter den erfassten CTCs waren EpCAM-CTCs signifikant häufiger als EpCAM + CTCs (115,7 vs. 39,1 CTCs/mL-1). Bei 95% der Patienten wurden auch Zellcluster von 2 oder mehr CTCs beobachtet. 79% dieser Cluster waren für die EpCAM-Expression negativ, während 35% Vimentin exprimierten, was auf einen EMT-Phänotyp hindeutet. Wiederhergestellte CTCs von Patienten mit RET-, ROS1- und ALK-Umlagerungen in Tumoren zeigten unter Verwendung der FISH-Analyse für jedes Gen Abbildungsfehler, die mit dem Primärtumor übereinstimmen.

Wir konnten CTCs in vitro erfolgreich ausbauen und die kultivierten Zellen übereinstimmende Mutationen tragen. Die Labyrinth-Vorrichtung demonstrierte die Vorteile von markerunabhängigen Trennungsvorgängen für heterogene CTC-Subpopulationen in einer CGD für die CTC-Dilatation, wodurch Medikamententests für Therapien durchgeführt werden können, die auf spezifische Treibermutationen abzielen. Die Möglichkeit, gewonnene CTCs mithilfe einer kontinuierlichen Verarbeitungstechnik vom Gerät zu sammeln, eröffnet nicht nur Möglichkeiten für die CTC-Erweiterung außerhalb des Chips, sondern auch Ex-vivo-Drogentests, um patientenspezifische Therapien zu steuern.

8 References

1. Alunni-Fabbroni, M, Sandri, MT: Circulating tumour cells in clinical practice: Methods of detection and possible characterization. *Methods*, 50: 289-297, 2010.
2. Tjensvoll, K, Nordgard, O, Smaaland, R: Circulating tumor cells in pancreatic cancer patients: Methods of detection and clinical implications. *International Journal of Cancer*, 134: 1-8, 2014.
3. Torphy, RJ, Tignanelli, CJ, Moffitt, RA, Soper, SA, Yeh, JJ: Circulating tumor cells as a biomarker of response to treatment in patient derived xenograft mouse models of pancreatic adenocarcinoma. *Journal of the American College of Surgeons*, 217: S30-S30, 2013.
4. Nagrath, S, Sequist, LV, Maheswaran, S, Bell, DW, Irimia, D, Ulkus, L, Smith, MR, Kwak, EL, Digumarthy, S, Muzikansky, A, Ryan, P, Balis, UJ, Tompkins, RG, Haber, DA, Toner, M: Isolation of rare circulating tumour cells in cancer patients by microchip technology. *Nature*, 450: 1235-U1210, 2007.
5. Bednarz-Knoll, N, Alix-Panabieres, C, Pantel, K: Plasticity of disseminating cancer cells in patients with epithelial malignancies. *Cancer and Metastasis Reviews*, 31: 673-687, 2012.
6. Kurihara, T, Itoi, T, Sofuni, A, Itokawa, F, Tsuchiya, T, Tsuji, S, Ishii, K, Ikeuchi, N, Tsuchida, A, Kasuya, K, Kawai, T, Sakai, Y, Moriyasu, F: Detection of circulating tumor cells in patients with pancreatic cancer: a preliminary result. *Journal of Hepato-Biliary-Pancreatic Surgery*, 15: 189-195, 2008.
7. Kanwar, N, Done, S: Circulating Tumour Cells: Implications and Methods of Detection. 2011.
8. Stott, SL, Hsu, CH, Tsukrov, DI, Yu, M, Miyamoto, DT, Waltman, BA, Rothenberg, SM, Shah, AM, Smas, ME, Korir, GK, Floyd, FP, Gilman, AJ, Lord, JB, Winokur, D, Springer, S, Irimia, D, Nagrath, S, Sequist, LV, Lee, RJ, Isselbacher, KJ, Maheswaran, S, Haber, DA, Toner, M: Isolation of circulating tumor cells using a microvortex-generating herringbone-chip. *Proceedings of the National Academy of Sciences of the United States of America*, 107: 18392-18397, 2010.
9. Zhang, Z, Nagrath, S: Microfluidics and cancer: are we there yet? *Biomedical microdevices*, 15: 595-609, 29 January 2013.
10. Khoja, L, Backen, A, Sloane, R, Menasce, L, Ryder, D, Krebs, M, Board, R, Clack, G, Hughes, A, Blackhall, F, Valle, JW, Dive, C: A pilot study to explore circulating tumour cells in pancreatic cancer as a novel biomarker. *British journal of cancer*, 106: 508-516, 2012.
11. Yu, M, Ting, DT, Stott, SL, Wittner, BS, Oszolak, F, Paul, S, Ciciliano, JC, Smas, ME, Winokur, D, Gilman, AJ, Ulman, MJ, Xega, K, Contino, G, Alagesan, B, Brannigan, BW, Milos, PM, Ryan, DP, Sequist, LV, Bardeesy, N, Ramaswamy, S, Toner, M, Maheswaran, S, Haber, DA: RNA sequencing of pancreatic circulating tumour cells implicates WNT signalling in metastasis. *Nature*, 487: 510-U130, 2012.
12. Armstrong, AJ, Marengo, MS, Oltean, S, Kemeny, G, Bitting, RL, Turnbull, JD, Herold, CI, Marcom, PK, George, DJ, Garcia-Blanco, MA: Circulating Tumor Cells from Patients with Advanced Prostate and Breast Cancer Display Both Epithelial and Mesenchymal Markers. *Molecular Cancer Research*, 9: 997-1007, 2011.
13. Stott, SL, Lee, RJ, Nagrath, S, Yu, M, Miyamoto, DT, Ulkus, L, Inserra, EJ, Ulman, M, Springer, S, Nakamura, Z, Moore, AL, Tsukrov, DI, Kempner, ME, Dahl, DM, Wu, CL, Iafrate, AJ, Smith, MR, Tompkins, RG, Sequist, LV, Toner, M, Haber, DA, Maheswaran, S: Isolation and Characterization of Circulating Tumor Cells from Patients with Localized and Metastatic Prostate Cancer. *Science Translational Medicine*, 2, 2010.
14. Cen, P, Ni, X, Yang, J, Graham, DY, Li, M: Circulating tumor cells in the diagnosis and management of pancreatic cancer. *Biochimica et biophysica acta*, 1826: 350-356, 2012.
15. de Albuquerque, A, Kubisch, I, Breier, G, Stamminger, G, Fersis, N, Eichler, A, Kaul, S, Stolz, U: Multimarker gene analysis of circulating tumor cells in pancreatic cancer patients: a feasibility study. *Oncology*, 82: 3-10, 2012.

16. Ren, CL, Han, CX, Zhang, JQ, He, P, Wang, DX, Wang, BH, Zhao, P, Zhao, XH: Detection of apoptotic circulating tumor cells in advanced pancreatic cancer following 5-fluorouracil chemotherapy. *Cancer Biology & Therapy*, 12: 700-706, 2011.
17. Han, L, Chen, W, Zhao, Q: Prognostic value of circulating tumor cells in patients with pancreatic cancer: a meta-analysis. *Tumour Biol*, 2013.
18. Crowley, E, Di Nicolantonio, F, Loupakis, F, Bardelli, A: Liquid biopsy: monitoring cancer-genetics in the blood. *Nature Reviews Clinical Oncology*, 10: 472-484, 2013.
19. M. Liberko, K. Kolostova, V. Bobek: Essentials of circulating tumor cells for clinical research and practice. *Critical reviews in oncology/hematology*, vol. 88, Nov. 2013.
20. Chen, CL, Mahalingam, D, Osmulski, P, Jadhav, RR, Wang, CM, Leach, RJ, Chang, TC, Weitman, SD, Kumar, AP, Sun, LZ, Gaczynska, ME, Thompson, IM, Huang, THM: Single-cell analysis of circulating tumor cells identifies cumulative expression patterns of EMT-related genes in metastatic prostate cancer. *Prostate*, 73: 813-826, 2013.
21. Pantel, K, Alix-Panabieres, C: Circulating tumour cells in cancer patients: challenges and perspectives. *Trends in Molecular Medicine*, 16: 398-406, 2010.
22. Ashworth, TR: A case of cancer in which cells similar to those in the tumours were seen in the blood after death. *The Medical Journal of Australia*, 14: 146-147, 1869.
23. Paget, S: The distribution of secondary growths in cancer of the breast. 1889. *Cancer Metastasis Rev*, 8: 98-101, 1989.
24. Yu, M, Bardia, A, Wittner, B, Stott, SL, Smas, ME, Ting, DT, Isakoff, SJ, Ciciliano, JC, Wells, MN, Shah, AM, Conncannon, KF, Donaldson, MC, Sequist, LV, Brachtel, E, Sgroi, D, Baselga, J, Ramaswamy, S, Toner, M, Haber, DA, Maheswaran, S: Circulating Breast Tumor Cells Exhibit Dynamic Changes in Epithelial and Mesenchymal Composition. *Science*, 339: 580-584, 2013.
25. Zhang, ZY, Ge, HY: Micrometastasis in gastric cancer. *Cancer Lett*, 336: 34-45, 2013.
26. E., K: Role of Epithelial-Mesenchymal Transition in Pancreatic Ductal Adenocarcinoma: Is Tumor Budding the Missing Link? *Frontiers in oncology*, 2013 Sep 17.
27. Satelli, A, Li, SL: Vimentin in cancer and its potential as a molecular target for cancer therapy. *Cellular and Molecular Life Sciences*, 68: 3033-3046, 2011.
28. Sarrio, D, Rodriguez-Pinilla, SM, Hardisson, D, Cano, A, Moreno-Bueno, G, Palacios, J: Epithelial-mesenchymal transition in breast cancer relates to the basal-like phenotype. *Cancer Research*, 68: 989-997, 2008.
29. Lee, JM, Dedhar, S, Kalluri, R, Thompson, EW: The epithelial-mesenchymal transition: new insights in signaling, development, and disease. *J Cell Biol*, 172: 973-981, 2006.
30. Kallergi, G, Papadaki, MA, Politaki, E, Mavroudis, D, Georgoulas, V, Agelaki, S: Epithelial to mesenchymal transition markers expressed in circulating tumour cells of early and metastatic breast cancer patients. *Breast Cancer Research*, 13, 2011.
31. Mendez, MG, Kojima, SI, Goldman, RD: Vimentin induces changes in cell shape, motility, and adhesion during the epithelial to mesenchymal transition. *Faseb Journal*, 24: 1838-1851, 2010.
32. Ivaska, J: Vimentin: Central hub in EMT induction? *Small GTPases*, 2: 51-53, 2011.
33. Kokkinos, MI, Wafai, R, Wong, MK, Newgreen, DF, Thompson, EW, Waltham, M: Vimentin and epithelial-mesenchymal transition in human breast cancer--observations in vitro and in vivo. *Cells Tissues Organs*, 185: 191-203, 2007.
34. Kalluri, R, Weinberg, RA: The basics of epithelial-mesenchymal transition. *J Clin Invest*, 119: 1420-1428, 2009.
35. Kalluri, R: EMT: When epithelial cells decide to become mesenchymal-like cells. 2015.
36. Beuran, M, Negoï, I, Paun, S, Ion, AD, Bleotu, C, Negoï, RI, Hostiuc, S: The epithelial to mesenchymal transition in pancreatic cancer: A systematic review. *Pancreatology*, 2015.

37. Lee, CJ, Dosch, J, Simeone, DM: Pancreatic cancer stem cells. *Journal of Clinical Oncology*, 26: 2806-2812, 2008.
38. Ischenko, I, Seeliger, H, Kleespies, A, Angele, MK, Eichhorn, ME, Jauch, KW, Bruns, CJ: Pancreatic cancer stem cells: new understanding of tumorigenesis, clinical implications. *Langenbecks Archives of Surgery*, 395: 1-10, 2010.
39. Nel, I, Jehn, U, Gauler, T, Hoffmann, A-C: Individual profiling of circulating tumor cell composition in patients with non-small cell lung cancer receiving platinum based treatment. *Translational Lung Cancer Research*, 3: 100-106, 2014.
40. Xu, L: Cancer stem cell in the progression and therapy of pancreatic cancer. *Frontiers in Bioscience-Landmark*, 18: 795-802, 2013.
41. Low, WS, Kadri, NA, Abas, WA: Computational fluid dynamics modelling of microfluidic channel for dielectrophoretic BioMEMS application. *ScientificWorldJournal*, 2014: 961301, 2014.
42. Polla, DL: BioMEMS Applications in Medicine. 2001.
43. Saliterman, SS: Fundamentals of BioMEMS and Medical Microdevices. 2006.
44. Daneshvar, ED: Conjugated Polymer Actuators for Articulating Neural Probes and Electrode Interfaces. 2014.
45. Borenstein, JT: BioMEMS Technologies for Regenerative Medicine. *Materials Research Society*, 1139, 2009.
46. B. Lin: Microfluidics, Technologies and Application. *Springer, New York, NY, USA*, 2011.
47. Qin, G, Liu, Y, Liu, H, Ding, Y, Qi, X, Du, R: Fabrication of bio-microelectrodes for deep-brain stimulation using microfabrication and electroplating process. *Microsystem Technologies*, 15: 933-939, 2009.
48. Guber, AE, Herrmann, D, Mühlberger, H, Hoffmann, W, Gerlach, A, Gottschlich, N: Lab-on-a-Chip-Systeme für die Online-Analytik. *Chemie Ingenieur Technik*, 76: 1332-1332, 2004.
49. Saem, S, Zhu, Y, Luu, H, Moran-Mirabal, J: Bench-Top Fabrication of an All-PDMS Microfluidic Electrochemical Cell Sensor Integrating Micro/Nanostructured Electrodes. *Sensors (Basel, Switzerland)*, 17: 732, 2017.
50. Yung-Chieh Tan, aJSF, a Alan I. Lee, a Vittorio Cristiniab and Abraham Phillip, Lee: Design of microfluidic channel geometries for the control of droplet volume, chemical concentration, and sorting. 2004.
51. Samuel K. Sia, GMW: Microfluidic devices fabricated in poly(dimethylsiloxane) for biological studies. *Electrophoresis*, 24, 3563-3576, 2003.
52. Liberko, M, Kolostova, K, Bobek, V: Essentials of circulating tumor cells for clinical research and practice. *Crit Rev Oncol Hemat*, 88: 338-356, 2013.
53. Gorges, TM, Pantel, K: Circulating tumor cells as therapy-related biomarkers in cancer patients. *Cancer immunology, immunotherapy : CII*, 62: 931-939, 2013.
54. Fiegl, M, Kircher, B, Zojer, N: Correspondence re: T. Fehm et al., cytogenetic evidence that circulating epithelial cells in patients with carcinoma are malignant. *Clin. Cancer Res.*, 8: 2073-2084, 2002. *Clinical Cancer Research*, 9: 1224-1225, 2003.
55. Moreno, JG, O'Hara, SM, Gross, S, Doyle, G, Fritsche, H, Gomella, LG, Terstappen, LW: Changes in circulating carcinoma cells in patients with metastatic prostate cancer correlate with disease status. *Urology*, 58: 386-392, 2001.
56. Moreno, JG, Miller, MC, Gross, S, Allard, WJ, Gomella, LG, Terstappen, LW: Circulating tumor cells predict survival in patients with metastatic prostate cancer. *Urology*, 65: 713-718, 2005.
57. Fizazi, K, Morat, L, Chauveinc, L, Prapotnich, D, De Crevoisier, R, Escudier, B, Cathelineau, X, Rozet, F, Vallancien, G, Sabatier, L, Soria, JC: High detection rate of circulating tumor cells in blood of patients with prostate cancer using telomerase activity. *Annals of Oncology*, 18: 518-521, 2007.

58. Danila, DC, Heller, G, Gignac, GA, Gonzalez-Espinoza, R, Anand, A, Tanaka, E, Lilja, H, Schwartz, L, Larson, S, Fleisher, M, Scher, HI: Circulating tumor cell number and prognosis in progressive castration-resistant prostate cancer. *Clinical Cancer Research*, 13: 7053-7058, 2007.
59. Wang, ZP, Eisenberger, MA, Carducci, MA, Partin, AW, Scher, HI, Ts'o, POP: Identification and characterization of circulating prostate carcinoma cells. *Cancer*, 88: 2787-2795, 2000.
60. Talasz, AH, Powell, AA, Huber, DE, Berbee, JG, Roh, KH, Yu, W, Xiao, WZ, Davis, MM, Pease, RF, Mindrinos, MN, Jeffrey, SS, Davis, RW: Isolating highly enriched populations of circulating epithelial cells and other rare cells from blood using a magnetic sweeper device. *Proceedings of the National Academy of Sciences of the United States of America*, 106: 3970-3975, 2009.
61. Ferreira, MM, Ramani, VC, Jeffrey, SS: Circulating tumor cell technologies. *Molecular Oncology*, 10: 374-394, 2016.
62. Pantel, K, Alix-Panabieres, C: Functional Studies on Viable Circulating Tumor Cells. *Clin Chem*, 62: 328-334, 2016.
63. Allard, WJ, Matera, J, Miller, MC, Repollet, M, Connelly, MC, Rao, C, Tibbe, AGJ, Uhr, JW, Terstappen, LWMM: Tumor Cells Circulate in the Peripheral Blood of All Major Carcinomas but not in Healthy Subjects or Patients With Nonmalignant Diseases. *Clinical Cancer Research*, 10: 6897-6904, 2004.
64. Miltenyi, S, Muller, W, Weichel, W, Radbruch, A: High gradient magnetic cell separation with MACS. *Cytometry*, 11: 231-238, 1990.
65. Peters, CE, Woodside, SM, Eaves, AC: Isolation of subsets of immune cells. *Methods Mol Biol*, 302: 95-116, 2005.
66. Neurauter, AA, Bonyhadi, M, Lien, E, Nokleby, L, Ruud, E, Camacho, S, Aarvak, T: Cell isolation and expansion using Dynabeads((R)). *Cell Separation: Fundamentals, Analytical and Preparative Methods*, 106: 41-73, 2007.
67. Gleghorn, JP, Pratt, ED, Denning, D, Liu, H, Bander, NH, Tagawa, ST, Nanus, DM, Giannakakou, PA, Kirby, BJ: Capture of circulating tumor cells from whole blood of prostate cancer patients using geometrically enhanced differential immunocapture (GEDi) and a prostate-specific antibody. *Lab on a Chip*, 10: 27-29, 2010.
68. Mikolajczyk, SD, Millar, LS, Tsinberg, P, Coutts, SM, Zomorodi, M, Pham, T, Bischoff, FZ, Pircher, TJ: Detection of EpCAM-Negative and Cytokeratin-Negative Circulating Tumor Cells in Peripheral Blood. *J Oncol*, 2011: 252361, 2011.
69. Murlidhar, V, Zeinali, M, Grabauskiene, S, Ghannad-Rezaie, M, Wicha, MS, Simeone, DM, Ramnath, N, Reddy, RM, Nagrath, S: A Radial Flow Microfluidic Device for Ultra-High-Throughput Affinity-Based Isolation of Circulating Tumor Cells. *Small*, 10: 4895-4904, 2014.
70. Stott, SL, Hsu, C-H, Tsukrov, DI, Yu, M, Miyamoto, DT, Waltman, BA, Rothenberg, SM, Shah, AM, Smas, ME, Korir, GK, Floyd, FP, Gilman, AJ, Lord, JB, Winokur, D, Springer, S, Irimia, D, Nagrath, S, Sequist, LV, Lee, RJ, Isselbacher, KJ, Maheswaran, S, Haber, DA, Toner, M: Isolation of circulating tumor cells using a microvortex-generating herringbone-chip. *Proceedings of the National Academy of Sciences of the United States of America*, 107: 18392-18397, 2010.
71. Sheng, WA, Ogunwobi, OO, Chen, T, Zhang, JL, George, TJ, Liu, C, Fan, ZH: Capture, release and culture of circulating tumor cells from pancreatic cancer patients using an enhanced mixing chip. *Lab on a Chip*, 14: 89-98, 2014.
72. Yoon, HJ, Kim, TH, Zhang, Z, Azizi, E, Pham, TM, Paoletti, C, Lin, J, Ramnath, N, Wicha, MS, Hayes, DF, Simeone, DM, Nagrath, S: Sensitive capture of circulating tumour cells by functionalized graphene oxide nanosheets. *Nat Nanotechnol*, 8: 735-741, 2013.
73. Kamande, JW, Hupert, ML, Witek, MA, Wang, H, Torphy, RJ, Dharmasiri, U, Njoroge, SK, Jackson, JM, Aufforth, RD, Snavely, A, Yeh, JJ, Soper, SA: Modular microsystem for the isolation, enumeration,

- and phenotyping of circulating tumor cells in patients with pancreatic cancer. *Analytical chemistry*, 85: 9092-9100, 2013.
74. Saliba, AE, Saias, L, Psychari, E, Minc, N, Simon, D, Bidard, FC, Mathiot, C, Pierga, JY, Fraissier, V, Salamero, J, Saada, V, Farace, F, Vielh, P, Malaquin, L, Viovy, JL: Microfluidic sorting and multimodal typing of cancer cells in self-assembled magnetic arrays. *Proc Natl Acad Sci U S A*, 107: 14524-14529, 2010.
 75. Earhart, CM, Hughes, CE, Gaster, RS, Ooi, CC, Wilson, RJ, Zhou, LY, Humke, EW, Xu, L, Wong, DJ, Willingham, SB, Schwartz, EJ, Weissman, IL, Jeffrey, SS, Neal, JW, Rohatgi, R, Wakelee, HA, Wang, SX: Isolation and mutational analysis of circulating tumor cells from lung cancer patients with magnetic sifters and biochips. *Lab Chip*, 14: 78-88, 2014.
 76. Winer-Jones, JP, Vahidi, B, Arquilevich, N, Fang, C, Ferguson, S, Harkins, D, Hill, C, Klem, E, Pagano, PC, Peasley, C, Romero, J, Shartle, R, Vasko, RC, Strauss, WM, Dempsey, PW: Circulating tumor cells: clinically relevant molecular access based on a novel CTC flow cell. *PLoS One*, 9: e86717, 2014.
 77. Harb, W, Fan, A, Tran, T, Danila, DC, Keys, D, Schwartz, M, Ionescu-Zanetti, C: Mutational Analysis of Circulating Tumor Cells Using a Novel Microfluidic Collection Device and qPCR Assay. *Translational oncology*, 6: 528-538, 2013.
 78. Ozkumur, E, Shah, AM, Ciciliano, JC, Emmink, BL, Miyamoto, DT, Brachtel, E, Yu, M, Chen, PI, Morgan, B, Trautwein, J, Kimura, A, Sengupta, S, Stott, SL, Karabacak, NM, Barber, TA, Walsh, JR, Smith, K, Spuhler, PS, Sullivan, JP, Lee, RJ, Ting, DT, Luo, X, Shaw, AT, Bardia, A, Sequist, LV, Louis, DN, Maheswaran, S, Kapur, R, Haber, DA, Toner, M: Inertial Focusing for Tumor Antigen-Dependent and -Independent Sorting of Rare Circulating Tumor Cells. *Science Translational Medicine*, 5, 2013.
 79. Saucedo-Zeni, N, Mewes, S, Niestroj, R, Gasiorowski, L, Murawa, D, Nowaczyk, P, Tomasi, T, Weber, E, Dworacki, G, Morgenthaler, NG, Jansen, H, Propping, C, Sterzynska, K, Dyszkiewicz, W, Zabel, M, Kiechle, M, Reuning, U, Schmitt, M, Lucke, K: A novel method for the in vivo isolation of circulating tumor cells from peripheral blood of cancer patients using a functionalized and structured medical wire. *Int J Oncol*, 41: 1241-1250, 2012.
 80. Liu, Z, Fusi, A, Klopocki, E, Schmitt, A, Tinhofer, I, Nonnenmacher, A, Keilholz, U: Negative enrichment by immunomagnetic nanobeads for unbiased characterization of circulating tumor cells from peripheral blood of cancer patients. *Journal of translational medicine*, 9: 70, 2011.
 81. Lara, O, Tong, X, Zborowski, M, Chalmers, JJ: Enrichment of rare cancer cells through depletion of normal cells using density and flow-through, immunomagnetic cell separation. *Experimental hematology*, 32: 891-904, 2004.
 82. Lara, O, Tong, X, Zborowski, M, Farag, SS, Chalmers, JJ: Comparison of two immunomagnetic separation technologies to deplete T cells from human blood samples. *Biotechnology and bioengineering*, 94: 66-80, 2006.
 83. Chen, CL, Chen, KC, Pan, YC, Lee, TP, Hsiung, LC, Lin, CM, Chen, CY, Lin, CH, Chiang, BL, Wo, AM: Separation and detection of rare cells in a microfluidic disk via negative selection. *Lab Chip*, 11: 474-483, 2011.
 84. Harouaka, RA, Nisic, M, Zheng, SY: Circulating tumor cell enrichment based on physical properties. *Journal of laboratory automation*, 18: 455-468, 2013.
 85. Sollier, E, Go, DE, Che, J, Gossett, DR, O'Byrne, S, Weaver, WM, Kummer, N, Rettig, M, Goldman, J, Nickols, N, McCloskey, S, Kulkarni, RP, Di Carlo, D: Size-selective collection of circulating tumor cells using Vortex technology. *Lab Chip*, 14: 63-77, 2014.
 86. Seal, SH: Silicone flotation: a simple quantitative method for the isolation of free-floating cancer cells from the blood. *Cancer*, 12: 590-595, 1959.

87. Rosenberg, R, Gertler, R, Friederichs, J, Fuehrer, K, Dahm, M, Phelps, R, Thorban, S, Nekarda, H, Siewert, JR: Comparison of two density gradient centrifugation systems for the enrichment of disseminated tumor cells in blood. *Cytometry*, 49: 150-158, 2002.
88. Muller, V, Stahmann, N, Riethdorf, S, Rau, T, Zabel, T, Goetz, A, Janicke, F, Pantel, K: Circulating tumor cells in breast cancer: Correlation to bone marrow micrometastases, heterogeneous response to systemic therapy and low proliferative activity. *Clinical Cancer Research*, 11: 3678-3685, 2005.
89. He, W, Kularatne, SA, Kalli, KR, Prendergast, FG, Amato, RJ, Klee, GG, Hartmann, LC, Low, PS: Quantitation of circulating tumor cells in blood samples from ovarian and prostate cancer patients using tumor-specific fluorescent ligands. *Int J Cancer*, 123: 1968-1973, 2008.
90. Campton, DE, Ramirez, AB, Nordberg, JJ, Drovetto, N, Clein, AC, Varshavskaya, P, Friemel, BH, Quarre, S, Breman, A, Dorschner, M, Blau, S, Blau, CA, Sabath, DE, Stilwell, JL, Kaldjian, EP: High-recovery visual identification and single-cell retrieval of circulating tumor cells for genomic analysis using a dual-technology platform integrated with automated immunofluorescence staining. *BMC Cancer*, 15: 360, 2015.
91. Gertler, R, Rosenberg, R, Fuehrer, K, Dahm, M, Nekarda, H, Siewert, JR: Detection of circulating tumor cells in blood using an optimized density gradient centrifugation. *Molecular Staging of Cancer*, 162: 149-155, 2003.
92. Naume, B, Borgen, E, Tossvik, S, Pavlak, N, Oates, D, Nesland, JM: Detection of isolated tumor cells in peripheral blood and in BM: evaluation of a new enrichment method. *Cytotherapy*, 6: 244-252, 2004.
93. Hayes, GM, Busch, R, Voogt, J, Siah, IM, Gee, TA, Hellerstein, MK, Chiorazzi, N, Rai, KR, Murphy, EJ: Isolation of malignant B cells from patients with chronic lymphocytic leukemia (CLL) for analysis of cell proliferation: validation of a simplified method suitable for multi-center clinical studies. *Leuk Res*, 34: 809-815, 2010.
94. Vona, G, Sabile, A, Louha, M, Sitruk, V, Romana, S, Schutze, K, Capron, F, Franco, D, Pazzagli, M, Vekemans, M, Lacour, B, Brechot, C, Paterlini-Brechot, P: Isolation by size of epithelial tumor cells - A new method for the immunomorphological and molecular characterization of circulating tumor cells. *American Journal of Pathology*, 156: 57-63, 2000.
95. Desitter, I, Guerrouahen, BS, Benali-Furet, N, Wechsler, J, Janne, PA, Kuang, Y, Yanagita, M, Wang, L, Berkowitz, JA, Distel, RJ, Cayre, YE: A new device for rapid isolation by size and characterization of rare circulating tumor cells. *Anticancer research*, 31: 427-441, 2011.
96. Adams, AA, Okagbare, PI, Feng, J, Hupert, ML, Patterson, D, Gottert, J, McCarley, RL, Nikitopoulos, D, Murphy, MC, Soper, SA: Highly efficient circulating tumor cell isolation from whole blood and label-free enumeration using polymer-based microfluidics with an integrated conductivity sensor. *Journal of the American Chemical Society*, 130: 8633-8641, 2008.
97. Harouaka, RA, Zhou, MD, Yeh, YT, Khan, WJ, Das, A, Liu, X, Christ, CC, Dicker, DT, Baney, TS, Kaifi, JT, Belani, CP, Truica, CI, El-Deiry, WS, Allerton, JP, Zheng, SY: Flexible micro spring array device for high-throughput enrichment of viable circulating tumor cells. *Clin Chem*, 60: 323-333, 2014.
98. Zhou, MD, Hao, S, Williams, AJ, Harouaka, RA, Schrand, B, Rawal, S, Ao, Z, Brenneman, R, Gilboa, E, Lu, B, Wang, S, Zhu, J, Datar, R, Cote, R, Tai, YC, Zheng, SY: Separable bilayer microfiltration device for viable label-free enrichment of circulating tumour cells. *Sci Rep*, 4: 7392, 2014.
99. Qin, X, Park, S, Duffy, SP, Matthews, K, Ang, RR, Todenhofer, T, Abdi, H, Azad, A, Bazov, J, Chi, KN, Black, PC, Ma, H: Size and deformability based separation of circulating tumor cells from castrate resistant prostate cancer patients using resettable cell traps. *Lab Chip*, 15: 2278-2286, 2015.
100. Sarioglu, AF, Aceto, N, Kojic, N, Donaldson, MC, Zeinali, M, Hamza, B, Engstrom, A, Zhu, H, Sundaresan, TK, Miyamoto, DT, Luo, X, Bardia, A, Wittner, BS, Ramaswamy, S, Shioda, T, Ting,

- DT, Stott, SL, Kapur, R, Maheswaran, S, Haber, DA, Toner, M: A microfluidic device for label-free, physical capture of circulating tumor cell clusters. *Nature methods*, 12: 685-691, 2015.
101. Kuo, JS, Zhao, Y, Schiro, PG, Ng, L, Lim, DS, Shelby, JP, Chiu, DT: Deformability considerations in filtration of biological cells. *Lab Chip*, 10: 837-842, 2010.
 102. Vasudha, M, Lianette, RB, Sunitha, N: Affinity Versus Label-Free Isolation of Circulating Tumor Cells: Who Wins? *Small*, 12: 4450-4463, 2016.
 103. Lin, E, Rivera-Báez, L, Fouladdel, S, Yoon, HJ, Guthrie, S, Wieger, J, Deol, Y, Keller, E, Sahai, V, Simeone, DM, Burness, ML, Azizi, E, Wicha, MS, Negrath, S: High-Throughput Microfluidic Labyrinth for the Label-free Isolation of Circulating Tumor Cells. *Cell Systems*, 5: 295-304.e294.
 104. Warkiani, ME, Guan, G, Luan, KB, Lee, WC, Bhagat, AA, Chaudhuri, PK, Tan, DS, Lim, WT, Lee, SC, Chen, PC, Lim, CT, Han, J: Slanted spiral microfluidics for the ultra-fast, label-free isolation of circulating tumor cells. *Lab Chip*, 14: 128-137, 2014.
 105. Becker, FF, Wang, XB, Huang, Y, Pethig, R, Vykoukal, J, Gascoyne, PR: Separation of human breast cancer cells from blood by differential dielectric affinity. *Proc Natl Acad Sci U S A*, 92: 860-864, 1995.
 106. Stoy, RD, Foster, KR, Schwan, HP: Dielectric properties of mammalian tissues from 0.1 to 100 MHz: a summary of recent data. *Physics in medicine and biology*, 27: 501-513, 1982.
 107. Gupta, V, Jafferji, I, Garza, M, Melnikova, VO, Hasegawa, DK, Pethig, R, Davis, DW: ApoStream(), a new dielectrophoretic device for antibody independent isolation and recovery of viable cancer cells from blood. *Biomicrofluidics*, 6: 24133, 2012.
 108. Polzer, B, Medoro, G, Pasch, S, Fontana, F, Zorzino, L, Pestka, A, Andergassen, U, Meier-Stiegen, F, Czyz, ZT, Alberter, B, Treitschke, S, Schamberger, T, Sergio, M, Bregola, G, Doffini, A, Gianni, S, Calanca, A, Signorini, G, Bolognesi, C, Hartmann, A, Fasching, PA, Sandri, MT, Rack, B, Fehm, T, Giorgini, G, Manaresi, N, Klein, CA: Molecular profiling of single circulating tumor cells with diagnostic intention. *EMBO molecular medicine*, 6: 1371-1386, 2014.
 109. Moon, HS, Kwon, K, Kim, SI, Han, H, Sohn, J, Lee, S, Jung, HI: Continuous separation of breast cancer cells from blood samples using multi-orifice flow fractionation (MOFF) and dielectrophoresis (DEP). *Lab Chip*, 11: 1118-1125, 2011.
 110. Peeters, DJ, De Laere, B, Van den Eynden, GG, Van Laere, SJ, Rothe, F, Ignatiadis, M, Sieuwerts, AM, Lambrechts, D, Rutten, A, van Dam, PA, Pauwels, P, Peeters, M, Vermeulen, PB, Dirix, LY: Semiautomated isolation and molecular characterisation of single or highly purified tumour cells from CellSearch enriched blood samples using dielectrophoretic cell sorting. *British journal of cancer*, 108: 1358-1367, 2013.
 111. Augustsson, P, Magnusson, C, Nordin, M, Lilja, H, Laurell, T: Microfluidic, label-free enrichment of prostate cancer cells in blood based on acoustophoresis. *Analytical chemistry*, 84: 7954-7962, 2012.
 112. Casavant, BP, Mosher, R, Warrick, JW, Maccoux, LJ, Berry, SM, Becker, JT, Chen, V, Lang, JM, McNeel, DG, Beebe, DJ: A negative selection methodology using a microfluidic platform for the isolation and enumeration of circulating tumor cells. *Methods*, 64: 137-143, 2013.
 113. Zuba-Surma, EK, Ratajczak, MZ: Analytical capabilities of the ImageStream cytometer. *Methods in cell biology*, 102: 207-230, 2011.
 114. Nieva, J, Wendel, M, Luttgen, MS, Marrinucci, D, Bazhenova, L, Kolatkar, A, Santala, R, Whittenberger, B, Burke, J, Torrey, M, Bethel, K, Kuhn, P: High-definition imaging of circulating tumor cells and associated cellular events in non-small cell lung cancer patients: a longitudinal analysis. *Physical biology*, 9: 016004, 2012.
 115. Krivacic, RT, Ladanyi, A, Curry, DN, Hsieh, HB, Kuhn, P, Bergsrud, DE, Kepros, JF, Barbera, T, Ho, MY, Chen, LB, Lerner, RA, Bruce, RH: A rare-cell detector for cancer. *Proc Natl Acad Sci U S A*, 101: 10501-10504, 2004.

116. Hillig, T, Horn, P, Nygaard, AB, Haugaard, AS, Nejlund, S, Brandslund, I, Soletormos, G: In vitro detection of circulating tumor cells compared by the CytoTrack and CellSearch methods. *Tumour Biol*, 36: 4597-4601, 2015.
117. Galanzha, EI, Zharov, VP: Circulating Tumor Cell Detection and Capture by Photoacoustic Flow Cytometry in Vivo and ex Vivo. *Cancers (Basel)*, 5: 1691-1738, 2013.
118. Lopez-Riquelme, N, Minguela, A, Villar-Permy, F, Ciprian, D, Castillejo, A, Alvarez-Lopez, MR, Soto, JL: Imaging cytometry for counting circulating tumor cells: comparative analysis of the CellSearch vs ImageStream systems. *APMIS : acta pathologica, microbiologica, et immunologica Scandinavica*, 121: 1139-1143, 2013.
119. Marrinucci, D, Bethel, K, Kolatkar, A, Luttgen, MS, Malchiodi, M, Baehring, F, Voigt, K, Lazar, D, Nieva, J, Bazhenova, L, Ko, AH, Korn, WM, Schram, E, Coward, M, Yang, X, Metzner, T, Lamy, R, Honnatti, M, Yoshioka, C, Kunken, J, Petrova, Y, Sok, D, Nelson, D, Kuhn, P: Fluid biopsy in patients with metastatic prostate, pancreatic and breast cancers. *Physical biology*, 9: 016003-016003, 2012.
120. Das, M, Riess, JW, Frankel, P, Schwartz, E, Bennis, R, Hsieh, HB, Liu, X, Ly, JC, Zhou, L, Nieva, JJ, Wakelee, HA, Bruce, RH: ERCC1 expression in circulating tumor cells (CTCs) using a novel detection platform correlates with progression-free survival (PFS) in patients with metastatic non-small-cell lung cancer (NSCLC) receiving platinum chemotherapy. *Lung cancer (Amsterdam, Netherlands)*, 77: 421-426, 2012.
121. Alix-Panabieres, C: EPISPOT assay: detection of viable DTCs/CTCs in solid tumor patients. *Recent results in cancer research Fortschritte der Krebsforschung Progres dans les recherches sur le cancer*, 195: 69-76, 2012.
122. Lu, J, Fan, T, Zhao, Q, Zeng, W, Zaslavsky, E, Chen, JJ, Frohman, MA, Golightly, MG, Madajewicz, S, Chen, WT: Isolation of circulating epithelial and tumor progenitor cells with an invasive phenotype from breast cancer patients. *Int J Cancer*, 126: 669-683, 2010.
123. Ramirez, JM, Fehm, T, Orsini, M, Cayrefourcq, L, Maudelonde, T, Pantel, K, Alix-Panabieres, C: Prognostic relevance of viable circulating tumor cells detected by EPISPOT in metastatic breast cancer patients. *Clin Chem*, 60: 214-221, 2014.
124. Alix-Panabieres, C, Pantel, K: Liquid biopsy in cancer patients: advances in capturing viable CTCs for functional studies using the EPISPOT assay. *Expert review of molecular diagnostics*, 15: 1411-1417, 2015.
125. Cayrefourcq, L, Mazard, T, Joosse, S, Solassol, J, Ramos, J, Assenat, E, Schumacher, U, Costes, V, Maudelonde, T, Pantel, K, Alix-Panabieres, C: Establishment and characterization of a cell line from human circulating colon cancer cells. *Cancer Res*, 75: 892-901, 2015.
126. Dong, Y, Skelley, AM, Merdek, KD, Sprott, KM, Jiang, C, Pierceall, WE, Lin, J, Stocum, M, Carney, WP, Smirnov, DA: Microfluidics and circulating tumor cells. *The Journal of molecular diagnostics : JMD*, 15: 149-157, 2013.
127. Aceto, N, Bardia, A, Miyamoto, DT, Donaldson, MC, Wittner, BS, Spencer, JA, Yu, M, Pely, A, Engstrom, A, Zhu, H, Brannigan, BW, Kapur, R, Stott, SL, Shioda, T, Ramaswamy, S, Ting, DT, Lin, CP, Toner, M, Haber, DA, Maheswaran, S: Circulating tumor cell clusters are oligoclonal precursors of breast cancer metastasis. *Cell*, 158: 1110-1122, 2014.
128. Shah, AM, Yu, M, Nakamura, Z, Ciciliano, J, Ulman, M, Kotz, K, Stott, SL, Maheswaran, S, Haber, DA, Toner, M: Biopolymer system for cell recovery from microfluidic cell capture devices. *Analytical chemistry*, 84: 3682-3688, 2012.
129. Gossett, DR, Weaver, WM, Mach, AJ, Hur, SC, Tse, HT, Lee, W, Amini, H, Di Carlo, D: Label-free cell separation and sorting in microfluidic systems. *Analytical and bioanalytical chemistry*, 397: 3249-3267, 2010.

130. Marrinucci, D, Bethel, K, Lazar, D, Fisher, J, Huynh, E, Clark, P, Bruce, R, Nieva, J, Kuhn, P: Cytomorphology of circulating colorectal tumor cells:a small case series. *J Oncol*, 2010: 861341, 2010.
131. Cristofanilli, M, Budd, GT, Ellis, MJ, Stopeck, A, Matera, J, Miller, MC, Reuben, JM, Doyle, GV, Allard, WJ, Terstappen, LWMM, Hayes, DF: Circulating tumor cells, disease progression, and survival in metastatic breast cancer. *New England Journal of Medicine*, 351: 781-791, 2004.
132. Andreopoulou, E, Yang, LY, Rangel, KM, Reuben, JM, Hsu, L, Krishnamurthy, S, Valero, V, Fritsche, HA, Cristofanilli, M: Comparison of assay methods for detection of circulating tumor cells in metastatic breast cancer: AdnaGen AdnaTest BreastCancer Select/Detect versus Veridex CellSearch system. *Int J Cancer*, 130: 1590-1597, 2012.
133. Zeinali, M, Murlidhar, V, Fouladdel, S, Shao, S, Zhao, L, Cameron, H, Bankhead, A, Shi, J, Cuneo, KC, Sahai, V, Azizi, E, Wicha, MS, Hafner, M, Simeone, DM, Nagrath, S: Profiling Heterogeneous Circulating Tumor Cells (CTC) Populations in Pancreatic Cancer Using a Serial Microfluidic CTC Carpet Chip. *Advanced Biosystems*, 0: 1800228, 2018.
134. L., SR, D., MK, Ahmedin, J: Cancer statistics, 2018. *CA: A Cancer Journal for Clinicians*, 68: 7-30, 2018.
135. Hezel, AF, Kimmelman, AC, Stanger, BZ, Bardeesy, N, DePinho, RA: Genetics and biology of pancreatic ductal adenocarcinoma. *Genes & Development*, 20: 1218-1249, 2006.
136. Hidalgo, M: Pancreatic Cancer. *New England Journal of Medicine*, 362: 1605-1617, 2010.
137. Chu, GC, Kimmelman, AC, Hezel, AF, DePinho, RA: Stromal biology of pancreatic cancer. *Journal of Cellular Biochemistry*, 101: 887-907, 2007.
138. Vogelstein, B, , K, K. W.: Cancer genes and the pathways they control. *Nature Medicine*, 10: 789-799, 2004.
139. Hingorani, SR, Wang, LF, Multani, AS, Combs, C, Deramaudt, TB, Hruban, RH, Rustgi, AK, Chang, S, Tuveson, DA: Trp53(R172H) and Kras(G12D) cooperate to promote chromosomal instability and widely metastatic pancreatic ductal adenocarcinoma in mice. *Cancer Cell*, 7: 469-483, 2005.
140. Guerra, C, Schuhmacher, AJ, Canamero, M, Grippo, PJ, Verdaguer, L, Perez-Gallego, L, Dubus, P, Sandgren, EP, Barbacid, M: Chronic pancreatitis is essential for induction of pancreatic ductal adenocarcinoma by k-Ras Oncogenes in adult mice. *Cancer Cell*, 11: 291-302, 2007.
141. Bardeesy, N, Aguirre, AJ, Chu, GC, Cheng, KH, Lopez, LV, Hezel, AF, Feng, B, Brennan, C, Weissleder, R, Mahmood, U, Hanahan, D, Redston, MS, Chin, L, DePinho, RA: Both p16(Ink4a) and the p19(Arf)-p53 pathway constrain progression of pancreatic adenocarcinoma in the mouse. *Proceedings of the National Academy of Sciences of the United States of America*, 103: 5947-5952, 2006.
142. Jones, S, Zhang, XS, Parsons, DW, Lin, JCH, Leary, RJ, Angenendt, P, Mankoo, P, Carter, H, Kamiyama, H, Jimeno, A, Hong, SM, Fu, BJ, Lin, MT, Calhoun, ES, Kamiyama, M, Walter, K, Nikolskaya, T, Nikolsky, Y, Hartigan, J, Smith, DR, Hidalgo, M, Leach, SD, Klein, AP, Jaffee, EM, Goggins, M, Maitra, A, Iacobuzio-Donahue, C, Eshleman, JR, Kern, SE, Hruban, RH, Karchin, R, Papadopoulos, N, Parmigiani, G, Vogelstein, B, Velculescu, VE, Kinzler, KW: Core signaling pathways in human pancreatic cancers revealed by global genomic analyses. *Science*, 321: 1801-1806, 2008.
143. Mahadevan, D, Von Hoff, DD: Tumor-stroma interactions in pancreatic ductal adenocarcinoma. *Mol Cancer Ther*, 6: 1186-1197, 2007.
144. Adwan, H, Zhivkova-Galunska, M, Georges, R, Eyol, E, Kleeff, J, Giese, NA, Friess, H, Bergmann, F, Berger, MR: Expression of HOXC8 is inversely related to the progression and metastasis of pancreatic ductal adenocarcinoma. *British journal of cancer*, 105: 288-295, 2011.
145. Miura, F, Takada, T, Amano, H, Yoshida, M, Furui, S, Takeshita, K: Diagnosis of pancreatic cancer. *HPB (Oxford)*, 8: 337-342, 2006.

146. Pierantoni, C, Pagliacci, A, Scartozzi, M, Berardi, R, Bianconi, M, Cascinu, S: Pancreatic cancer: progress in cancer therapy. *Crit Rev Oncol Hematol*, 67: 27-38, 2008.
147. Matsuda, Y, Hagio, M, Ishiwata, T: Nestin: a novel angiogenesis marker and possible target for tumor angiogenesis. *World J Gastroenterol*, 19: 42-48, 2013.
148. Malafa, JKaMP: "Early Detection of Pancreatic Cancer : Why , Who , and How to Screen,". vol. 15, 2008.
149. Greenhalf, W, Grocock, C, Harcus, M, Neoptolemos, J: Screening of High-Risk Families for Pancreatic Cancer. *Pancreatology*, 9: 215-222, 2009.
150. Larghi, A, Verna, EC, Lecca, PG, Costamagna, G: Screening for Pancreatic Cancer in High-Risk Individuals: A Call for Endoscopic Ultrasound. *Clinical Cancer Research*, 15: 1907-1914, 2009.
151. Faca, VM, Song, KS, Wang, H, Zhang, Q, Krasnoselsky, AL, Newcomb, LF, Plentz, RR, Gurumurthy, S, Redston, MS, Pitteri, SJ, Pereira-Faca, SR, Ireton, RC, Katayama, H, Glukhova, V, Phanstiel, D, Brenner, DE, Anderson, MA, Misek, D, Scholler, N, Urban, ND, Barnett, MJ, Edelstein, C, Goodman, GE, Thornquist, MD, McIntosh, MW, DePinho, RA, Bardeesy, N, Hanash, SM: A mouse to human search for plasma Proteome changes associated with pancreatic tumor development. *Plos Medicine*, 5: 953-967, 2008.
152. Bidard, FC, Huguet, F, Louvet, C, Mineur, L, Bouché, O, Chibaudel, B, Artru, P, Desseigne, F, Bachet, JB, Mathiot, C, Pierga, JY, Hammel, P: Circulating tumor cells in locally advanced pancreatic adenocarcinoma: the ancillary CirCe 07 study to the LAP 07 trial. *Annals of Oncology*, 24: 2057-2061, 2013.
153. Bissolati, M, Sandri, MT, Burtulo, G, Zorzino, L, Balzano, G, Braga, M: Portal vein-circulating tumor cells predict liver metastases in patients with resectable pancreatic cancer. *Tumour Biol*, 36: 991-996, 2015.
154. Rhim, AD, Mirek, ET, Aiello, NM, Maitra, A, Bailey, JM, McAllister, F, Reichert, M, Beatty, GL, Rustgi, AK, Vonderheide, RH, Leach, SD, Stanger, BZ: EMT and dissemination precede pancreatic tumor formation. *Cell*, 148: 349-361, 2012.
155. Qiang Ding, Yumi Miyazaki, Koichiro Tsukasa, Shyuichiro Matsubara, Makoto Yoshimitsu, Takao, S: CD133 facilitates epithelial-mesenchymal transition through interaction with the ERK pathway in pancreatic cancer metastasis. *Molecular Cancer*, 2014.
156. Hori, Y: Prominin-1 (CD133) Reveals New Faces of Pancreatic Progenitor Cells and Cancer Stem Cells: Current Knowledge and Therapeutic Perspectives. *Adv Exp Med Biol*, 777: 185-196, 2013.
157. Hatina, J: The dynamics of cancer stem cells. *Neoplasma*, 59: 700-707, 2012.
158. Hatina, J, Schulz, WA, Fischer, J, Wahl, J, Debatin, KM, Beltinger, C: Tumour stem cells - a new concept in tumour biology. *Deutsche Medizinische Wochenschrift*, 132: 1629-1632, 2007.
159. Moriyama, T, Ohuchida, K, Mizumoto, K, Cui, L, Ikenaga, N, Sato, N, Tanaka, M: Enhanced cell migration and invasion of CD133+ pancreatic cancer cells cocultured with pancreatic stromal cells. *Cancer*, 116: 3357-3368, 2010.
160. Zhang, Y, Wei, JS, Wang, H, Xue, XF, An, Y, Tang, D, Yuan, ZX, Wang, FT, Wu, JL, Zhang, JJ, Miao, Y: Epithelial mesenchymal transition correlates with CD24(+)CD44(+) and CD133(+) cells in pancreatic cancer. *Oncology Reports*, 27: 1599-1605, 2012.
161. Ding, Q, Yoshimitsu, M, Kuwahata, T, Maeda, K, Hayashi, T, Obara, T, Miyazaki, Y, Matsubara, S, Natsugoe, S, Takao, S: Establishment of a highly migratory subclone reveals that CD133 contributes to migration and invasion through epithelial-mesenchymal transition in pancreatic cancer. *Human Cell*, 25: 1-8, 2012.
162. Li, Y, Cheng, X, Chen, Z, Liu, Y, Liu, Z, Xu, S: Circulating tumor cells in peripheral and pulmonary venous blood predict poor long-term survival in resected non-small cell lung cancer patients. *Scientific Reports*, 7: 4971, 2017.

163. Zhang, Z, Ramnath, N, Nagrath, S: Current Status of CTCs as Liquid Biopsy in Lung Cancer and Future Directions. *Frontiers in oncology*, 5: 209, 2015.
164. Santarpia, M, Liguori, A, D'Aveni, A, Karachaliou, N, Gonzalez-Cao, M, Daffina, MG, Lazzari, C, Altavilla, G, Rosell, R: Liquid biopsy for lung cancer early detection. *Journal of thoracic disease*, 10: S882-s897, 2018.
165. Faugeroux, V, Pailler, E, Auger, N, Taylor, M, Farace, F: Clinical Utility of Circulating Tumor Cells in ALK-Positive Non-Small-Cell Lung Cancer. *Frontiers in Oncology*, 4, 2014.
166. Cancer.Lung., AJCo: Non-Small Cell Lung Cancer Early, Detection, Diagnosis, and Staging. In: *AJCC Cancer Staging Manual 8th ed New York, NY: Springer*, 2017.
167. Wiener, RS, Schwartz, LM, Woloshin, S, Welch, HG: Population-based risk for complications after transthoracic needle lung biopsy of a pulmonary nodule: an analysis of discharge records. *Annals of internal medicine*, 155: 137-144, 2011.
168. Murlidhar, V, Ramnath, N, Nagrath, S, Reddy, R: Optimizing the Detection of Circulating Markers to Aid in Early Lung Cancer Detection. *Cancers*, 8: 61, 2016.
169. van Zandwijk, N: Neoadjuvant strategies for non-small cell lung cancer. *Lung cancer (Amsterdam, Netherlands)*, 34 Suppl 2: S145-150, 2001.
170. Ilie, M, Hofman, V, Long, E, Bordone, O, Selva, E, Washetine, K, Marquette, CH, Hofman, P: Current challenges for detection of circulating tumor cells and cell-free circulating nucleic acids, and their characterization in non-small cell lung carcinoma patients. What is the best blood substrate for personalized medicine? *Annals of translational medicine*, 2: 107, 2014.
171. Pantel, K, Speicher, MR: The biology of circulating tumor cells. *Oncogene*, 35: 1216-1224, 2016.
172. Murlidhar, V, Reddy, RM, Fouladdel, S, Zhao, L, Ishikawa, MK, Grabauskiene, S, Zhang, Z, Lin, J, Chang, AC, Carrott, P, Lynch, WR, Orringer, MB, Kumar-Sinha, C, Palanisamy, N, Beer, DG, Wicha, MS, Ramnath, N, Azizi, E, Nagrath, S: Poor Prognosis Indicated by Venous Circulating Tumor Cell Clusters in Early-Stage Lung Cancers. *Cancer Research*, 77: 5194-5206, 2017.
173. Zhang, Z, Shiratsuchi, H, Palanisamy, N, Nagrath, S, Ramnath, N: Expanded Circulating Tumor Cells from a Patient with ALK-Positive Lung Cancer Present with EML4-ALK Rearrangement Along with Resistance Mutation and Enable Drug Sensitivity Testing: A Case Study. *Journal of Thoracic Oncology*, 12: 397-402, 2017.
174. Tanaka, F, Yoneda, K, Kondo, N, Hashimoto, M, Takuwa, T, Matsumoto, S, Okumura, Y, Rahman, S, Tsubota, N, Tsujimura, T, Kuribayashi, K, Fukuoka, K, Nakano, T, Hasegawa, S: Circulating tumor cell as a diagnostic marker in primary lung cancer. *Clin Cancer Res*, 15: 6980-6986, 2009.
175. Rolfo, C, Castiglia, M, Hong, D, Alessandro, R, Mertens, I, Baggerman, G, Zwaenepoel, K, Gil-Bazo, I, Passiglia, F, Carreca, AP, Taverna, S, Vento, R, Santini, D, Peeters, M, Russo, A, Pauwels, P: Liquid biopsies in lung cancer: the new ambrosia of researchers. *Biochimica et biophysica acta*, 1846: 539-546, 2014.
176. Perez-Callejo, D, Romero, A, Provencio, M, Torrente, M: Liquid biopsy based biomarkers in non-small cell lung cancer for diagnosis and treatment monitoring. *Transl Lung Cancer Res*, 5: 455-465, 2016.
177. Hou, JM, Krebs, M, Ward, T, Sloane, R, Priest, L, Hughes, A, Clack, G, Ranson, M, Blackhall, F, Dive, C: Circulating tumor cells as a window on metastasis biology in lung cancer. *The American journal of pathology*, 178: 989-996, 2011.
178. Tong, B, Xu, Y, Zhao, J, Chen, M, Xing, J, Zhong, W, Wang, M: Prognostic significance of circulating tumor cells in non-small cell lung cancer patients undergoing chemotherapy. *Oncotarget*, 8: 86615-86624, 2017.
179. Fiorelli, A, Accardo, M, Carelli, E, Angioletti, D, Santini, M, Di Domenico, M: Circulating Tumor Cells in Diagnosing Lung Cancer: Clinical and Morphologic Analysis. *The Annals of thoracic surgery*, 99: 1899-1905, 2015.

180. Ilie, M, Hofman, V, Long-Mira, E, Selva, E, Vignaud, JM, Padovani, B, Mouroux, J, Marquette, CH, Hofman, P: "Sentinel" circulating tumor cells allow early diagnosis of lung cancer in patients with chronic obstructive pulmonary disease. *PLoS One*, 9: e111597, 2014.
181. Krebs, MG, Sloane, R, Priest, L, Lancashire, L, Hou, JM, Greystoke, A, Ward, TH, Ferraldeschi, R, Hughes, A, Clack, G, Ranson, M, Dive, C, Blackhall, FH: Evaluation and prognostic significance of circulating tumor cells in patients with non-small-cell lung cancer. *Journal of clinical oncology : official journal of the American Society of Clinical Oncology*, 29: 1556-1563, 2011.
182. Hofman, V, Ilie, MI, Long, E, Selva, E, Bonnetaud, C, Molina, T, Venissac, N, Mouroux, J, Vielh, P, Hofman, P: Detection of circulating tumor cells as a prognostic factor in patients undergoing radical surgery for non-small-cell lung carcinoma: comparison of the efficacy of the CellSearch Assay (TM) and the isolation by size of epithelial tumor cell method. *International Journal of Cancer*, 129: 1651-1660, 2011.
183. Isobe, K, Hata, Y, Kobayashi, K, Hirota, N, Sato, K, Sano, G, Sugino, K, Sakamoto, S, Takai, Y, Shibuya, K, Takagi, K, Homma, S: Clinical significance of circulating tumor cells and free DNA in non-small cell lung cancer. *Anticancer research*, 32: 3339-3344, 2012.
184. Hirose, T, Murata, Y, Oki, Y, Sugiyama, T, Kusumoto, S, Ishida, H, Shirai, T, Nakashima, M, Yamaoka, T, Okuda, K, Ohnishi, T, Ohmori, T: Relationship of circulating tumor cells to the effectiveness of cytotoxic chemotherapy in patients with metastatic non-small-cell lung cancer. *Oncology research*, 20: 131-137, 2012.
185. Ke, Z, Lin, M, Chen, J-F, Choi, J-s, Zhang, Y, Fong, A, Liang, A-J, Chen, S-F, Li, Q, Fang, W, Zhang, P, Garcia, MA, Lee, T, Song, M, Lin, H-A, Zhao, H, Luo, S-C, Hou, S, Yu, H-h, Tseng, H-R: Programming Thermoresponsiveness of NanoVelcro Substrates Enables Effective Purification of Circulating Tumor Cells in Lung Cancer Patients. *ACS Nano*, 9: 62-70, 2015.
186. Kallergi, G, Vetsika, EK, Aggouraki, D, Lagoudaki, E, Koutsopoulos, A, Koinis, F, Katsarlinos, P, Trypaki, M, Messaritakis, I, Stournaras, C, Georgoulas, V, Kotsakis, A: Evaluation of PD-L1/PD-1 on circulating tumor cells in patients with advanced non-small cell lung cancer. *Therapeutic advances in medical oncology*, 10: 1758834017750121, 2018.
187. Ilie, M, Hofman, V, Leroy, S, Cohen, C, Heeke, S, Cattet, F, Bence, C, Lalvee, S, Mouroux, J, Marquette, CH, Hofman, P: Use of circulating tumor cells in prospective clinical trials for NSCLC patients - standardization of the pre-analytical conditions. *Clinical chemistry and laboratory medicine*, 56: 980-989, 2018.
188. Hou, HW, Warkiani, ME, Khoo, BL, Li, ZR, Soo, RA, Tan, DS, Lim, WT, Han, J, Bhagat, AA, Lim, CT: Isolation and retrieval of circulating tumor cells using centrifugal forces. *Sci Rep*, 3: 1259, 2013.
189. McDonald, JC, Duffy, DC, Anderson, JR, Chiu, DT, Wu, H, Schueller, OJ, Whitesides, GM: Fabrication of microfluidic systems in poly(dimethylsiloxane). *Electrophoresis*, 21: 27-40, 2000.
190. Campo, Ad, Greiner, C: SU-8: a photoresist for high-aspect-ratio and 3D submicron lithography. *Journal of Micromechanics and Microengineering*, 17: R81-R95, 2007.
191. Zhou, J, Ellis, AV, Voelcker, NH: Recent developments in PDMS surface modification for microfluidic devices. *Electrophoresis*, 31: 2-16, 2010.
192. Meghna Waghay, MY, Michele Dziubinski, Mina Zeinali, Marguerite Erkkinen,, Huibin Yang, KAS, Sumithra Urs, Marina Pasca Di Magliano, Theodore H. Welling,, Phillip L. Palmbo, EVA, Vaibhav Sahai, Sunitha Nagraath, Lidong Wang, Diane M. Simeone.: GM-CSF Mediates Mesenchymal–Epithelial Cross-talk in Pancreatic Cancer. *cancer discovery*, May 16, 2016.
193. Han, B, Mehra, R, Dhanasekaran, SM, Yu, J, Menon, A, Lonigro, RJ, Wang, X, Gong, Y, Wang, L, Shankar, S, Laxman, B, Shah, RB, Varambally, S, Palanisamy, N, Tomlins, SA, Kumar-Sinha, C, Chinnaiyan, AM: A fluorescence in situ hybridization screen for E26 transformation-specific aberrations: identification of DDX5-ETV4 fusion protein in prostate cancer. *Cancer Res*, 68: 7629-7637, 2008.

194. Han, B, Mehra, R, Suleman, K, Tomlins, SA, Wang, L, Singhal, N, Linetzky, KA, Palanisamy, N, Zhou, M, Chinnaiyan, AM, Shah, RB: Characterization of ETS Gene Aberrations in Select Histologic Variants of Prostate Carcinoma. *Modern pathology : an official journal of the United States and Canadian Academy of Pathology, Inc*, 22: 1176-1185, 2009.
195. Bhalla, R, Kunju, LP, Tomlins, SA, Christopherson, K, Cortez, C, Carskadon, S, Siddiqui, J, Park, K, Mosquera, JM, Pestano, GA, Rubin, MA, Chinnaiyan, AM, Palanisamy, N: Novel dual-color immunohistochemical methods for detecting ERG-PTEN and ERG-SPINK1 status in prostate carcinoma. *Mod Pathol*, 26: 835-848, 2013.
196. Lee, HJ, You, DD, Choi, DW, Choi, YS, Kim, SJ, Won, YS, Moon, HJ: Significance of CD133 as a cancer stem cell markers focusing on the tumorigenicity of pancreatic cancer cell lines. *Journal of the Korean Surgical Society*, 81: 263-270, 2011.
197. Waghray, M, Yalamanchili, M, Dziubinski, M, Zeinali, M, Erkinen, M, Yang, H, Schradle, KA, Urs, S, Pasca Di Magliano, M, Welling, TH, Palmbos, PL, Abel, EV, Sahai, V, Nagrath, S, Wang, L, Simeone, DM: GM-CSF Mediates Mesenchymal-Epithelial Cross-talk in Pancreatic Cancer. *Cancer Discov*, 6: 886-899, 2016.
198. Báez, LR: Application of Label-free Microfluidic Technologies for the Enrichment, Expansion and Characterization of Circulating Tumor Cells in Pancreatic Cancer. 2017.
199. Karachaliou, N, Chaib, I, Cardona, AF, Berenguer, J, Bracht, JWP, Yang, J, Cai, X, Wang, Z, Hu, C, Drozdowskyj, A, Servat, CC, Servat, JC, Ito, M, Attili, I, Aldeguer, E, Capitan, AG, Rodriguez, J, Rojas, L, Viteri, S, Molina-Vila, MA, Ou, SI, Okada, M, Mok, TS, Bivona, TG, Ono, M, Cui, J, Cajal, SRY, Frias, A, Cao, P, Rosell, R: Common Co-activation of AXL and CDCP1 in EGFR-mutation-positive Non-smallcell Lung Cancer Associated With Poor Prognosis. *EBioMedicine*, 29: 112-127, 2018.
200. Alix-Panabieres, C, Pantel, K: Challenges in circulating tumour cell research. *Nat Rev Cancer*, 14: 623-631, 2014.
201. Xiao, D, He, J: Epithelial mesenchymal transition and lung cancer. *Journal of thoracic disease*, 2: 154-159, 2010.
202. Gorges, TM, Tinhofer, I, Drosch, M, Rose, L, Zollner, TM, Krahn, T, von Ahsen, O: Circulating tumour cells escape from EpCAMbased detection due to epithelial-to-mesenchymal transition. *BMC Cancer*, 12: 178, 2012.
203. Sieuwerts, AM, Kraan, J, Bolt, J, van der Spoel, P, Elstrodt, F, Schutte, M, Martens, JW, Gratama, JW, Sleijfer, S, Foekens, JA: Anti-epithelial cell adhesion molecule antibodies and the detection of circulating normal-like breast tumor cells. *J Natl Cancer Inst*, 101: 61-66, 2009.
204. Hong SH, Misek DE, Wang H, Puravs E, Hinderer R, Giordano TJ, al, GJe: Identification of a specific vimentin isoform that induces an antibody response in pancreatic cancer. *Biomark Insights*, 2006.
205. Ren, C, Chen, H, Han, C, Jin, G, Wang, D, Tang, D: Detection and molecular analysis of circulating tumor cells for early diagnosis of pancreatic cancer. *Med Hypotheses*, 80: 833-836, 2013.
206. Fazlul H. Sarkar, Yiwei Li, Zhiwei Wang, Kong, D: Pancreatic cancer stem cells and EMT in drug resistance and metastasis. *Minerva chirurgica*, 64: 489-500, Oct. 2009.
207. Yamada, S, Fuchs, BC, Fujii, T, Shimoyama, Y, Sugimoto, H, Nomoto, S, Takeda, S, Tanabe, KK, Kodera, Y, Nakao, A: Epithelial-to-mesenchymal transition predicts prognosis of pancreatic cancer. *Surgery*, 154: 946-954, 2013.
208. Lahat, G, Lubezky, N, Loewenstein, S, Nizri, E, Gan, S, Pasmanik-Chor, M, Hayman, L, Barazowsky, E, Ben-Haim, M, Klausner, JM: Epithelial-to-Mesenchymal Transition (EMT) in Intraductal Papillary Mucinous Neoplasm (IPMN) is Associated with High Tumor Grade and Adverse Outcomes. *Annals of Surgical Oncology*, 21: 750-757, 2014.

209. Hiroshi, K, Sonshin, T, Kosei, M, Yuko, M, Taisaku, K, Koki, M, Qiang, D, Masahiko, S, Satoshi, I, Sumiya, I, Shinichi, U, Hiroyuki, S, Shoji, N: Epithelial–mesenchymal transition and mesenchymal–epithelial transition via regulation of ZEB-1 and ZEB-2 expression in pancreatic cancer. *Journal of Surgical Oncology*, 105: 655-661, 2012.
210. Lianyu Chen¹, Jie Fan³, , HC, 2, Zhiqiang Meng^{1,2}, Zhen Chen^{1,2}, Peng Wang^{1,2} & Luming Liu^{1,2}: The IL-8/CXCR1 axis is associated with cancer stem cell-like properties and correlates with clinical prognosis in human pancreatic cancer cases. *Sci Rep*, Aug 2014.
211. Tai, MH, Chang, CC, Kiupel, M, Webster, JD, Olson, LK, Trosko, JE: Oct4 expression in adult human stem cells: evidence in support of the stem cell theory of carcinogenesis. *Carcinogenesis*, 26: 495-502, 2005.
212. Chengzhi He¹, Hua Jiang¹, Shasha Geng¹, Haihui Sheng³, Xiaoying Shen³, Xiaoyan Zhang³, Shizhang, Zhu³, XC, Changqing Yang², HengJun Gao^{2,3}: Expression of c-Myc and Fas correlates with perineural invasion of pancreatic cancer. May 30, 2012.
213. Yu-Jun Li, Z-MW, Yun-Xiao Meng, Xiang-Rui Ji: $\delta\zeta$ -catenin up-regulates the expression of cyclinD1, c-myc and MMP-7 in human pancreatic cancer: Relationships with carcinogenesis and metastasis. *World J Gastroenterol* 2004.
214. Proctor, E, , W, M., , L, C. J., , H, D. G., , Y, M., , L, C., , B, F., , S, D. M.: Bmi1 enhances tumorigenicity and cancer stem cell function in pancreatic adenocarcinoma. *PLoS One*, 8: e55820, 2013.
215. Nakajima, S, Doi, R, Toyoda, E, Tsuji, S, Wada, M, Koizumi, M, Tulachan, SS, Ito, D, Kami, K, Mori, T, Kawaguchi, Y, Fujimoto, K, Hosotani, R, Imamura, M: N-Cadherin Expression and Epithelial-Mesenchymal Transition in Pancreatic Carcinoma. *Clinical Cancer Research*, 10: 4125, 2004.
216. Gagliano, N, Celesti, G, Tacchini, L, Pluchino, S, Sforza, C, Rasile, M, Valerio, V, Laghi, L, Conte, V, Procacci, P: Epithelial-to-mesenchymal transition in pancreatic ductal adenocarcinoma: Characterization in a 3D-cell culture model. *World Journal of Gastroenterology*, 22: 4466-4483, 2016.
217. Maithel, SK, Coban, I, Kneuert, PJ, Kooby, DA, El-Rayes, BF, Kauh, JS, Sarmiento, J, Staley, CA, 3rd, Volkan Adsay, N: Differential expression of ERCC1 in pancreas adenocarcinoma: high tumor expression is associated with earlier recurrence and shortened survival after resection. *Ann Surg Oncol*, 18: 2699-2705, 2011.
218. Akita, H, Zheng, Z, Takeda, Y, Kim, C, Kittaka, N, Kobayashi, S, Marubashi, S, Takemasa, I, Nagano, H, Dono, K, Nakamori, S, Monden, M, Mori, M, Doki, Y, Bepler, G: Significance of RRM1 and ERCC1 expression in resectable pancreatic adenocarcinoma. *Oncogene*, 28: 2903-2909, 2009.
219. Ormanns, S, Siveke, JT, Heinemann, V, Haas, M, Sipos, B, Schlitter, AM, Esposito, I, Jung, A, Laubender, RP, Kruger, S, Vehling-Kaiser, U, Winkelmann, C, Fischer von Weikersthal, L, Clemens, MR, Gauler, TC, Märten, A, Geissler, M, Greten, TF, Kirchner, T, Boeck, S: pERK, pAKT and p53 as tissue biomarkers in erlotinib-treated patients with advanced pancreatic cancer: a translational subgroup analysis from AIO-PK0104. *BMC Cancer*, 14: 624, 2014.
220. Hay, N: The Akt-mTOR tango and its relevance to cancer. *Cancer Cell*, 8: 179-183, 2005.
221. Si, L, Xu, L, Yin, L, Qi, Y, Han, X, Xu, Y, Zhao, Y, Liu, K, Peng, J: Potent effects of dioscin against pancreatic cancer via miR-149-3P-mediated inhibition of the Akt1 signalling pathway. *British Journal of Pharmacology*, 174: 553-568, 2017.
222. Köninger, J, Giese, NA, di Mola, FF, Berberat, P, Giese, T, Esposito, I, Bachem, MG, Büchler, MW, Friess, H: Overexpressed Decorin in Pancreatic Cancer. *Clinical Cancer Research*, 10: 4776, 2004.
223. Schonleben, F, Qiu, W, Remotti, HE, Hohenberger, W, Su, GH: PIK3CA, KRAS, and BRAF mutations in intraductal papillary mucinous neoplasm/carcinoma (IPMN/C) of the pancreas. *Langenbecks Arch Surg*, 393: 289-296, 2008.
224. Garcia-Carracedo, D, Chen, ZM, Qiu, W, Huang, AS, Tang, SM, Hruban, RH, Su, GH: PIK3CA mutations in mucinous cystic neoplasms of the pancreas. *Pancreas*, 43: 245-249, 2014.

225. Chen, L, Fan, J, Chen, H, Meng, Z, Chen, Z, Wang, P, Liu, L: The IL-8/CXCR1 axis is associated with cancer stem cell-like properties and correlates with clinical prognosis in human pancreatic cancer cases. *Scientific Reports*, 4: 5911, 2014.
226. Hollstein, M, Moeckel, G, Hergenhausen, M, Spiegelhalder, B, Keil, M, Werle-Schneider, G, Bartsch, H, Brickmann, J: On the origins of tumor mutations in cancer genes: insights from the p53 gene. *Mutation Research/Fundamental and Molecular Mechanisms of Mutagenesis*, 405: 145-154, 1998.
227. Gorges, TM, Tinhofer, I, Drosch, M, Rose, L, Zollner, TM, Krahn, T, von Ahsen, O: Circulating tumour cells escape from EpCAM-based detection due to epithelial-to-mesenchymal transition. *BMC Cancer*, 12: 178, 2012.
228. Krebs, MG, Hou, JM, Sloane, R, Lancashire, L, Priest, L, Nonaka, D, Ward, TH, Backen, A, Clack, G, Hughes, A, Ranson, M, Blackhall, FH, Dive, C: Analysis of circulating tumor cells in patients with non-small cell lung cancer using epithelial marker-dependent and -independent approaches. *Journal of thoracic oncology : official publication of the International Association for the Study of Lung Cancer*, 7: 306-315, 2012.
229. The Cancer Genome Atlas Research, N: Comprehensive molecular profiling of lung adenocarcinoma. *Nature*, 511: 543, 2014.
230. The Cancer Genome Atlas Research, N: Comprehensive genomic characterization of squamous cell lung cancers. *Nature*, 489: 519, 2012.
231. Arora, A, Scholar, EM: Role of tyrosine kinase inhibitors in cancer therapy. *The Journal of pharmacology and experimental therapeutics*, 315: 971-979, 2005.
232. Ahn, MJ, Sun, JM, Lee, SH, Ahn, JS, Park, K: EGFR TKI combination with immunotherapy in non-small cell lung cancer. *Expert opinion on drug safety*, 16: 465-469, 2017.
233. Gerber, DE, Gandhi, L, Costa, DB: Management and future directions in non-small cell lung cancer with known activating mutations. *American Society of Clinical Oncology educational book American Society of Clinical Oncology Annual Meeting*: e353-365, 2014.
234. Socinski, MA, Villaruz, LC, Ross, J: Understanding Mechanisms of Resistance in the Epithelial Growth Factor Receptor in Non-Small Cell Lung Cancer and the Role of Biopsy at Progression. *The oncologist*, 22: 3-11, 2017.
235. Arcila, ME, Oxnard, GR, Nafa, K, Riely, GJ, Solomon, SB, Zakowski, MF, Kris, MG, Pao, W, Miller, VA, Ladanyi, M: Rebiopsy of lung cancer patients with acquired resistance to EGFR inhibitors and enhanced detection of the T790M mutation using a locked nucleic acid-based assay. *Clinical cancer research : an official journal of the American Association for Cancer Research*, 17: 1169-1180, 2011.
236. Yoon, HJ, Lee, HY, Lee, KS, Choi, Y-L, Ahn, M-J, Park, K, Ahn, JS, Sun, J-M, Kim, J, Kim, TS, Chung, MJ, Yi, CA: Repeat Biopsy for Mutational Analysis of Non-Small Cell Lung Cancers Resistant to Previous Chemotherapy: Adequacy and Complications. *Radiology*, 265: 939-948, 2012.
237. Lecharpentier, A, Vielh, P, Perez-Moreno, P, Planchard, D, Soria, JC, Farace, F: Detection of circulating tumour cells with a hybrid (epithelial/mesenchymal) phenotype in patients with metastatic non-small cell lung cancer. *British journal of cancer*, 105: 1338-1341, 2011.
238. Hong, Y, Fang, F, Zhang, Q: Circulating tumor cell clusters: What we know and what we expect (Review). *International Journal of Oncology*, 49: 2206-2216, 2016.
239. Marchetti, A, Del Gramastro, M, Felicioni, L, Malatesta, S, Filice, G, Centi, I, De Pas, T, Santoro, A, Chella, A, Brandes, AA, Venturino, P, Cuccurullo, F, Crino, L, Buttitta, F: Assessment of EGFR mutations in circulating tumor cell preparations from NSCLC patients by next generation sequencing: toward a real-time liquid biopsy for treatment. *PLoS One*, 9: e103883, 2014.
240. Provencio, M, Pérez-Callejo, D, Torrente, M, Martin, P, Calvo, V, Gutiérrez, L, Franco, F, Coronado, MJ, Cruz-Bermúdez, JL, Ruiz-Valdepeñas, AM, Cruz-Bermúdez, A, Sánchez-Beato, M, Romero, A,

- García-Grande, A: Concordance between circulating tumor cells and clinical status during follow-up in anaplastic lymphoma kinase (ALK) non-small-cell lung cancer patients. *Oncotarget*, 8: 59408-59416, 2017.
241. Kang, JH, Krause, S, Tobin, H, Mammoto, A, Kanapathipillai, M, Ingber, DE: A combined micromagnetic-microfluidic device for rapid capture and culture of rare circulating tumor cells. *Lab Chip*, 12: 2175-2181, 2012.
 242. Zhang, L, Ridgway, LD, Wetzel, MD, Ngo, J, Yin, W, Kumar, D, Goodman, JC, Groves, MD, Marchetti, D: The identification and characterization of breast cancer CTCs competent for brain metastasis. *Sci Transl Med*, 5: 180ra148, 2013.
 243. Yu, M, Bardia, A, Aceto, N, Bersani, F, Madden, MW, Donaldson, MC, Desai, R, Zhu, H, Comaills, V, Zheng, Z, Wittner, BS, Stojanov, P, Brachtel, E, Sgroi, D, Kapur, R, Shioda, T, Ting, DT, Ramaswamy, S, Getz, G, Iafrate, AJ, Benes, C, Toner, M, Maheswaran, S, Haber, DA: Cancer therapy. Ex vivo culture of circulating breast tumor cells for individualized testing of drug susceptibility. *Science*, 345: 216-220, 2014.
 244. Zhang, Z, Shiratsuchi, H, Lin, J, Chen, G, Reddy, RM, Azizi, E, Fouladdel, S, Chang, AC, Lin, L, Jiang, H, Waghray, M, Luker, G, Simeone, DM, Wicha, MS, Beer, DG, Ramnath, N, Nagrath, S: Expansion of CTCs from early stage lung cancer patients using a microfluidic co-culture model. *Oncotarget*, 5: 12383-12397, 2014.
 245. Costello, E, Greenhalf, W, Neoptolemos, JP: New biomarkers and targets in pancreatic cancer and their application to treatment. *Nat Rev Gastroenterol Hepatol*, 9: 435-444, 2012.
 246. Jack, RM, Grafton, MM, Rodrigues, D, Giraldez, MD, Griffith, C, Cieslak, R, Zeinali, M, Kumar Sinha, C, Azizi, E, Wicha, M, Tewari, M, Simeone, DM, Nagrath, S: Ultra-Specific Isolation of Circulating Tumor Cells Enables Rare-Cell RNA Profiling. *Advanced science (Weinheim, Baden-Wurttemberg, Germany)*, 3: 1600063, 2016.
 247. MD-Anderson: Personalized Cancer Therapy.
 248. Perkel, JM: Single-cell biology: The power of one. 2015
 249. Care-for-a-Cure: New Drug Testing Method Could Speed Up Development of Breast Cancer Treatments. 2016.
 250. Bilimoria, KY, Bentrem, DJ, Ko, CY, Ritchey, J, Stewart, AK, Winchester, DP, Talamonti, MS: Validation of the 6th Edition AJCC Pancreatic Cancer Staging System - Report from the National Cancer Database. *Cancer*, 110: 738-744, 2007.
 251. Nagrath, S, Jack, RM, Sahai, V, Simeone, DM: Opportunities and Challenges for Pancreatic Circulating Tumor Cells. *Gastroenterology*, 151: 412-426, 2016.
 252. Zhang, Y, Wang, F, Ning, N, Chen, Q, Yang, Z, Guo, Y, Xu, D, Zhang, D, Zhan, T, Cui, W: Patterns of circulating tumor cells identified by CEP8, CK and CD45 in pancreatic cancer. *International Journal of Cancer*, 136: 1228-1233, 2015.
 253. Ankeny, JS, Hou, S, Lin, M, OuYang, H, Song, M, Rochefort, MM, Girgis, MD, Isacoff, WH, Wainberg, ZA, Tseng, H-R, Tomlinson, JS: Pancreatic circulating tumor cells as a diagnostic adjunct in pancreatic cancer. *Journal of Clinical Oncology*, 32: 175-175, 2014.
 254. Kulemann, B, Pitman, MB, Liss, AS, Valsangkar, N, Fernández-del Castillo, C, Lillemoe, KD, Hoepfner, J, Mino-Kenudson, M, Warshaw, AL, Thayer, SP: Circulating Tumor Cells Found in Patients With Localized and Advanced Pancreatic Cancer. *Pancreas*, 44: 547-550, 2015.
 255. Vladimir Bobek, Robert Gurlich, Petra Eliasova, Kolostova, K: Circulating tumor cells in pancreatic cancer patients: Enrichment and cultivation. 2014 December.
 256. Hanssen, A, Loges, S, Pantel, K, Wikman, H: Detection of Circulating Tumor Cells in Non-Small Cell Lung Cancer. *Frontiers in oncology*, 5: 207, 2015.
 257. Pailler, E, Adam, J, Barthelemy, A, Oulhen, M, Auger, N, Valent, A, Borget, I, Planchard, D, Taylor, M, Andre, F, Soria, JC, Vielh, P, Besse, B, Farace, F: Detection of circulating tumor cells harboring a

- unique ALK rearrangement in ALK-positive non-small-cell lung cancer. *Journal of clinical oncology : official journal of the American Society of Clinical Oncology*, 31: 2273-2281, 2013.
258. Dorsey, JF, Kao, GD, MacArthur, KM, Ju, M, Steinmetz, D, Wileyto, EP, Simone, CB, 2nd, Hahn, SM: Tracking viable circulating tumor cells (CTCs) in the peripheral blood of non-small cell lung cancer (NSCLC) patients undergoing definitive radiation therapy: pilot study results. *Cancer*, 121: 139-149, 2015.
259. Hosokawa, M, Kenmotsu, H, Koh, Y, Yoshino, T, Yoshikawa, T, Naito, T, Takahashi, T, Murakami, H, Nakamura, Y, Tsuya, A, Shukuya, T, Ono, A, Akamatsu, H, Watanabe, R, Ono, S, Mori, K, Kanbara, H, Yamaguchi, K, Tanaka, T, Matsunaga, T, Yamamoto, N: Size-based isolation of circulating tumor cells in lung cancer patients using a microcavity array system. *PLoS One*, 8: e67466, 2013.

9 Appendix

9.1 Different design configurations of immunoaffinity microfluidic devices

We undertook a pilot exploratory study comparing five different immunoaffinity CTC Chip devices to determine the highest capture efficiencies. Different micropost distributions and arrangement were tested in this study including, CTC Original, Split, Modified, Rotated, and Carpet Chip.

9.1.1 Original vs. Split CTC chip

The Original CTC Chip was modified to a Split chamber CTC Chip to enhance the % capture efficiencies. The expression of EpCAM on PC-3 cell line was checked prior to the experiments with western blot analysis (section 3.3.1) (Figure 3-13). 1000 fluorescently-labeled with green CellTracker PC-3 cell line were spiked into buffer and the % capture efficiencies of EpCAM on the CTC Original and Split Chip at 10 mL hr⁻¹ flow rate were analyzed. The results showed higher capture efficiencies in the Original (20.1%) compared to the Split Chip (12.4%) (Figure 9-1).

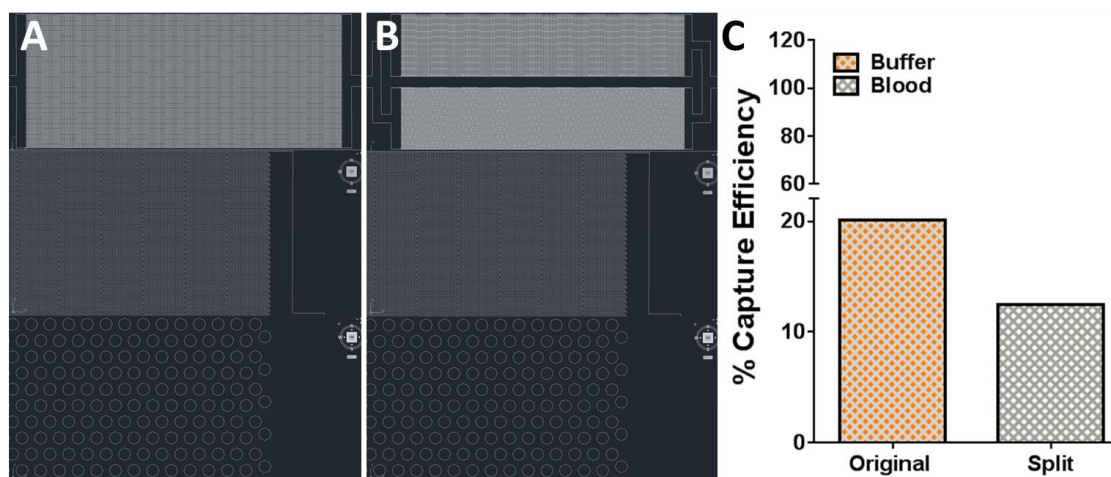


Figure 9-1: Original vs. Split CTC Chip. A) AutoCAD design of the Original CTC Chip, B) and the Split CTC Chip. C) % Capture efficiency of EpCAM with 1,000 spiked pre-labeled PC-3 cell line into buffer at 10 mL hr⁻¹ flow rate showed higher %capture efficiency in the Original CTC Chip (20.1%) compare to the Split device (12.4%).

9.1.2 Original vs. Modified CTC Chip

Original Chip was re-designed to Modified Chip to make it more refined for capturing purpose. 1000 fluorescently-labeled with green CellTracker PC-3 cell line were spiked into buffer and blood. % Capture efficiencies of EpCAM with the CTC Original and Modified Chips at 1 mL hr⁻¹ flow rates were analyzed. % Capture efficiencies in blood were slightly higher in the Modified device compare to the Original device (71.9% vs. 67%) (Figure 9-2).

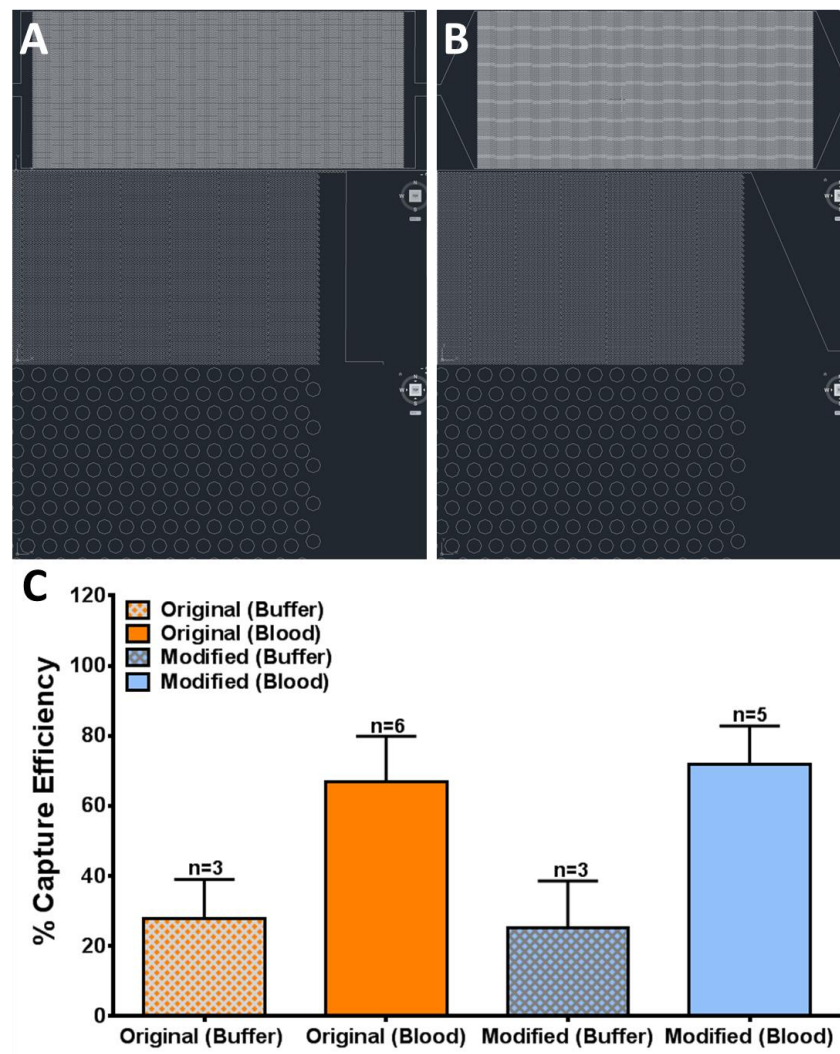


Figure 9-2: Original vs. Modified CTC Chip. A) AutoCAD design of the Original CTC Chip, B) and the Modified CTC Chip. C) % Capture efficiencies of EpCAM with spiked pre-labeled PC-3 cell line into buffer and blood at 1 mL hr⁻¹ flow rate. The CTC Modified Chip showed 71.9% capture efficiency with the PC-3 cell line into blood.

9.1.3 Modified vs. Rotated CTC Chip

Due to low capture efficiencies of the Modified Chip, the Rotated device had been designed based on the rotating the arrays 10° relative to the previous array until reaching a total rotation of 180° and then decreasing rotation from 180° to 0° for the subsequent row. By this new configuration, capture efficiencies of pre-labeled PC-3 cells spiked into blood increased 11.8% at 1 mL hr^{-1} flow rate compare to the Modified CTC Chip (83.7% vs.71.9%) (Figure 9-3).

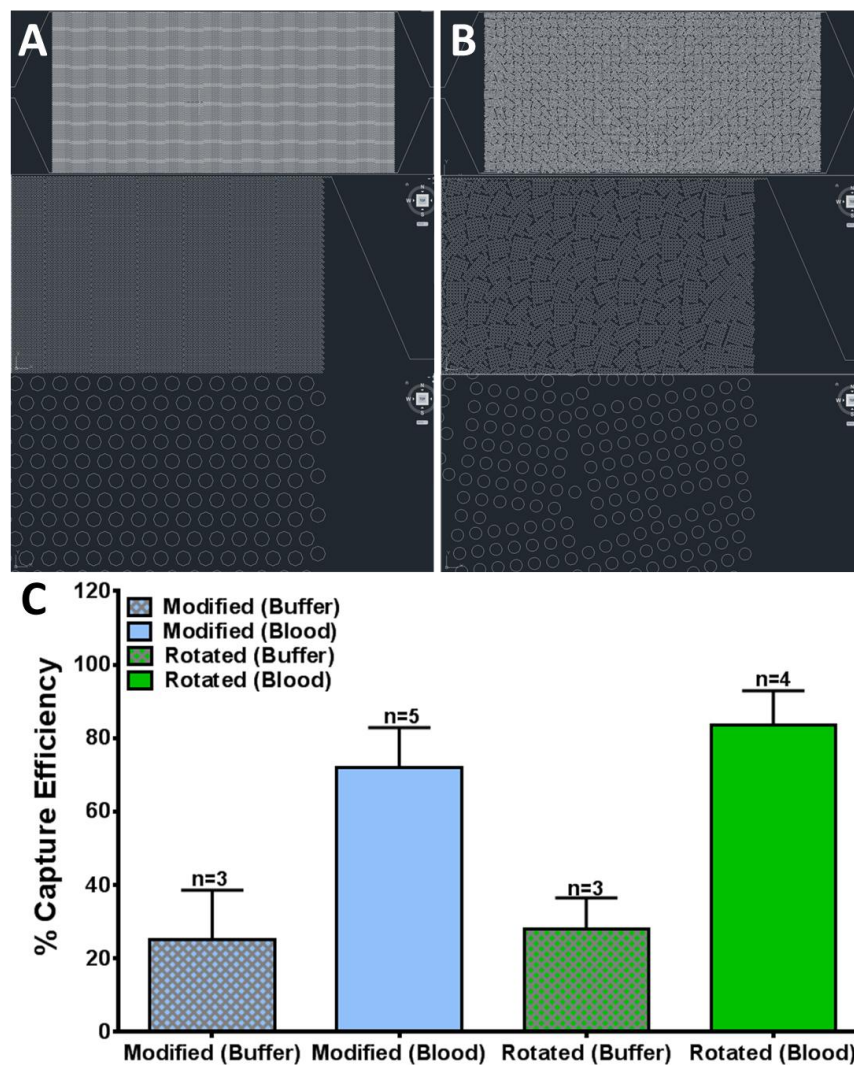


Figure 9-3: Modified vs. Rotated CTC Chip. A) AutoCAD design of the Modified CTC Chip, B) and the Rotated CTC Chip. C) % Capture efficiency of EpCAM with spiked pre-labeled PC-3 cell line into buffer and blood at 1 mL hr^{-1} flow rate. The CTC Rotated Chip showed 83.7% capture efficiency with the PC-3 cell line into blood.

9.1.4 Rotated vs. Carpet CTC chip

In order to increase the specificity and sensitivity of capturing CTCs, CTC Carpet Chip was designed based on an 18° rotation of hexagonal arrays of $100\ \mu\text{m}$ posts, by which capture efficiencies increased to 87.7% with pre-labeled PC-3 cell line spiked into blood at $1\ \text{mL hr}^{-1}$ flow rate compare to the Rotated Chip (83.7%) (Figure 9-4).

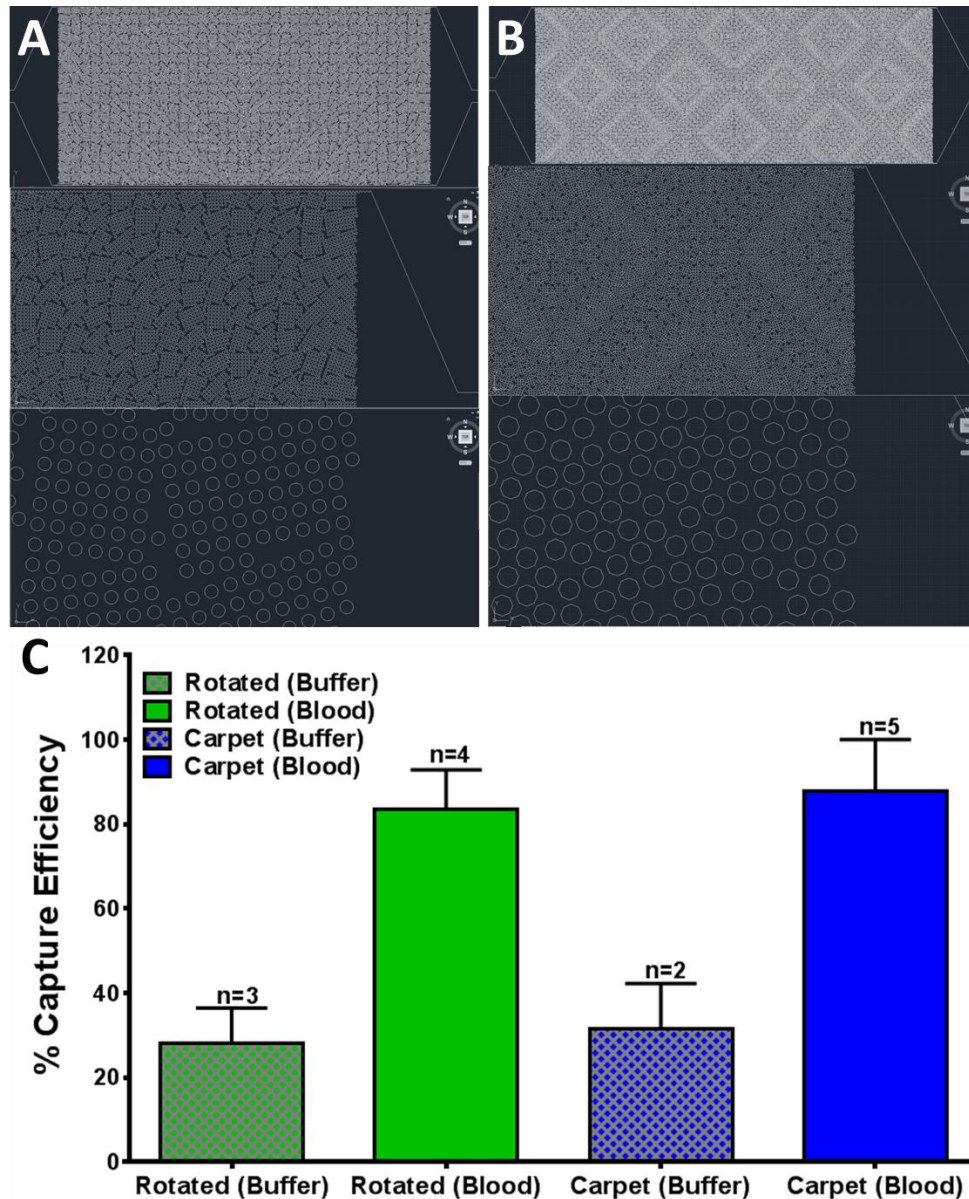


Figure 9-4: Rotated vs. Carpet CTC Chip. A) AutoCAD design of the Rotated CTC Chip, B) and the Carpet CTC Chip. C) % Capture efficiency of EpCAM with spiked pre-labeled PC-3 cell line into buffer and blood at $1\ \text{mL hr}^{-1}$ flow rate. The CTC Carpet Chip showed 87.7% capture efficiency with the PC-3 cell line into blood.

9.2 List of Tables

Table 9-1: Staging of pancreatic cancer ²⁵⁰

Stage	Tumor grade	Nodal status	Distant metastases	Median survival	Characteristics
-	TX	NX	MX	-	Primary tumor cannot be assessed
-	T0	N0	M0	-	No evidence of primary tumor
0	Tis	N0	M0	-	Carcinoma in situ
IA	T1	N0	M0	24.1	Tumor limited to the pancreas, ≤2 cm in greatest diameter (localized within pancreas)
IB	T2	N0	M0	20.6	Tumor limited to the pancreas, >2 cm in greatest diameter (localized within pancreas)
IIA	T	N0	M0	15.4	Tumor extends beyond the pancreas but does not involve the celiac axis or superior mesenteric artery (locally invasive, resectable)
IIB	T1/2/3	N1	M0	12.7	Regional lymph-node metastasis (locally invasive, resectable)
III	T4	Any N	M0	10.6	Tumor involves the celiac axis or the superior mesenteric artery (locally advanced, unresectable)
IV	Any T	Any N	M1	4.5	Distant metastasis

N; denotes regional lymph nodes, M; distant metastases, and T; primary tumor.

NX; Regional nodes cannot be assessed, N0; No regional lymph node metastasis, N1; Regional lymph node metastasis

MX; Distant metastasis cannot be assessed, M0; No distant metastasis, M1; Distant metastasis

Table 9-2: CTC detection techniques in pancreatic cancer ²⁵¹

Platforms	Enrichment technology	Number of PDAC patients	Detection rate (%)	Reference
CellSearch	Immunomagnetic	16	2±6 CTCs 7.5mL ⁻¹	63
		26	42%	6
		79	11%	152
		20	45%	153
Multi marker RT-PCR	Immunomagnetic	34	47.1%	15
CTC-iChip	Immunomagnetic, Inertial sorting	6	66.7%	78
Ultra-specific CTC isolation platform	Immunomagnetic, Inertial sorting	14	100%	246
Immunofluorescence and in situ hybridization (FISH) of chromosome 8	Negative Enrichment	40	90%	252
CTC-Chip	Immunoaffinity	15	100%	4
Thermoplastic modular microsystem	Immunoaffinity	12	100%	73
GEDI	Immunoaffinity	11	73%	67
GEM	Immunoaffinity	18	94.4%	71
OncoBean	Immunoaffinity	2	100%	69
NanoVelcro	Immunoaffinity	32	62.5%	253
ISET	Size-based filtration		93%	10
ScreenCell	Size-based filtration	11	73%	254
MetaCell	Size-based filtration	24	66.7%	255
Immunocytogenetics		22	4 CTCs 7.5mL ⁻¹	252
Immunocytochemistry		41	≥1 CTCs 7.5mL ⁻¹	16
HD-CTC		18	50%	119

Table 9-3: Staging of Lung Cancer ¹⁶⁶

Stage	Tumor grade	Nodal status	Distant metastases	Characteristics
	TX	N0	M0	No evidence of primary tumor
0	Tis	N0	M0	Tumor is found in only the top layers of the cells lining the air passages
IA1	T1mi/T1a	N0	M0	Minimally invasive adenocarcinoma, tumor size <1 cm
IA2	T1b	N0	M0	Tumor size >1 cm but not <2 cm
IA3	T1c	N0	M0	Tumor size >2 cm but not <3 cm
IB	T2a	N0	M0	Tumor size >3 cm but not <4 cm Grown into a main bronchus, visceral pleura, clogging the airways.
IIA	T2b	N0	M0	Tumor size >4 cm but not <5 cm Grown into a main bronchus, visceral pleura, clogging the airways.
IIB	T1a/T1b/T1c	N1	M0	Tumor size <3 cm but has spread to lymph nodes
	T2a/T2b	N1	M0	Tumor size >3 cm but not <5 cm Grown into a main bronchus, visceral pleura, clogging the airways (specific sizes). Cancer has spread to lymph nodes
	T3	N0	M0	Tumor size >5 cm but not <7 cm Grown into the chest wall, the phrenic nerve, or membrane of the sac surrounding the heart
IIIA	T2a/T2b	N2	M0	Tumor size >3 cm but not <5 cm Grown into a main bronchus, visceral pleura, and clogging the airways (specific sizes). Cancer has spread to lymph nodes around the carina or into the space between the lungs.
	T3	N1	M0	Tumor size >5 cm but not <7 cm Grown into the chest wall, partial pleura, the phrenic nerve, or membrane of the sac surrounding the heart. Cancer has spread to lymph nodes
	T4	N0/N1	M0	Tumor size >7 cm Grown into the space between lungs, the heart, aorta, trachea, esophagus, diaphragm, the backbone, or the carina. May or may not spread to the lymph nodes.
	T2a/T2b	N3	M0	Tumor size >3 cm but not <5 cm Grown into the bronchus, visceral pleura, and clogging the airways (specific sizes). Cancer has spread to lymph nodes near the collarbone.
	T3	N2	M0	Tumor size >5 cm but not <7 cm Grown into the chest wall, partial pleura, the phrenic nerve, or membrane of the sac surrounding the heart. There are >2 separate tumor nodules. Has spread to lymph nodes around the carina
	T4	N2	M0	Tumor size >7 cm Grown into the space between lungs, the heart, aorta, trachea, esophagus, diaphragm, the backbone, or the carina. There are >2 separate tumor nodules. Has spread to the lymph nodes around the carina.

IIIB	T1a/T1b/T1c	N3	M0	Tumor size <3 cm Not grown into the membrane surrounded the lung. Cancer spread to lymph nodes near the collarbone on either side, or to hilar or mediastinal lymph nodes on the other side of the body from the main tumor. Cancer has not spread to distant sites
	T2a/T2b	N3	M0	Tumor size >3 cm but not <5 cm Grown into a main bronchus, visceral pleura, and clogging the airways. Cancer has spread to lymph nodes near the collarbone on either side or to hilar or mediastinal lymph nodes on the other side of the body from the main tumor. Cancer has not spread to distant sites.
	T3	N2	M0	Tumor size >5 cm but not <7 cm Grown into the chest wall, partial pleura, and the phrenic nerve. There are >2 separate tumor nodules. Cancer has spread to lymph nodes around the carina or mediastinum. Cancer has not spread to distant sites.
	T4	N2	M0	Tumor size >7 cm Grown into the space between lungs, the heart, the trachea, the esophagus, the diaphragm, the backbone, or the carina. There are >2 separate tumor nodules. Cancer has spread to the lymph nodes around the carina or mediastinum. Cancer has not spread to distant sites.
IIIC	T3	N3	M0	Tumor size >5 cm but not <7 cm Grown into the chest wall, partial pleura, the phrenic nerve, or membrane of the sac surrounding the heart. There are >2 separate tumor nodules. Cancer has spread to the lymph nodes around the collarbone.
	T4	N3	M0	Tumor size >7 cm Grown into the space between lungs, the heart, aorta, trachea, esophagus, diaphragm, the backbone, or the carina. There are >2 separate tumor nodules. Cancer has spread to the lymph nodes around the carina.
IVA	Any T	Any N	M1a	Cancer has spread to the other lung, cancer cells are found in the fluid around the lung, and heart
	Any T	Any N	M1b	Has spread as a single tumor outside of the chest (lives, bones, or brain)
IVB	Any T	Any N	M1c	Has spread as more than one tumor outside of the chest (lives, bones, or brain)

N; denotes regional lymph nodes, M; distant metastases, and T; primary tumor.

Table 9-4: CTC detection technologies in NSCLC ²⁵⁶

Platforms	Enrichment technology	Number of NSCLC patients	Detection rate (%)	Reference
CellSearch	Immunomagnetic	101	21	181
		210	39	182
		152	31	174
		24	33	183
		33	36	184
CTC-Chip	Immunoaffinity	55	100	4
Graphene oxide chip	Immunoaffinity	4	100	72
OncoBean Chip	Immunoaffinity	2	100	69
		35	83.3	172
Vortex Chip		8	100	85
Dean Flow Fractionation		20	100	188
ISET	Size-based filtration	210	50	182
		40	80	228
		32	100	257
Negative depletion		43	100	39
Telomerase-based		30	65	258
MCA		22	77	259
NanoVelcro	Immunoaffinity	7	100	185

Table 9-5: Optimization of panel of antibodies for CTCs detection in pancreatic cancer patients.

Sample	EpCAM chip		CD133 chip		Antibodies	
	EpCs	EMTCs	EpCs	EMTCs	Cytokeratin	Vimentin
S 01	0	NA	0	0	CK 7&8 (IgG2a/BD)	Vimentin (Rabbit mAb/Cell Signaling)
S 02	0	NA	2	0	CK 7&8 (IgG2a/BD)	Vimentin (Rabbit mAb/ Cell Signaling)
S 03	0	0	0	0	CK 7&8 (IgG2a/BD) + CK 8/18/19 (IgG2a/Invitrogen)	Vimentin (Rabbit pAb/ Santa Cruz)
	0	0	0	3	CK 7&8 (IgG2a/BD)	Vimentin (IgG1/BD)
S 04	0	NA	0	6	CK 7&8 (IgG2a/BD)	Vimentin (IgG1/BD)
S 05	2	NA	0	6	CK 7&8 (IgG2a/BD)	Vimentin (IgG1/BD)
S 06	2	NA	0	4	CK 7&8 (IgG2a/BD)	Vimentin (IgG1/BD)
S 07	6	NA	0	7	CK 7&8 (IgG2a/BD)	Vimentin (IgG1/BD)
S 08	0	4	0	0	CK 7&8 (IgG2a/BD)	Vimentin (IgG1/BD)
S 09	0	0	0	2	CK 7&8(IgG2a/BD)	Vimentin (IgG1/BD)
S 10	0	0	0	0	CK 7&8 (IgG2a/BD)	Vimentin (IgG1/BD)
S 11	0	0	1	8	PanCK (IgG2a/Abcam)	Vimentin (IgG1/BD)
S 12	10	NA	0	3	-PanCK (IgG2a/BioRad) for EpCAM chip -CK 7&8 (IgG2a/BD) for CD133 chip	Vimentin (IgG1/BD)
S 13	4	NA	0	10	-PanCK (IgG2a/ BioRad) for EpCAM chip -CK 7&8 (IgG2a/BD) for CD133 chip	Vimentin (IgG1/BD)
S 14	2	NA	NA	NA	-CK 7&8 (IgG2a/BD)	NA
	8	NA	NA	NA	-PanCK (IgG2a/ BioRad)	NA
S 15	2	NA	NA	NA	-CK 7&8 (IgG2a/BD)	NA
	7	NA	NA	NA	-PanCK (IgG2a/ BioRad)	NA
S 16	6	NA	NA	NA	-CK 7&8 (IgG2a/BD)	NA
	13	NA	NA	NA	-PanCK (IgG2a/ BioRad)	NA

EpCs; epithelial CTCs, EMTCs; EMT-like CTCs

Table 9-6: Clinical characterization of pancreatic cancer patients (n=40) (immunoaffinity CTC Carpet Chip study)

Sample	CTC	EMT	Gender	Age	Stage	T (mm)	N	M	Tumor status	CA19-9 U mL ⁻¹	CEA ng mL ⁻¹	Therapy	Pathology	Death	OS	PFS
P 01	30	26	F	74	IIA	-	N0	M0	Resected	2011	-	Res	AD	Dead	463	279
P 02	25	17	M	51	IIA	-	N0	M0	Resected	44	-	Rad/Res	AD	Dead	667	494
P 03 ¶*	9	201	M	63	IIA	19	N0	M0	Resected	42	-	Res	AD	Alive	1000	977
P 04 ¶	13	101	M	63	IIA	32	N0	M0	Locally Advanced	52	2	No	AD	Alive	907	208
P 05 ¶*	44	73	M	71	IIA	24	N0	M0	Resected	16	-	Res	AD	NA	181	169
P 06	25	44	M	74	IIB	22	N1	M0	Resected	11	-	No	AD	Alive	1508	1292
P 07*	10	77	F	64	IIB	19	N1	M0	Resected	381	-	No	AD	Alive	1314	835
P 08	64	50	M	69	IIB	-	N1	M0	Resected	84	3.3	NA	AD	Alive	1245	1218
P 09 ¶	38	92	M	65	IIB	45	N1	M0	Locally Advanced	524	4	No	AD	Dead	612	612
P 10	36	180	M	74	IIB	40	-	M0	Locally Advanced	2128	5	No	AD	Dead	223	223
P 11 ¶*	21	118	M	68	IIB	29	N1	M0	Resected	4	7	Res	AD	Dead	319	55
P 12 ¶	16	42	M	76	IIB	18	N1	M0	Locally Advanced	688	-	No	AD	Dead	99	99
P 13 ¶	5	127	M	56	IIB	23	N1	M0	Borderline Resectable	1033	3	No	AD	Dead	539	471
P 14 *	10	93	M	40	IIB	15	N1	M0	Resected	3	<1	Chemo/Res	AD	Alive	1112	1112
P 15 ¶	9	78	F	55	III	23	N0	M0	Locally advanced	21	2	No	AD	Alive	654	344
P 16	0	15	F	53	III	-	N0	M0	Locally advanced	2485	-	No	AD	Dead	670	573
P 17	8	40	F	60	III	-	N0	M0	Borderline Resectable	27	-	Chemo	AD	NA	364	161
P 18	8	26	F	66	III	-	N0	M0	Locally Advanced	325	-	NA	AD	Dead	321	321
P 19	9	27	F	70	III	-	N1	M0	Locally advanced	3693	-	No	AD	Dead	602	465
P 20	8	183	F	60	III	13	N1	M0	Locally advanced	619	-	No	AD	Dead	1363	373
P 21 ¶	39	87	F	55	III	17	N0	M0	Locally advanced	21	2	No	AD	Alive	723	351
P 22 ¶	57	73	M	64	III	27	N0	M0	Locally advanced	52	2	No	AD	Alive	1011	1005
P 23 ¶	30	15	M	63	III	44	-	M0	Locally advanced	-	-	No	AD	Dead	482	254
P 24	9	48	F	81	IV	43	-	M1-Liver	Locally advanced	17408	-	Chemo	AD	Dead	519	519
P 25	9	21	M	66	IV	-	N0	M1	Metastatic	1109	-	No	AD	Dead	130	91
P 26	5	105	M	73	IV	-	N1	M1	Metastatic	145	-	NA	AD	NA	14	14

P 27	67	66	F	50	IV	35	-	M1-Liver	Metastatic	-	-	Chemo	AD	Dead	548	72
P 28 ¶	29	147	M	51	IV	34	N1	M1-Liver	Metastatic	4	-	No	AD	Dead	131	52
P 29	31	36	F	58	IV	39	N1	M1-Breast	Metastatic	56	29	No	AD	Dead	167	99
P 30 ¶	13	51	M	60	IV	44	N0	M1-Lung	Metastatic	4232	-	No	AD	Dead	367	137
P 31 ¶	35	236	M	66	IV	80	N1	M1-Liver	Metastatic	3116	12	No	AD	Dead	450	55
P 32 ¶	13	128	M	74	IV	56	N1	M1-Peritoneum	Metastatic	45	9	No	AD	Dead	169	139
P 33 ¶	9	83	M	65	IV	65	N1	M1-Liver	Metastatic	652518	-	No	AD	Dead	437	169
P 34 ¶*	44	207	M	78	IV	60	N1	M1-small bowel	Metastatic	19712	26	No	AD	Dead	76	76
P 35	7	85	F	58	IV	60	N1	M1-Liver, Peritoneum	Metastatic	-	-	Chemo/Rad	AD	Dead	734	143
P 36*	-	-	M	64	III	14	N1	M0	Locally advanced	204	1	Chemo	AD	Alive	1127	936
P 37 *	-	-	F	65	IIB	29	N1	M1-Liver	Metastatic	97	-	Chemo/Rad	AD	Alive	496	265
P 38 *	-	-	F	78	IIB	15	N1	M1-Liver	Metastatic	132	-	Chemo	Ad	Alive	440	440
P 39 *	-	-	F	74	IIA	30	N0	M1-Liver	Metastatic	29	<1	Chemo	AD	Dead	462	134
P 40 *	-	-	M	61	IIA	22	N0	M1-Liver	Metastatic	21	<1	Chemo	AD	Dead	514	259
HC 01	F	33	0	-	-	-	-	-	-	-	-	-	HC	Alive		
HC 02	F	27	2	-	-	-	-	-	-	-	-	-	HC	Alive		
HC 03	M	27	3	-	-	-	-	-	-	-	-	-	HC	Alive		
HC 04	M	24	1	-	-	-	-	-	-	-	-	-	HC	Alive		
HC 05	F	45	2	-	-	-	-	-	-	-	-	-	HC	Alive		
HC 06	M	40	0	-	-	-	-	-	-	-	-	-	HC	Alive		
HC 07	F	57	6	-	-	-	-	-	-	-	-	-	HC	Alive		
HC 08	M	90	3	-	-	-	-	-	-	-	-	-	HC	Alive		
HC 09	M	66	0	-	-	-	-	-	-	-	-	-	HC	Alive		

CA19-9, Carbohydrate antigen 19-9; CEA, carcinoembryonic antigen; Chemo, Chemotherapy; Rad, Radiation; Res, Resected; AD, Adenocarcinoma; NA, not Available; HC, healthy controls; OS, overall survival; PFS, progression free survival. RNA analyses were done for patients marked with ¶. Tissues samples of patients marked with* were analyzed for IHC analysis.

Table 9-7: Treatment of pancreatic cancer patients in different visits (immunoaffinity CTC Carpet Chip study)

Sample	Gender	Age	Stage	N	M	Visit 1	Visit 2	Visit 3	Visit 4
P 04	Male	63	IIA	N0	/	6/30/2014	1/6/2015	/	/
							Received clinical trial treatment UMCC, A Dose Escalation Trial of the Wee1 Inhibitor MK1775, I in combination with gemcitabine (+radiation) - 6 cycles completed		
P 20	Female	60	III	N1	/	6/17/2013	9/22/2014	3/2/2015	6/1/2015
							Completed 4 cycles Folfirinox & 4 cycles of FOLFOX, then chemo+radiation (55 Gy) and gastrojejunostomy	On palliative treatment (Gemcitabine, Abraxane, Xeloda)	Received previous treatment
P 21	Female	39	III	N0	/	7/14/2014	8/7/2014	9/8/2014	12/8/2014
							Completed two weeks of gemcitabine with AZD1775 (wee1 inhibitor)	Received 31.5 Gy (out of a planned 52.5 Gy) radiation with concurrent gemcitabine and AZD1775	On chemotherapy with gemcitabine
P 22	Male	57	III	N0	/	7/28/2014	8/14/2014	9/8/2014	4/14/2015
							Completed two weeks of gemcitabine with AZD1775 (wee1 inhibitor)	Received 31.5 Gy (out of a planned 52.5 Gy) radiation with concurrent gemcitabine and AZD1775	Off chemotherapy, last dose was 1/13/15
P 29	Female	58	IV	N1	BREAST	8/4/2014	12/22/2014	4/28/2015	
							Patient began Wee-1 inhibitor clinical trial (a dose escalation trial of the Wee1 inhibitor MK1775, in combination with gemcitabine (+radiation)), the patient switched to FOLFIRI (completed 1 cycle)	Received FOLFIRI then switched to mFOLFIRINOX, currently on this tx at time of sample	
P 30	Male	60	IV	N0	LUNG	8/4/2014	1/12/2015	/	/
							Received 6 cycles gemcitabine + Cisplatin		
P 31	Male	66	IV	N1	LIVER	8/11/2014	12/22/2014	/	/
							Given Gemcitabine+Abraxane then began on FOLFOX (still on FOLFOX at time of sample)		
P 33	Male	65	IV	N1	LIVER	8/18/2014	1/20/2015	/	/
							Completed 5 cycles of OMP-59R5 in Combination With Nab-Paclitaxel and Gemcitabine (APLINE trial)		

Visit 1: no prior treatment; different patients received different treatments in their visits 2, 3 and 4.

Table 9-8: Clinical characterization of treatment naïve patients with pancreatic cancer (Labyrinth)

Sample	Gender	Age	Tumor status	CA19-9 (U/mL)	Name of chemotherapy received	Type and Gy of Radiation received	Total CTCs	Epithelial CTCs	EMT-like CTCs
P 01	M	64	Resectable	55	Gemcitabine, Abraxane		0	0	0
P 02	M	76	Resectable	262	C1D1 Gemcitabine, Abraxane		0	0	0
P 03	M	74	Resectable	20523			0	0	0
P 04	F	56	Resectable	24			2	1	1
P 05	F	69	Resectable	160	Gemcitabine/Abraxane		2	0	2
P 06	F	62	Resectable	518	Gemcitabine		3	0	3
P 07	M	73	Resectable	94	Gemcitabine/Cisplatin		3	0	3
P 08	M	73	Resectable	27	FOLFIRINOX		3	0	3
P 09	M	55	Resectable	90	none		4	4	0
P 10	M	46	Resectable	18			4	2	2
P 11	F	72	Resectable	1103	Gemcitabine		4	2	2
P 12	F	73	Resectable	376			5	0	5
P 13	M	70	Resectable	35			5	0	5
P 14	M	68	Resectable	158	Gemzar/Xeloda, Capecitabine		5	0	5
P 15	F	74	Resectable	29	Gem/Cisplatin		6	3	3
P 16	M	73	Resectable	46	OSH		6	0	6
P 17	F	68	Resectable	173			8	0	8
P 18	M	69	Resectable	64	Gemcitabine		8	0	8
P 19	M	72	Resectable	688	Gemcitabine	24.4/36Gy	9	3	6
P 20	F	78	Resectable	132			12	3	9
P 21	M	46	Resectable	14	Gem/Abraxane		12	3	9
P 22	F	67	Resectable	243			12	0	12
P 23	M	69	Resectable	35	none		13	4	9
P 24	F	63	Resectable	95	Gemcitabine (Xeloda starting 3/13/16)		13	11	2
P 25	F	62	Resectable	24	Gemcitabine, Capecitabine (OSH)		13	0	13
P 26	F	82	Resectable				13	0	13
P 27	M	72	Resectable	16	NAB-PACLITAXEL + GEMCITABINE		18	18	0
P 28	F	59	Resectable	9	none		23	15	8
P 29	M	51	Resectable	2058	Oxaliplatin/5-FU		27	11	16
P 30	M	79	Resectable	19	Gem/Abraxane		28	0	28
P 31	M	82	Resectable	60	none		33	22	11
P 32	F	58	Resectable	105	FOLFIRINOX		46	34	12
P 33	F	77	Resectable	307	none		52	26	26

P 34	F	86	Resectable	51	Capecitabine		57	34	23
P 35	M	85	Resectable	43	Gemcitabine		61	23	38
P 36	M	72	Borderline Resectable	2884	FOLFIRINOX		3	0	3
P 37	M	72	Borderline Resectable	3079			5	5	0
P 38	M	60	Borderline Resectable	271	FOLFIRINOX, FDR-Gemcitabine	52.5 Gy	5	0	5
P 39	M	62	Borderline Resectable	83			5	0	5
P 40	F	59	Borderline Resectable	15	mFOLFIRINOX		6	3	3
P 41	F	49	Borderline Resectable	163			6	0	6
P 42	M	56	Borderline Resectable	<2	2011.007 trial: FOLFIRINOX, FDR-Gemcitabine + IMRT	50 Gy	6	0	6
P 43	F	65	Borderline Resectable	104	UMCC 2011.007: mFOLFIRINOX, Gemcitabine + IMRT	50 Gy	6	0	6
P 44	M	71	Borderline Resectable	56	GEMCITABINE + ABRAXANE		12	4	8
P 45	F	77	Borderline Resectable	1524			13	4	9
P 46	F	56	Borderline Resectable	425	FOLFIRINOX - OSH		13	0	13
P 47	M	70	Borderline Resectable	1150			15	5	10
P 48	M	69	Borderline Resectable	1671	1. FOLFIRINOX, 2. Gemcitabine	50 Gy	16	0	16
P 49	M	66	Borderline Resectable	none			20	13	7
P 50	F	58	Borderline Resectable	1674	Gem/Abraxane		21	3	18
P 51	M	60	Borderline Resectable	14	Neoadjuvant at OSH		22	18	4
P 52	F	86	Borderline Resectable	none	1. GEMCITABINE + ABRAXANE, 2. Gemcitabine, 3. Capecitabine		22	22	0
P 53	F	75	Borderline Resectable	4818	Gem/Abraxane		23	10	13
P 54	M	63	Borderline Resectable	135	mFOLFIRINOX		25	23	2
P 55	F	65	Borderline Resectable	none	GEMCITABINE + ABRAXANE at OSH		26	13	13
P 56	M	68	Borderline Resectable	1159	1. FOLFOX, 2. FOLFIRINOX		26	20	6
P 57	F	58	Borderline Resectable	215	GEMCITABINE + ABRAXANE at OSH		27	18	9
P 58	F	54	Borderline Resectable	518	UMCC 2011.007 M-FOLFIRINOX	50	27	5	22
P 59	M	82	Borderline Resectable	329	Gemcitabine at OSH (then added Abraxane)		31	22	9
P 60	M	54	Borderline Resectable	345	Gemcitabine AZD-1775	IMRT, 52.5 Gy	31	13	18
P 61	F	69	Borderline Resectable	1289			33	0	33
P 62	M	62	Borderline Resectable	241	FOLFIRINOX (12 cycles)		58	22	36
P 63	F	49	Borderline Resectable	188	FOLFIRINOX	IMRT, 50 Gy	71	45	26
P 64	F	84	Borderline Resectable	1337	1. GEMCITABINE, 2. GEMCITABINE + ABRAXANE		71	49	22
P 65	F	62	Borderline Resectable	none	1. GEMCITABINE + ABRAXANE, 2. GEMCITABINE + ABRAXANE	IMRT, 55 Gy	80	80	0
P 66	M	59	Borderline Resectable	5	FOLFIRINOX		101	56	45
P 67	F	71	Borderline Resectable	510	FOLFIRINOX		117	67	50
P 68	F	67	Locally Advanced	82			0	0	0

P 69	F	69	Locally Advanced	2209	GEMCITABINE	52.5	0	0	0
P 70	F	78	Locally Advanced	553			3	3	0
P 71	M	63	Locally Advanced	179			3	0	3
P 72	M	56	Locally Advanced	1618			4	0	4
P 73	M	62	Locally Advanced	204			5	5	0
P 74	M	81	Locally Advanced	41	Gem/Abraxane		6	0	6
P 75	F	68	Locally Advanced	2402	Wee-1 clinical trial	52.5	6	0	6
P 76	M	66	Locally Advanced	6	Gemzar/Abraxane		6	0	6
P 77	F	62	Locally Advanced	2245			7	0	7
P 78	F	52	Locally Advanced	2436	none		8	4	4
P 79	F	68	Locally Advanced	2			9	3	6
P 80	F	54	Locally Advanced		OSH		9	0	9
P 81	M	56	Locally Advanced	29			11	9	2
P 82	M	60	Locally Advanced	none	none		16	13	3
P 83	M	68	Locally Advanced	524	GEMCITABINE + ABRAXANE	52.8 Gy	17	0	17
P 84	F	59	Locally Advanced	4348	Gemcitabine	52.5	23	0	23
P 85	M	79	Locally Advanced	1678	1. Gemcitabine, 2. Capecitabine, 3. 5-FU/LV		23	23	0
P 86	M	67	Locally Advanced	510	1. FOLFIRINOX, 2. Gemcitabine		26	13	13
P 87	F	58	Locally Advanced	169	Gemcitabine	IMRT	27	13	14
P 88	F	58	Locally Advanced	4	FOLFIRINOX		27	9	18
P 89	F	70	Locally Advanced	2002			27	21	6
P 90	F	57	Locally Advanced	none	1. FOLFIRINOX at OSH, 2. GEMCITABINE + ABRAXANE		31	27	4
P 91	F	84	Locally Advanced	204	none		31	15	16
P 92	F	80	Locally Advanced	687	Gemcitabine		64	49	15
P 93	F	72	Metastatic	2657	1. FOLFOX 6, 2. GEMCITABINE + ABRAXANE		0	0	0
P 94	M	68	Metastatic	671	1. UMCC 2013.030 PHASE 2: ALPINE 2. Gem/Abraxane		0	0	0
P 95	M	65	Metastatic		OSH		0	0	0
P 96	M	63	Metastatic	346	Gemcitabine		3	3	0
P 97	F	51	Metastatic	1982			3	0	3
P 98	M	80	Metastatic	229	C1D1 Gemcitabine, Abraxane		3	0	3
P 99	F	69	Metastatic	6345	1. UMCC 2013.030, 2. FOLFOX		4	4	0
P 100	M	70	Metastatic	1653	Gemcitabine		4	2	2
P 101	M	75	Metastatic	17217			5	0	5
P 102	M	64	Metastatic	61881	1. UMCC 2013.030 PHASE 2: ALPINE 2. FOLFOX		6	6	0
P 103	F	63	Metastatic				6	0	6

P 104	M	64	Metastatic	9377	1. Gemcitabine/Cisplatin, 2. Olaparib	6	0	6
P 105	F	46	Metastatic			6	0	6
P 106	M	59	Metastatic	1444	UMCC 2015.055 Gemcitabine/Abraxane	8	3	5
P 107	F	46	Metastatic	2391	1. GEMCITABINE + ABRAXANE, 2. FOLFOX6, 3. Gemcitabine + Cisplatin + Lynparza, 4. FOLFIRI	8	4	4
P 108	M	53	Metastatic	none	unknown	8	4	4
P 109	M	61	Metastatic	1825	Gem/Abraxane	8	0	8
P 110	M	54	Metastatic	605	FOLFIRINOX	8	0	8
P 111	M	69	Metastatic	481	1. Gemzar/Abraxane, 2. FOLFOX	9	9	0
P 112	F	47	Metastatic	2463	1. FOLFIRINOX 2. Gem/Abraxane	9	6	3
P 113	M	59	Metastatic	397	UMCC 15.055 Gem/Abraxane	9	9	0
P 114	F	67	Metastatic	163		9	0	9
P 115	M	81	Metastatic	3561	Gemcitabine	9	0	9
P 116	M	66	Metastatic	429		9	0	9
P 117	F	47	Metastatic	x		10	6	4
P 118	M	52	Metastatic	91		10	0	10
P 119	F	51	Metastatic	35477	alternative regimen - OSH	10	0	10
P 120	M	61	Metastatic	22711		11	0	11
P 121	M	79	Metastatic	1393634	Gemcitabine	11	0	11
P 122	F	56	Metastatic	none	none	12	8	4
P 123	M	65	Metastatic	149	GEMCITABINE + ABRAXANE at OSH	13	13	0
P 124	M	44	Metastatic	7064	GEMCITABINE + ABRAXANE	13	13	0
P 125	M	76	Metastatic	34		13	9	4
P 126	M	59	Metastatic	7373	clinical trial: Gemcitabine, Cisplatin	13	0	13
P 127	F	77	Metastatic	50974	Gemcitabine	16	3	13
P 128	F	66	Metastatic	4030		16	5	11
P 129	F	75	Metastatic	none	none	17	4	13
P 130	F	55	Metastatic	34		18	9	9
P 131	F	69	Metastatic	2		18	0	18
P 132	M	66	Metastatic	931		21	2	19
P 133	M	75	Metastatic	159		23	10	13
P 134	F	66	Metastatic	624	1. UMCC 2013.030, 2. M-FOLFOX6	31	18	13
P 135	M	67	Metastatic	464	none	31	22	9
P 136	M	62	Metastatic	6980	FABLOx phase I clinical trial	34	17	17
P 137	M	68	Metastatic	30	1.YOSEMITE study: Gemzar/Abraxane, 2. Gemcitabine/Abraxane	46	0	46
P 138	M	75	Metastatic	8493	1. GEMCITABINE, 2. GEMCITABINE + ABRAXANE	53	53	0

P 139	F	68	Metastatic	1907	1. GEMCITABINE + ABRAXANE, 2. GEMCITABINE + ABRAXANE	58	58	0
P 140	M	78	Metastatic	343		62	62	0
P 141	F	34	Metastatic	120082	1. ALPINE trial (OMP-59R5 in Combination With Nab-Paclitaxel and Gemcitabine), 2. FOLFOX6	97	57	40
H 01	M	52				0	0	0
H 02	F	51				0	0	0
H 03	M	55				0	0	0
H 04	F	66				2	0	2
H 05	M	50				0	0	0
H 06	F	77				0	0	0
H 07	F	57				0	0	0
H 08	M	63				8	0	8
H 09	M	66				2	0	2
H 10	M	51				3	0	3
H 11	M	73				6	0	6
H 12	M	81				0	0	0

CA19-9, Carbohydrate antigen 19-9; P, patient sample; H, healthy controls

Table 9-9: Clinical characterization of patients with pancreatic cancer pre and post-surgery (Labyrinth)

Sample	Gender	Age	Tumor status pre-Surgery	Tumor status post-surgery	Total CTCs pre- Surgery	Total CTCs post-Surgery	Epithelial CTCs pre- surgery	Epithelial CTCs post- surgery	EMT-like CTCs pre- surgery	EMT-like CTCs post-surgery
P 01	F	49	Borderline	Resected	71	3	45	0	26	3
P 02	M	65	Resectable	Resected	22	3	/	0	/	3
P 03	F	86	Resectable	Resected	57	64	34	37	23	27
P 04	M	85	Resectable	Resected	61	0	23	0	38	0
P 05	M	59	Borderline	Resected	101	10	56	0	45	10
P 06	M	82	Resectable	Resected	16	70	0	54	16	16
P 07	M	55	Resectable	Resected	17	17	9	9	9	9
P 08	F	86	Borderline	Resected	22	6	22	0	0	6
P 09	F	66	Borderline	Resected	71	0	/	0	/	0
P 10	F	53	Borderline	Resected	4	3	/	0	/	3
P 11	F	73	Resectable	Resected	5	3	/	3	/	0
P 12	F	74	Resectable	Resected	6	6	3	6	3	0
P 13	M	68	Resectable	Resected	26	8	20	3	6	5
P 14	F	68	Resectable	Resected	8	2	0	0	8	2
P 15	F	54	Borderline	Resected	27	16	5	0	22	16
P 16	M	69	Resectable	Resected	8	10	0	0	8	10
P 17	F	78	Resectable	Resected	12	29	3	6	9	23
P 18	F	63	Resectable	Resected	13	3	11	0	2	3
P 19	M	63	Borderline	Resected	25	9	23	0	2	9
P 20	M	63	Resectable	Resected	13	12	3	0	10	12
P 21	M	46	Resectable	Resected	6	6	0	0	6	6
P 22	F	73	Resectable	Resected	5	14	0	0	5	14
P 23	F	62	Resectable	Resected	13	6	0	3	13	3
P 24	M	70	Resectable	Resected	5	6	0	3	5	3
P 25	M	68	Resectable	Resected	5	3	0	0	5	3
P 26	M	73	Resectable	Resected	6	0	0	0	6	0
P 27	M	73	Resectable	Resected	3	17	0	0	3	17
P 28	M	74	Resectable	Resected	0	3	0	0	0	3
P 29	M	64	Resectable	Resected	5	10	0	5	5	5

Table 9-10: Clinical characterization of patients with pancreatic cancer pre- and on-Chemotherapy (Labyrinth)

Sample	Gender	Age	Tumor status pre-Chemotherapy	Tumor status on-Chemotherapy	Total CTCs pre-Chemo	Total CTCs on-Chemo	Epithelial CTCs pre-Chemo	Epithelial CTCs on-Chemo	EMT-like CTCs pre-Chemo	EMT-like CTCs on-Chemo
P 01	M	59	Borderline	Resected	101	10	56	0	45	10
P 02	M	67	Locally Advanced	Metastatic	26	10	13	/	13	/
P 03	F	46	Metastatic	Metastatic	8	60	4	/	4	/
P 04	F	58	Locally Advanced	Locally Advanced	27	14	9	3	18	11
P 05	F	66	Metastatic	Metastatic	31	15	18	3	13	12
P 06	F	65	Borderline	borderline	26	0	13	0	13	0
P 07	F	69	Metastatic	Metastatic	4	26	4	5	0	22
P 08	M	44	Metastatic	Metastatic	13	0	13	0	0	0
P 09	M	54	Borderline	Locally Advanced	31	9	13	9	18	0
P 10	F	53	Borderline	Borderline	4	0	/	0	/	0
P 11	F	74	Resectable	resected	6	6	3	6	3	0
P 12	F	58	Locally Advanced	Locally Advanced	17	21	13	6	14	15
P 13	M	65	Metastatic	Metastatic	16	3	/	3	/	0
P 14	M	67	Metastatic	Metastatic	0	22	/	3	/	19
P 15	F	58	Resectable	resectable	46	3	34	0	12	3
P 16	F	63	Resectable	resected	13	3	11	0	2	3
P 17	F	59	Borderline	borderline	6	36	3	10	3	26
P 18	M	81	Metastatic	Metastatic	16	16	/	0	/	16
P 19	M	62	Metastatic	Metastatic	34	0	17	0	17	0
P 20	M	51	Borderline Resectable	Borderline Resectable	27	10	11	0	16	10
P 21	M	60	Borderline Resectable	Borderline Resectable	5	0	0	0	5	0
P 22	M	80	Metastatic		3	5	0	0	3	5
P 23	M	69	Borderline Resectable		16	3	0	0	16	3
P 24	F	68	Unresectable	Unresectable	6	3	0	0	6	3
P 25	M	68	Metastatic	Metastatic	46	0	0	0	46	0
P 26	M	68	Resected	Resected	3	5	0	0	3	5
P 27	M	64	Metastatic	Metastatic	6	3	0	0	6	3

P 28	F	46	Metastatic	Metastatic	0	6	0	0	0	6
P 29	M	56	Borderline Resectable	Borderline Resectable	6	5	0	0	6	5
P 30	M	64	Unresectable	Unresectable	12	3	6	0	6	3
P 31	M	73	Resected	Resected	17	6	0	0	17	6
P 32	M	66	Unresectable	Unresectable	6	1	0	0	6	1
P 33	M	59	Metastatic	Metastatic	13	7	0	0	13	7
P 34	M	76	Resectable	Resectable	0	0	0	0	0	0
P 35	M	54	Metastatic	Metastatic	8	0	0	0	8	0

Chemotherapy, Chemo

Table 9-11: Clinical characterization of patients with pancreatic cancer pre- and post-Chemotherapy (Labyrinth)

Sample	Gender	Age	Tumor status pre-Chemotherapy	Tumor status post-Chemotherapy	Total CTCs pre-Chemo	Total CTCs post-Chemo	Epithelial CTCs Pre-Chemo	Epithelial CTCs Post-Chemo	EMT-like CTCs pre-Chemo	EMT-like CTCs post-Chemo
P 01	M	82	Borderline	Resectable	31	16	22	0	9	16
P 02	F	62	Borderline	Locally Advanced	80	21	80	0	0	21
P 03	F	58	Locally advanced	Metastatic	27	14	9	3	18	11
P 04	F	84	Borderline	Locally Advanced	71	12	49	12	22	0
P 05	F	86	Borderline	Resected	22	6	22	0	0	6
P 06	F	68	Metastatic	Metastatic	58	18	58	3	0	15
P 07	F	53	Borderline	Resected	4	3	/	0	/	3
P 08	F	59	Borderline	Locally Advanced	3	7	0	0	3	7
P 09	M	68	Resectable	Resected	26	8	20	3	6	5
P 10	F	54	Borderline	Resected	27	16	5	0	22	16
P 11	F	75	Borderline	Borderline	23	6	10	0	13	6
P 12	M	61	Metastatic	Metastatic	8	23	0	0	8	23
P 13	M	69	Resectable	Resected	8	10	0	0	8	10
P 14	F	59	Borderline	Locally Advanced	6	3	3	0	3	3
P 15	M	63	Borderline	Resected	25	9	23	0	2	9
P 16	M	81	Metastatic	Metastatic	16	6	/	3	/	3
P 17	F	61	Metastatic	Metastatic	24	3	/	0	/	3
P 18	M	59	Metastatic	Metastatic	8	6	3	0	5	6
P 19	F	58	Borderline	Borderline	21	33	3	6	18	27
P 20	M	51	Borderline Resectable	Borderline Resectable	27	4	11	0	16	4
P 21	M	46	Resectable	Resectable	12	6	3	0	9	6
P 22	F	56	Borderline Resectable	Borderline Resectable	13	0	0	0	13	0

Chemotherapy, Chemo

Table 9-12: Clinical characterization of patients with pancreatic cancer pre- and post-Radiation (Labyrinth)

Sample	Gender	Age	Tumor status pre-Radiation	Tumor status post-Radiation	Total CTCs pre-Rad	Total CTCs post-Rad	Epithelial CTCs pre-Rad	Epithelial CTCs post-Rad	EMT-like CTCs pre-Rad	EMT-like CTCs post-Rad
P 01	F	49	Borderline	Resected	71	3	45	0	26	3
P 02	F	62	Borderline	Locally Advanced	80	21	80	0	0	21
P 03	F	87	Resected	Resected	6	5	0	0	6	5
P 04	F	73	Locally Advanced	Locally Advanced	20	8	0	1	20	7
P 05	M	54	Borderline	Locally Advanced	31	9	13	9	18	0
P 06	F	53	Borderline	Resected	0	3	0	0	0	3
P 07	F	59	Borderline	Locally Advanced	3	7	0	0	3	7
P 08	F	58	Locally Advanced	Locally Advanced	17	21	13	6	14	15
P 09	F	75	Borderline	Borderline	23	6	10	0	13	6
P 10	F	63	Resectable	Resected	13	3	11	0	2	3
P 11	F	59	Borderline	Locally Advanced	6	3	3	0	3	3
P 12	M	51	Borderline Resectable	Borderline Resectable	10	4	0	0	10	4

Radiation, Rad

Table 9-13: Clinical characterization of patients with NSCLC

Sample	Gender	Age	Stage	Node status	Tumor	Adenocarcinoma subtype	Smoking status	Mutation	Treatment
P 01	F	39	IV	N0	T2	ALK	No	Alk Mutation	Crizotinib
P 02	F	55	IV	N3	T2	ROS-1	80 PY	ROS1 Mutation	Crizotinib (switched from Carbo/Taxol due to neuropathy - was taking Carbo/Taxol prior to baseline)
P 03	F	40	IV	N2	T1	ROS-1	No	ROS1 rearrangement	Crizotinib (stopped 12/10/2017). Started Entrectinib 12/26/2017.
P 04	M	85	IV	N1	T2	ROS-1	30PY	ROS1 rearrangement	Crizotinib
P 05	F	78	IV	N2	T3	EGFR	No	EGFR mutant AC with T790M mutation	Osimertinib
P 06 [¶]	F	49	IV	N0	T4	EGFR	25PY	T790M mutation	Osimertinib
P 07	F	77	IV	N1	T3	EGFR	No	EGFR mutant AC	Disease progression on Erlotinib so switched to Afatinib on 1/10/2017
P 08	M	81	IV	N2	T1	EGFR	No	EGFR mutant AC	Afatinib reduced dose started on 12/31/2016. On hold as of 2/14/2017 to improve QOL
P 09 [¶]	F	43	IV	N2	T2	ROS-1	No	ROS 1 Mutation	Progressed on Crizotinib. Started on Ceritinib
P 10	M	58	IV	N0	T3	ROS-1	No	ROS 1 Mutation	Crizotinib
P 11	M	60	IV	N0	T2	Alk	23PY	Alk translocation +	Crizotinib
P 12	F	57	IV	N0	T4	EGFR	5PY	EGFR mutation	Erlotinib and Zometa
P 13	M	62	IV	N2	T3	EGFR	No	EGFR mutation	Afatinib, Switched to Osimertinib (due to rash)
P 14	F	58	IV	N0	T2	EGFR	5PY	EGFR mutation	Pemetrexed maintenance - cycle 1 initiated on 7/12/2017; prior to this patient received 4 cycles of Carboplatin/Pemetrexed.
P 15	F	61	IV	N0	T2	EGFR	10PY	EGFR exon 19 deletion	Tarceva
P 16	F	80	IV	N0	T2	EGFR	No	EGFR L858R, T790M	Osimertinib
P 17	M	58	IV	Nx	T3	Alk	No	TTF-1, Napsin, ALK positive	Alectinib (stopped Crizotinib)
P 18	F	61	IV	N3	T2	EGFR	No	EGFR L858R, T790M	Osimertinib
P 19	M	50	IV	N2	T2	Alk	Former	ALK EML-4 fusion	Alectinib
P 20	F	45	IV	N3	T4	EGFR	Former	EGFR, Exon 19 deletion, PDL1 10%	Tagrisso
P 21	F	63	IV	N3	T3	ROS-1	No	ROS-1	Carboplatin/Pemetrexed
P 22*	F	49	IV	Nx	T2	EGFR	No	EGFR insertion/deletion19 and a variant of unknown significance in ERBB2. ALK1 and ROS1 negative.	Afatinib + Cetuximab. 10/27/2017 switched to Taxotere+Cyamza+Tagrisso
P 23*	F	43	IV	N0	T2A	RET	No	RET Mutation	Alectinib
P 24**	M	53	/	/	/	/	/	CK7, TTF-1, Napsin-A positive PD-L1 5%	Pembrolizumab + ePancreatic cancerdostat

[¶] Analyzed for PanCK CTC only. * Discarded from the analysis due to the different sample processing. ** Withdraw from the project by the clinic due to the PDL1 mutation.

Table 9-14: CTC enumeration of patients with NSCLC

Sample	PanCK+ CTCs	EpCAM+ CTCs	Vimentin+ CTCs	Double+ CTCs	Total CTCs	Processed with
P 01	121.4	0.0	11.3	8.5	141.2	Single Labyrinth
P 02	34.4	0.0	7.4	54.0	95.7	Single Labyrinth
P 03	96.9	14.2	23.6	33.1	167.8	Single Labyrinth
P 04	100.9	38.2	30.0	2.7	171.8	Single Labyrinth
P 05	273.8	5.0	7.5	0.0	286.3	Single Labyrinth
P 06 [¶]	76.8	0	0	0	76.8	Single Labyrinth
P 07	24.0	0.0	57.6	122.4	204.0	Single Labyrinth
P 08	167.3	0.0	2.4	12.1	181.8	Single Labyrinth
P 09 [¶]	631.4	0.0	0.0	0.0	631.4	Single Labyrinth
P 10	30.1	7.5	0.0	7.5	45.2	Single Labyrinth
P 11	350.0	0.0	7.9	44.7	402.6	Single Labyrinth
P 12	189.3	5.2	59.6	25.9	280.0	Single Labyrinth
P 13	31.6	0.0	0.0	7.9	39.5	Single Labyrinth
P 14	21.8	0.0	9.5	2.7	34.1	Single Labyrinth
P 15	42.4	4.4	0.0	5.9	52.7	Single Labyrinth
P 16	7.3	0.0	1.5	1.5	10.2	Single Labyrinth
P 17	71.3	0.0	11.3	56.3	138.8	Single Labyrinth
P 18	38.5	0.0	52.5	0.0	91.0	Single Labyrinth
P 19	6.4	6.4	22.4	35.2	70.4	Single Labyrinth
P 20	82.5	0.0	20.6	4.1	107.3	Single Labyrinth
P 21	41.6	6.9	263.5	239.2	551.2	Single Labyrinth
P 22*	0.0	0.0	0.0	3.2	3.2	Double Labyrinth
P 23*	13.8	0.0	4.2	0.0	18.0	Double Labyrinth
P 24**	NA	NA	NA	NA	NA	Single Labyrinth
HC 01	3.0	0.0	0.0	0.0	30	Single Labyrinth
HC 02	0.0	0.0	0.0	0.0	0.0	Single Labyrinth
HC 03	0.0	0.0	0.0	0.0	0.0	Single Labyrinth

[¶] Analyzed for PanCK CTC only. * Discarded from the analysis due to the different sample processing. ** Withdraw from the project by the clinic due to the PDL1 mutation.

Table 9-15: Clinical information of NSCLC patients (P 03 and P 22) over the treatment.

Study ID	Mutation	Treatment	Baseline Blood Draw	Medication Start	Visit 2	Visit 3	Visit 4	Visit 5	Visit 6	Visit 7	Visit 8	Visit 9	Visit 10	Comments
P 03	ROS1 rearrangement	Crizotinib (stopped 12/10/2017). Entrectinib Started 12/26/2017.	12/6/2016	11/8/2013	4/18/2017	8/29/2017	12/5/2017	1/22/2018	3/19/2018	5/14/2018	6/8/2018	7/13/2018	8/31/2018	11/21/2017- progressed in the brain. 1/20/2018- MRI Brain- slight increase in fullness of L frontal brain tumor. CT (chest, abdomen, pelvis) no change in bone mets, no new mets. 3/19/2018- cancer progression in the brain only, but at several spots. Entrectinib continued as treatment. 7/11/2018- Continue Entrectinib for now, has likely stable disease, recent MRI findings more likely treatment-related/radiation necrosis and less likely progression.
P 22	EGFR insertion/deletion19	10/27/2017 Docetaxel + Ramucirumab Discontinued Docetaxel on 4/13/2018 (due to fatigue and taste changes). Discontinued Ramucirumab on 6/15/2018 due to progression on MR brain with two new lesions. 6/15/2018 started on Osimertinib.	10/21/2016	10/28/2016	12/16/2016	3/10/2017	6/23/2017	8/18/2017	10/27/2017	2/16/2018	3/30/2018	8/8/2018		Disease progression to liver and new lung, brain tumor increasing in size. 12/29/2017 Brain MRI- No significant interval change. 2/13/2018 Chest CT- Interval decrease in lung nodules and liver lesions. Withdrew consent further blood draws on 6/15/2018. Brain MR on 6/11/2018 demonstrated two new brain lesions. Discontinued ramucirumab due to new lesions and started on Osimertinib.

9.3 Table of Figures

Figure 1-1: Pancreatic precursor lesions in pancreatic adenocarcinoma progression.....	29
Figure 1-2: Cell components of pancreatic cancer	31
Figure 1-3: Schematic representative images of the immunoaffinity CTC Carpet Chip.....	36
Figure 1-4: Size-based separation Labyrinth device.....	38
Figure 1-5: Pie chart of NSCLC mutations	39
Figure 2-1: Microfabrication process	42
Figure 2-2: Photolithography process.....	44
Figure 2-3: Rapid prototyping of PDMS devices.....	45
Figure 2-4: Silanization of plasma-exposed PDMS	46
Figure 2-5: Biotinylated functionalized PDMS micropost chamber.....	47
Figure 2-6: PDMS surface modification and functionalization.....	48
Figure 2-7: BioMark HD Real-Time PCR system.....	57
Figure 3-1: AutoCAD design of different version of the Original CTC Chip.	62
Figure 3-2: AutoCAD design of different configurations of the CTC Chip.....	63
Figure 3-3: % Capture efficiencies among different configuration of the CTC Chip	64
Figure 3-4: The effect of different cell %confluency of HT-29 cell line on the capture efficiencies of EpCAM	65
Figure 3-5: The effect of different blocking reagents on the capture efficiencies of EpCAM.	66
Figure 3-6: The effect of backward and forward PBS wash on the % purity	66
Figure 3-7: Schematic representation of CTC Carpet Chip	67
Figure 3-8: Finite element simulations of the CTC Carpet Chip.....	68
Figure 3-9: The effect of different distances between posts of CTC Carpet Chip and different flow rates on the capture efficiencies of EpCAM	69
Figure 3-10: The effect of different cell line on the capture efficiencies of EpCAM	70
Figure 3-11: Profile capturing across the CTC Carpet Chip.....	71
Figure 3-12: Representative image of a dual CTC Carpe Chip.....	72
Figure 3-13: Western blot analysis of EpCAM and CD133 on HT-29 and PC-3 cell lines.	72
Figure 3-14: The FACS analysis to check the expression of capture antibodies (EpCAM and CD133) on different cell lines.	73
Figure 3-15: FACS analysis to check the expression of detection antibodies (CK) on different cell lines	74
Figure 3-16: FACS analysis to check the expression of detection antibodies (Vimentin) on different cell lines	75
Figure 3-17: Sensitivity and specificity of the capture efficiencies of the dual CTC Carpet chip.....	76
Figure 3-18: Comparison between CK7&8 and PanCK in detecting the EpCs in pancreatic cancer patient samples (n=3).....	77
Figure 3-19: Analysis of pancreatic cancer patient samples (n=16) with triple staining (CK, Vimentin, and CD45) for each CTC Carpet Chip	78
Figure 3-20: CTC Carpet Chip cell line immunofluorescence staining. Anti-human CD45, anti-human PanCK, and anti-human Vimentin antibodies were tested with cancer cell lines.....	79
Figure 3-21: The effect of Chip's order on the numbers of captured cells on dual study.....	80
Figure 3-22: Characterization of circulating epithelial CTCs (EpCs) in the EpCAM Carpet Chip from pancreatic cancer patients.	81

Figure 3-23: Characterization of circulating EMT-like CTCs (EMTCs) in the CD133 Carpet Chip from pancreatic cancer patients	82
Figure 3-24: Analysis of EpCs and EMTCs from pancreatic cancer patient samples compared to the healthy controls.....	83
Figure 3-25: Analysis of EpCs and EMTCs from pancreatic cancer patient samples based on their clinical outcomes.....	85
Figure 3-26: Clustering heat map of gene expression profiling of CTCs in pancreatic cancer patients samples (n=17).....	87
Figure 3-27: Gene expression profiling in pancreatic cancer patients CTC samples (n=17) based on the capture device.	88
Figure 3-28: Immunohistochemistry of the primary tumor tissues of PDAC patients.....	90
Figure 3-29: Gene expression profiling of CTCs based on stage IIA pancreatic cancer patients. Stage IIA samples (n=5) compared to the rest of stages (n=30) analysis.	91
Figure 3-30: Gene expression profiling of CTCs based on stage IIB&III pancreatic cancer patients	92
Figure 3-31: Gene expression profiling of CTCs based on stage IV pancreatic cancer patients.	93
Figure 3-32: Relationship between CTCs gene expression and prognosis.....	94
Figure 3-33: CTC numbers of pancreatic cancer patient samples (n=8) over the treatment	96
Figure 3-34: Gene expression analysis of pancreatic cancer patient samples (n=5) over the treatment.....	97
Figure 3-35: Strategies of the application of CTC Carpet Chip to isolate both CTCs and CFCs from pancreatic cancer mouse model.	99
Figure 3-36: Pancreatic cancer cells transduced with a luciferase-expressing lentivirus were subcutaneously injected alone or with CAF or CA-MSC into NOD/SCID mice.....	100
Figure 3-37: Representative images of captured circulating GFP+ tumor cells (CTCs) using CTC Carpet Chip from mice blood samples	101
Figure 3-38: Quantification of circulating GFP+ tumor cells (CTCs) in tumor alone, tumor plus CAF, and CA-MSC groups and DsRed+ fibroblasts cells (CFCs) in tumor+CAF and CA-MSC groups.....	102
Figure 3-39: The effect of the reinjection on the number of GFP positive cells on the tumor, tumor plus CAF CA-MSC groups	103
Figure 3-40: Experimental outline for isolation of CTCs in pancreatic cancer patients using Labyrinth technology.....	104
Figure 3-41: The illustration of Labyrinth device	105
Figure 3-42: Characterization of heterogonous CTC populations in pancreatic cancer using Labyrinth	106
Figure 3-43: CTC enumeration of treatment naïve pancreatic cancer patients using Labyrinth	108
Figure 3-44: KM curve for overall survival probability in treatment naïve (A), and in treatment naïve samples grouped by cancer stage (B)	108
Figure 3-45: CTC enumeration for pre- and post-surgery cohort (n=29).....	110
Figure 3-46: CTC enumeration for pre- and on-chemotherapy cohort (n=35)	111
Figure 3-47: CTC enumeration for pre and post chemotherapy cohort (n=22).....	111

Figure 3-48: CTC enumeration for pre- and post-radiation cohort (n=12).	112
Figure 3-49: CTC counts to predict the prognosis in pancreatic cancer.	113
Figure 3-50: High throughput and label-free Labyrinth device demonstrated the advantages of marker-independent separation methods in identifying heterogonous CTC sub-population in non-small cell lung cancer patients.	114
Figure 3-51: Labyrinth optimization using PC-9 cell line for cell recovery	115
Figure 3-52: Labyrinth optimization using H1975 cell line for cell recovery	116
Figure 3-53: Labyrinth optimization using HCC827 cell line for cell recovery.	117
Figure 3-54: Labyrinth optimization using H1650 cell line.	118
Figure 3-55: Immunofluorescence staining optimization using NSCLC cell lines	118
Figure 3-56: Immunofluorescence staining images of the representative images of some CTCs recovered from NSCLC patients samples.	119
Figure 3-57: Isolation of CTCs from NSCLC patients (n=21)	120
Figure 3-58: Immunofluorescence staining images of the representative images of heterogeneous CTC subpopulations recovered from NSCLC patients samples	121
Figure 3-59: Identification of heterogeneous CTC subpopulations isolated from NSCLC patient samples (n=19)	122
Figure 3-60: Analysis of total numbers of CTCs mL ⁻¹ in different subpopulation of CTCs.	123
Figure 3-61: Immunofluorescence staining images of the representative recovered CTC clusters in NCSLC patients	124
Figure 3-62: Identification of CTC clusters recovered from NSCLC patient samples (n=19).	125
Figure 3-63: Analysis of CTCs clusters mL ⁻¹ in different subpopulation of CTCs	125
Figure 3-64: Genomic analysis of NSCLC patient samples using Fluorescence in situ hybridization (FISH) analysis.	126
Figure 3-65: Patient-derived CTC expansion utilizing different culture conditions.	128
Figure 3-66: Cell viability check on the patient-derived expanded CTC using 3D models.	129
Figure 3-67: RBC removal techniques optimization.	132
Figure 3-68: RBC removal techniques optimization using cell strainer	133
Figure 3-69: RBC removal techniques optimization using Ficoll	134
Figure 3-70: Representative images of the NSCLC patient-derived expanded CTCs (P 03).	135
Figure 3-71: Genomic analysis of NSCLC patient sample (P 03) using FISH analysis.	136
Figure 3-72: Representative images of the NSCLC patient-derived expanded CTCs (P 22).	137
Figure 3-73: CTC enumeration of two NSCLC patients over the treatment regime.	139
Figure 3-74: IC50 values of different drugs on NSCLC cell lines using CellTiter 96® Aqueous One Solution Cell Proliferation Assay.	141
Figure 3-75: IC50 values of different drugs on NSCLC cell lines using CellTiter-Glo® Luminescent Cell Viability Assay.	143
Figure 3-76: IC50 values of crizotinib on NSCLC cell lines using CellTiter-Glo luminescent cell viability assay (2D kit) vs. CellTiter-Glo 3D Cell Viability Assay (3D kit).	144
Figure 3-77: LIVE/DEAD viability/cytotoxicity kit optimization using different NSCLC cell lines.	145
Figure 3-78: IC50 values of different drugs on the expanded CTCs from patient P 03-V6.	146
Figure 3-79: IC50 values of different drugs on the expanded CTCs from patient P 22-V8.	148

Figure 5-1: Biomarker independent microfluidics strategy and the future direction for CTC based tumor models in lung cancer	169
Figure 9-1: Original vs. Split CTC Chip	193
Figure 9-2: Original vs. Modified CTC Chip	194
Figure 9-3: Modified vs. Rotated CTC Chip	195
Figure 9-4: Rotated vs. Carpet CTC Chip	196

9.4 Table of Tables

Table 1-1: Classification of EMT according to the biological context	12
Table 1-2: CTC isolation technologies.....	25
Table 2-1: Table of 96 genes analyzed by TaqMan Gene Expression Assays	56
Table 3-1: Comparison between different microfluidic devices, including, Original, Modified, Rotated, and Carpet.....	64
Table 3-2: Numbers of GFP+ tumor cells (CTCs) in tumor alone, tumor plus CAF, and CA-MSC groups and DsRed+ fibroblasts cells (CFCs) in tumor+CAF and CA-MSC groups	102
Table 3-3: Numbers of GFP positive tumor cells (CTCs) in tumor, tumor plus CAF and CA-MSC groups in the first and second injection.	103
Table 3-4: The effects of different drugs on of NSCLC cell lines.	142
Table 3-5: Comparison of IC50 values with two different cell viability assays.....	142
Table 3-6: Comparison of IC50 values with two different cell viability assays 2D vs. 3D	144
Table 3-7: IC50 values of different drugs on the expanded CTCs from patient P 03-V6. Data are means \pm standard deviation of three independent experiments.....	147
Table 3-8: IC50 values of TKIs tested in patients' CTCs or NSCLC cell line. Data are means \pm standard deviation of three independent experiments.	147
Table 9-1: Staging of pancreatic cancer	197
Table 9-2: CTC detection techniques in pancreatic cancer	198
Table 9-3: Staging of Lung Cancer.....	199
Table 9-4: CTC detection technologies in NSCLC	201
Table 9-5: Optimization of panel of antibodies for CTCs detection in pancreatic cancer patients.	202
Table 9-6: Clinical characterization of pancreatic cancer patients (n=40) (immunoaffinity CTC Carpet Chip study)	203
Table 9-7: Treatment of pancreatic cancer patients in different visits (immunoaffinity CTC Carpet Chip study).....	205
Table 9-8: Clinical characterization of treatment naïve patients with pancreatic cancer (Labyrinth).....	206
Table 9-9: Clinical characterization of patients with pancreatic cancer pre and post-surgery (Labyrinth).....	211
Table 9-10: Clinical characterization of patients with pancreatic cancer pre- and on-Chemotherapy (Labyrinth)	212
Table 9-11: Clinical characterization of patients with pancreatic cancer pre- and post-Chemotherapy (Labyrinth)	214
Table 9-12: Clinical characterization of patients with pancreatic cancer pre- and post-Radiation (Labyrinth).....	215
Table 9-13: Clinical characterization of patients with NSCLC	216
Table 9-14: CTC enumeration of patients with NSCLC	217
Table 9-15: Clinical information of NSCLC patients (P 03 and P 22) over the treatment.	218

10 Curriculum Vitae

Personal data

Name: Mina Zeinali
DOB: 01.08.1981
POB: Tehran, Iran
Marital Status: Single
Father: DarvishAli Zeinali
Mother: Mahin Hasani

School (Education)

(1988) – (1992) Elementary school, Imam Bagher, Tehran-Iran
(1992) – (1994) Middle school, Imam Sadegh, Tehran-Iran
(1994) – (1997) High school, Imam Sadegh, Tehran-Iran
(1997) – (1998) Pre-University Course, Aain Tarbiyat, Tehran-Iran

University (Education)

WS2004 Biology
Islamic Azad University, Tehran-Iran
June 2004 Bachelor of Science (B.Sc.)
WS2008 Biotechnology
Mannheim University of Applied Sciences
Thesis: Differentiation of human Mesenchymal Stem Cells (MSCs)
under shear stress.
09 April 2010 Master of Science (M.Sc.) Note: 2.1

11 Professional Work and Research Cited

Summary:

- 5 published papers, 1 submitted paper, 3 in-preparation papers, 1 oral presentation, 2 conference presentations, 7 poster presentations (over 160 citations)
- Google Scholar Profile:
<https://scholar.google.com/citations?user=YtI4vxIAAAAJ&hl=en>

Publications:

- **Zeinali, M**, Murlidhar, V, Fouladdel, S, Shao, S, Zhao, L, Cameron, H, Bankhead, A, Shi, J, Cuneo, KC, Sahai, V, Azizi, E, Wicha, MS, Hafner, M, Simeone, DM, Nagrath, S: Profiling Heterogeneous Circulating Tumor Cells (CTC) Populations in Pancreatic Cancer Using a Serial Microfluidic CTC Carpet Chip. *Advanced Biosystems*, 0: 1800228, 2018.
- Jack, R, Hussain, K, Rodrigues, D, **Zeinali, M**, Azizi, E, Wicha, M, Simeone, DM, Nagrath, S: Microfluidic continuum sorting of sub-populations of tumor cells via surface antibody expression levels. *Lab Chip*, 17: 1349-1358, 2017.
- Waghray, M, Yalamanchili, M, Dziubinski, **M, Zeinali, M**, Erkinen, M, Yang, H, Schradle, KA, Urs, S, Pasca Di Magliano, M, Welling, TH, Palmbo, PL, Abel, EV, Sahai, V, Nagrath, S, Wang, L, Simeone, DM: GM-CSF Mediates Mesenchymal-Epithelial Cross-talk in Pancreatic Cancer. *Cancer Discov*, 6: 886-899, 2016.
- Jack, RM, Grafton, MM, Rodrigues, D, Giraldez, MD, Griffith, C, Cieslak, R, **Zeinali, M**, Kumar Sinha, C, Azizi, E, Wicha, M, Tewari, M, Simeone, DM, Nagrath, S: Ultra-Specific Isolation of Circulating Tumor Cells Enables Rare-Cell RNA Profiling. *Advanced science (Weinheim, Baden-Wurttemberg, Germany)*, 3: 1600063, 2016.
- Murlidhar, V, **Zeinali, M**, Grabauskienė, S, Ghannad-Rezaie, M, Wicha, MS, Simeone, DM, Ramnath, N, Reddy, RM, Nagrath, S: A Radial Flow Microfluidic Device for Ultra-High-Throughput Affinity-Based Isolation of Circulating Tumor Cells. *Small*, 10: 4895-4904, 2014.
- **M. Zeinali**, M. Lee, A. Nadhan, A. Mathur, E. Lin, R. Harouaka, M. S. Wicha, N. Palanisamy, M. Hafner, R. Reddy, G. P. Kalemkerian, B. J. Schneider, K. A. Hassan, N. Ramnath*, S. Nagrath*. High Throughput label-free isolation of heterogeneous CTCs from Non-small cell lung cancer patients. (Submitted to JTO, 2019).
- **M. Zeinali**, S. Owen, S. Nagrath. *Small methods journal. Bio-applications of Microfluidic Devices. (In preparation)*
- **M. Zeinali**, W. Huang, R. Rishindra, N. Ramnath, S. Nagrath. High throughput size-based isolation of Lung CTCs for molecular diagnosis and drug testing. *(In preparation)*

- L. Rivera, V. Sahai, **M. Zeinali**, C. Dunlay, D. M. Simeone, S. Nagrath. Analysis of circulating tumor cells in pancreatic cancer using size-based microfluidic technology, (In preparation)

Oral Presentations:

- Analysis of circulating epithelial and EMT like CTCs in pancreatic cancer using sensitive microfluidic “CTC Carpet chip”. **M. Zeinali**, V. Murlidhar, S. Fouladdel, M. S. Wicha, M. Hafner*, E. Azizi, D. M. Simeone, S. Nagrath*. 21st IAMA -Las Vegas 2014 (Invited speakers).

Conference Presentations:

- Molecular Genetics of β -Thalassemia in Iran. V. Lotfi, P. Fouladi, M. Masrouri, A. Abdolhosseini, B. Azimifar, M.M Sajedi Far, **M. Zeinali**, M. Feizpour, S. Foroughi, F. Mollazadeh, S. Zeinali. Genetics Conference, Kerman, Iran, 2006.
- The report of 1520 cases of prenatal diagnosis of β -Thalassemia as the best consequences of the preventive program in the country. V. Lotfi, B. Azimifar, P. Fouladi, M. Masrouri, Z. Jamali, S. Abdi, A. Abdolhosseini, F. Hashemi, F. Ehterami, M. Feizpour, S. Foroughi, F. Mollazadeh, A. Jodaki, F. Chehelcheraghi, M. M.Sajedi Far, **M. Zeinali**, A. Fahim, S. Zeinali. The First Iranian Medical Laboratory Scientists conference in Iran, Tehran, Iran. Jan 2007.

Posters:

- High Throughput isolation of circulating tumor cells (CTCs) from Non-small cell lung cancer (NSCLC) patients for personalized treatments. Authors: **Mina Zeinali**, Arthi Nadhan, Anvya Mathur, Maggie Lee, Wei Huang, Mathias Hafner, Nithya Ramnath, Sunitha Nagrath. **Fifth AACR-IASLC International Joint Conference 2018: Lung Cancer Translational Science from the Bench to the Clinic, San Diego.**
- Epithelial-Mesenchymal Transition-like CTCs reveals signatures of poor outcomes in pancreatic cancer. Authors: **Mina Zeinali**, Vasudha Murlidhar, Shamileh Fouladdel, Mathias Hafner, Shimeng Shao, Lili Zhao, Heather Cameron, Armand Bankhead III, Jiaqi Shi, Kyle C.Cuneo, Vaibhav Sahai, Ebrahim Azizi, Max S. Wicha, Diane M. Simeone, Sunitha Nagrath. **AACR 2018, Chicago.**
- Increased number of EMT-like CTCs relative to Epithelial CTCs reveal signatures of poor out-comes in pancreatic cancer. Authors: **M. Zeinali**, V. Murlidhar, S. Fouladdel, M. Hafner, S. Shao, L. Zhao, H. Cameron, A. Bankhead III, J. Shi, K. C.Cuneo, V. Sahai, E. Azizi, M. S. Wicha, D. M. Simeone, S. Nagrath. **AACR 2016, Florida.**
- Mesenchymal stem cells in pancreatic cancer possess unique properties in promoting tumor growth and metastasis. Authors: M. Waghray, G. Grace, M.

Yalamanchili, L. Wang, M. Dziubinski, **M. Zeinali**, S. Nagrath, D. Simeone. **AACR 2015, Philadelphia.**

- Analysis of circulating epithelial and EMT-like CTCs in pancreatic cancer using a sensitive microfluidic CTC capture device. Authors: **M. Zeinali**, V. Murlidhar, S. Fouladdel, M. Hafner, S. Shao, E. Azizi, M. S Wicha, K. Cuneo, D. M Simeone, S. Nagrath. **AACR 2015, Philadelphia.**
- A Radial Flow Microfluidic Device for Ultra-high-throughput Affinity-based Isolation of Circulating Tumor Cells. Authors: V. Murlidhar, **M. Zeinali**, S. Grabauskiene, M. Ghannad-Rezaie, M. S. Wicha, D. M. Simeone, N. Ramnath, R. M. Reddy, S. Nagrath. **AACR 2014, San Diego.**
- Integrated Microfluidic Chip for high throughput CTC Sorting and Detection with High Specificity. Authors: M. MG Grafton*, R. M Jack*, D. Rodrigues, C. Griffin, D. Jue, R. Cieslak, **M. Zenali**, M.S. Wicha, D.M. Simeone, S. Nagrath. **AACR 2014, San Diego.**

12 Acknowledgments

I would like to express my deep appreciation and gratitude to my advisors at the Institute for Medical Technology of Heidelberg University and Mannheim University of Applied Sciences Professor Dr. rer.nat. habil., Mathias Hafner, and at the University of Michigan, Professor Dr. Sunitha Nagrath, for their supports and the opportunity they provided, all the way from when I was first considering applying to this PhD program in the University of Heidelberg, through to completion of this degree. Their extreme patience in the face of numerous obstacles and the encouragements inspired me during the course of my graduate studies. Sunitha's intellectual heft in matched only by her genuinely good nature and down-to-earth humility, and I am truly honored to have had the opportunity to work with her. I have learned many lessons from her, both personally and professionally. I also specifically would like to thank Mathias for his positive unconditional help and support during my study.

I also would like to thank my dissertation committee members, professor Dr. Norbert Gretz, professor Dr. Frank A. Giordano, professor Dr. Bernd Krüger, and professor Joerg Lahann for accepting to be on my dissertation committee.

I also would like to acknowledge a multiple of people for their friendly guidance, thought provoking suggestions and the general collegiality that offered to me over the years. I am grateful to Dr. Diane Simone and Dr. Vaibhav Sahai for their help, support and providing the pancreatic patient's blood samples and the clinical specimen coordinator Heather Cameron, Kara Schradle, and Kirk Herman. I also would like to thank Dr. Meghna Waghray for her help for building the xenograft PDAC mice model study, Dr. Vasudha Murlidhar, Dr. Lianette Rivera, Christopher Dunlay, and Maggie Lee for their help and support on the pancreatic project.

In the same vein, I would like to thank to Dr. Nithya Ramnath and Dr. Rishindra Reddy for being a wonderful collaborators and for immensely useful insights and feedback on my work on lung cancer. Also, I would like to thank to the clinical lung cancer specimen coordinators Shari Barnett. I am thankful to our collaborators Dr. Max Wicha, Dr. Ebrahim Azizi, Shamileh Fouladdel, and Dr. Ramdane Harouaka for the contributions they made to my intellectual growth during my years of study. I would like to acknowledge Dr. Nallasivam Palanisamy, Dr. Armand Bankhead, Dr. Lili Zhao, and Dr. Jiaqi Shi for their help with the sample analysis. I am also thankful to Dr. Meggie Grafton and Dr. Mostafa Ghannad-Rezaie for their help in AutoCAD design of the immunoaffinity microfluidic devices, Saeedeh Noroozi and Ali Attari for helping with animations images and video the Carpet CTC chip, Rork Kuick for his help with statistical analysis of the RNA expression profiling and review of the manuscript, Dr. Molly Kozminsky, and Emma Purcell for giving me valuable feedback. Also, I am grateful to Dr. Eric Lin to provide the size-based separation technology and his feedback on the projects and to Dr. Wei Huang for performing the drug testing experiments. I am thankful to all undergraduate and graduate students and research fellows in Nagrath's group for being great colleagues and friends and persuading me to reach to this final stage.

Additionally, I also thankfully acknowledge all the staff at Lurie Nanofabrication Facility at College of Engineering-University of Michigan, who provides an excellent micro-fabrication research facility, and the staff of MIL at University of Michigan for providing access to their instruments and facilities for Confocal and SEM imaging. The research histology and immunoperoxidase laboratory at the University of Michigan

Comprehensive Cancer Center for performing the IHC of primary tumors. This work was supported by the National Institutes of Health (NIH), a Career Development Program of the Gastrointestinal Specialized Program of Research Excellence (GI SPORE) award, and a Department of Defense (DoD) Office of the Congressionally Directed Medical Research Programs (CDMRP) Career Development Award. I also would like to express my gratitude to the all patients who participate in this study and the healthy volunteers who contributed blood samples.

Last but certainly not least, I sincerely thank all of my friends for taking the blows and giving me a chance to thrive, for being there and taking care of me in every way possible in all hardships and joyful moment of my life during my study far from home. Words cannot describe how much your friendship means to me.

I would be remiss if I did not acknowledge the innumerable sacrifices made by all of my family members. Word cannot express my thankfulness to have them as a family. So here by I dedicate all of my work to them.